An Assessment of Environmental Magnetics and Particle Size Distribution Analyses as Proxies for Variations in the Intensity of the East Asian Monsoon.

Thesis submitted in accordance with the requirements of the
University of Liverpool for the degree of Doctor of Philosophy
Eleanor Jane Parker

September 30th 1999

An Assesment of Environmental Magnetics and Particle Size Distribution Analyses as Proxies for Variations in the Intensity of the East Asian Monsoon.

Abstract

High-resolution records of rapid climate change during the last glacial-interglacial cycle are biased by European and North Atlantic data sets. The Chinese loess Plateau also has the potential for high resolution climate proxy records. Loess from the north western Chinese loess plateau is typically coarse-grained and the palaeosols relatively weakly developed as a result of the climate gradients of dust storm intensities and precipitation. Past research has shown that variations in magnetic susceptibility and bulk particle size may be used as proxies for the intensity of the East Asian summer and winter monsoons respectively. However aridity in northern China prevents marked changes between palaeosols, incipient soils and slightly altered loess This study shows that a multi-proxy approach using magnetic susceptibility, magnetic remanence and parametric particle size distributions allows a more detailed reconstruction of environmental processes and their response to climate variability

Analysis of a 45 m section at Caoxian in the Jingyuan basin, north western China, has identified 4 typical particle size distributions for loess arid palaeosols deposited during the last 130 ka. Each type is reflected by distinctive variations In magnetic grain size and mineralogy. It is suggested that one type reflects initial dust transport mechanisms and associated magnetic parameters reflect the primary detrital magnetic composition. The remaining three particle size distribution types reflect pedogenic alteration of the primary loess. The type and degree of pedogenesis is quantified by magnetic frequency dependent susceptibility and magnetic remanence parameters.

I declare that the content of this thesis is my own work and that it has not been submitted for examination at any other university.

Eleanor Jane Parker

September 30th 1999

Acknowledgements

Dedication

This thesis is dedicated to my father. Wish he could have read it.

Table of Figures

Table of Tables

1. Introduction

1.1. 'Global Warming' and Climatic Variability

The three principal factors which have influenced climate in the past are variations in solar radiation, earth surface conditions and general atmospheric circulation. These factors have been joined in the recent past by the influence of anthropogenic activity. Recent human activity has not only altered the Earth's surface but also the atmosphere. How fast climate may change in the future may be answered by investigating how fast climate changed in the past. Climate change research is one field where the present is not the key to the past, indeed it may be more precise to say that the past is the key to the future. The recent decade has seen environmental issues grow in political importance probably none more so than 'Global Warming'. The World Meteorological Organisation (WMO) and the United Nations Environment Programme (UNEP) established the Intergovernmental Panel on Climate Change (IPCC) in 1988. The IPCC was established to assess scientific, technical and socio-economic information relevant to understanding the risk of human-induced climate change. A report in 1995 (IPCC Working Group 1) stated that in order "to distinguish anthropogenic climate changes from natural variations, it is necessary to identify the anthropogenic signal against the background noise of natural climate variability" (www.ipcc.ch pp 3). The aim of this research is to attempt to quantify the "background noise of climate variability" in the recent past, prior to any significant anthropogenic influence.

The palaeoclimatic record has provided convincing evidence of large-scale climate changes. At present high-resolution climate proxy records, with good chronologies, that allow analysis of very abrupt or relatively small scale changes are rare. A recent IPCC report (1995) stated that "the range of natural year to year temperature variations is quite similar to the size of the warming that appears to have occurred over the past century (0.3-0.6° C). Moreover, the 16th to 18th centuries appear to have been cold, linked possibly to the Maunder Minimum, and the climate may still be recovering from that time". The Maunder Minimum was the period from 1640-1710 when almost no sunspots were observed. It coincided with a period of colder than average temperatures in northern Europe i.e. the Little Ice Age. Ice cores provide direct evidence of past

methane and CO_2 concentrations and the pace of the rise in concentrations of these greenhouse gases over the last century is unprecedented in the 400 ky ice record. However, the present concentration is within the range of past variations (Raynaud et al, 1997).

Past abrupt climate changes appear on several occasions to have severely strained natural ecosystems. The importance of assessing the scale, rate of climate change and spatial and temporal connections of past variability will give further evidence that can be used in climate prediction models. Following the pioneering work of the COHMAP project several large scale initiatives have been set up in recent years; CLIVAR, ACE-ASIA, PAGES (IGBP, geosphere biosphere interactions) to name a few. For example PEP's (Pole-Equator-Pole Palaeoclimate) aim is to analyse inter-hemispheric linkages of climate past and present. By quantifying responses of environmental systems to global changes and then linking them to responses in other regions an insight into the global climate change mechanism can be gained. The East Asian monsoon is an important component of the climate system and its reactions to changes in atmospheric and oceanic circulations are reflected to some extent by the extensive loess deposits in China. This thesis concentrates on the high resolution climate proxy potential of the north western Chinese loess Plateau. The following discussion will show that high resolution climate proxies have a North Atlantic bias. This research aims to rectify this by augmenting evidence from Asia.

1.2. Timescales and Mechanisms of Climate Change

1.2.1. Earth Orbital Forcing of Climate

Evidence has mounted for a link between the earth's orbital parameters and long term climate variations (Imbrie et al, 1984). Milankovitch theory states that glacial cycles are related to changes in earth orbital parameters due to gravitational interactions with the sun and other planets. Variations in obliquity and precession of the Earth's rotational axis and cyclical changes in eccentricity of its orbit have main periodicities of 41, 23 – 19 and 100 ky. Solar radiation is the primary energy input to the Earth's climate system. Astronomical parameters such as the distance between the earth and the sun, the inclination of the Earth's axis and the speed of rotation, modify the sun's

energy input. Atmospheric circulation arises from the uneven heating of the Earth's surface, as a result of latitudinal variations due to a tilted rotating axis and the variation in the thermal and reflective properties of land and oceans. Many climatic proxies from the deep-sea (Ruddiman and McIntyre, 1984) and ice cores (Imbrie et al, 1984) have been shown to vary with clearly defined orbital cycles. In the 1970s and 1980s, palaeoclimate research focused on Milankovitch forcing of the climate system and specifically the global ice volume. Abrupt changes in the climate became high profile after the publication of Heinrich's paper in 1988 (Heinrich 1988), in which he showed significant and abrupt iceberg discharge events punctuated the normal marine sedimentary regime in the North Atlantic. Subsequently, the possible role of the ice sheets in the climate cycle has become the subject of extensive debate. It is accepted that seasonal changes in the distribution of insolation induced by orbital cycles are the primary mechanism for driving the glacial-interglacial fluctuations of Quaternary ice sheets. The fluctuations in ice volume appear to have a major influence on short term ocean-atmosphere reorganisations.

1.2.2. The 100 ka cyclicity and Loess

Climate over the past million years has been dominated by glaciation cycles with periods near 23, 41 and 100 kys. In a linear version of the Milankovitch theory, the first two cycles can be explained as responses to insolation cycles driven by precession and obliquity (Imbrie et al, 1984). The 100 ky radiation cycle (arising from eccentricity variation) is too small in amplitude and too late in phase to produce the corresponding climate cycle by direct forcing (Imbrie et al, 1993). 100 ky cyclicity, evident in ice and marine core records, led to the proposal that something more than orbital forcing was controlling the climate since it was not specifically predicted by the Milankovitch hypothesis (Imbrie et al, 1993). It was proposed that ice sheets, forced by precession and obliquity, exceeded a critical size and stopped responding linearly to Milankovitch forces.

Large ice sheets may drive atmospheric and oceanic responses in a similar way to external forces. This non-linear response was evident in many records from 0.78 Ma onwards and its onset may be linked to the Tibetan plateau reaching a critical height and altering atmospheric circulation

14

(Ruddiman et al, 1990; Kutzbach et al, 1993). Figure 1.1 shows the 100, 41, 23, 19 ka orbital frequencies reflected in the Central Chinese Loess Plateau at Baoji by spectral analysis (Ding et al, 1995).

1.2.3. North Atlantic Deep Water Circulation (NADW)

Broecker and Denton (1989) proposed that the Quaternary glacial cycles (and possibly interglacial cycles: Adkins et al, 1997) were dominated by abrupt reorganisations of the ocean-atmosphere system, which were primarily driven by orbitally induced changes in freshwater transport. In turn, these impacted on the ocean's salt structure (Broecker et al, 1985). In explanation, Broecker hypothesised the existence of the North Atlantic conveyer belt or North Atlantic thermohaline circulation system in which, warm low-salinity waters transfer heat energy from low latitudes to high latitudes. A high rate of evaporation would cause precipitation over the poles and the growth of ice sheets. Residual dense, salty, cold, water sinks to form North Atlantic Deep Water (NADW), which upwells in the Indian and Pacific oceans. The North Atlantic and in particular the Labrador Sea components appeared to be crucial in convection variability in Broecker's model.

In this model, evaporation is the driving force of the Atlantic saline conveyor. The transport of freshwater is northward (Bond and Lotti, 1995). Stommel's (1961) box model proposed a southward transport of fresh water. Although both models were based on density differences, only one can be valid. Rahmstorf's (1994; 1996) computer model showed that heat is supplied in the South Atlantic. If the conveyor is switched off, salinity decreases in the North Atlantic and heat builds up in the southern hemisphere. He proposed that the conveyor transports warm salty surface water to high latitudes. The computer model shows that the conveyor can be sustained without significant evaporation. Rahmstorf's model is precariously balanced: cooling and fresh water influx reduces salinity and density. If readjustment is tardy the conveyor breaks down gradually over a century or, more (horizontal forces). A second circulation threshold is based on vertical mixing. If vertical mixing ceases, a shift in the position of NADW formation sites may follow or in extreme cases, the conveyor may stop within a decade.
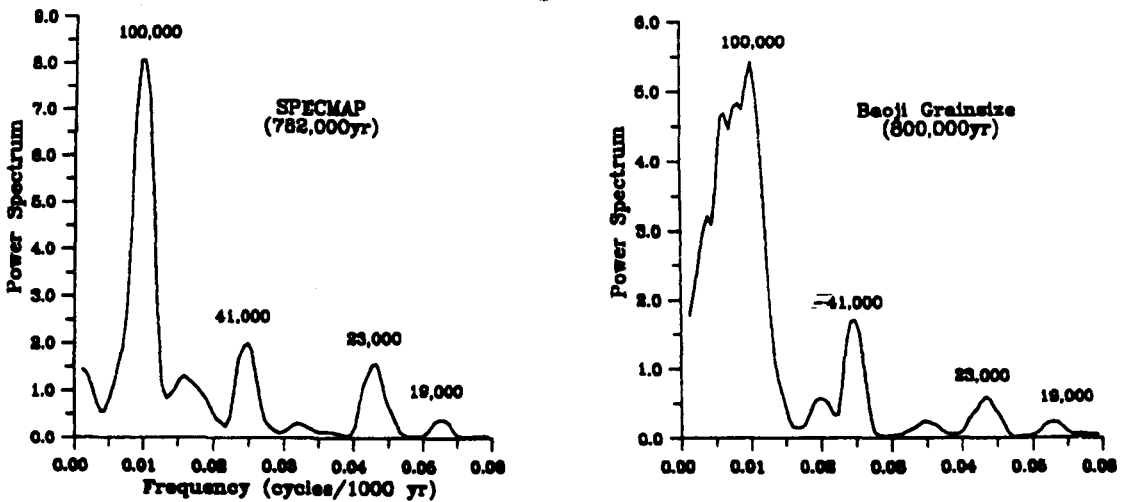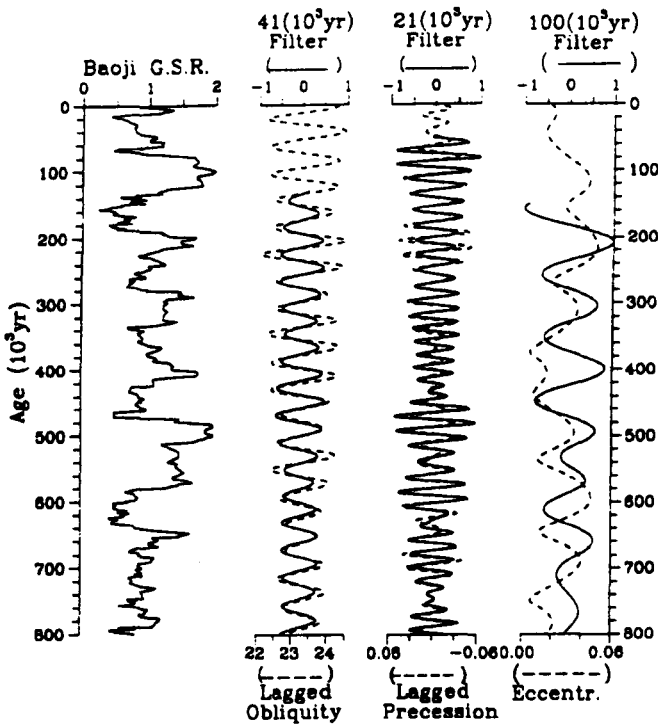
Figure 1.1 Baoji particle size (top) time series and SPECMAP stack (bottom) for the past 800 ka. Frequencies are in cycles per 1000 yr. (After Ding et al, 1995)

16

There is now substantial evidence for a 'flickering switch' of late Pleistocene climate change, which may be primarily driven by ice and salinity variation (Taylor et al, 1993b). Marine core evidence for the existence of a link between deep-ocean thermohaline circulation and abrupt interstadials is growing (Lehman and Keigwin, 1992; McManus et al, 1999). Whether changed ocean circulation is the cause of interstadials or an associated reaction to another forcing mechanism is unclear. That the Greenland ice cores and marine sediment cores from the tropical Atlantic (Hughen et al, 1996) to the Polar North Atlantic show high resolution rapid changes throughout the last glacial cycle is not disputed.

Recent evidence also indicates millennial scale variations in north Atlantic circulation during the Holocene (Marchitto et al, 1998). Atlantic and Pacific circulations are only weakly connected in Ramhstorf's model and do not respond as one system: in contrast Broecker's model proposes a global conveyor. Very little evidence of glacial-interglacial and short cyclicity variation exists for the Pacific. The mechanism and significance of teleconnection of climate variability through ocean circulation is still a matter of some debate (Shackleton et al, 1983; Kotilainen and Shackleton, 1995).

1.2.4. Heinrich Events and Bond and Dansgaard and Oeschger Cycles

Whatever the cause, rapid climate variations certainly have a northern hemisphere signal. Ice cores provide nearly continuous evidence about local temperature, precipitation, humidity, and wind speed variations. Ice cores also record changes in the composition of the atmosphere. Bond cycles, 10 ky cooling cycles, evident in Greenland ice cores, are made up of bundles of progressively cooler interstadials. Dansgaard-Oeschger (D-O) cycles last approximately 1000 years (Dansgaard et al, 1993; Taylor et al, 1993a). D-O cycles may also be connected to small scale ice sheet instability over millennial time scales (Bond and Lotti, 1995). The gradual cooling of the interstadials during the Bond cycles probably reflects a strengthening of the polar cell (Bond et al 1992; 1993).

Each Bond cycle culminates in a cold stadial and subsequent Heinrich event - iceberg calving as a result of ice sheet collapse characterised by layers of ice rafted debris and decreases in salinity in North Atlantic marine sediments

and microfauna (fig 1.3). These sequences of events form the characteristic asymmetrical saw tooth patterns evident in the ice core climate proxy records (GRIP members, 1993) fig 1.2 and fig 1.3. Moderate calving associated with short-term ice volume fluctuations during glacials, termed 'binge-purge' oscillations by MacAyeal (1993), may have been enough to cause cyclic disruption of the salt structure of the Atlantic (Duplessy et al, 1992) and hence, lead to feedback amplification or a mechanism of teleconnection. Bond (1993) suggests that after massive calving, and melt water dispersion, the ice sheet retreat may have been so extensive (possibly due to isostatic anomalies) that subsequent iceberg-dilution was insignificant and allowed full North Atlantic thermohaline circulation to re-establish itself.

There is a close relationship between ice-core temperature cycles and Heinrich events (Heinrich, 1988) recorded in the marine record. Low ocean salinity and iceberg discharges only occurred during the cold stadials and were followed by abrupt shifts to warmer sea surface temperatures. The correlation of Heinrich events in marine cores to stadials, periods of 'cold ice',
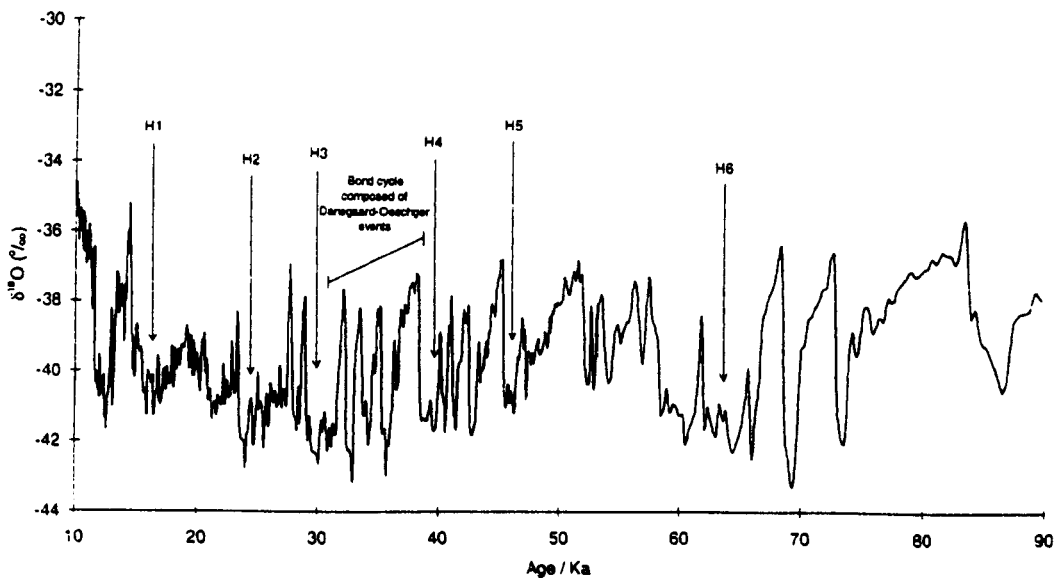
Figure 1.2 $\delta^{18}O$ record from the GISP2 ice core record demonstrating interstadial cooling events defined as Bond cycles. Each cooling phase is composed of Dansgaard- Oeschger events characterised by saw-tooth stepwise cooling. Each Bond cycle is terminated by a cold Heinrich Event.

reinforces the idea that these events are linked in some way to atmospheric cooling. The warming at the end of the Younger Dryas was estimated to be of the order of 7°C in a few decades (Johnsen et al, 1992, Grootes et al, 1993). A similar and correlative event occurred in the tropical North Atlantic (Hughen et al, 1996). Similar events have been recognised in the Santa Barbara Basin in the Eastern Pacific (Kennett and Ingram, 1995; Behl and Kennett, 1996; Lund and Mix, 1998).

Andrews' (1998) paper drew into attention to the concept of time transgression of sedimentary profiles and problems of accurately dating 'abrupt' climatic events such as Heinrich events. He stated the need to reduce the uncertainty of dates to ± 50yrs. Age estimates for Heinrich event 4 range from 33 – 39 ky. Dating of marine and terrestrial records using radiocarbon techniques with a resolution of ± 2000 ky affects attempts to correlate abrupt climate events (Andrews, 1998); the 'count from the top' procedure, which has been used to date layers in ice cores shows recent abrupt events have occurred over decades not millennia.

The Antarctic Vostok ice core contains a 160 ka climate record of the southern hemisphere (Barnola et al, 1987). Only eight of the nine Dansgaard – Oeschger events that last longer than 2 ka are visible in the Antarctic Vostok ice core (Jouzel et al, 1990; Lorius et al, 1993; Bender et al, 1994). It is unclear whether cooling cycles are forced by internal dynamics of all ice sheets or simply reflect a different mode of climate forcing. Decadal-to-centennial variability is evident in the top of the Greenland ice core records. They show a resolution approaching annual. Fluctuations in ice conductivity on scales of <5-20 yrs reflect rapid oscillations of the dust content of the atmosphere, suggesting extremely rapid reorganisations of atmospheric circulation as well as ocean circulation (Taylor et al 1993).

The isotope and dust content of the GRIP ice core was initially thought to show rapid shifts to cooler conditions during the last interglacial, the Eemian (MIS 5e) (GRIP members 1993; Dansgaard et al, 1993).
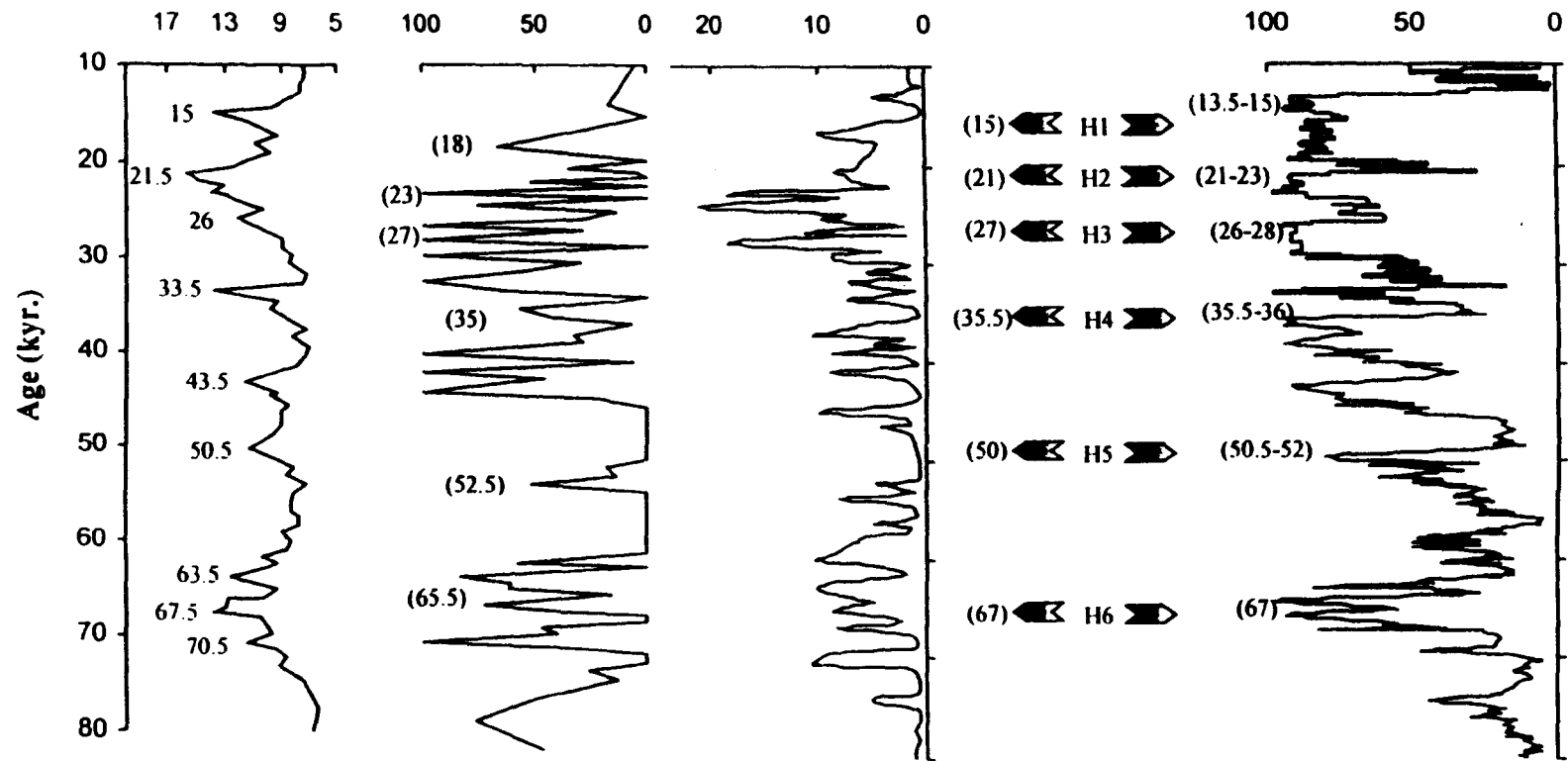
Figure 1.3 Covariance of Heinrich type events across the northern hemisphere. Quartz- only median diameter from the Luochuan loess section is a possible indicator of winter monsoon intensity. Al % contribution is from western sources - indicator of detrital input. The Ca content of GRIP ice core is an indicator of variations of aerosol mineral dust. Heinrich events are dated from IRD layers from the North Atlantic; N Pachyderma is a cold water indicator.

This has since been discounted and is now thought to reflect disturbed basal ice layers (Johnsen et al, 1995). The deep-sea record from the mid North Atlantic (Keigwin et al, 1994; McManus et al., 1994) does not support the presence of climate instability during the last interglacial. However, the marine records from higher latitudes contain evidence of an unstable climate during this time (Lauritzen 1995; Seidenkrantz et al., 1995; Fronval et al., 1995;), as do Norwegian speleotherms (Winograd and Ludwig, 1996). French lake deposits reveal an unstable climate during the Eemian interglacial (Thunell and Mortyn, 1995). Field et al (1994) considered that European pollen records record an unstable climate. At low and mid latitudes, variations in precipitation may have been a more important driving force than temperature variations during D-O events. Cold North Atlantic sea-surface temperatures are known to have a dramatic effect on regions directly down wind (DeMenocal, 1993). Climate instability in Europe during the last glacial has been detected in the lake sediments of France (Thouveny et al, 1994; Thunell et al, 1995) and in deep-sea sediment cores from the North Pacific (Thunell and Mortyn, 1995, Kotilainen and Shackleton 1995). New evidence of sub-millennial scale variations during the Holocene and other periods of low ice volume indicate that the relationship between ice volume and climate is extremely complex (MacAyeal, 1998).

Several conflicting hypotheses exist regarding the mechanism of abrupt global climate change. The first involves synchronous changes in atmospheric and ocean circulation, while the second is predicated upon reorganisation in the North Atlantic having a global feedback effect with the amplitude and phase depending on geographical position (Fanning and Weaver, 1997).

1.3. History of Loess research

Loess deposits in China are valuable high resolution records of abrupt climate change. The term loess is derived from the German meaning 'loose' and was first used to describe the friable silty deposits along the River Rhine. The origins of loess did not become widely accepted in the west until 1868 with von Richthofen's geological investigations in China. It was J.G. Anderson in 1923 who designated all the 'loose soils above the Pliocene red clay' as loess in China. Obruchev (1945) made a firm distinction between loess of aeolian

origin and loess delivered by non-aeolian processes or reworked loess. Pye (1989) states "in China the relationship between wind-blown dust and loess, known locally as *huangtu* meaning 'yellow earth', was understood more than 2000 years ago". The aeolian origin of Chinese loess is now widely accepted.

There is still considerable discussion as to what the determining characteristics of loess are. Definitions based on physical and mineralogical characteristics are not entirely satisfactory (Pye, 1987). Loess is defined by the INQUA Loess Commission as a sediment whose 'dominant fraction .... is within 60-20μm, is unstratified, primary calcareous, quite porous capillary network, on the whole, dry material is yellow, buff, brownish yellow' (Rogers and Smalley, 1993). Recent work has shown that not all loess is calcareous and it may have significant sand (desert loess) or clay content (Thailand) and the colour can vary from red brown to grey.

1.3.1. Chinese Loess Stratigraphy

Loess deposits across the globe are generally less than 30m thick. Greater thicknesses only occur in areas where huge and sustained quantities of dust are supplied over a prolonged period. In regions of North America, the Argentine and the Danube, deposits occur locally when dust is trapped by vegetation or at a change in topography. In contrast, loess deposits in China cover 630 000 km^2 or 6.6 % of the country at thicknesses up to 400m at the north western plateau margin.

The loess sequence in China is divided into four major formations: the Wucheng loess (2.4 – 1.15 Ma BP), Lishi loess (1.15 – 0.1 Ma), Malan loess (0.1 – 0.01 Ma) and the Holocene black loam (Liu, 1962; Heller and Liu, 1982; Ding et al, 1992). It is now accepted that soils are formed during interglacial periods on loess sub-base formed during the intervening glacial periods. At the Baoji sections in the central loess plateau, the 32 units defined within these formations are well developed A, B and C horizons (Rutter et al, 1991) (fig 1.4). The pedostratigraphic subdivision of Quaternary Chinese loess is based on the S-L system. S defines a well-developed soil horizon and the associated number.

Xifeng

Lithology	Polarity	*Log* susceptibility (SI - units)
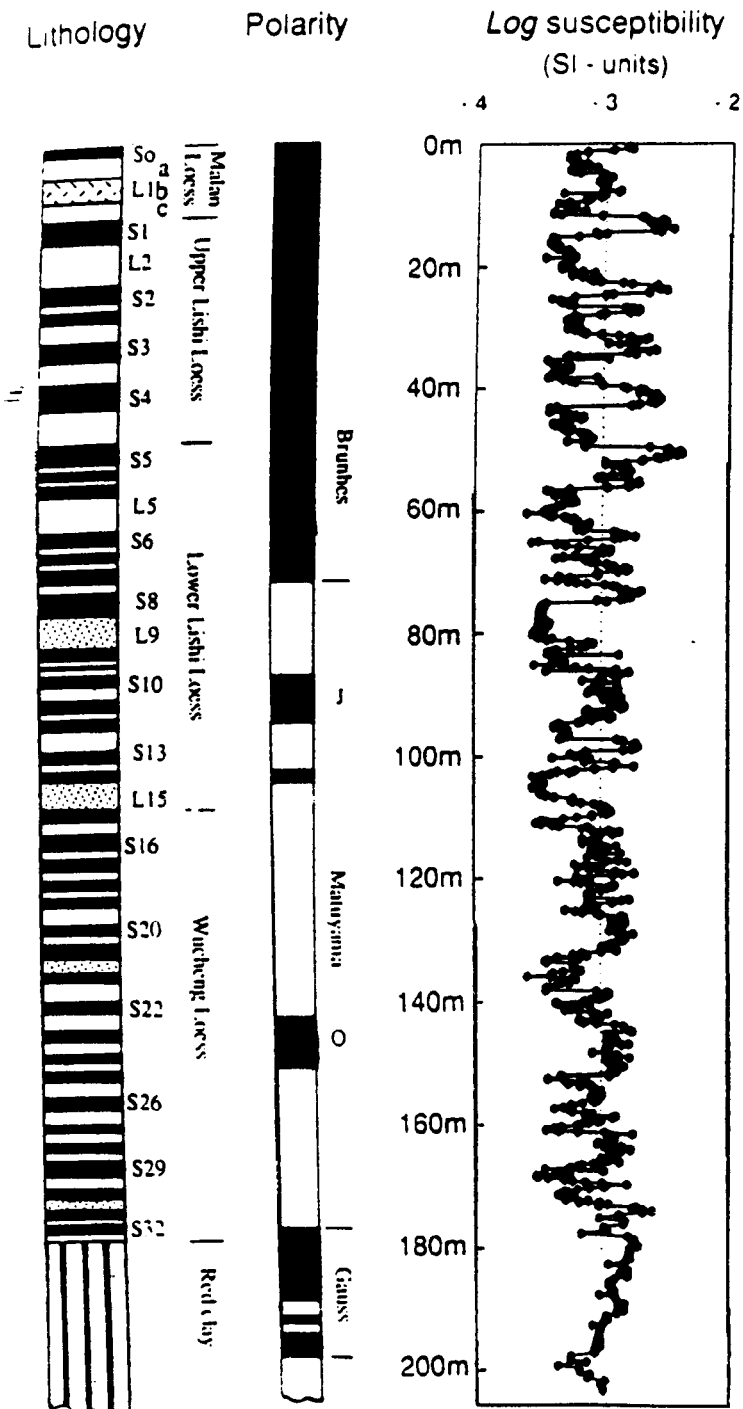
Figure 1.4 Sequence of alternating Loess (L) and palaeosols (S) covering the Wucheng, Lishi and Malan loess formations. Polarity boundaries as defined by measurement of the stable natural remanent magnetisation (After Rutter et al, 1991).

relates to its stratigraphic position. L notation defines the intervening loess deposit.

The Wucheng loess is underlain by the red clay. Palaeomagnetic measurements demonstrate that the contact between the red clay and the Wucheng loess dates from around the Matuyama / Gauss geomagnetic reversal (Heller and Liu, 1982; Kukla and An, 1989; Ding et al, 1992; Sun et al, 1992). Time series analysis of long loess sections at Baoji revealed strong spectral peaks at periods of 100 ka and 40 ka in agreement with the other climate records (Ding et al, 1995). There was also strong evidence for a 400 ka periodicity prior to 1.32 million years ago; this is predicted by astronomical calculations, but had rarely been recognised in geological data. It appears from palaeomagnetic results that a slow and constant sedimentation rate for the red clay continued from 7.05 to 2.58 Ma (Ding 1998). It is widely accepted that loess deposition proper began at 2.4Ma (Ding et al, 1992, Ding et al, 1997).

In the north western loess plateau loess is typically coarse-grained, and the palaeosols relatively weakly developed. The loess deposition rate is approximately 4 to 5 times greater (Chen et al, 1993), and up to 7 times greater than in the Central Loess Plateau. It has been suggested this is the most sensitive region to global changes in China (Yie et al, 1990; An et al. 1993; An et al, 1991a; Li et al, 1988). Loess regions have been defined on the basis of the NW-SE climate gradient across the plateau, with sandy loess in northernmost areas, followed to the south east by a zone of loess and then clayey loess. This progression has been dynamically linked to modern dust storm intensities and precipitation (Liu, 1985).

1.4. High Resolution Proxy Climate Records

Most high quality, high-resolution records of rapid climate change during the last glacial-interglacial cycle are biased by European and North Atlantic data sets. However, it is becoming increasingly clear that the Chinese loess Plateau has great potential for high resolution climate proxy records. The stratigraphy of the Chinese loess plateau shows clear alternating soil and loess horizons. Early correlation with the marine record showed that these soil horizons corresponded to periods of more negative $\delta^{18}O$ values or interglacials in deep-sea sediments (Heller and Liu, 1984; Kukla et al, 1988; 1990). Early

chronologies used orbitally tuned oxygen isotope record (SPECMAP – Imbrie et al 1984; Ocean Drilling Program Site 677).

Climate records deposits other than loess also exist from East Asia. The $\delta^{18}O$ record in the 309 m long Guliya ice core indicate a close correlation between the temperature variation on the Tibetan Plateau and solar activity (Yao et al, 1997). [36]Cl data (Thompson et al, 1997) suggest that the ice core recovered from the Guliya ice cap may be more than 500 ka. A comparison of the Guliya ice core with the Greenland and the Antarctic ice records shows similar temperature variation events but with a different amplitude. The similarity of the Guliya pattern to that of CH_4 records from a polar ice core indicate that global CH_4 levels and the tropical hydrological cycles are linked.

The Late glacial stage record of the Guliya ice core contains 200 year oscillations in $\delta^{18}O$ values and in dust content. Analysis of the upper most section of the ice core shows the variation of precipitation has been relatively small compared with that of temperature during the past 2000 years. The long term variation of temperature correlates positively with precipitation estimates from the Guliya ice core record, but the variation of precipitation lags behind the variation of temperature (Yao et al, 1996).

A previous core (Thompson et al, 1993) from the Dunde ice cap on the northern flank of the Tibetan plateau covered 40,000 years. Pollen preserved in the Dunde ice cap provides a sensitive record of Holocene climatic change and vegetational response in the northern Tibetan Plateau at time scales of millennia to centuries and decades. Prominent pollen changes during the Medieval Warm Period (790-620 yr BP) and the Little Ice Age (330-80 yr BP) suggest that the vegetation in the Tibetan Plateau region is sensitive to abrupt, century scale climatic changes (Liu et al, 1998).

Lake records in China can provide significant information about Asian monsoon activity and induced changes in the environment. Magnetic susceptibility, geochemical and pollen fluctuations in a 120 m long core of lacustrine and fluvial sediments from the Zoige Basin, eastern Tibetan Plateau, appear to be related to global changes in ice volume over the last 800 ka (Chen et al, 1999). Other lake cores from Gaxun Nor in the Badain Juran desert cover

approximately 950 ka, the last 140 ka of which have been matched to the Guliya ice core.

Published data indicates climate instability in the region during the Eemian, a phenomenon not positively detected in the Greenland ice core record (Wu and Wang, 1997). In the Tengger Desert palaeolake levels at Baijian Hu are evident in raised shorelines and stratified carbonates formed during the last 40 ka (Pachur et al, 1995). Microfossil evidence from lakes has been used to reconstruct precipitation, temperature and humidity during the last glacial cycle in north western China.

The isotopic composition from deposits in the Qaidam Basin together with the activity of H_2O of fluid inclusions in primary halite were used to determine variations in regional precipitation and hence, paleoclimatic changes on the Tibetan Plateau during the past 50 ka (Yang et al, 1995). The $\delta^{18}O$ values of fossil ostracods from Lake Qinghai provide a record of isotopic chemistry of the lake waters that can be related to the precipitation / evaporation budgets that have controlled the palaeolake levels. The precipitation / evaporation budget for the Lake Qinghai, as with other lakes in the region, appears to be largely determined by the Asian monsoon system.

As mentioned previously high resolution records of rapid climate variability have inherent problems of dating and correlation. A recent paper by Walker et al, (1999) proposed the concept of event stratigraphy rather than conventional stratigraphic procedures. Their discussion of the late Pleistocene climate variability recorded in the GRIP ice core seems particularly pertinent to the analysis and interpretation of north western Chinese loess climate proxies. Attention was drawn to the problems and practicalities of correlations based on lithostratigraphic or biostratigraphic evidence with reference to type-sites for fine scale stratigraphic records.

Terrestrial records are prone to erosional hiatii, time transgression and considerable spatial variation (Derbyshire et al, 1995b) and in such cases an alternative approach is required. Walker et al, (1999) prefer the use of 'events'. These are short lived occurrences, i.e. volcanic eruptions, floods, sea level rise, glacier margin oscillations etc., that have left an imprint on the geological record and can therefore be used as a basis for correlation. Such events would

be interpreted from a wide range of sedimentary environments using evidence appropriate to each sequence, not the conventional use of stratotypes. Since the events are the important elements of the record not the boundaries between them, problems such as time transgression can be more easily accommodated. It was recommended that the GRIP oxygen isotope record of the last glacial interglacial cycle be used as an event stratotype for the North Atlantic region with the possibility that it could be extended to a hemispherical event stratotype. The appropriateness of correlating proxies of aridity from loess profiles with Greenland interstadial events is discussed in chapter 6.

1.5. 'Proto-loess' and 'Loess-like' deposits

In discussing the formation of "loess", it is important to define precisely what is meant by the 'origin' of loess and the concepts of primary and secondary loess. The term 'loess' is often used to describe particles at source or in the atmosphere, but better terms may be 'dust' or 'proto-loess'.

In this discussion the definition of "origin" refers to the continuous processes of particle formation, transport and deposition. Contrary to Zhang et al, (1991) modification of primary loess once on the loess plateau by pedogenic process etc. is dealt with separately from the "origin" of loess dust. In this discussion, primary loess is the pristine loess after deposition, i.e., prior to any post depositional biochemical or physical alteration. Clearly, the period a loess deposit remains in the primary state is limited by environmental conditions, largely precipitation. This definition of primary loess is pertinent to loess deposits close to the plateau margins. Loess deposited in the central and southern loess plateau may contain a component of re-entrained primary loess from the northern plateau.

Obruchev (1911) designated secondary loess as loess formed by redeposition and reaccumulation of primary loess. He intended this definition to distinguish aeolian deposits from loess reworked by non-aeolian processes. This is not the definition used in subsequent discussions here. In this thesis, the term secondary loess is applied to all loess altered by pedogenic processes after deposition (Yakimenko, 1995). Sediments described as loess-like deposits (alluvial loess, loess loam etc.,) have usually been reworked by slope or water processes after aeolian deposition. In this discussion the term 'secondary

loess' is used to describe dust altered in situ by chemical and physical processes. The term 'loess-like' will be used to describe deposits that have undergone some form of non-aeolian redistribution after their initial phase of aeolian deposition such as gravity-induced slumping, collapse or aqueous deposition.

The definition of palaeosols in loess and their inherent characteristics is also problematic. Loess may be modified markedly by weathering. Palaeosols are usually decalcified and contain a higher percentage of clay minerals and aggregates than pristine loess (Assallay, 1998; Kemp et al, 1995; 1999; Kalm et al, 1996). Whether or not palaeosols should be described as secondary loess or as loess-like or modified loess is unclear in the literature. A distinction between palaeosols and incipient soils and slightly altered loess is especially relevant to the NW loess plateau where aridity prevents marked changes but allows subtle modification may be significant with respect to particular types of climate proxy analysis. It will be shown that when field stratigraphy is unclear, magnetic and particle size distribution criteria can be used.

1.5.1. Uncertainties involved in proxy interpretation

The application of parameters as proxies for environmental processes depends on how realistic the underlying assumptions are. The use of climate proxies is essential to allow the formulation of climate prediction models. It has been stated that "the instrumental record is barely adequate for studying the characteristics of decadal – centennial scale climate variability and the record can only be extended using proxy paleoclimatic information from different sources" (U.S Global Change Research Program, 1996). Various parameters obtained from Chinese loess have been used as climate proxies with varying degrees of success. Data including the magnetic susceptibility, granulometry, mineralogy, geochemistry, micromorphology, fossil content, and inorganic and organic carbon content of Asian loess-palaeosol series have been used as proxies of palaeoclimates.

Early workers used paleontological evidence to infer glacial and interglacial oscillations on the loess plateau based on quantities of fossil cold-drought resistant mammals. The remains of molluscs have been used more

28

recently (Keen, 1995). The analysis of amino acids racemisation from such remains can also be used to date the material (Oches and McCoy, 1995).

More recently, cores from Lake Qinghai have been shown to reflect monsoon and insolation fluctuations over the northern Tibet-Qinghai Plateau. The δO^{18} values of fossil ostracods provide a record of changes in the isotopic chemistry of the lake waters that can be related to precipitation and evaporation budgets that have controlled the palaeolevels for Lake Qinghai (Lister et al, 1991). It was concluded that the precipitation/evaporation budget for the Lake Qinghai region is largely determined by the Asian monsoon system. Terrestrial mollusc assemblages from Luochuan loess have been investigated to reconstruct environmental changes. This is a time consuming technique that has so far not been used for high resolution analysis (< 10cm intervals). Molluscs may potentially be a more sensitive climatic indicator than magnetic susceptibility (Keen, 1995). However, north western loess sections are lacking in suitable quantities of paleontological material in general including molluscs.

A pollen record from Weinan loess section revealed possible climate-induced vegetation variations, in the form of a succession of steppe and meadow-steppe environments during the past 100 ka (Sun and Ding, 1998). Dating pollen concentrated from aeolian sediments was also attempted so as to establish a chronological framework (Zhou et al, 1997). It was shown that pollen deposited simultaneously with sediment in a stable environment could provide reliable ages. Some researchers are still sceptical about the usefulness of pollen data in an aeolian dominated environment.

High resolution ^{14}C chronology, $\delta^{13}C$ values and organic carbon content from loess/palaeosol sequences and peats in China demonstrate century scale paleoclimatic fluctuations and precipitation variability within the last deglaciation (Zhou et al, 1997). The ^{14}C dating of organic fractions from palaeosol layers has yielded results that are quite often much younger than the true age of these sediments, probably due to the percolation of modern organic materials from agricultural activities (Head et al, 1989).

Bronger and Heinkele (1989) discussed the formation of palaeosols and variations in micromorphology of a Luochuan loess section. They concluded that pedostratigraphic variations had environmental implications. Subsequently,

detailed analysis from north western loess sections revealed cryogenic microfabric, thin soil crusting etc., not visible to the naked eye (Derbyshire et al, 1997). Such features may be used as indications for morphostratigraphic and climatic correlation (Guo et al, 1996; 1998). There are again drawbacks of inadequate sampling interval and long preparation time.

Geochemical analysis has become an increasingly used tool in paleoenvironmental reconstruction in China. Profiles of soluble salts and carbonates have been used to infer precipitation, weathering and soil moisture content (Chen et al, 1997). Suites of elements have also been used as palaeodust source tracers; Clarke's (1995) rare earth element analysis. Elemental analysis of modern dust material along a transport pathway has allowed individual storm tracks to be followed for great distances (Zhang et al, 1994; Zhang et al, 1996; Zhang et al, 1999). The flux of chemical elements to deep-sea sediments is affected by in situ biogeochemical processes and volcanic events. However, a close correlation between the chemical compositions of Chinese loess, marine aerosol and pelagic clays from the North Pacific Ocean has been noted (Zhang and Huang, 1992).

Berylium 10 (^{10}Be) is an isotope produced by the interaction of cosmic rays and the upper atmosphere. It has been used to determine past ice accumulation rates in Greenland and the same principle has been applied to Chinese loess (Beer et al, 1993). Deposition of the isotope is assumed to be constant (Shen et al, 1990). Shen et al (1992) found that the ^{10}Be concentration shows a tendency to decrease with increasing bulk particle size. The ^{10}Be record in loess showed features similar to those observed in δ^{18}O records from deep sea sediments and ice cores. This allowed a time scale to be established. Based on this time scale, accumulation rates of loess and ^{10}Be fluxes were calculated revealing higher values for cold, arid and windy periods than for warm, humid intervals. Correlation with magnetic susceptibility also revealed a similar relationship (Beer et al, 1993). This methodology depended on correlation and lacked an independent chronology. Estimates of changes in erosion rates in source regions have also been attempted using *in situ* cosmogenic ^{10}Be in loess quartz (Shen et al, 1992b).

The most widely utilised palaeoclimate proxies for loess are rock magnetic parameters, particularly magnetic susceptibility. Variations in the magnetic susceptibility of the Chinese loess and its interbedded palaeosols were found to correlate well with the deep-sea oxygen isotope record, and isotopic curves of Vostok and Greenland ice cores (Li et al, 1992; Liu and Ding, 1993; Ding et al, 1995; Shackleton et al, 1995). Enhancement of the bulk susceptibility by in situ formation of magnetite occurs in palaeosols. The formation and preservation of this pedogenic magnetite is dependent on soil-forming conditions and hence reflects the regional climate (Maher and Thompson, 1991). Other rock magnetic properties can reveal more detailed changes in magnetic mineral type and magnetic grain size that may also be climate driven. It has been assumed that regional and global paleoclimatic development of the East Asian Summer Monsoon during the last 2.5 Ma can be reconstructed from susceptibility records in the central loess plateau (Liu et al, 1992).

Temporal variations of loess particle size have been used to illustrate changes in the strength of the transporting winds. It has been inferred that lower mean wind speeds during interglacial periods lead to reduced mean particle size of the aeolian dust (Ding et al, 1992; Liu and Ding, 1993). Derbyshire et al (1997) stated that particle size might be a more sensitive record of climatically driven changes than magnetic susceptibility in the north western part of the plateau.

1.6. Aims of thesis

Chapter 1 has shown that there is a significant North Atlantic bias to high resolution climate reconstructions. Since the mid 1980's the potential of the terrestrial record from the central loess plateau has been realised. The primary aim of this research is to assess the usefulness of variations in bulk particle size distribution and magnetic susceptibility as proxies for the intensity of the Winter Monsoon and East Asian Summer respectively. The majority of assumptions made about the provenance, dust transportation and deposition of Chinese loess are made with respect to sites in the central Chinese loess plateau. Chapter 2 reviews factors influencing aspects of loess formation from silt production to post depositional modification. The proximity of the site under

31

analysis to the source area is particularly important; a detailed discussion of the types and climate induced variability of dust transport mechanisms is included. Chapter 2 also discusses the potential effects of climate change in the source area, pedogenesis and variable weathering rates, and how they may be reflected at the depositional site. Chapter 3 discusses the methodologies employed to analyse environmental magnetic and granulometric properties of the loess. Chapter 4 pays particular attention to defining a preparation method for loess particle size analysis. An understanding of the influence of the preparation technique is critical in interpreting the particle size distribution (PSD) results. Results in Chapter 5 and discussion in chapter 6 will be used to reconstruct in detail the environment in and around the loess plateau margin during the last 130 ka. The importance of temporal and spatial variation of environmental factors discussed in chapter 2 will be highlighted in the reconstruction. Particular attention is paid to variations in the PSD and its potential to provide increased or corroboratory evidence for rapid and abrupt climate variation on the Chinese loess plateau usually derived from bulk grain size and magnetic susceptibility variations. Although this study concentrates on local and regional climate influences on environmental process, in order to address the potential global significance of the climate variations recorded in the loess record, endeavours are made to link fluctuations with other records. The majority of this thesis concentrates on the interpretation of environmental magnetic and bulk particle size results from a north westerly site, Caoxian, Gansu County. It will be shown that critical examination of assumptions underlying the use of magnetic and particle size data as surrogate measures of palaeoclimate is imperative for sites at the Chinese loess plateau margins.

2. Variation of Environmental Processes in North Western China

2.1. Introduction

This chapter aims to summarise the influences of environmental processes on the stages leading to the formation of the loess profile. Processes are discussed in order, from silt particle formation through transportation and depositional mechanisms and post depositional modification. Particular attention is paid to the effect of climate variations on critical environmental factors. Assumptions made in previously published literature are discussed with respect to their applicability to the interpretation of climate proxies from sites in the northwestern part of China.

2.2. The Chinese Loess Plateau and The East Asian Monsoon System

Chinese climate alternates between the influence of two monsoonal systems, the East Asian winter and summer monsoons. 'Monsoon' is defined as a climatological phenomenon manifesting itself by marked changes in wind direction (Zhang and Lin, 1992). These changes result from seasonal variations in the thermal structure of the land and sea surfaces. The definition also includes the occurrence of distinct rainy and dry seasons. The meridional winds flowing from mid to high latitudes are very sensitive to changes in surface conditions at high latitudes (Kiladis et al, 1994), and it has previously been suggested that northern hemisphere ice sheets control the variations in the meridional atmospheric winds beyond mid latitudes (Ding et al, 1992). This winter wind system may play a significant part in the transfer of high latitude climate signals to lower latitudes (Ding et al, 1994).

2.2.1. The Tibetan plateau

Global climate models (GCMs) indicate that the uplift of the Tibetan plateau has played a critical role in the initiation and development of the Asian monsoon system (Ruddiman and Kutzbach, 1989; Clemens and Prell, 1990; Prell and Kutzbach, 1992; Ruddiman, 1997). The Asian monsoon system consists of two branches, the Indian monsoon and the East Asian monsoon.

The uplift of the Tibetan plateau appears to have blocked the direct influence of the Indian monsoon on the loess plateau. However, marine core records from the Indian Ocean also show rapid climate change (Clemens et al 1991; Colonna et al, 1996) which can be linked to North Atlantic variability (Colin et al, 1998). Ding (1994) suggested that the onset of loess deposition was caused by the Tibetan plateau reaching a critical height around 2.4 Ma BP.

Recent analysis of a 7 Ma aeolian sequence from the north central loess plateau provides evidence that the underlying red clay deposits may also be aeolian in origin (Ding et al, 1998; 1999; Sun et al, 1998). Studies of the pedogenic development of the red clay indicate that the summer monsoon was strongest between 7.05 to 2.6 Ma. This implies that the Tibetan plateau reached a critical height to induce some wind erosion and deposition around 7.05 Ma in the late Miocene (aeolian sedimentation rate of 2.98 cm/ka Ding pre-print). This dust has been heavily weathered due to the proposed slow sedimentation rate and high precipitation levels. Analysis of the red clay and the non-linear pattern of development of the summer monsoon system led Ding to speculate that the uplift of the Tibetan plateau prior to 2.6 Ma was not the sole climate forcing mechanism. This late Miocene dust was probably transported and deposited by a stable wind system, significantly different from the monsoonal wind system that has developed subsequently.

The change from homogeneous red clay deposition to loess-palaeosol deposition after 2.6 Ma, marks a major reorganisation in the monsoonal system to one with high amplitude fluctuations. The high degree of pedogenesis of soils S32 to S26 (2.6 –1.8 Ma) intercalated with loess layers demonstrates the increasing influence of the winter monsoon, with a strong summer monsoon control. Soil development between 1.8 and 1.2 Ma shows a weakening of the summer monsoon. Since 0.8 Ma the intensity of the Mongolian-Siberian high has increased, probably due to further uplift of the Tibetan plateau as shown by Ding et al, (1995) in figure 2.1, and most recently in rock magnetic and particle size results by Fang et al, (1999b). This resulted in an increased dust flux to the loess plateau and a decrease in pedogenesis. The height of the Tibetan plateau was crucial in the initiation of the two monsoon systems. The combined Indian and East Asian monsoons seem to have been active from 7.05 Ma, and separation of the East Asian summer monsoon occurred at ~2.6 Ma

34

(Ruddiman, 1997). The long term evolution of the Asian summer monsoons is evident in upwelling and palaeosalinity records of the Arabian and South China Sea (Clemens and Prell, 1990; Rea 1994; Emeis et al, 1995). Winter flow was enhanced by increasing flow around Tibet rather than over the plateau. Yellow River terraces at 0.8, 0.6, 0.15, 0.05 and 0.01 Ma indicate the recent uplift stages of the plateau (Li et al, 1997).

2.2.2. The Mongolian-Siberian high and the Pacific Aleutian low

During the winter half year (October - May), pressure fields are dominated by a strong cold anticyclone over Mongolia – the Mongolian Siberian high. Temperature differences between the cold Eurasian continent and the warm surrounding oceans (higher heat capacity) during the winter cause high-pressure at the surface over Mongolia and Siberia. The present January position is 100°N 50°S (fig 2.2a). When the East Asian summer monsoon is strong, cold, dry mid-latitude air flows NW-SE. The Tibetan plateau blocks the influence of these on the Indian monsoon. During the summer half year (June – September) an intense warm low develops over northern India and Pakistan and south west China and a strong subtropical high over the western Pacific resulting in a south and easterly summer wind regime (fig 2.2b). At present, the length of the rainy season decreases in a north-westerly direction. The annual advance of the summer monsoon into the continental interior is gradual but its retreat is rapid (Zhang and Lin, 1992).

Ding (1994) speculated that during glacial periods the enlarged ice sheets of the Northern hemisphere intensified the Mongolian-Siberian high and/or displaced it southwards. Inferred increases in aridity of source areas and extension of deserts combined with strengthened cold, dry winds caused an increase in dust flux and particle size that could potentially be transported on to the plateau. Present dust flux maxima occur in March – July, with corresponding storm minima during November and December, probably due to seasonal freezing of the surface (Derbyshire et al, 1998).
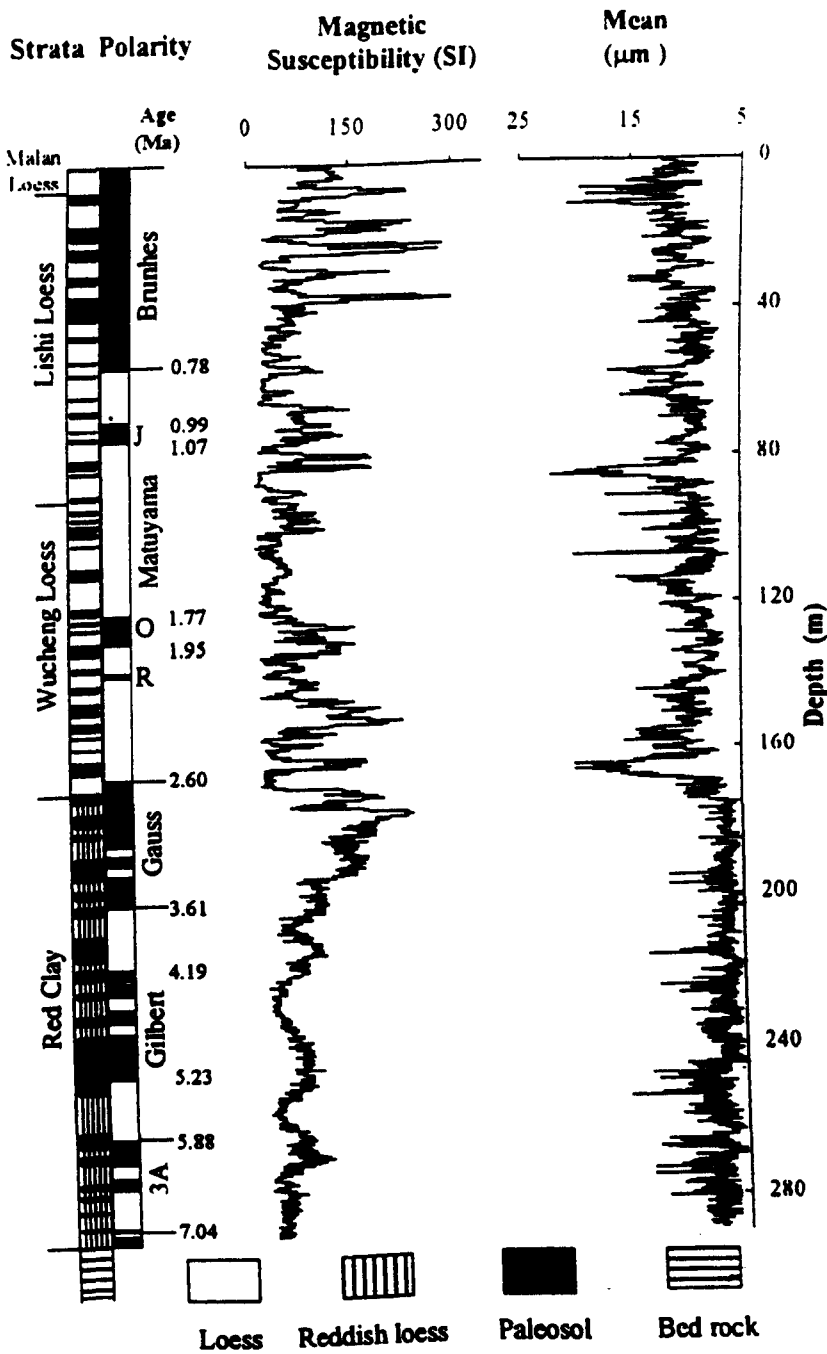
Figure 2.1 Sequence of alternating loess and palaeosol horizons. Peaks in magnetic susceptibility correspond to warm periods. Note the change in variability of both the particle size and susceptibility records after 2.64 Ma. (After Ding et al, 1992)
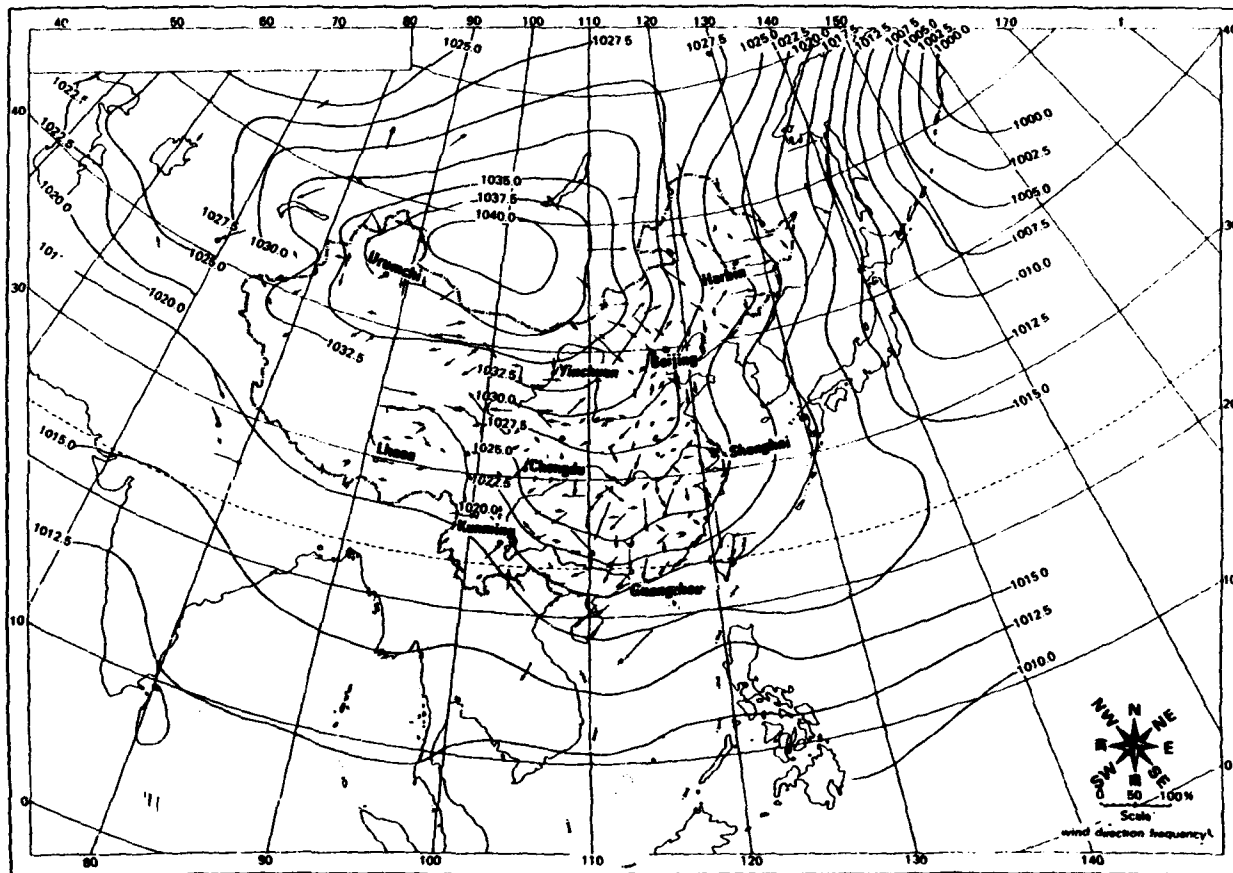
Figure 2.2a. Mean January sea surface pressure (hPa) over China. Arrows indicate seasonal wind directions (After Zhang and Lin 1992, from the Climatic Atlas of the P. R. of China).
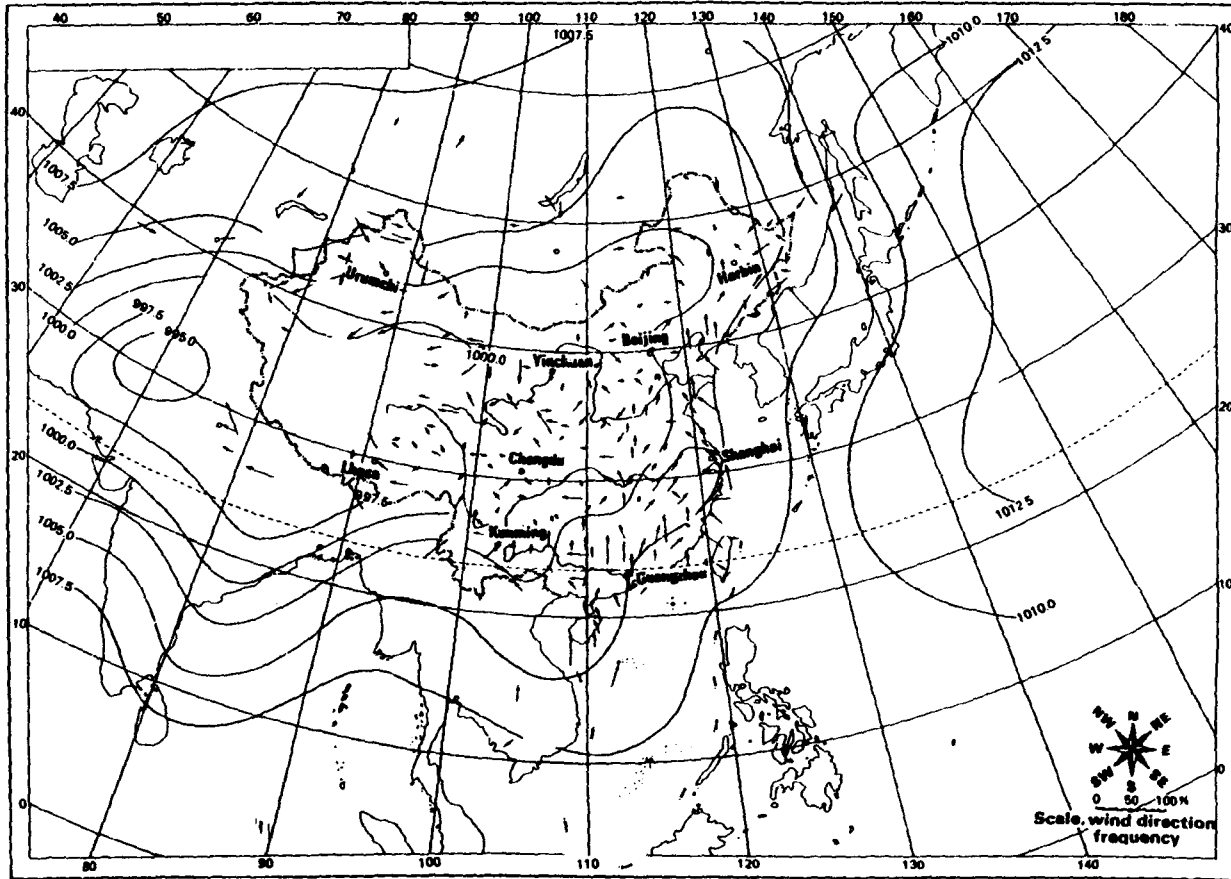
Figure 2.2b. Mean July sea surface pressure (hPa) over China. Arrows indicate seasonal wind directions (After Zhang and Lin 1992, from the Climatic Atlas of the P. R. of China).

Massive cold waves cause the intense dust storms characteristic of the loess plateau. A cold wave is preceded by a warm front with warm temperatures and may deliver rain or snow. The strong anticyclonic cold wave generally has a leading edge with a large pressure gradient causing exceptional wind speeds and an abrupt drop in temperature. The minimum temperature usually occurs after the storm winds have abated. A characteristic drop in temperature is > 10°C in 48 hrs with a minimum below 4°C and winds stronger than Beaufort force 5 (Zhang and Lin, 1992). At present in the northwest of the loess plateau, there is an average of five storms per year concentrated during early spring and late autumn i.e. associated with the migratory system, not the steady winter season. The trajectories of cold waves across China at present are commonly west to east or north to south, the direction depending on the movement of the high-pressure centre. Significantly, the progression of a cold wave affects the upper air circulation and jet stream (see section 2.3.4).

There is increasing evidence for teleconnections between the Asian monsoonal system and other widely distributed ocean and atmosphere systems. There is some indication that the Asian monsoon system interacts with the El Niño Southern Oscillation (ENSO). This is presently an important issue for climate modellers due to the social and economic effects of erratic weather conditions. More frequent cold waves in east Asia associated with a strengthening winter monsoon can enhance cumulus convection over the equatorial Pacific and may strengthen the 30-60 day oscillation in the western Pacific which may trigger ENSO events (Wang and Li, 1990). It has been suggested that convective activity over the warm pool of the western Pacific influences the intensity and location of the East Asian monsoon rain-band. Webster and Yang (1992) proposed that monsoon variations precede variations in the southern oscillation index (SOI). The monsoon may force changes in ENSO. Chen et al (1998) speculate that precipitation variations are closely related to the interactions between the Asian Monsoon Activities and El Niño events. Frequent El Niño occurrences may be due to strengthened winter monsoon during cold periods.

The Aleutian low in the North Pacific appears to be the main cause of local ocean climate variability. Between 1945 and 1997 the regimes of Pacific North America, North Atlantic Oscillation, Western Pacific and Polar/Eurasian teleconnections were monitored to define which patterns were important in each month. Significant shifts in the Aleutian low (strongest in winter) were well correlated with the three teleconnection patterns and are almost equally influenced by variability in the central Pacific and the NE Asian region. Shifts in the Aleutian low in the 1970's and early 1990's resulted in warming of ~5°C over Alaska (NOAA, Arctic Research Initiative). The presence of mobile pressure systems, especially those over or near the poles, may be used to explain the global propagation of paleoclimatic changes, through changes in the energy exchange and meridional air masses (Leroux, 1993). Such conclusions are drawn from directly monitored data. The retrieval of very high resolution proxy records from the region is important if a long term assessment of the cyclicity is to be made.

During the last glaciation, the strong winter monsoon seems to have been responsible for cooling the surface of the South China Sea. The reduced area of the South China Sea and Pacific warm pool due to falling glacial sea levels would have resulted in decreased moisture reaching the margins of the north western Chinese loess plateau. The short pulses of variability evident in records of the East Asian monsoon from the SCS are concurrent with short intervals of drought in southern California, (Site ODP 893 Santa Barbara Basin, Kennett and Ingram, 1995; Behl and Kennett, 1996). This implies that the Asian monsoon region and low latitude eastern Pacific are connected.

Elevated values in microparticle numbers and mass, especially during the Younger Dryas (YD), have been directly related to northern hemisphere aridity and the subsequent increase in dust available for long-range transport to Greenland. The sub-micron dust concentrations and calcium content of Younger Dryas recorded in GISP ice are 4 times higher and the micron dust concentrations are 7 times higher than the Preboreal concentrations (Taylor et al, 1997). The colder climatic conditions result from an expanded polar vortex (spatially and temporally). Peaks in mean particle size in the ice record have been used as a proxy for increased strength of zonal westerly winds (Zielinski

and Mershon 1997). Highs in the earlier part of the record often coincide with number and mass peaks reflecting increased temperature and pressure gradients of the polar vortex. Comparison of the clay mineralogy and Sr, Nd and Pb isotope data showed the composition of ice dust was very close to that in eastern Asia. The dust was not derived from the mid-continental United States or Sahara (Biscay and Grousset, 1998). The source area of the dust transported to the ice caps appears not to have changed significantly during times of variably higher dust fluxes. The annual layering of the ice (corrected for flow) shows that these changes occurred rapidly. Shifts in the YD dust concentration occur in three ~5yr steps over a ~40 yr period (Alley et al 1993). The associated sudden change in snow accumulation rate at the GISP site is too rapid to be a response of precipitation to increased warm airflow. A storm track shift because of latitudinal movement of the pressure systems is the suggested cause, although the intensity of the pressure zone would also decrease with warming (Kapsner et al, 1995.) Stratigraphic records from polar ice caps (Bender et al 1994; Mayewski et al, 1994), tropical ice caps (Thompson et al, 1986, 1993; Yao et al, 1997), marine sediments (Pye and Zhou, 1989; Hovan et al, 1989; Hovan and Rea, 1991; Rea, 1994; Heusser and Morley, 1997) and loess deposits (Ding, 1994) show that dust deposition rates were 2-20 times higher during the last glacial maximum.

Spectral analysis of marine particle size records has shown that an external orbital insolation signal and an internal ice volume signal can be defined (Clemens and Prell, 1990; Hovan et al, 1989; 1991). Studies of marine pelagic sediments over 2000km from the aeolian source have been interpreted as recording abrupt changes in the intensity of the transporting winds (Janenek et al, 1985). Comparison of mollusc records from the Luochuan loess sequence with those of particle-size and aridity index from core RC 27-61 in the Indian Ocean reveals obvious similarities suggesting that climate variations in the Loess Plateau may have been also subjected to the influences of the Indian monsoon to a certain extent in the geological past (Wu et al 1996). In conclusion, evidence from outside China shows not only the far reaching effects of monsoon variability but also the potential rapidity of change.

2.3. Factors Controlling the Characteristics of Pristine Loess Deposits in NW China

2.3.1. Introduction

Hardcastle (1890, quoted by Smalley, 1995) stated that four factors are required for the production of a massive deposit of dust. These are 1) sources of dust, 2) winds to transport the dust, 3) vegetation to trap the dust, and 4) sufficient time for accumulation. This was simplified by Smalley (1983) to 1) formation of loess particles, 2) transport of loess material, 3) deposition of loess material, and 4) post depositional modification. The present author prefers a combination of the two in the context of north western loess, as follows 1) formation of silt sized particles; 2) transport and sorting of the material into a deflation-prone sediment, 3) wind velocity reduction and dust trapping elements, i.e. deposition > erosion; and 4) post depositional modification.

Several 'standard' assumptions have regularly been made in published literature regarding silt production, provenance and deposition in China. The most significant are outlined below and a discussion of the validity of such assumptions follows.

- The majority of silt particles are formed by glacial grinding.
- Loess dust is blown from a spatially and temporally constant source area.
- Distinctions can not be made between the characteristics of dust from different source areas in the past.
- The dominant source areas are 'the Gobi desert' and other areas in the north of China and Mongolian borders.
- Coarse silt and sand particles can not be transported significant distances even by storm winds.
- Deposition on the loess plateau is by dry air fall.
- The majority of dust is deposited during perennial winter periods by storm events.
- Soil formation occurs on a previously deposited loess base.
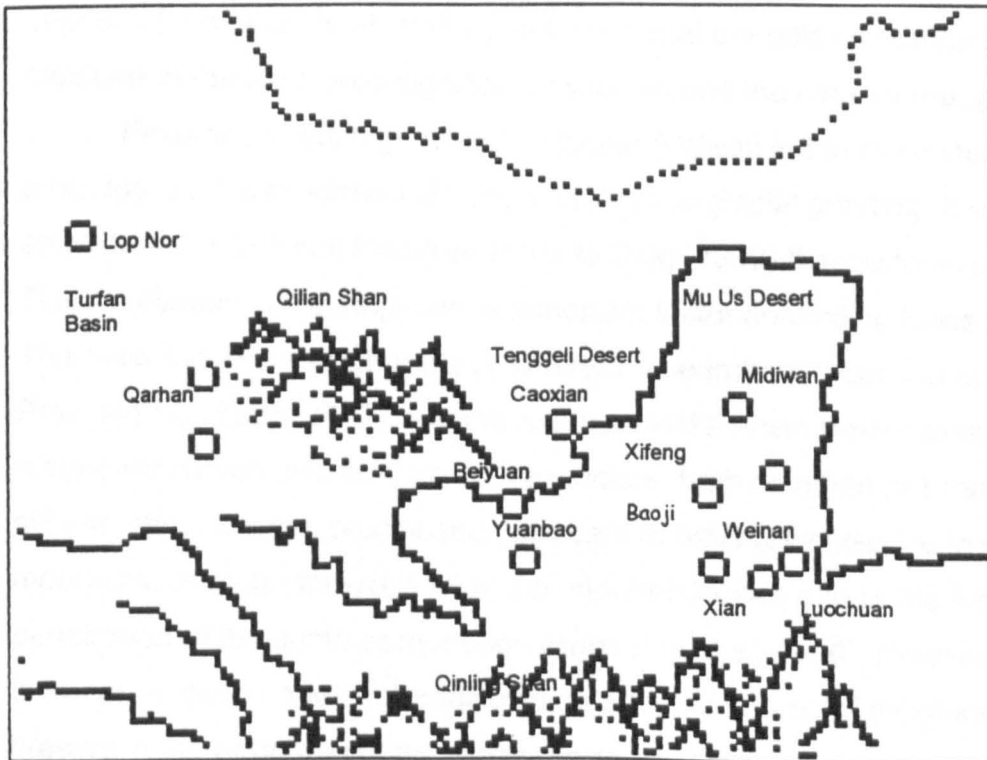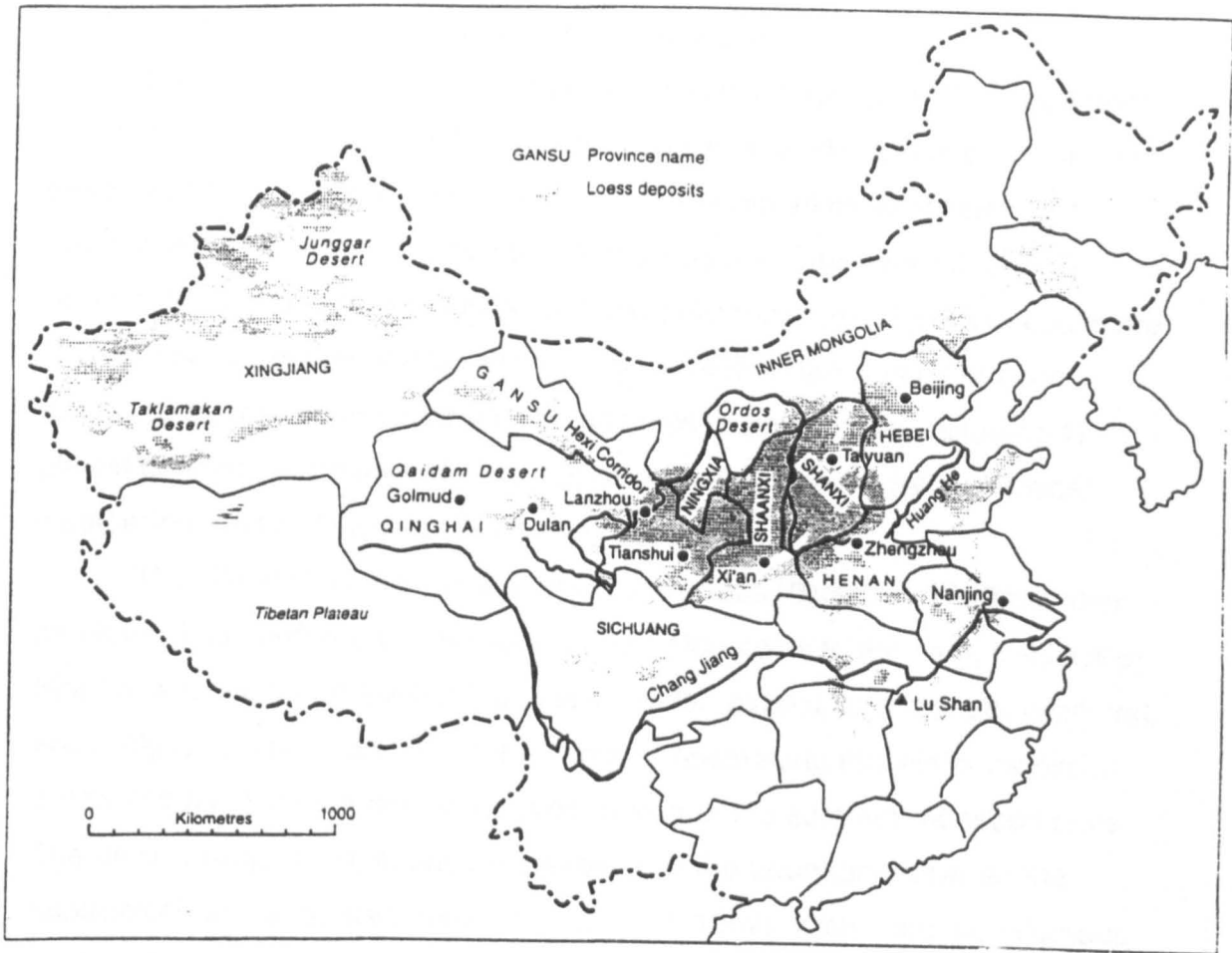
Figure 2.3 Map of potential source areas and depositional sites.

2.3.2. Silt Production and the Source of Proto-Loess.

Western literature directly concerned with the source of Chinese Loess and its relationship with the depositional area is surprisingly scarce, although there has been a significant increase in the two last years as western researchers realise its importance and implications. Charlesworth (1957) described loess as "the most important periglacial deposit". Loess deposits are largely associated with the Quaternary. Several mechanisms have been proposed for the formation of silt size particles or proto-loess, including 1) glacial grinding, 2) frost weathering, 3) aeolian abrasion, 4) salt / chemical weathering, and 5) fluvial abrasion and crushing.

The Western Loess Plateau or Longxi Loess Plateau is 2000m above sea level. It is bordered by the Liupan Shan Mountains to the east, the Qinling Shan to the south and the north eastern Tibetan plateau to the south-west and south (fig 2.3). These are important barriers, obstructing the winter monsoon winds and blocking the northward progression of the summer monsoon rains. The west Qinling Shan, at 3000m elevation, is the boundary between the subtropical and temperate zones (Porter et al, 1992). Within the mountainous north eastern Tibetan Plateau soil development in basins is evident in loess-like deposits (Lehmkuhl et al, 1998b) indicating that periodic increases in soil moisture in the past were significant even beyond the plateau margins.

Proximity to the high altitude Tibetan Plateau led to the consensus that proto-loess silt was formed almost entirely from glacial grinding. It was well established in Chinese literature (prior to Ding, 1999) that tectonic uplift of the Tibetan plateau is the single most important factor controlling loess formation. This view has been scrutinised by western researchers (Harrison et al, 1992, Prell and Kutzbach, 1992). An intense periglacial environment exists in these mountains, which also contain active glaciers; both common pre-requisites for silt formation. Limited precipitation appears to have restricted ice to the high mountainous marginal areas after the mid-Pleistocene due to the limited penetration of the summer monsoon winds (Liu et al, 1996). However, the summer monsoon does not appear to be the only source of moisture. At present in the northeast of the Tibetan plateau, mountain ranges receive up to 800 mm a^{-1} at the snowline (~5000m). The influence of the Indian monsoon in

44

the northern and north western parts of the Tibetan plateau is largely unquantified.

Data accumulated during investigations of terminal moraine (Lehmkuhl, 1998a, 1998b) and lake level fluctuations indicate that up to four Pleistocene glaciations occurred in the Tibetan Plateau and the adjacent Himalayan Mountains (Zheng and Rutter, 1998). Even during glacial maxima, morainic evidence shows that few extensive glaciers existed and only a small ice cap was present at the source of the Yellow River. There is evidence for a glacial advance between 30 - 23/21 Ka BP and accompanying alluvial and ice contact fan aggradation (Lehmkuhl et al, 1998). Sedimentalogical evidence suggests that the period 21-13 ka was cataglacial, i.e. conditions were unfavourable for glaciers followed by dissection and terracing before 10 ka (Li et al, 1997). According to Derbyshire et al. (1991) sand wedge casts in sediments date from the LGM (18 ka), and the presence of loess horizons above solifluction layers indicate high aridity during the LGM in the source area. The presence of loess layers also indicates a change from debris transport and deposition to aeolian deposition (Lehmkuhl et al, 1998). The largest continental ice fields at present (1978 NASA Landsat 30135-04492) are located in the Kunlun Shan, 9973 km^2, and Tian Shan, 9196 km^2 (fig 2.4). Here precipitation is in the region of 300 - 1000mm annually and mean temperatures at the snowline are between -6 and -15°C. Since the beginning of the Holocene permafrost conditions have dominated in most of this area.

Chen et al (1999a) discussed loess-like deposits within these mountain regions and concluded that these were 'cold' loess deposits derived directly from the Tibetan plateau. At Hezuo on the north-eastern margin of the plateau, a loess palaeosol sequence of a few tens of metres has formed since the last interglacial. Planation surfaces show the remains of tropical and subtropical deep weathered soils, intercalated with periglacial soils. This shows that precipitation had reached significant levels in the last 75 ky. Whether this reflects northward penetration of the summer monsoon winds is not stated.

Chen et al (1999b) state that 'hot' loess is derived principally from the Asian interior, especially the Gobi Desert. Researchers concluded that glacially ground silt was not a direct source of loess (Derbyshire, 1983). It is likely that Chen's 'hot' loess is partly contributed to by glacially ground 'cold' loess.

The Neotectonic movement at the margins of the Tibetan plateau has formed complex fault systems and many subsiding basins. These semiarid basins may also be a source for the proto-loess. The basin rim sediments contain extensive alluvial fans formed by perennial streams and rivers that rise in the mountain ranges. The altitude, weathering regime and gradient dictates the amount of sediment supplied to the intermontane basins. Their sedimentology shows that when sedimentary environments were dominated by perennial streams, fans experienced humid conditions. During periods of increasing aridity, coarse fanglomerates were deposited by ephemeral

Figure 2.4 Landsat image (ST040-609-024) of the Kunlun fault and associated drainage patterns, rivers and lakes and snow cover.

streams and active-layer structures were produced by permafrost within the alluvial fan sediments. The alluvial fans have been deformed, faulted by small thrust faults that propagate from the mountain fronts. Localised uplift rates are in the order of 0.1 to 1 m Ky^{-1} (Owen et al, 1997) allowing a potentially significant rate of denudation. During periods of increased sediment yield to mountain valleys during the late Pleistocene large alluvial fans formed upon which loess-like deposits have formed. Alluvial deposition and dissection terracing followed by pedogenesis are assumed to occur sequentially during the change from glacial to interglacial environment and that loess like material is deposited during extreme cold events (Lehmkuhl, 1998b). Most alluvial fans in north western China are aggrading at present, characterised by sheet flooding and lateral channel migration. Since new material is regularly supplied, boulder cover does not form and the silt can be readily deflated (Derbyshire et al, 1998).

Kuenen (1960) conducted experiments and found that silt sized material was not formed during abrasion by saltating grains. Later desert sources were proposed as a major supplier of silt sized particles (Liu, 1974). This view has since been much debated. Aeolian abrasion because of grain - grain collision during saltation may break solid particles and crusts and disaggregate pedogenic material (Smith and Whalley, 1982; 1987; Pye, 1983; 1989). Whalley et al, (1982) proposed that impacting sand grains were a mechanism of silt size particle formation. Wright (1995) also showed in laboratory experiments that abrasion of sand sized quartz could produce notable quantities of silt material relatively rapidly. However, in an early paper by Liu (1985), it was proposed that sand dune deposits and loess were a manifestation of proximal and distal sorting of material from alluvial fans and mountain piedmonts. This mechanism accounts for the very limited silt content in desert sand dune environments. This does not negate the possibility of silt production by other weathering processes in desert basins under suitable hydrological conditions.

The Taklimakan Desert within the Tarim basin is one of the largest internal drainage basins in the world. Landsat images reveal complex palaeodrainage and channel systems of the Tarim River (rising in the Kunlun Shan). The old channels are now covered by drifting sediment. In 1905, 35

47

brackish lakes were mapped in the area, but Landsat imagery shows that very few remain 80 years later. Although this is probably an anthropogenic effect, it hints at the speed of change in such environments.

Fluvial erosion in the Taklimakan, Turfan, and Junggar deserts has exposed Mesozoic and Cenozoic sandstone, siltstone and mudstones which can be considered silt sources. The Taklimakan and Junggar deserts have been described as deflation zones composed of 'black Gobi' or unsorted loose angular quartzite gravels. Temperatures in the basin can reach a maximum of 47°C with severe winters. Although rainfall is limited, there are several artesian springs. Sediment in foreland and intermontane basins has been reworked and undergone a degree of pedogenesis.
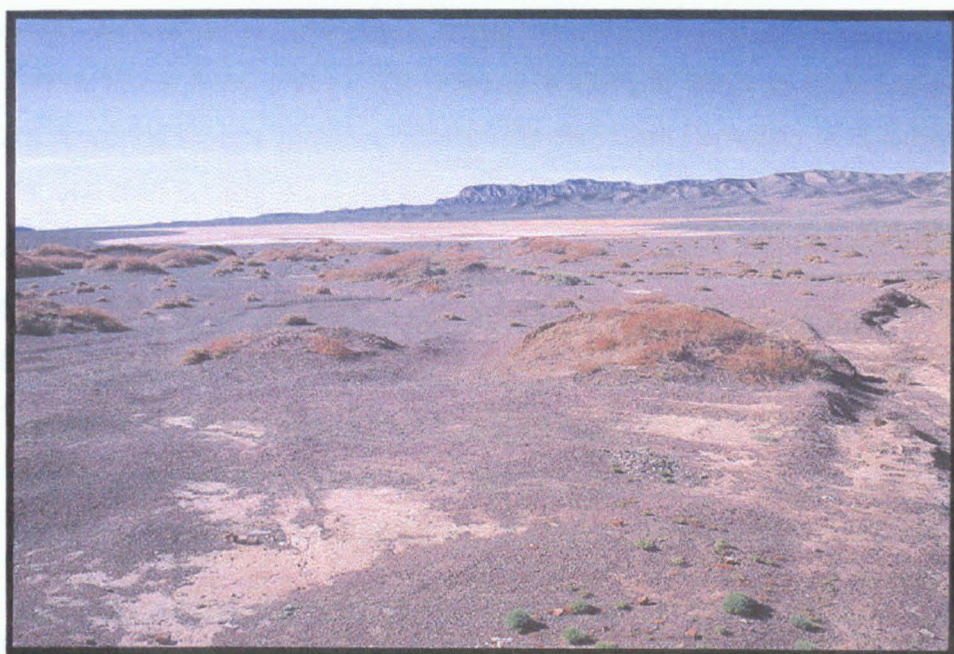
Fig 2.5 the Turfan basin indicating the hydrological conditions and type of vegetation. (Photo courtesy of Fletcher and Baylis, http://www.science.ubc.ca)

Particle size and micromorphological analysis showed these sediments were not true loess but loessic colluvium, perhaps a precursor to true loess. Although active dunes contain little silt, recent investigations have observed that sand dunes stabilised by vegetation and irrigated by man have an increased amount of silt (Derbyshire, 1998), although no mention of the date of stabilisation is mentioned, the implication is of relatively recent stabilisation.

This may reflect reduced winnowing of stabilised dunes or trapping dust by vegetation, rather than rapid silt production in stabilised dunes due to pedogenesis.

Large-scale sheet wash, karst outflow and slope collapse deposits may be reworked by wind or water and subsequently provide a further secondary dust source. The Yellow River is one of the most turbulent and flashy on Earth. Fluvial abrasion and crushing of larger particles may occur. The contribution of fluvially derived loess to the Chinese loess Plateau is not widely discussed. Smalley and Smalley (1983) discussed research into New Zealand loess that showed that high-energy rivers associated with deformable rocks could produce silt sized material. However, New Zealand loess is associated with volcanics, especially soft pyroclastic, materiel in alpine terrain, although high-energy river abrasion may provide a fining mechanism. Considering the extent of the Yellow River flood plain in the past, it is likely to have been a significant source of reworked loess made available for deflation (Smalley and Smalley, 1983). Fluvial and fluvioglacial transport is a particularly efficient sorting mechanism. Removal of the finest fraction leaves a non-cohesive deposit that is more easily entrained (Pye, 1995). Neotectonic movement and climate change has resulted in down cutting by the rivers and exposure of the Cenozoic rocks. These exposures provide stable areas for loess deposition and possibly an additional source.

Chinese researchers consider the Tarim a closed basin at present and therefore a minor dust source. Modern dust storms have been observed emanating from the basin. Large fan terraces and playas are formed and the nature of the local wind regime appears to deflate and transport a significant percentage of the silt material to higher elevations. Billard (1999) suggests that the basin may have been a significant source in the past due to enhancement of the north-easterly branch of the winter monsoon winds (division of the winter airflow by the Qilian Shan). The eastern end of the Tarim joins the Hexi corridor, so that environmental changes may have resulted in massive quantities of silt in the basin being made available for transport along the corridor.

Many basins contain evidence of large interconnecting paleolacustrine/playa lake deposits. The Qaidam Basin sediments record the

temporal evolution of saline lake to saline-lake-margin subenvironmental stages (dilute lake, saline lake, saline pan, and desiccated pan) fig 2.6.

Figure 2.6. Topography in and surrounding the Qaidam Basin. (Photo courtesy of Fletcher and Baylis, http://www.science.ubc.ca)

At present aeolian abrasion and salt weathering dominate the Qaidam Basin and the piedmont of the Kunlun Mountains. A study by Goudie et al (1979) showed silt production by salt weathering in deserts was feasible. Recent sediments from the Qarhan Salt Plain consist of mud-halite couplets, which represent one shallowing- and concentrating-upwards succession. This succession records the flooding and desiccation of a 200 km² lake, with water depths of 2.2 - 3.0 m (Schubel and Lowenstein, 1997). Silt grains, of late Pleistocene age, have been found within halite layers of the Qarhan Playa (Kezao and Bowler, 1986). These authors believe that the silt was generated by glacial and periglacial processes at high latitudes and subsequently transported to the outwash plain rather than being produced within the basin. Lop Nor in the Tarim basin is perhaps the most studied lake (Zhao and Xia, 1984). Salt crust and saline soil occupy more than 35% of the Lop Nor environment.

Heavy mineral analysis of the Taklimakan desert determined the dominant source to be from the weathering of bedrock of the surrounding mountains (Zhu, 1984). REE analysis of loess from the central loess plateau found that no distinction could be made between loess and palaeosol horizons and concluded that the source was uniform throughout glacial interglacial cycles (Gallet et al, 1996). Previous research had shown that the chemical compositions of regolith over northern China could not be differentiated (Wen, 1989). Therefore, it was considered unlikely that source areas could be distinguished on the basis of bulk elemental analysis. However, the REE results of Clarke (1995) determined a Kunlun Mountain silt source for loess in the NW of the plateau, confirming that wind from the west northwest carried dust up towards Lanzhou basin. Crucially the LREE of the samples from the Tibetan front compares favourably with those of loess from the central plateau. This was one of the first reports defining links between particular sources and depositional area. Complementary research of Zhang (1994) at the Luochuan section concluded that the coarse fraction at Luochuan might be from a different source from the fine fraction. At present two regions with high dust fluxes have been identified, the "Western High-Dust Desert" and the "Northern High-Dust Desert," with Taklimakan Desert and Badain Juran Desert as their respective centres. The Mu Us desert bounds the loess plateau directly and it has been proposed that the desert has expanded into the loess region in the past (Ding et al, 1999). Sand beds (0.5 – 3.2 m light yellow sand) intercalated with loess in the marginal deposits contained less than 10% fine silt, the dominant fraction being 10-50µm. The profile is indicative of desert expansion and contraction with climate (Ding et al, 1999) (fig 2.7). This would appear to be a major contributory factor in the extensive thickness deposited at the loess plateau margin during the last glacial cycle, as compared to other loess deposits.

Smalley (1995) states that there are no mechanisms capable of producing large quantities of silt within lowland desert basins: a combination of high relief, aqueous transport/sorting and semiarid desert processes are required. The loess plateau is ideally situated to receive material from many potential sources.
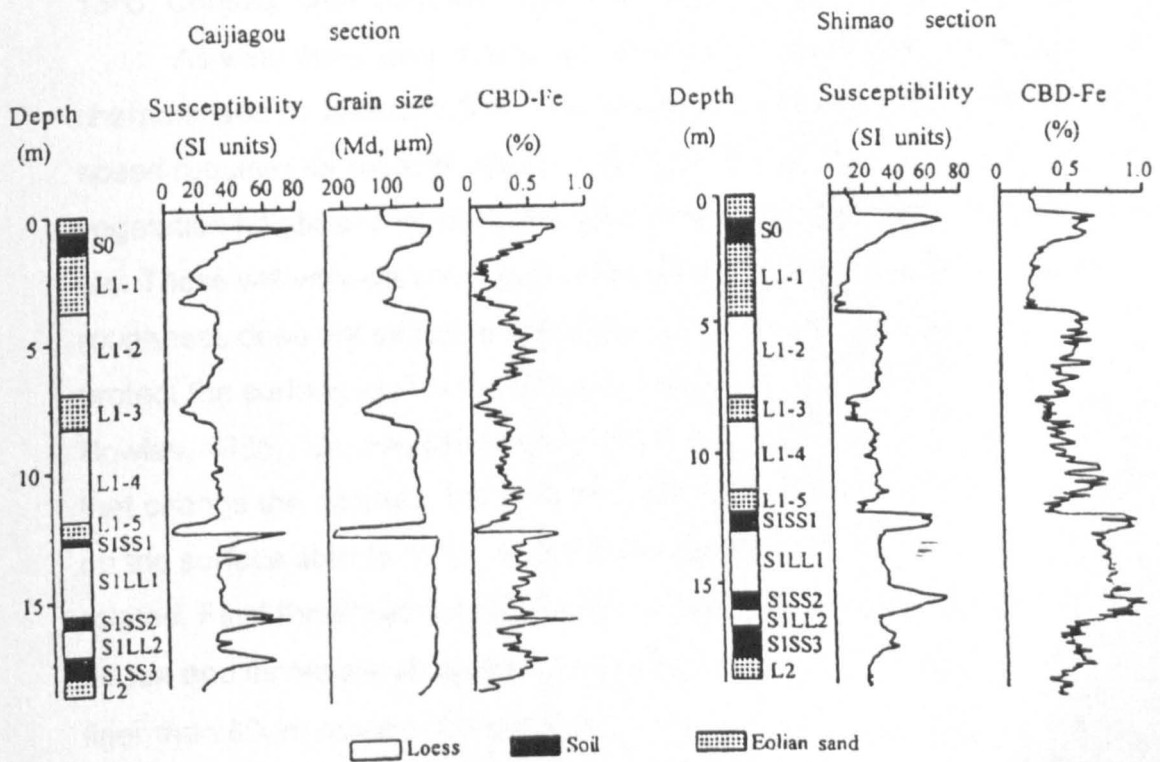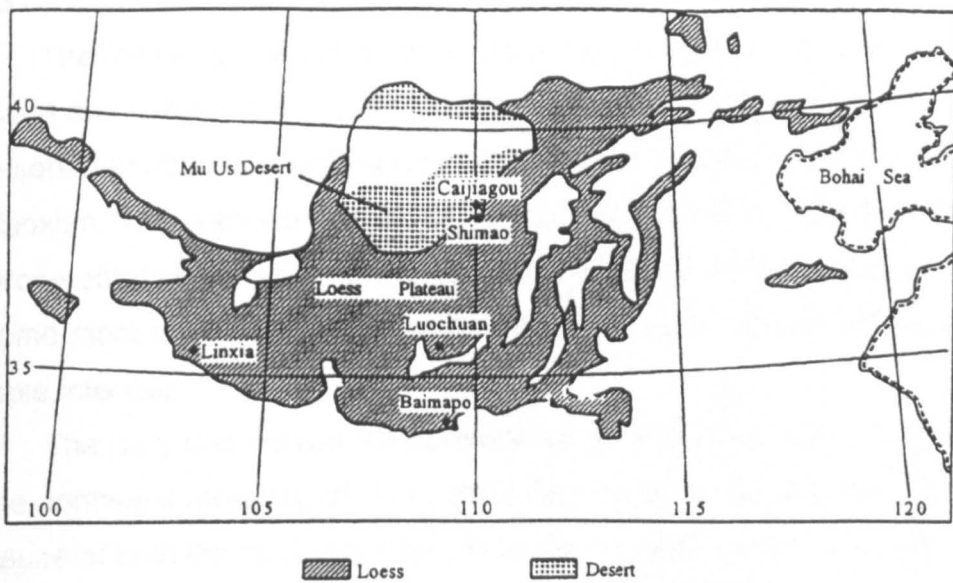
Figure 2.7a Map of Mu Us desert showing the location of Caijiagou and Shimao on the eastern margin. Figure 2.7b shows the stratigraphic profiles of the two sites, with sand layers indicating desert expansion. (After Feng et al, 1998).

2.3.3. Factors affecting Deflation Processes in Source Areas

The following discussion of deflation and associated factors is deemed relevant due to the proximity of Caoxian to the Hexi corridor, and hence the high sedimentation rate and high resolution potential of the particle size record at Caoxian. The author believes the relevance of climate induced changes to environmental processes in the source area and along the transport route become more critical when analysing a thick depositional profile at small sample intervals.

The daily and annual temperature range increases from the south east to the northwest more rapidly than other regions of similar latitude. This is because of both the rapid decrease in winter temperatures northward and the increased continentality. The autumn sees the largest diurnal temperature range, as high as 18°C in the Tarim and the longest duration of sunshine in the Qaidam basin and northern Gansu. The annual mean range at Lanzhou is 13°C. Consequently both the air and the soil are drier in the northwest.

As wind flows over a natural surface it is slowed by surface friction and characterised by turbulent flow. The roughness of the surface dictates the wind speed required for particle deflation (fig 2.8). Roughness elements include the vegetation height and density, diameter of the particles on the bed, potholes etc. These will vary with changes in the climate (fig 2.9). Surficial element roughness does not increase indefinitely. At a critical density, the elements protect the surface and the likelihood of entrainment is reduced (Mclaren and Bowles, 1985). Continued selective entrainment of grains can form bed defects that change the deflating PSD (Best, 1992). At the fluid threshold, the particles on the surface start to move. Fluid threshold velocity and particle diameters are related. Fluid threshold velocity attains a minimum value at diameters around 80 μm and increases as diameter increases. Surfaces covered by particles finer than 80μm require a greater drag to set grains in motion (Pye, 1987) (fig 2.10). The upturn in the relationship at 80um may be due to Reynolds number effects or interparticle cohesion caused by moisture, van der Waals forces, etc. So in fact, depending on the particle size distribution, roughness and the wind velocity, those particles picked up first are not necessarily the finest.
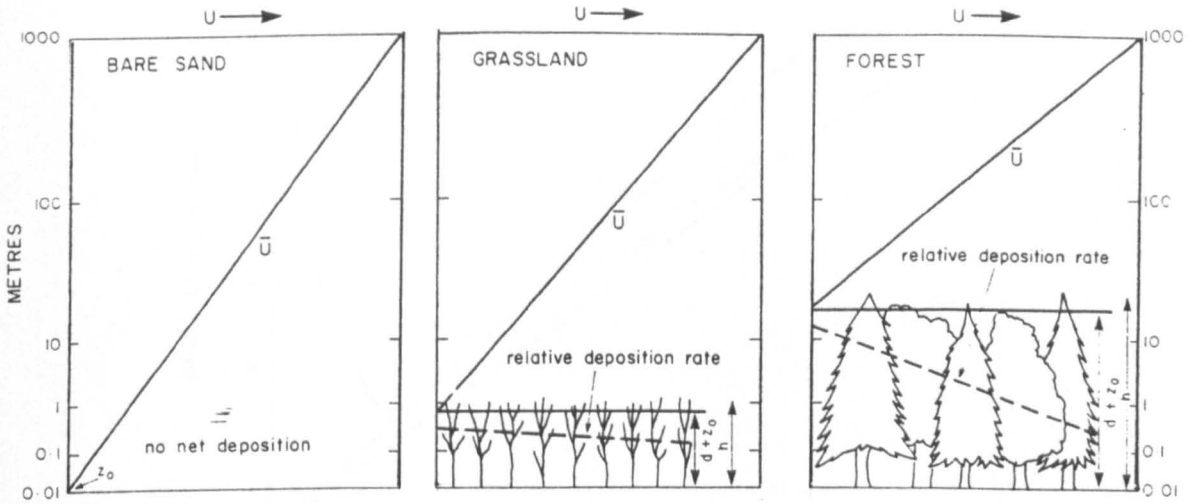
Figure 2.8 Schematic diagram showing the effect of changes in surface roughness on the wind velocity profile and the height of effective zero velocity (Z_o) and associated decrease in deposition rate. (After Tsoar and Pye 1987)
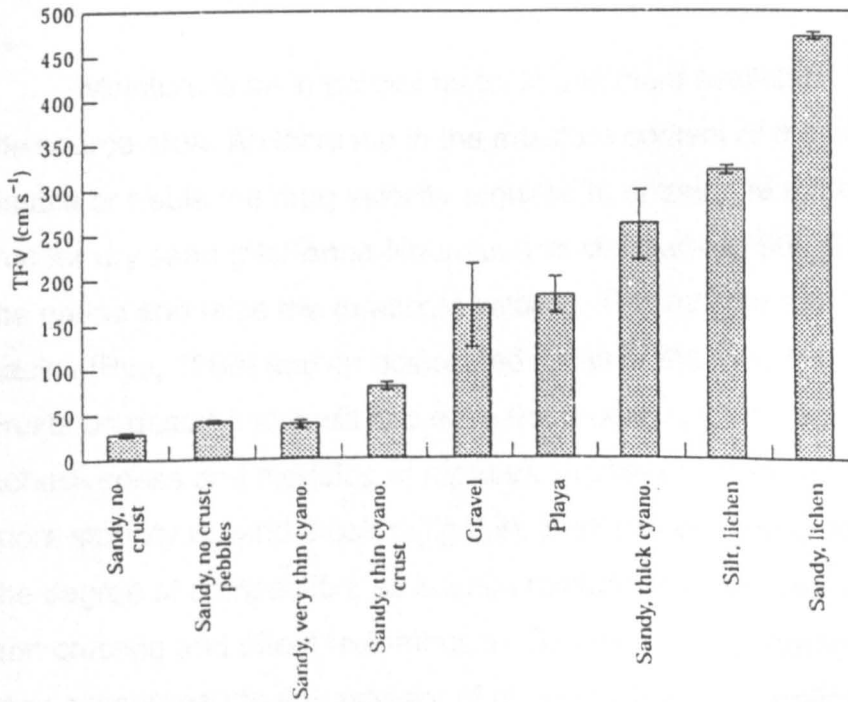
Figure 2.9 Comparison of threshold frictional velocities for a variety of surfaces, sites in USA (After McKenna Neuman and Maljaars 1998)
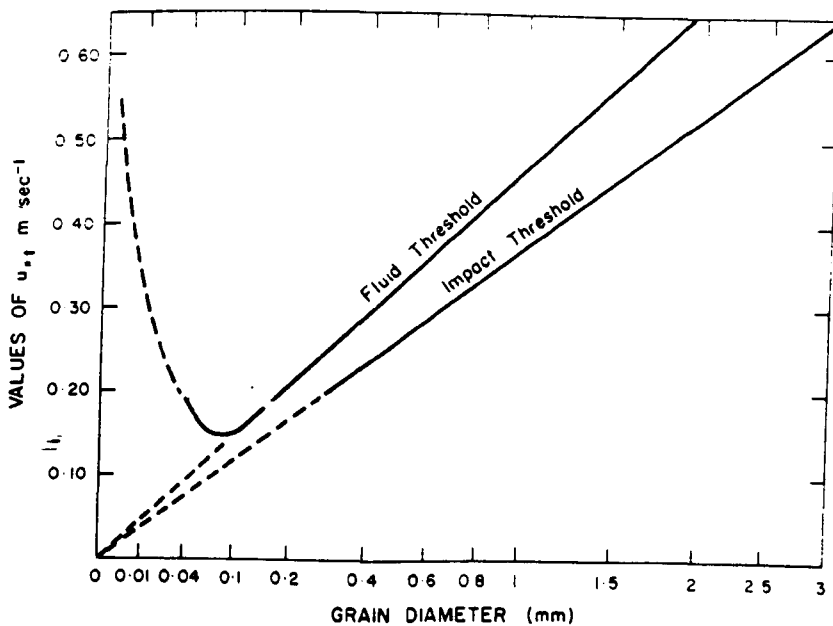
Figure 2.10 Relationship of fluid/ frictional threshold velocity (u_t) and impact threshold velocity (u_-) to median particle diameter as determined by Bagnold (1941). Values for particles < 60μm are approximate. (After Pye, 1987). Note the up turn in u_t for particles finer than 80 μm i.e. for loess ease of deflation decreases with increasing u_t.

Moisture is an important factor in sediment availability i.e. precipitation in the source area. An increase in the moisture content of the soil, at source, can double or treble the drag velocity required to entrain the material compared to that for dry sand (McKenna-Neuman and Malijaars, 1998). Salt can also bind the grains and raise the threshold velocity. This may be significant in desert basins (Pye, 1980) and on desiccated areas of the river flood plain. Clay rich crusts on desert floors will decrease the erodibility of the surface (increase in cohesiveness and modulus of rupture). Pebble covered surfaces (Gobi) exhibit more stability to wind erosion (fig 2.9). Surface deflation is also influenced by the degree of compaction, so intense rainfall may increase surface compaction and crusting and effect redistribution. Saltating grains during local redistribution may encourage the entrainment of others by bouncing grains into the air stream, and breaking up crusts and aggregates. Studies of the Mu Us desert showed that 4.5m/s was a general threshold velocity for sand transport. Such wind speeds occurred 85-370 times a year, (meteorological records), nearly all

55

sand movement took place in spring (Ding et al, 1998). The amount of silt available varies according to surface character. Little research into the relationship between changes in surface character velocity and silt deflation has been done. Such research would improve an understanding of the relationship between particle size and velocity.

2.3.4. Factors affecting suspension of dust particles

The velocity and turbulence of the air mass will dictate the size of entrained grains and their fall velocity. If the vertical component of the velocity exceeds the settling velocity then particles will remain in suspension. The settling velocity depends on the particle characteristics (mass, shape). The settling velocity of spherical quartz grains (1-50μm) can be calculated using Stokes' law. The majority of loess grains has previously been shown to be blade shaped (8:5:2 axial ratio, Rogers et al, 1994) or to travel as aggregates (Derbyshire et al 1998). A small but significant proportion of fines (<9μm) in African plain dust was transported as aggregates of diameter 15-45μm (McTainsh et al, 1997). Derbyshire et al (1998) states that a negligible amount of Asian dust less than 5μm travels as single particles. The greater surface area and lower density of aggregates means that they travel further than an equivalent sized solid particle. Modified Stokes' law calculations would be complex. Derbyshire's investigations of modern dust revealed a higher proportion of aggregates in distal dust. Although this may have implications for the interpretation of particle size distribution results the simple assumption that the volume of fines increases with distance still holds, although PSD can not then be directly related to particle size. The fine skew and unusually poorly sorted nature of analysed loess is undoubtedly related to disaggregation after deposition and during preparation (see page 78).

April mean wind speed in the northwest is 3 – 6 m/s prolonged winds reach in excess of 17m/s and gusts up to 40 m/s during gales (10-15 days per month in spring, maximum in May). Speeds decrease to 2-3 m/s in the summer. Local wind patterns are affected by diurnal and seasonal variations and topography. Wind speeds reach a maximum in the late afternoon, as the air masses become unstable due to heating of the land surface. Local winds

such as mountain, valley, lake and glacier breezes are affected by diurnal heating variations which can cause inversion of wind directions during a 24 hr period. Mountain breeze tends to dominate over valley breeze on a seasonal basis, and is more intense during the winter due to snow cover or frozen ground (Zhang and Lin, 1992). The mean speed of these local winds is not insignificant, reaching 4m/s (u* not quoted) (Zhang and Lin, 1992). Any large-scale circulation patterns will override them, so they tend to dominate during the stable winter monsoon period and become negligible during migration of pressure systems in spring and autumn. Funnel topography can concentrate flows and raise wind intensity. The degree of erosion and reworking will vary locally.

A degree of vertical mixing is required to carry particles of a particular size to a particular height within the boundary layer. There is an approximately exponential decrease of diameter with height above the surface. Field tests and laboratory based wind tunnel investigations of the vertical distribution of particle size parameters during storms in the Taklimakan desert yielded results directly related to loess source areas. Surface deposits in the desert basin consist of well sorted dune material, 80% fine and very fine sand (Chen. W, 1993) and multimodal less well sorted material at the rim and interdune areas. The vertical distribution of particle size above the surface was found to affect the dispersion distance, fig 2.11 (Chen and Fryear, 1996). The height above the surface of any particle size fraction was related to wind velocity. In wind speeds greater than 10m/s, particles up to 0.09 mm were carried to a height of 4 cm in the creep/saltation zone. In the saltation layer, particle size was found to decrease as a power function of height. In the higher layers particle size decreased logarithmically with height. Wind tunnel experiments also showed that particle size parameters change irregularly at heights of 14 cm above the surface. The total percentage of silt sized particles increases at 2m above the surface as the mean velocity, U increases, on though theory states particles finer than 80μm are increasingly difficult to deflate.

If the associated air mass remains in equilibrium it does not tend to sink or rise. Air masses that are warmer than the surroundings will rise,
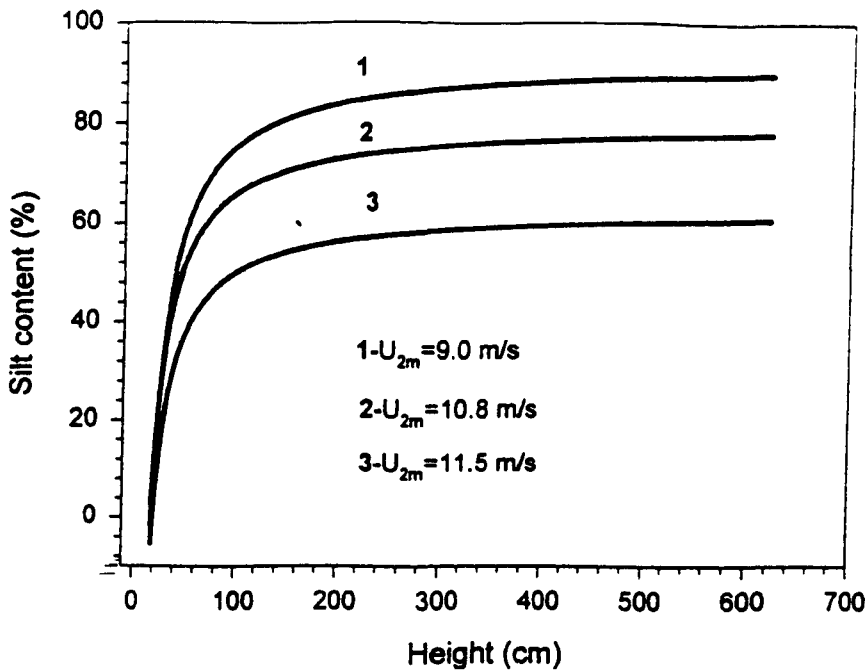
Figure 2.11. Vertical distribution trends of silt content for wind speeds of 9, 10.8, and 11.5, m/s at 2m above the surface. Maximum variability between 0 and 0.8m above the surface of the Taklimakan desert. (after Chen and Fryrear 1996)
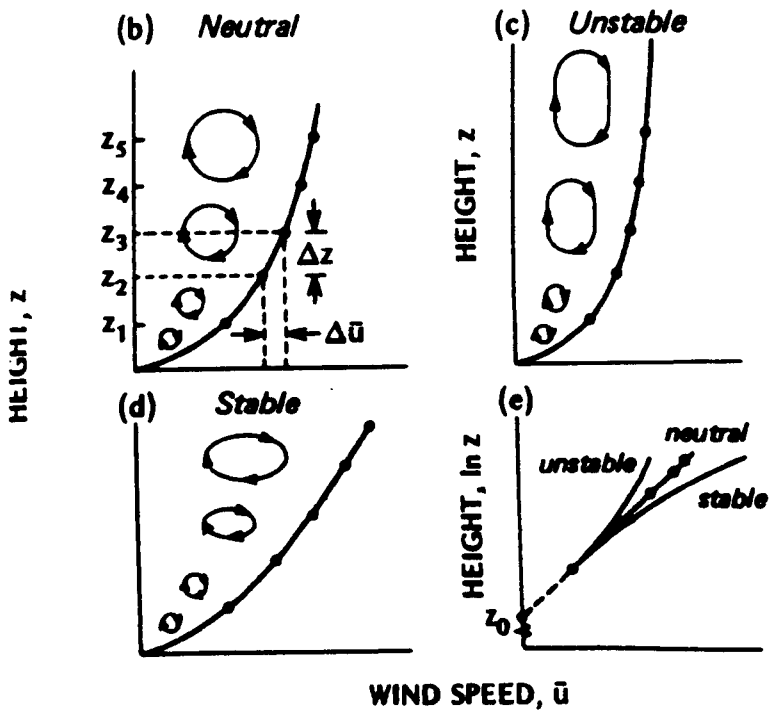
Fig 2.12. Schematic diagram of stable neutral and unstable states.(after Pye 1989)

and vice versa if it is cooler. These are known as unstable and stable states respectively, fig 2.12, (Pye, 1989). Moisture in the atmosphere will result in unstable conditions, moist air being less dense. In unstable states convection is important and can raise the dust higher than turbulence alone (A. P. Morse pers com). Conversely, in stable state the dust may become trapped at a lower level. Turbulence is greatest in the lower part of the boundary layer. Cloudiness is not as low as might be expected in the NW, at approximately 5/10, slightly higher in spring and summer and lower in winter, but low level cloud is rare (Zhang and Lin, 1992)

A mean upward velocity greater than 4cm/s will keep particles of 25μm suspended up to several hundred metres. If the particles are to undergo long range transport they need to be lifted through the mixed layer (day time convection only) and past the low updraft velocity zone at the base of the high level cloud layer (Rea, 1994). Within clouds (cumulus clouds) high updraft values occur (Oke, 1987). It is likely that particles greater than 25μm can reach the higher levels of the cloud layer. Coarser particles will either require very severe storm turbulence and updrafts or travel by modified saltation. Winter monsoon conditions are characterised by stable cool air masses. Regional deposition over land (loess plateau) and long distance deposition at sea (NW Pacific) are due to differing transport mechanisms (Pye, 1987; Pye and Zhou, 1989; Zhang et al, 1996). Moderate north westerly winds can raise the dust to a height of 1.5 km, deposition being local and directly downstream. Stronger baroclinic conditions and a dry front can give rise to pronounced vertical air motion, raising dust to heights of more than 3 km. The importance of an upper level jet in long range transport has been identified (Liu, T. 1981; Hovan et al, 1989; Hovan and Rea, 1991). A predominant long distance transport path was shown to be easterly over the north Pacific (Merrill, 1994). Seasonal peaks in dust over the north Pacific is closely related to frequency of dust storm events in Asia.

In the 1980 dust storm, dust was initially entrained by warm winds blowing ahead of a cold front. Rising air in front of the depression caused downward movement of energy from the westerly jets. This resulted in increased speed and turbulence of the surface winds. Vertical air motion

59

caused dust to be incorporated in the jet stream and then rapidly transported eastwards. The speed of the jet stream was 144-180 km/hr, and dust haze reached the northern China plain, 1500km from source in 10 hrs. The flow over east-central China resulted in a dust haze for the following two days observed as far afield as Korea and Japan. Liu et al (1992) reported that 90% of the dust storm deposit was material coarser than 30μm, at a distance 3000 km from source. Dust storm data (Liu et al, 1981) collected during 17-21 April storm in 1980 revealed a sedimentation rate of 0.01mm/day in Beijing. Particles were carried by near surface winds.

The dust storm of May 5th 1993 was caused by the south easterly movement of a southwest - northeast aligned cold front. Water vapour near the desert surface increased before the storm broke causing mesoscale convective conditions. The moisture increase was attributed to local circulation between the mountainous areas and the desert (Takemi, 1997). Initial wind speeds were of the order of 12 –17 m/s. Retardation and constriction of pressure systems by the east west orientated Tian Shan caused increased wind speed. Wind speeds reached 30-34 m/s channelled along the Hexi corridor. At the mouth of the corridor the flow split into two branches, one to the north and one to the south spreading out over the loess plateau. Over 70 000km^2 was affected by the storm. In Beiying, the storm mass appeared to be 300 meters high and contained three layers, a low dark layer, mid red layer and upper yellow layer. Visibility was less than 10 metres and temperatures fell to –6.6°C (Derbyshire et al., 1998). Figure 2.13 shows satellite images of the 16th of April 1998 dust storm progressing eastwards across the Pacific reaching the western coast of the USA on the 24th of April. Asian dust was held at high levels in suspension for a prolonged period of time in the jet stream. In summary, this section shows that dusts storms are associated with unstable climatic conditions i.e. a shift from predominant winter to summer monsoon in spring. Violent and long lived storms associated with cold fronts usually result in a degree of precipitation. Dust deflated by these storms are carried by two distinct mechanisms; local and regional transport by saltation and low level suspension and high level distal transport by the jet stream.
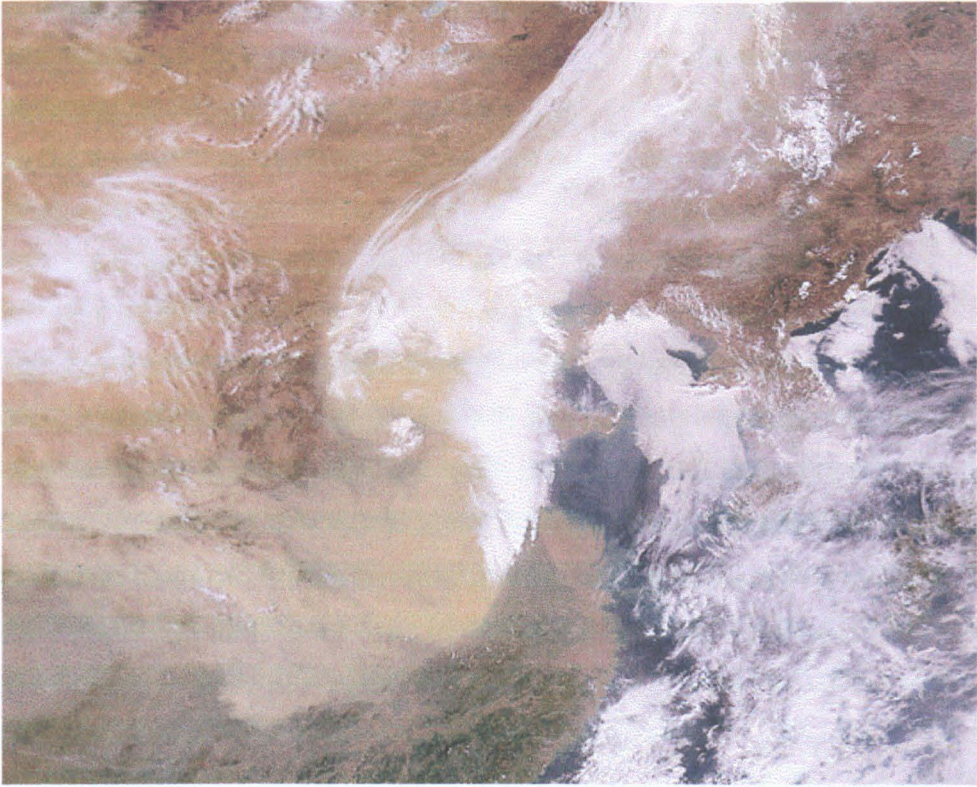
Figure 2.13 Satellite image of the April 16 1998 dust storm as it crosses the Pacific Ocean reaching the states April 25.
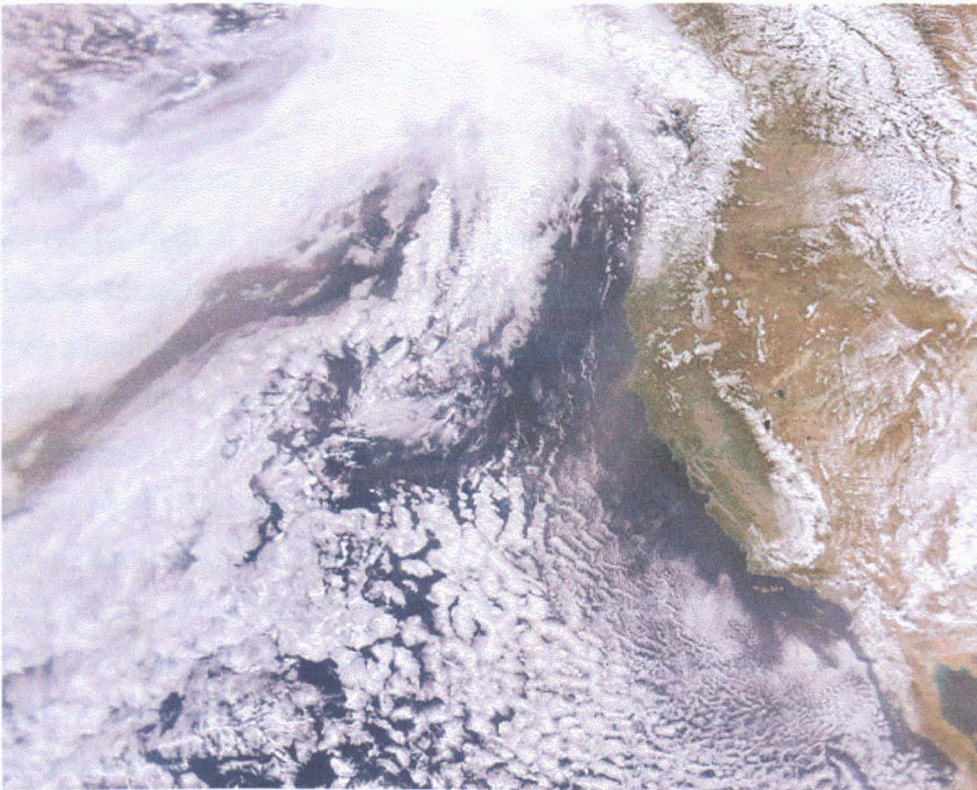
2.3.5. Dust Flux and Accumulation Rate

Observation of the storm of May 5[th]1993 revealed that close to sources of sand and silt the particle content of the air was 1016mg/m^3, containing 90% sand content moving by creep saltation and suspension up to 30m. These data indicate an underestimation of Chen and Fryears (1996) field and wind tunnel experiments. The suspension load coarse silt of the 1993 May 5th storm reached at least as far as the Qinling Shan (south of Xian). It is important to note that observations made during the on going ACE-ASIA programme (http://saga.pmel.noaa.gov/aceasia/index.html), particles much larger than those expected from modelling experiments reached as far as Hawaii.

Modelling simulations of dust in response to wind intensity and the hydrological cycle have been carried out by Joussaume (1990), Joussaume and Jouzel 1993, Genthon, (1992), Anderson et al (1998), and Yung et al (1996). The expansion of the source area was not considered in these models and failed to duplicate the measured dust flux at the poles during the LGM ice core records. Increasing the available dust by decreasing soil moisture and hence vegetation cover improved the model but still did not recreate the dust concentrations preserved in the polar ice cores. Recent models by MAGIC (Mineral Aerosols and Glacial Interglacial Cycles) show that changes in source area characteristics due to a reduction in vegetation (lowered CO_2 fewer C_3 plants) and an increase in the exposed source area is important in the simulation of LGM dust fluxes (Mahowald et al, 1999).

Loess deposits of the last glacial in Europe exhibit 2-5 cm thick bands of sandy loess laminae that fine upward. It was concluded that this indicated an uneven sedimentation rate (Kukla and Cilek, 1996). It also points to decreasing energy of the wind that carries the dust during an individual storm or over the medium term. Such resolution of grain size records has not yet been possible in China. It should be borne in mind that finer particles take relatively more energy to deflate. Due to their small size and relatively large attractive forces they require a larger TFV to detach them from a surface. It may be expected that during a sustained period of erosion the source will become better sorted until a point where grains susceptible to deflation have been removed. The author envisages that this period will be seasonal unless a reduction in

seasonality occurs where either silt production or transportation is limited. Then replenishment or a change in the environment (drying, reduction in vegetation etc.) will be required before significant deflation can resume. Zhang et al (1999) state that on a regional-scale the effects of dust storms appear to cause fluctuations in dust fluxes that are more pronounced during glacial than interglacial conditions. This conclusion is based on the observed similarities between the PSD of the dust collected during dust storm conditions and particle size distributions in glacial age loess. The comparison was made between glacial dust from Luochuan and modern day dust storm dust PSD collected from a desert source, this author believes that they are not comparable (see PSD evidence in chapters 5 and 6).

Another consideration is that dust flux in air ($gm^{-2}ky^{-1}$) is not necessarily equivalent to accumulation rate (cm/yr). If a coarse PSD dominates in the source area, a more open particle packing structure will result at the depositional site, and a finer PSD will settle into a denser, thinner deposit. An equivalent flux of mineral aerosols can be produced by different wind speeds and available source PSD.

It has been suggested that 'typical dust storm' weather is restricted to north of the Qinling Shan and floating dust weather occurs to the south (Ding et al, 1994). Modern estimates of daily dry deposition flux are found to be higher during dust storm events but, in most cases, the monthly averaged flux was found to be attributable to non dust storm dust i.e. floating dust (Zhang et al, 1998). Mass spectrometry results of elemental concentrations (Al, Fe, Mg, Sc) in modern dust, collected during storm and "non-storm" events, has shown significant differences between storm and non-storm aerosols. In addition, the signature of a particular source was traceable between source area and a site over 400 km away (Zhang et al, 1996). Non dust storm dust travels under quite different conditions from dust storm dust and therefore a distinct particle size distribution may be expected (see chapter 6). The simple assumption that particle size is directly proportional to wind speed and therefore a useful proxy for winter monsoon intensity is subject to question since it takes no account of changes in aeolian transport mechanisms and sediment availability.

2.3.6. Depositional Processes on the Chinese Loess Plateau

The mechanism of deposition is largely dictated by atmospheric conditions. Deposition occurs because of a drop in velocity and turbulence, increases in atmospheric moisture (humidity or snow and rainfall) or crossing of a roughness boundary. An increase in humidity will encourage agglomeration of particles and deposition occurs when the increase in weight results in the threshold settling velocity being met. Precipitation will wash the dust particles out of the atmosphere. US loess travels a few 10-100's of m (J. Mason pers comm) by repeated entrainment by saltation until it reaches areas that limit transport by the nature of the topography (steep valleys, deeply entrenched streams, etc.). Coarse, low level mineral aerosols in China follow a similar path. On the loess plateau squally winds cause flurries of dust that are carried 10 - 100's of metres before losing energy at a change in topography (i.e. gullies, hill tops etc.) and dumping the silt. Resuspension is also avoided in the lee of such obstacles. Resuspension is significantly reduced as vegetation cover increases, although the ever present dust layer within cities, and indeed within rooms, showed that there was a good deal of low level suspended fine particles.

In areas of the world where loess accumulated in the Pleistocene under forest conditions the thickness of the deposit decreases rapidly away from the roughness boundary. Under grass steppe conditions by way of contrast, the decrease is much more gradual (Oke, 1987).

Present day dust deposition at a site may be overestimated due to remobilised local material (McTainsh et al, 1997). Formal terms are required to distinguish inputs of material from mid and long distances transported into the area as opposed to locally mobilised dust. African Harmattan winds were investigated in order to distinguish between urban and agricultural local wind induced deflation and larger scale regional plume dust. Local dust inputs were episodic and caused greatly increased dust levels; long distance plume dust fines were persistent (McTainsh et al., 1997). Analysis showed that particle size distributions reflect mixing of these various types. Any bimodality in the suspended sediment is an indication of mixed sources. Although the PSD of loess has been shown to be unimodal, a similar mechanism is proposed for the processes on the loess plateau and has complex implications for the

interpretation of particle size analysis. Two distinct regions of loess thickness maxima are known, one at the mouth of Hexi corridor with mountains and deserts beyond and the other in the northern loess plateau between the loess plateau and the Mongolian deserts and uplands.

2.3.7. Vegetation on the loess plateau

Palynological and carbon isotope analysis has been applied to various sediment types, lakes and marine cores, to construct changes in biozones that are related to climate variation (de Beaulieu and Reille, 1992; Pons et al, 1992; Goslar et al, 1993; Heusser and Morley, 1997). There is the potential to derive cyclicity on orbital scales and higher (Harrison et al 1995; Harrison and Tarasov, 1996). The primary controlling factors on the loess plateau and surrounding deserts have been shown to be precipitation and evapotranspiration, evidence from tree ring width data (Wu and Zhan, 1991), and lake levels (van Campo and Gasse, 1993; van Campo et al, 1996). These processes are primarily controlled by the shifting pressure systems (Miehe, 1996). Vegetation patterns are assumed to change in line with the shifting climate gradient (Sun and Chen 1991). However, pollen records from the loess plateau region have been viewed with some scepticism due to the dominance of the aeolian transport mechanism. Vegetation in the source area is presently composed of grasses and shrubs concentrated between dunes in basins and on plains where ground water is near the surface. Riverine forest vegetation (*Poplar, Tamarix, Elaegnus*) is concentrated on the river deltas and may result in local dust trapping. The desert regions of western and north western China are characterised by vegetation of a xerophytic type: these shrubs include short grasses and small flowering plants which flower quickly following the summer rains, and then disappear again as the dry season sets in. Shrubs are more common on dry slopes and semi-saline flat land while grasses grow in moister places (Thorp, 1936). On the edges of these regions are areas of discontinuous desert sand dunes where vegetation is sparse or entirely lacking, encouraging deflation of any available silt material. In parts of the Ordos and Inner Mongolia where low dunes are common on flat land and the water table is high, *Tamarix* is common. It thrives in moderately sandy saline poorly drained desert regions that include stony land and many small areas of saline and alkaline soils.

These saline/alkaline soil areas occur on flat poorly drained desert and semiarid regions of northern China. Plants that are true halophytes and mere salt tolerant plants such as *Artemisia* are also common (Thorp, 1936).

South of Lanzhou and Xian the vegetation characteristics are modified by humans. The region was once more densely forested than further to the north east (Zhou et al, 1997). Where the soils are thick and rich some evergreen broad leaf trees survive, while on poorer soil pines were common. At present the area is covered in grass and used to feed animals. Most soils have been cultivated and over-grazed and the natural ecology severely disturbed. Historical records going back to the Han dynasty (206 BC) recount periods of sufficient rainfall for good harvest interspersed with periods of crop failure, due to lack of rains (Liu, 1988). However, on the steep slopes where cultivation has not been carried out, modified natural vegetation has taken hold. Man probably planted a mixture of thorny shrubs (Zizyphus) tall and short grasses and trees in inhabited areas. These include *Thuja orientalis*, (pagoda tree) *Sophora japonica*, poplars, pines and occasional cedars. Southerly regions of the loess plateau are scarcely vegetated but were probably covered by mixed deciduous and coniferous forest, oak (*Quercus*) elms (*Ulmus*), chestnuts *Castanea*, maples (*Acer*), *Sophora*; and conifers (*Pinus, Thuja, Juniperus*) (Liu, 1988). The forests do not reproduce themselves quickly under present conditions and have been destroyed due to man's need for fuel and timber. The long dry season makes it difficult for young trees to gain a foothold. Under a tree canopy, moisture would have been conserved, but now rapid run off, a lowered water table, deep gullies, and rapid evaporation means desertification is a problem.

In the past, summer and winter monsoons may have differed in rate and degree of response to the northern insolation variations affecting the vegetation zones. Carbon isotope evidence of variations in the quantities of C^3 and C^4 plant, has been used to construct a record of vegetation variability during stadial and interstadial periods (Frakes and Sun, 1994). Feng et al (1998) showed evidence from pollen that indicated a forest-steppe environment dominated in the northwest during MIS 5. Coniferous forest emerged at the MIS 5 - MIS 4 transition in cold and moist conditions. The Mongolian High became dominant when the northern insolation entered a stadial state (MIS 4). Feng et

al (1998) suggest that the lower latitude oceans were still capable of supplying water vapour to the continental interior, thus maintaining arboreal vegetation. Coniferous forest dominated MIS 4, but thereafter deteriorated to a grass steppe towards the end of the MIS 4, probably because the lower latitude oceans failed to supply water vapour to the interiors as shown in figure 2.14

The following paragraph summarises the results of palynoflora studies by Ma et al, (1998) on the Duantouliang section, 39°40'N, 103°55'E. The section consisteed of palaeolake deposits and is situated in the north western Tengger Desert. Spore and pollen assemblages were used to reconstruct the palaeoenvironment. The major vegetation and climatic environment phases between 42 to 23 (ky BP) could be subdivided. From 42 000 to 38 000 BP, a mixed conifer/deciduous broad-leaved forests developed on mountain and foothill regions where bare gobi-desert is at present. At that time, *Populus* and *Salix* forests and grassland surrounded the lake, and the climate was much warmer and humid than today.

From 38000 to 31 000 BP, the climate was warm and moist and was the most suitable period for the plant growth. The studied area was dominated by temperate and warm-temperate mixed broad-leaf deciduous and needle-leaf forest. Grass meadow developed on the river sides and lake beaches. From 31 000 to 30 000 BP, the needle-leaf forests and cold-temperate *Salix oritrepha* shrubs were flourishing, and the climate at that time was relatively cold. From 30 000 to 28 000 BP, the temperatures began increasing. Lake levels were high and surrounded by meadows and swamps. From 28 000 to 23 000 BP temperate *Cupressaceae* and *Betula* mixed conifer - deciduous forests grew on mountain and foothill regions, while grassland with shrubs (*Salix*) developed on plain areas, lake and river sides. This indicates a warm and moist climate condition that was drier than the earliest period (Ma 1998). Further evidence from Tengri Nor in Tibet indicates high lake levels during MIS 3 between 39-21 ka, and higher rainfall probably induced by the westerlies. Sedimentary evidence from MIS 2, 18-13 ka, showed dessication of the lake and increased aeolian activity. Such dry, cold conditions suggest an intensification of the winter monsoon. From 13 ka onwards there appears to have been an increase in summer monsoon activity.
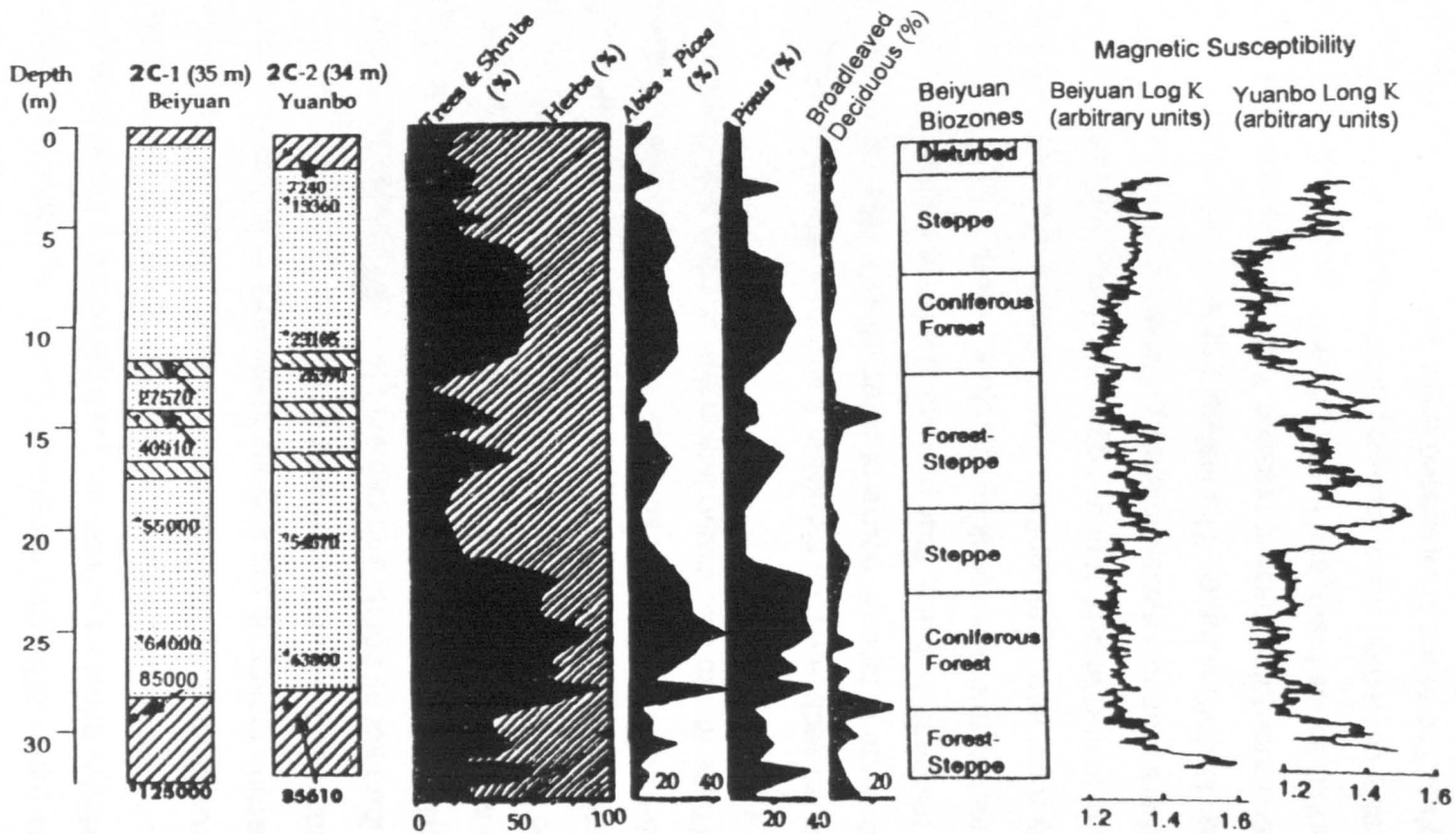
Figure 2.14 Pedostratigraphic Columns of the Beiyuan and Yuanbao sections and their magnetic susceptibility curves, together with the pollen sequence and pollen assemblage biozones of the Beiyuan section. (from Feng et al 1998,)

2.3.8. Characteristics of Pristine Loess

The dominant minerals in Chinese loess are quartz (50 - 80wt%), feldspars (up to 25%) clay minerals (10-20% - see later discussion) and calcite (12%). Heavy minerals (zircon etc.) are generally < 2% and there are small amounts of micas, pyroxenes and hornblende (Kukla, 1970). Three fractions and corresponding particle size boundaries for loess have been defined. The > 10μm fraction makes up the skeletal framework of the loess structure (70-75%). Those particles 2-10 μm in diameter fill some of the void spaces (10-16%) and those < 2μm act as bonds and cement (10 - 15%) (Assallay, 1998). Krinsely and Smalley (1973) suggest that the crystalline characteristics of quartz, silt and clay size particles tend to be blade shaped or platy. Rogers et al (1994) proposed a first approximation of particle dimensions of 8:5:2, but with considerable variability around this ratio. Fine silt particles can easily form aggregates due to their small size and high surface forces in relation to particle weight. These forces also cause adsorption of clays and fine silts onto the surface of larger silt grains.

Air fall sedimentation results in a structure of primary loess that is edge to edge or edge to face (a 'house of cards effect'). After deposition, carbonate and clay minerals mobilise, thus permitting a small degree of cementation to hold the metastable open packing structure. Pores > 100μm are probably formed by roots and plant capillaries, bioturbation or dissolution of salts. Pores 10 -100μm, inter-granular or inter-aggregate pores, account for 15-28% of total voids and are probably synsedimentary. Pores which are < 10μm are intra-aggregate (18-25% volume). The limited extent of 'cementation' is clear in the field. When metastable loess is pressed firmly between the fingers or wetted the cemented bonds break and the loess becomes a powder or slurry. Even so, in this weakly cemented state, loess deposits are self supporting at very steep slope angles. The effect of increased water held in the sediment will affect this structure and ultimately lead to a modified or secondary loess soil structure.

Dry bulk density analysis by Vandenberghe et al (1997) showed that soils had a higher dry bulk density than loess, probably due to clay formation and illuviation. Their investigation of the Luochuan section revealed the surface

density of loess was 1.35 g/m^3 and that of soil was 1.65 g/m^3. An increase in the density of both loess and soils to a maximum of 1.85 g/m^3 occurred between the surface and 120 m (approximately 2.2My).

2.4. Post Depositional Modification of Loess

2.4.1. Introduction

Chemical aspects of the pedogenic processes involved in loess soil development are not widely discussed in the literature. An understanding of the conditions that are required for initiation of in situ magnetic mineral formation is important with respect to the site under investigation at Caoxian. It is also important to consider physical changes that may occur to the primary PSD when using particle size parameters as climate proxies. To gain reliable information from a deposit requires disentangling the effects of time/soil formation periods, other soil forming factors and the effect of overburden compaction. Aeolian deposits should be considered as horizons showing pedogenic development to a greater or lesser degree (Catt, 1995). Where pedogenesis is not obvious, microscopic changes in structure may give a more detailed understanding of environmental changes than environmental magnetic susceptibility or silt - clay ratio measurements (Kemp et al, 1995; Derbyshire et al, 1995).

When the summer monsoon is dominant, the assumption is that dust flux is reduced and precipitation increases. Pedogenesis occurs, altering the nature of the primary wind blown deposit. The SE-NW rainfall gradient which exists across the plateau results in higher rainfall and more intense pedogenesis at southerly latitudes, reflecting the onshore flow of warm, moist, Pacific air. Evidence from palaeoclimate records suggests that this gradient has been present for the last 2.6 Ma (An et al, 1991). Susceptibility profiles of modern and ancient soils have been used in attempts to reconstruct the precipitation gradient across the plateau (Maher and Thompson, 1995).

Southerly sites suffer from superimposition of soil layers due to the depth of the influence of weathering being greater than the sedimentation rate (Bronger and Heinkele, 1989). NW sites, however, are assumed to be aggrading even during periods dominated by the summer monsoon (Kemp et al, 1995). A detailed study of micromorphological variation at Jiuzhoutai (Kemp

et al 1999) has shown that it is possible to define horizons of relatively reduced and increased loess accretion at north western sites. The location of the Lanzhou loess' at the arid end of the climate gradient and close to the source has resulted in a higher sedimentation rate and lower rainfall on average than the type-sites around Luochuan. At present the annual precipitation at Caoxian is ~300mm, whereas further south it may be >700mm (Zhang and Lin, 1992).

Processes significant in loess are:

Chemical

Dissolution and precipitation of soluble salts

Decalcification

Decomposition of organic matter

Release of Fe or Al from primary oxides or hydroxides.

Accumulation of gypsum

Gleying in waterlogged conditions

Physical

Eluviation of fines in percolating water

Freeze-thaw

Bioturbation

Consolidation changes in bulk density

Earthquake/landslip erosion

Temporal variation of these processes affects how magnetic and PSD data from a palaeosol horizon can be interpreted. The extent to which sediment has been altered after deposition dictates how precisely any primary characteristics can be interpreted. The importance of these processes with respect to the northwest plateau loess is discussed below.

2.4.2. The Effect of Water on Loess

Water is perhaps the most critical factor driving all the processes listed above. Gao (1988) proposed characteristic stages of development in the loess pile. He summarised development into five stages: the loessisation stage, the formation stage, the development stage, the degeneration stage, and the clayisation stage. During the loessisation stage, he states that primary dust

particles are deposited dry. Periodic rainfall provides pore water that causes clay aggregate formation and limited dissolution of carbonate. Periodic wetting and drying results in reprecipitation of the carbonate into discrete $1\mu m$ grains thus strengthening the loess into its characteristic metastable form during the formation stage. Initial pedogenesis causes degeneration of the structure and intense pedogenesis causes clayisation.

The author believes that hydrogen bonds are active at the point of deposition and the first phase of drying results in some structural stability. This assumption is based on the fact that laboratory experiments with dry 'airfall loess' subsequently wetted failed to form the open packing structure characteristic of the marginal loess deposits (Assalley, 1998). Slightly 'sticky' loess is more likely to provide this initial structure (Assalley, 1998). Subsequent wetting may then enhance the strength of the structure by mobilising clay particles and cation cement. At present the majority of dust storms occur in spring and involve some element of atmospheric moisture/precipitation. It seems a reasonable extrapolation of present day processes to assume that the highest number of storms occurred during periods of extreme migration of pressure cells i.e. during shifts from perennial winter monsoon to summer monsoon dominance or vice versa.

Evidence shows that clay crusts are quick to form on the surface, possibly during or immediately after the storm event. Although their presence does not significantly reduce the amount of surface erosion it considerably increases the ratio of surface flow and sheet wash to infiltration. Surface flow is then concentrated into gullies and loess karst. A sealing effect is proposed as preserving the characteristics of the loess. Moderately sorted layers (< 5mm long and 1.5 mm thick) of clay grading into fine and coarse silt also show micas and linear organics aligned parallel to the layers. Described as afterflow or crust features (Kemp et al, 1995), they may be formed by water reworking and differential settlement of surficial sediment at a sparsely vegetated surface after intense rainfall and ponding.

Rainfall intensities during the summer season may reach upwards of 50mm hour^{-1}. Field experiments showed that infiltration rate was more strongly influenced by vegetation cover than by surface gradient (Billard et al, 1999).

Although only directly applicable to comparisons of grassland pasture which have a higher infiltration rate, and modern tilled land on loess deposits, this may have implications for changes in vegetation zones in the past. Clay seals developed very quickly on bare soil (in less than 2 minutes) whereas on good grass pasture infiltration was aided by stem and root flow whilst the surface was protected from compaction by the leaf canopy (Derbyshire et al, 1999). Crusts are strong enough to significantly reduce soil erodibility and deflation potential. Only very limited infiltration can explain the presence of highly soluble salts within recent loess layers (gypsum etc.). Present ambient soil moisture contents are 5-12%, maintaining high pore-water tensions that also increase the strength of the deposit.

Tectonic movement and overburden pressures form cracks along which the overland flow moves creating loess karst, so that secondary permeability is more important than porosity and connectivity. Dating of alluvial terraces gives fault offsets of 9-12 m since the late Holocene, and slip rates imply that M 8 earthquakes may occur every 800-1000 yr (Yin et al, 1998). The high frequency of surface fractures directly influences the loess hydrology. In very cold periglacial conditions processes dependent on water are reduced due to freezing. The effects are most easily seen in thin section. Discontinuous bands of silty clay (5 - 500μm thick and 2.5 mm long) have been identified in Chinese loess and have been reproduced by freeze thaw action. Freeze thaw alteration of the soils is minimal at present, due to the low moisture content during the dry winter months (Derbyshire et al, 1991; Derbyshire, 1991). Luminescence dates constrain the age of formation of permafrost structures showing a phase of permafrost development during the latter part of the last glacial (22 to 15 ka) that resulted in cryoturbated sediments and ice-wedge casts. Furthermore, permafrost degradation occurred during Late glacial times (13-10 ka) and was absent during the early Holocene. These permafrost structures mark the southernmost evidence of permafrost in northern Asia during late Quaternary times and indicate that the mean annual air temperature was below -6 °C during formation (Owen et al, 1998).

Due to the proximity of the north western part of the plateau to the source, a reduced but continuous supply of dust can be expected during soil

forming periods. The depth of development of a soil into pre-existing loess will be dictated by the sedimentation rate, as will the potential for well-developed B horizons. It is envisaged that dust deposited during warm, wet periods characterised by significant pedogenesis will fail to form the metastable packing structure described by Gao (1988) during the formation stage. Bioturbation, increased primary clay content and increased infiltration in vegetated regions means that new dust will quickly be mixed into the soil. Hydrogen and other van der Waals bonding will become increasingly important over ionic carbonate bonds.

2.4.3. Soil Structure and Moisture

Storage (evapo-transpiration, infiltration etc.) of water is critical in pedogenic processes. Infiltration is dependent on rooting depth and bioturbation. In northern Gansu, annual potential evapotranspiration exceeds precipitation by over 1000mm (Zhang and Lin, 1992).

Kemp et al, (1995) studied the microstructure of loess from the Lanzhou area. The microstructure of pristine loess is described as massive, becoming more spongy and channelled due to faunal reworking (excrement) and flora (plant roots). It is the author's opinion that this statement is not meant to imply a temporal but a spatial progression from massive to spongy microstructure across the plateau in accordance with precipitation evidence. The organic content of glacial loess is low especially in the Longxi plateau: approximately 0.2-0.3%, and up to 1.8% in palaeosols.

The degree of clay aggregation increases in line with increasing pedogenesis. Scanning electron micrographs of Malan loess taken from a site close to Lanzhou (Derbyshire et al, 1999) show evidence of occasional aggregate break down and some carbonate coatings on grains. The loess appears to have been only slightly altered by soil moisture. A further micrograph of last glacial maximum age (20ka) from Dajing 150 km north of Lanzhou, revealed coarse clean grains of silt rarely cemented and almost no aggregates. In reference to the previous discussion regarding transport of fine particles as aggregates, the lack of any 'primary' aggregates appears contradictory. One possible interpretation is that wind conditions effectively sorted coarse single grains from less dense aggregates and transported the

74

latter further down wind. So the higher percentage of clay grade particles in the south is a composite of both distal deposition and pedogenesis (see page 59). The very limited precipitation and soil moisture in the northern loess plateau had barely any effect on the pristine loess structure.

2.4.4. Soil Water and Chemistry

Water combined with carbonic and organic acids hydrolyses alkalis (Na and K) and alkali earths (Ca and Mg). These combine with the carbonic acid in the soil water to form carbonates and bicarbonates in B-horizons leaving depletion pedofeatures in A-horizons. In semi arid soils, large quantities of carbonate in migrating fluids can reprecipitate in microvoids. Calcium carbonate can occur as coatings on quartz grains and nodular concretions. Known as loess dolls they are often hollow inside and are up to 60mm in size (Kemp et al 1995). Leaching experiments carried out on Malan and Lishi loess samples from the Lanzhou area showed that percolation waters were heavily charged with cations of sodium, and anions of sulphates and hydrogen carbonates. A very fast dissolution of the soluble Na, Ca and Mg chlorides and sulphates occurred. Increased alkalinity of the waters may enhance later dissolution of Na and K carbonates and bicarbonates. Geochemical analysis of Luochuan loess from the central loess plateau showed that Rb, Sr, U, and Ce were strongly controlled by the breakdown of primary minerals. This resulted in their concentration in palaeosols and relative depletion in loess layers (Gallet et al, 1996).

Nd and Ce are rare earth elements and presumably are linearly related on deposition. Weathering subsequently controls Ce concentrations; the ratio of Ce/Nd could be expected to decrease with increasing pedogenesis due to dissolution of Ce, (Chen et al, 1997; Gallet, 1996). Chen et al (1999) used the Rb/Sr ratio as an indicator of chemical weathering at Luochuan and Huanxian (200km north of Luochuan). The similarity in size of Rb and K ions means substitution occurs. Relatively high concentrations of Rb are found in K feldspar. Sr generally substitutes for Ca and Na ions in carbonates and sodic or calcic aluminosilicates. Carbonates and alumino silicates are more prone to weathering, and therefore a relative enrichment of Rb over Sr can be expected in palaeosols. K/Rb remains relatively unchanged during the early stages of

weathering, and changes in this ratio act as an indicator of more intense pedogenesis. Chen et al (1999) found an excellent correlation between Rb/Sr and magnetic susceptibility, with high values in weathered layers, indicating that a similar process must drive them. Zr and Al and Nd may be taken as constant, although Gallet (1996) has shown that heavy minerals such as Zr may be prone to enrichment in the coarse fraction due to the aeolian transport process.

2.4.5. Post Depositional Changes in the Clay Fraction of Loess

Aggregation is an important feature of loess soil structure. Silt and clay particles combine in soils to form globular aggregates, with sizes between 10 and 100μm, some larger than 350μm (Medvadev, 1996). Evidence from Russian loess). Clay sized particles flocculate in the presence of a high concentration of alkali ions. Aggregates have varying water resistance depending on the type of bonds between the particles (Rowell, 1996). Feldspars and ferromagnesian minerals produce a series of clays of different composition. Type of clay depends on temperature and moisture conditions and the length of time the material is exposed to water. The disassociation of water into H^+ and OH^- ions is strongly temperature dependent, and may be critical in weathering. Temperature largely influences the rates of weathering, a 10°C increase in temperature enhances weathering reactions by a factor of 2 – 3. However, this factor has a less dramatic effect on clay mineral type than does precipitation (Brady and Weil, 1999).

In general, the formation of secondary clay minerals depends on the balance between the rate of dissolution of primary minerals and the rate of flushing of solutes by water. The leaching experiments carried out by Billard et al (1999) found that the maximum suspended load in percolation water did not correspond to the highest concentration of cations. The suggested mechanism is that water with high concentrations of Na^+ and basic anions destabilises the aggregates. Subsequently less alkali water breaks up the aggregates and carries them away. The transport of small particles from the A to the B horizons results in enrichment of illuvial clay in the B horizon. Analysis of Baoji loess (north central loess plateau) found major components of the clay mineral

fraction to be illite (55-75%) kaolinite (10-20%) mixed layer chlorite-vermiculite (10-20%) chlorite (<7%) and small amounts of smectite (<5%) (Kalm et al, 1996). Clay minerals can be used to show weathering, precipitation, climate gradient or changes in drainage. Clay minerals at Baoji section Showed an increase in chlorite and chlorite-vermiculite up section indicating a decrease in weathering intensity. Increase in the percentage of illite since 1.2 Ma in both soil and loess indicates increasing aridity over time.

2.4.6. Classification of Chinese Loess Plateau Soils

Classifications of the soil types on the loess plateau described the present north western soil horizons as light to very light imperfectly developed chestnut soils (Thorp 1936). Chestnut soils undergo similar processes as chernozems. The horizons are similar, as are the soil forming processes. However, because of the semi-arid environment and the significantly reduced moisture availability, the soils never become true chernozem or chestnut soils. Where loess is constantly aggrading the dark A-horizon is more calcareous than it would otherwise be. Below, the B-horizon shows some carbonate enhancement. In the southern part of the chestnut range there are notable differences between the adret and ubac hill slopes. The generally weaker soil development on the adret slopes commonly gives rise to light or very light chestnut earths (Thorp, 1936). Thorp (1936) described present day surface soils on the loess plateau and related them to climate and vegetation as follows.

Reddish brown soil: reddish surface horizon, on a redder horizon and a light coloured horizon with carbonate accumulation formed under warm, temperate to tropical, to semiarid climates. (NW Gansu during the Eemian) Chinese classification describes the last interglacial calcic drape soils as luvisols or cambisols.

Chernozem: soils characterised by a dark, usually deep, humic A horizon saturated with cations of calcium and magnesium (a mollic epipedon) thin, brown B horizon with clay accumulation, and a calcareous sub soil. Formed under temperate to cool sub-humid climate associated with long grass steppe. (NW Gansu during the Holocene) Chinese classification describes the weak palaeosols of light chernozems during the last glacial and Holocene as

heilusols, kastanozems or sierozems (calcisols) indicating increasing aridity (Fang et al, 1994).

Chestnut soil: soils characterised by less distinct horizons than a chernozem, a dark horizon lying on a lighter subsoil which shows signs of clay accumulation, often associated with specks of gypsum (calcium sulphate) and calcium carbonate accumulation. This soil development is usually associated with short grass steppe in a semi arid environment and light chestnut soils dominate the north western loess plateau.

2.5. Environmental Magnetic Studies of Chinese Loess

2.5.1. Magnetic Mineral fraction

Numerous environmental magnetic studies found that, in general, loess soil horizons contained an enhanced magnetic susceptibility signal. A benefit of the use of magnetic susceptibility is that a significantly narrower band may be identified as 'true' palaeosol than that applied in the field by eye. Using thermomagnetic techniques, several authors found that magnetite dominates the susceptibility signal, e.g. Heller et al (1991); Liu et al (1992); Maher and Thompson (1992). These conclusions have been supported by Mossbauer spectroscopy (Vandenberghe et al, 1992). However, XRD analysis pointed to significant contributions from maghemite. Eyre and Shaw (1994) used thermal demagnetisation of low temperature isothermal remanent magnetisation and thermomagnetic curves to conclude that there was a very significant maghemite component, particularly in palaeosols.

Citrate-Bicarbonate-Dithionate (CBD) technique, although time dependent (Liu X et al, 1995), was used with limited success to separate magnetite from maghemite and quantify pedogenesis in loess (Verosub et al 1993). Several explanations for the relative concentrations (enhancement) of the loess susceptibility record were suggested. Heller and Liu (1984, 1986) proposed concentration of the magnetic mineral component by decalcification and soil compaction. Following the work by Heller and Liu (1986); Kukla and An (1989) and Kukla et al (1988) it was proposed that a constant flux of fine grained magnetic material from a distant source was diluted periodically by a weak magnetic local source. These two models could not account for the scale of variation of magnetic susceptibility in loess.

The accumulation rates of magnetic minerals were shown to vary both temporally and spatially invalidating the constant flux theory of Kukla. (Maher and Taylor, 1988; Zhou et al, 1990; Maher and Thompson, 1991; Zheng et al 1991; Hus and Han, 1992; Banerjee et al, 1993; Verosub et al, 1993; Heller et al, 1993; Liu et al, 1993; Rolph et al, 1993; Verosub et al, 1993; Evans and Heller, 1994). Differences between loess and palaeosol layers were found in both concentration and magnetic grain size distribution. Heller (1991) found evidence for a partly pedogenic origin of the ultrafine grains. Two types of magnetic particle in the ultrafine fraction were identified - those produced during inorganic precipitation and rarer particles possibly of bacterial origin.

Analysis of magnetic grain size fractions showed that susceptibility increased with decreasing grain size (Zheng, 1991). Detailed quantitative estimates of the magnetic grain size fractions, using microscopy and magnetic hysteresis modelling (Maher and Thompson, 1992) identified the principal detrital ferrimagnetic minerals as multidomain (titano)magnetite or cation deficient magnetite. Subsequent investigation of the magnetic remanence characteristics of different magnetic grain size categories showed a larger multidomain fraction in soils than in loess, as well as particles at the SD/SP boundary, $\sim$ 0.03 μm (Liu et al., 1994). This indicated possible leaching of carbonate and relative enhancement of the coarse fraction. This author's research will show an alternative suggestion for increased concentration of MD grains in loess horizons (Chapter 5 and 6)

Ultra fine magnetite and maghemite was recognised as an important source of the magnetic susceptibility signal (Kukla et al, 1988). Palaeosol horizons were found relatively enriched in magnetic grains around the SSD/SP boundary (Zheng et al, 1991) associated with an increase in pedogenic clays. Fang et al (1999) used low-temperature remanence studies to analyse variations in the concentration of superparamagnetic (SP) grains from S_1. The SP concentration pedogenic proxy showed millennial scale variations indicating that the last interglacial period was characterised by rapid climate fluctuations. Assuming an aeolian origin of the red clay (Ding et al, 1998; 1999), it is interesting to note that, although micromorphological and clay mineral analysis has shown a greater degree of pedogenic development than in younger

palaeosols, the magnetic susceptibility of the red clay is less than in the overlying palaeosols. This must have implications for the use of susceptibility as a proxy of rainfall relating to the summer monsoon. Variations within the local region and variations in source material must limit the degree of enhancement in soils.

2.5.2. *Possible Mechanisms of Formation and Preservation of Magnetic Material in Loess*

Redoximorphic features, formed by the distribution of iron oxides associated with periodic water saturation but not water logging, have been identified in loess palaeosols (Liu et al, 1995). In order for a soil layer to become 'enhanced' magnetically some paramagnetic or antiferromagnetic iron oxides, silicates or oxyhydroxides must convert to ferrimagnetic material. Migration of organic rich water helps to keep any dissolved iron in suspension. Ferrimagnets may be formed via the production of ferrihydrite (Dearing et al, 1996). 'Micro-niches' formed soon after the initiation of pedogenesis (J Dearing pers comm) has been proposed as possible sites for SP magnetite formation. The potential for the massive structure of loess; house of card effects, with well supported pore spaces as sites for the in situ production of ferrimagnetic material is discussed in chapter 6.

A suitable environment for the production of secondary magnetic minerals may form even earlier due to the adhesion of water, charged micelle films and water held by capillary action. It can be shown that (chapter 6) very weakly developed pedogenic horizons, indicating very low soil moisture, exhibit enhancement. SEM studies have indicated that ferrimagnetic grains formed within the soil matrix (Maher, 1998) are sub-micron cryptocrystalline in structure, often occurring as discrete single grains and sometimes as magnetosome chains formed by magnetotactic bacteria (Lovley et al, 1987). Such chains were found in S1 palaeosol at Luochuan in small quantities (Thompson and Maher, 1992). Susceptibility values can be enhanced by the presence of less than 0.1 % of ultrafine ferrimagnetic material (Maher, 1998) with other iron oxides making up 2-5 weight percent. Because of this, there is usually little correlation between total iron and magnetic susceptibility (see Chapter 6).

Dearing et al (1996) showed a weak correlation between soil iron content and susceptibility in U.K soils. The supply of iron may be the major limiting factor in the in situ formation of ferrimagnets. Maher (1998) points out that the highest susceptibilities are rarely associated with the highest soil iron content, and argues that soil conditions of conversion and preservation of magnetic grains are more important. Analysis of CBD extracted ferric iron oxides at Caijiagou and Shimao at the margin of the Mu Us desert (Ding et al, 1999a) shows a very close positive correlation with susceptibility. There is more likely to be some correlation between susceptibility, organic content and cation exchange capacity, although it should be borne in mind that high amounts of organic matter may act to dilute the magnetic signal.

Iron manganese speckles in well developed soils in the southern loess plateau (S_{1-3} and S_5) indicate very warm and very humid conditions with acidic soils with strong hydrolytic and oxidative reactions. The resulting iron compounds are weakly magnetic hematite and or goethite. Under these conditions, any ferrimagnetic material would have been removed if ever formed at all. Laboratory experiments on magnetite synthesis showed that a neutral pH soil was most conducive to the formation of ultrafine magnetite (Maher and Taylor, 1987; Taylor et al, 1987). The carbonate rich loess in China may act as a pH buffer and be advantageous in ferrimagnetic production (Maher, 1998). The author notes that in S_1 palaeosol development carbonate dissolution occurs with reprecipitation below the horizon of maximum enhancement (Chapter 5 and 6). Oxidation appears to favour the production of non-ferrimagnets. Periods of reduction may be a prerequisite for ferrimagnetic production (magnetite). Subsequent oxidation of magnetite may lead to maghemite production, a ferrimagnetic mineral with a slightly lower susceptibility than magnetite. If this is the case, one may suppose that the formation of these two species in situ is competitive. Ferrimagnetic material must be resistant to subsequent pedogenic processes of dissolution and indeed, it appears from Maher's research (1998) that ferrimagnetic production is highest in well drained soils with wet-dry alternations. Gleying conditions in Scottish soils resulted in the depletion of ferrimagnetic material (Maher, 1998). Maher (1998) also expresses concern that accumulation rates may be over estimated for Chinese palaeosols. She states that "soils are not essentially a

deposit but are superimposed on previously deposited glacial loess"; and continues "it is possible that loess and palaeosol units remain at the surface for approximately equivalent periods (~10ka) constrained, respectively by burial rates during glacial periods and by the duration of the interglacial periods". The presence of magnetic enhancement in short lived interstadial soils (An et al, 1991) is a significant piece of evidence against this suggestion. Sections from the western loess plateau at Beiyuan and Yuanbao contain incipient soil development within S_m characterised by organic enrichment of the A horizon and lacking a B horizon (Chen, 1997). This indicates that the accumulation rate was rapid (Feng, et al 1998) and the depth of influence of weathering was low. Problems remain in determining the rate of dust input to soil horizons during pedogenesis and its significance for enhancement.

Maher's (1998) paper, although valuable, concentrates on re-analysis of well-developed, overprinted soils. The inherent problems involved in gaining a detailed understanding of environmental processes have been widely reported. It is unlikely that a realistic rate of ferrimagnetic production can be gained by studying central loess plateau palaeosols alone. This thesis will show that the initiation of the enhancement process is rapid, occurring over a period of less than a few hundred years. It is also possible that detailed analysis of these incipient soils will give some insight into the initial processes of magnetic mineral formation.

3. Methodology and Techniques

3.1. Introduction

The sample site location and sampling method is described here, followed by a brief discussion of the theory of each analytical laboratory technique used and how the loess samples were prepared and tested.

Figure 3.1 Photograph of the Caoxian section

The section is located in Caoxian village, Gansu province, approximately 150 km north of Lanzhou. Situated in the Jingyuan basin, the site is close to the mouth of the Hexi corridor to the northwest and the border of the Mu Us desert in the northeast. In the Jingyuan basin, loess has been deposited on the 6th terrace of the Yellow River. The region is characterised by 500 m thick deposits of loess over Palaeozoic granite and Neogene conglomerates, these forming the drainage divide areas between rivers. The area is characterised by yuan (flat plateau surface) and steep unstable valley sides. Streams cutting into the soft loess have incised narrow valleys. The hillside that was excavated was composed of over-steepened consolidated older (Wucheng and Lishi) loess, with 65-75° slope angles. The upper 50m, where the samples were taken, sloped more gently at an angle close to 35°. There was evidence of rotational and slab instability in the upper loess on proximal valley sides (see Derbyshire et al, 1993) and some gullying. Vegetation on the valley sides was limited to low growing woody plants and shrubs, Artemisia etc. The plateau surface was cultivated and fertilised. The present annual precipitation is ~300 mm (370 mm, Chen et al, 1999) falling in concentrated events between June and September.

The period of sampling was mid April to mid May 1996. The weather was moderate to good, although occasional downpours and brief dust storms delayed sampling. The start of fieldwork was postponed by several weeks due to heavy snow in the area. Therefore the loess at depths greater than one metre was moist and weakly bound.

Two types of samples were collected: unorientated broken samples and orientated block samples. Broken samples were taken from a freshly dug 'stepped' trench situated on a west facing valley side, 500 m out of the village along the 'main road'. The trench base was at a depth of 1.5 to 2 m below the yuan topographic surface. Samples were taken at 2 cm intervals from the vertical front face of the steps, 2100 samples being collected over the length of the 45 m trench. The approximate mass taken was 60g. Levelled orientated block samples were also taken using a spirit level and compass, for use in geomagnetic secular variation experiments (Heslop, 1998).

The top of the section (0-50 cm), being early to mid Holocene soil, (S_0 noted as unit 1 in the field) was disturbed by farming. Therefore, a second sampling site of three metres depth was located at the back of the government buildings in the centre of the village. Here, the top of S_0 was sampled, the continuation of which was sampled (0-2m) in the trench. From 2-32m, friable yellow loess was sampled containing occasional 1-2 mm gypsum nodules, described as units 2, 3 and 4 (see Chapter 5 for detailed log). The remaining 32-43 m reached the base of a well-developed soil, unit 5. This unit was characterised by reddening and higher clay content.

3.2. Environmental Magnetic Methods

3.2.1. Introduction

Paleomagnetism, the study of natural remanent magnetism, has long been used to reconstruct changes in the Earth's magnetic field. More recently, magnetic studies have been used to investigate environmental factors. Investigations of sediment provenance, lithostratigraphic correlation and identification of pedogenic or weathering processes have been carried out using a magnetic approach. Magnetic measurements are rapid, sensitive and non-destructive and have been applied to a variety of sediment types. All materials respond when a magnetic field is applied. Some have the ability to retain a record of the induced magnetism after the field has been removed. Magnetic fields within materials are the result of the motion of electrons, either orbital motion around the nucleus or spinning motion about the central axis. Material may be weakly or strongly affected by an induced field depending on the nature of the material.

There are five possible magnetic responses. The most fundamental is diamagnetism. Diamagnetism is only exhibited in the presence of an external field. The applied field causes electron orbits within the diamagnetic material to become aligned in the opposite direction to the applied field. Quartz, orthoclase feldspar, calcium carbonate, organic matter and water all show diamagnetic characteristics, i.e. weak negative magnetisation in an applied field (Thompson and Oldfield, 1986). Such materials are slightly repelled by a strong applied magnetic field. The effects of the field are not retained once the field is removed. Diamagnetic responses usually act to dilute the signal of other

magnetic constituents and only in extreme cases such as pure quartz, limestone and feldspar, would the diamagnetic effect be significant.

Paramagnetic material has permanent magnetic dipoles, which align along the direction of an applied field due to the magnetic moment. Transition metals, those with an unfilled 3d electron, have a magnetic moment and are central to most magnetic investigations. In the absence of any external field, the net magnetisation of paramagnetic material is zero due to the random orientation of the magnetic moments. The arrangement of dipoles in the field is adversely affected by thermal agitation. The amount of paramagnetism is temperature dependent; i.e. a greater amount of energy is required to induce magnetisation as temperature increases – unlike diamagnetism (Rolph et al, 1993). On application of a field, the magnetic moments align themselves in a direction parallel to the field. Once the field is removed, the effect of the induced magnetism is lost. Minerals, such as olivine, pyroxene, garnet, biotite, and carbonates of iron and manganese exhibit paramagnetic behaviour. The paramagnetic effect is generally one or two orders of magnitude greater than diamagnetic effects (Smith et al, 1999). In soils, paramagnetic behaviour is significant where the soil is iron rich but poor in ferrimagnets.

Ferromagnetic material posses a particular crystallographic arrangement where neighbouring atoms with magnetic moments interact. The spins become aligned in the absence of an externally applied field. The magnetic moment of ferromagnets is much greater than either diamagnets or paramagnets. In such cases, it is possible for a record of an induced field to be retained by the material, i.e. remanence. Ferromagnetic materials behave as paramagnets above their Curie temperature, again due to disruptive thermal energy (Sears, 1951). Below this temperature, ferromagnets can hold a strong remanent magnetism.

Different forms of ferromagnetic behaviour result from the arrangement of atoms in the crystal lattice. Ferrimagnetic minerals are a permutation of ferromagnets. Ferrimagnets have antiparallel layers of magnetic moments (Thompson and Oldfield, 1986). Ferrimagnetism is common in iron oxides because the intermediate layers of oxygen atoms result in alternate layers being magnetised in opposite directions (Smith et al, 1999). If one direction is stronger than the other a net magnetisation in one direction results. Magnetite

and maghemite are perhaps the most frequently referred to natural ferrimagnets. Magnetite in soils may be allochthonous or autocthonous, derived from igneous rocks or by in situ pedogenic reactions. Maghemite always occurs as a secondary mineral.

Antiferromagnets are again a category of ferromagnets. They too have antiparallel moments, but they are of equal strength and so antiferromagnets have a zero bulk magnetisation. Imperfect antiferromagnets may exhibit a bulk magnetisation due to incomplete antiparallelism. Hematite and goethite have imperfect antiferromagnetic structures resulting from spin canting; hence they are capable of retaining remanent magnetisation.

3.2.2. Magnetic Hysteresis

Hysteresis is "the lag in a variable property of a system with respect to the effect producing it" (The Concise Oxford English Dictionary 1996, pp 377). In the case of a material subjected to a magnetic field, the strength of the induced field lags behind that of the charging external field. A magnetic hysteresis loop can be used to illustrate the magnetisation behaviour of a material under applied fields. At low applied fields, magnetisation slowly increases and changes are reversible, and this can be used as a measure of the initial magnetic susceptibility of a material. Diamagnetic material has a negative susceptibility, while paramagnetic material has a weak positive susceptibility. For imperfect antiferromagnetic material the range is from $0.3 - 2$ x $10^{-6}m^3kg^{-1}$ and ferrimagnetic material 250-450 x $10^{-6}m^3kg^{-1}$ for maghemite and up to 1000 x $10^{-6}m^3kg^{-1}$ for magnetite (Smith et al, 1999). Beyond a critical field, the magnetisation of ferromagnets is not reversible, i.e. on removal of the field the material exhibits a remanence. Magnetisation increases with increasing field to a maximum known as saturation magnetism (Ms). On removal of the field magnetisation drops to the saturation isothermal remanence magnetisation (SIRM or Mrs). The application of fields in the opposite direction will eventually reduce the induced magnetisation back to zero. The reverse field required to reduce the magnetisation back to zero is the coercivity, B_oc, (in field measurement). The magnitude of the reverse field required to reduce the remanence to zero (out of field) is the coercivity of remanence, B_ocr.

Hysteresis properties of ferromagnets are controlled by domain walls, and their arrangement and changes in wall positions during and after the application of a field. Domain walls, a ~1 μm unit where the direction of magnetisation spirals through 180°, divide a material into domains that can be spontaneously magnetised in different directions. They exist in order to reduce the magnetostatic energy allowing the grain to exist in the most energetically favourable state.
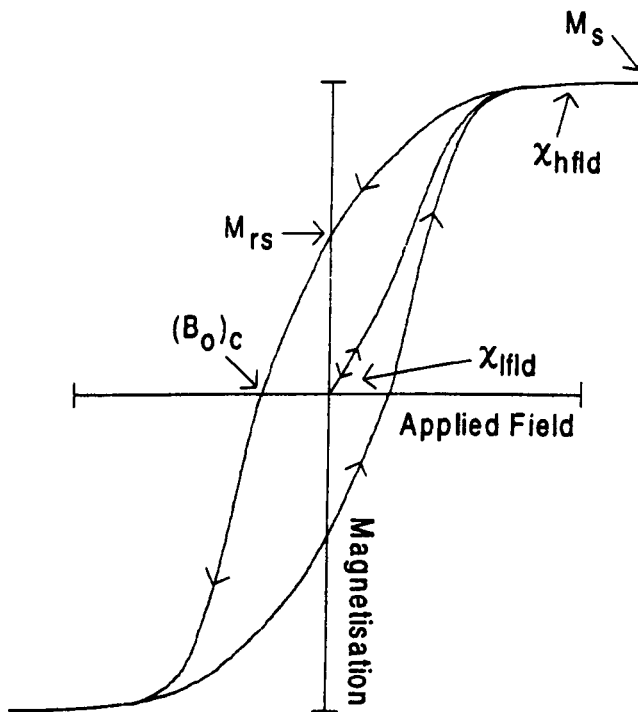
Figure 3.2 Schematic diagram of hysteresis behaviour

Large grains are likely to exhibit multidomain (MD) behaviour. Ferrimagnetic grains larger than ~110μm behave as MD grains (Dearing, 1999). If these domains are aligned randomly then the grain will possess a net magnetisation of zero. On the application of an external field, the domain walls will shift allowing alignment in the same direction as the applied field. As the field increases, the boundary walls move to positions of least energy. A MD grain is saturated once all domains are aligned in the direction of the field. The value of Ms is invariant of grain size but varies with mineralogy. Above a certain field the walls 'block' and retain the alignment of the external field after it is

removed, resulting in remanent magnetisation. The value of the remanence will be lower than the magnetisation achieved in field since some relaxation of domain walls will occur.

SD behaviour of ferrimagnetic material applies to grains < 2 μm. It is not energetically favourable for small grains to contain domain walls. SD grains show several characteristic hysteresis loops depending on their shape and orientation in the applied field. The saturation remanence of SD grains is higher than that of MD grains. Pseudo-single domain (PSD) behaviour is characterised by MD grains with ten or fewer domains (Smith et al, 1999) and applies to ferrimagnetic material with grain sizes between 2-110μm (Dearing, 1999). They are very stable and are able to hold remanences for prolonged periods (Merrill et al, 1996).

Superparamagnetic grains (SP) are ultra-fine ferro and ferrimagnetic particles (< 0.03μm diameter for magnetite) (Dunlop, 1973). The magnitude of their magnetic energy is equal to the thermal energy at room temperature and consequently they cannot retain stable remanent magnetism due to thermal agitation. However, they exhibit large in field magnetisation i.e. high susceptibility values. SP behaviour is strongly temperature dependent: sufficient cooling will reduce thermal agitation and allow stable single domain behaviour. They do have an extremely strong magnetic alignment, similar to, but much stronger than paramagnetism.

Most natural samples contain a mixture of different minerals and domain and grain sizes. The magnetic parameters retrieved from analysis of natural samples are therefore a composite of all of these factors affecting the magnetic response. This study uses concentration parameters and interparametric ratios to define the contributions and importance of various magnetic mineral types. Concentration parameters give an indication of the quantity of magnetic mineral present, but mineral type, size, and shape affects the values. Interparametric ratios give an indication of the quality or types of mineral i.e. to infer domain size and mineralogy.

3.2.3. Magnetic Susceptibility

Magnetic susceptibility is a measure of the ease with which a material can become magnetised (Thompson and Oldfield, 1986). Therefore, susceptibility is often interpreted as an indicator of the total magnetic mineral concentration (Dearing, 1994). The bulk susceptibility of a sample is the total contribution of each of the magnetic material types and their relative concentrations – diamagnetic, paramagnetic, ferrimagnetic etc. at room temperature. Where present, the major contribution to the susceptibility will be from ferrimagnetic minerals. Susceptibility increases exponentially in SP grains as size decreases (Maher, 1987).

The ferrimagnetic contribution of grain sizes ranging from SSD to SP can be expressed as the difference between contributions to low and high frequency fields. The decrease in induced magnetisation between low and high frequency is termed frequency dependent susceptibility. If normalised and expressed as a percentage;

$$\chi_{FD}\% = 100(\chi_{LF} - \chi_{HF})/\chi_{LF}$$

χ_{LF} is the susceptibility measured at a frequency of 0.47 kHz

χ_{HF} is the susceptibility measured at 4.7 kHz on the Bartington MS2B susceptibility meter gives the proportion of grains at the SSD/ SP boundary. In samples where the values of $\chi_{FD}\%$ are very low, mass specific frequency dependent loss of susceptibility can be used

$$\chi_{FD} = \chi_{LF} - \chi_{hf}$$

and gives the concentration of SP-SSD grains (Dearing et al, 1996). This parameter can be used as an indicator of environmental conditions and the degree of pedogenesis (as discussed in chapter 2 and 6). Samples with a significant proportion of SSD/SP grains may have $\chi_{FD}\%$ values > 6%. Values of < 5 % typify assemblages dominated by non SSD/SP grains or very fine grains dominate the SP fraction (< 0.005 μm) (Dearing, 1999). Values of $\chi_{FD}\%$ will be lowered by the presence of frequency independent grains.

3.2.4. Remanence Parameters

Isothermal Remanent magnetism (IRM) is the remanence retained by a particle exposed to a steady field at a constant temperature (room

90

temperature). Increasing the field stepwise up to 1T gives a suite of IRM results for each sample related to the ferromagnetic component of the sample. Diamagnetic and paramagnetic material does not contribute to remanence parameters. Particles with a coercive force higher than the applied field will remain unaffected. IRM can be used to estimate the relative contributions of soft or low coercivity magnetic minerals and hard or high coercivity magnetic minerals i.e. indicative of mineralogy. Magnetite is soft, and its IRM curve shows rapid saturation at an applied field of approximately 300 mT. Hematite is hard and continues to be magnetised up to fields greater than 1 T. SIRM, in the case of hematite, may be limited by the size of the field the equipment can impart to the sample – in these cases; the true SIRM may not be reached. The SIRM of a sample is strongly dependent on mineralogy and grain size. The strength of fine grained ferrimagnets present in the sample may obscure the response of any imperfect antiferromagnetic minerals to the induced fields. SIRM is a good measure of magnetite content but is also dependent on grain size and is influenced by other magnetic minerals such as hematite. SIRM is highest for small SSD and lower for MD grains and the range of values through these grain sizes is much greater than for χ_{LF}

Relaxation of magnetic grains and their domains can greatly affect the interpretation of IRM and SIRM results. The relaxation time is the time required for the grain to reach equilibrium after the removal of the external field. The specific relaxation time required by a particle depends on grain size and temperature. SP/SSD grains are the most viscous, contributing to the initial rapid viscous loss in a sample; MD grains may lose 1-2-% of their total remanence over 24hrs.

HIRM parameter is a measure of the proportion of high coercivity, hard imperfect antiferromagnetic material. Minerals such as hematite and or goethite dominate this parameter's response. In order to define samples with significantly different imperfect canted antiferromagnetic content the S-ratio is calculated. S-ratio is usually calculated as the ratio of IRM_{100mT} to SIRM. In this case, IRM_{300mT} is used. It is based on the principle that all soft ferrimagnetic material will have saturated by 300mT and the remainder will be hard imperfect canted antiferromagnetic material, hematite of goethite.

3.2.5. Anhysteretic remanent magnetism

Anhysteretic remanent magnetism (ARM) is acquired when a sample is subjected to a small steady (DC) field during the gradual decay of an alternating frequency (AC) demagnetising field. The small positive field intensifies the positive half of the alternating field. Therefore, on removal of both fields a net positive remanence remains in the material. Only those grains with domains capable of being realigned in a field greater than the peak alternating field will retain a remanence: smaller grains will be demagnetised. ARM is particularly useful for estimating the concentration of SD grains in a sample. ARM normalised by the biasing field (χ_{ARM}) is strongly sensitive to grain size variations across the PSD size range, χ_{ARM} ($m^3Am^2kg^{-1}$) (Maher, 1988). As illustrated by Maher (1988) ARM is highly selective of true stable single domain ferrimagnetic grains in the $0.02 - 0.4$ μm range. However this parameter is concentration dependent. Similar values may be produced by a high concentration of relatively coarse MD grains (>1 μm). It has been suggested that IRM_{20mT}/χ_{ARM} ratios provide a way of discriminating between an SSD and MD dominated assemblage. However variations in this parameter are complicated by the influence of SP grains, where present in the sample. The magnitude of the remanence is an indication of the concentration of SD grains. The intensity of the ARM moment is dependent on mineral concentration and grain size. ARM is believed to be more discriminating of SSD grain sizes than SIRM.

ARM measurements suffer from errors caused by grain interaction. Where individual magnetic grains touch, i.e. the concentration is high, and then their fields interact. This modifies the behaviour of the magnetic assemblage by altering the effective magnetic grain size and hence domain states. High concentrations of SD grains are prone to MD behaviour (Robinson, 1997) i.e. an increase in modal particle size. This results in a decrease in the material's apparent ARM and IRM and an increase in susceptibility. Grain interaction also affects the SP range by decreasing the grain size for SP behaviour. The combined effect of this behaviour results in a broadening of the range of SD

behaviour of the material (Dunlop, 1981). In contrast, grain interaction has very little effect on the susceptibility and remanence behaviour of true MD grains.

3.3. Magnetic Measurements

3.3.1. Sample Preparation

Air dried sub-samples were packed tightly into 10 cc plastic pots lined with cling film to ensure the grains could not move and distort remanence analyses. The mass of the sample was recorded to 3 decimal places. Initial sub-sampling was carried out at 8cm intervals for the entire 42.5 m section to define the magnetic susceptibility characteristics of the site. Subsequently sub-samples were packed and measured continuously at 2cm intervals from two parts of the section (5 to 26m and 35 to 42.5 m). This allowed high resolution comparison of a well developed soil horizon Unit 5, with incipient soil development, unit 3, and relatively pristine loess, Unit 2.

3.3.2. Susceptibility Measurements

The magnetic susceptibility of the samples was measured using a Bartington MS2B susceptibility meter. The machine generates a weak 0.1mT field from an oscillating current of 0.47 kHz (low frequency). A calibration sample of magnesium carbonate (156×10^{-10} m^3 total susceptibility) was measured at the beginning of each period. An error of $\pm$ 1% was acceptable for the calibration. The low frequency magnetic susceptibility of each sample was measured three times. The ambient background air was measured between each repeat and subtracted from the sample measurement, thus correcting for any drift. The three corrected values were then averaged. The direct measurement from the meter is the volume susceptibility, κ. χ is the mass corrected susceptibility ($m^3 kg^{-1} \times 10^{-8}$).

The procedure was repeated using an oscillating current of 4.7 kHz to give high frequency susceptibility. As described previously the frequency dependent susceptibility (χ_{FD} or χ_{FD} %) can then be calculated to give an estimate of the SSD/SP grain concentration. The use of diamagnetic cling film in the pots has been shown to have a negligible diluting effect on the measured susceptibility of most natural soil samples (Clifton, 1997).

3.3.3. Anhysteretic Remanent Magnetisation Measurements

The same group of sub-samples in 10 cc pots was used for ARM analysis. The ARM was imparted using the DTECH demagnetiser and controlled using a portable PC. A 100 mT peak alternating field and a 0.1 mT biasing field reduced at 0.016 mT per cycle were used. After imparting the ARM the remanence was measured in a Molspin fluxgate spinner magnetometer. The spinner was calibrated regularly using a standard sample of known remanence, 1684×10^{-8} Am^2. Raw values in 10^{-8}Am^2 were divided by the value of the biasing field and mass corrected units of 10^{-5}Am^{2}kg^{-1} (χ_{ARM}).

3.3.4. Isothermal Remanent Magnetisation Measurements

The same samples that were used in susceptibility and ARM analysis were measured for their 'high' field remanence behaviour. A Trilec pulse magnetometer was used to impart an electromagnetic field. The Trilec can generate fields between 0 and 8 T. The initial approach used was to apply a field and measure the remanence immediately using a Molspin fluxgate spinner magnetometer. This was found unsatisfactory since the relaxation time was initially very rapid. The dominant factor effecting the variability between samples was the time between imparting the field and measuring the IRM.

Tests for viscous loss of remanence were carried out. It was established that loess and especially palaeosols suffered significant viscous loss so the effect of variable relaxation time between loess and palaeosol horizons was removed by imparting the field and then leaving the samples for 24hrs to relax before measuring the IRMs. This results in the contribution of stable remanence carrying grains being measured. This method combined with regular calibration, resulted in more consistent results. Three fields were imparted 1T (SIRM), -0.02 T and -0.3 T. Data was corrected for mass and IRM/SIRM ratios calculated and converted into percentages of soft or hard material present.

3.3.5. Preparation of Particle Size Fractions for Vibrating Sample Magnetometer (VSM) Measurements

Detailed analyses of remanence properties of selected bulk and particle size fractions of loess samples were carried out. Bulk loess samples of 0.650g were placed into small plastic holders and packed tightly with cling film. In order to perform hysteresis analysis on the coarse >63 μm, 63 – 40 μm and <40 μm fraction selected bulk samples were wet sieved. Approximately 60g of loess material was mixed with 500ml double distilled water and sieved roughly at 63μm. The >63μm fraction was then placed in an ultrasonic bath for 3 minutes in a 0.5 % Calgon solution and re-sieved; the > 63 μm fraction was then amalgamated with the previously removed coarse residue.

The < 63, 40 – 63 and <40 μm fractions were centrifuged to remove the majority of the calgon solution. These fractions were also placed in an ultrasonic bath for 3 minutes and re sieved. All fractions were then oven dried at a low temperature (40° C to avoid oxidation). Dry samples were packed into 0.5g plastic pots with cling film for VSM analysis.

3.3.6. VSM analysis of Selected Samples

The remanence properties of selected samples were measured in greater detail using a Molspin Nuvo vibrating sample magnetometer (VSM). The VSM can generate fields between +1 and –1 T at intervals of 0.1 mT intervals. The VSM was calibrated using a palladium sample of 31.23 Am^{-1} volume magnetisation. Selected fields were applied and the in field magnetisation of the sample was recorded. The field then reduces to 0.1mT and the remanence magnetisation of the sample recorded.

The pre-selected fields applied were 0.1, 5, 10, 20, 80, 100, 300, 1000, -10, -20, -80, -100 mT. Parameters gained from results were low and high field susceptibility, IRMs, in field magnetisation, Ms and derived ratios again used to discriminate between magnetic material. In order to characterise samples, percent ferrimagnetic and paramagnetic susceptibility using low (χ_{low}, $10^{-6}m^3kg^{-1}$, approximately equivalent to χ_{LF}) and high (χ_{high}, $10^{-6}m^3kg^{-1}$) susceptibility were calculated. χ_{high} is measured as the slope of the hysteresis loop between 800 and 1000mT, and indicates the susceptibility of the paramagnetic

component. The mass specific component of ferrimagnetic material, χ_{ferri} ($10^{-6}m^3kg^{-1}$) was calculated from the difference between χ_{high} and χ_{low} susceptibility.

3.4. Particle Size analysis

3.4.1. Introduction

The particle size distribution of consecutive 2 cm interval samples from units 2, 3, and 5 was determined using a Coulter LS 130 laser diffraction particle size analyser. The methods used to determine the preparation technique for particle size analysis using the Coulter LS130 are reviewed in detail in chapter 4. This section gives a brief description of the principles of laser diffraction analysis and the configuration of the LS130 Coulter and the preparation technique used to analyse this suite of loess samples.

3.4.2. Laser Diffraction Particle Size Analysis

The technique is based on the principle that a particle of a given size will diffract light through a known angle. The size of this angle increases as the size of a particle decreases. The Coulter LS130 uses a laser light source to measure larger particles, 0.4 - 900μm and a white light source to analyse fine particles 0.1 - 0.4μm (PIDS). The Coulter is able to define 72 particle size 'bins' between 0.4 - 900μm. The distribution of the scattered light is converted to a particle size distribution using the Fraunhofer theoretical model. The software uses an algorithm and displays the results graphically as volume % against particle size for each sample.

3.4.3. Preparation method

An air-dried loess sub-sample of 1.5g was placed in a 50ml screw top pot, 25ml of fresh sodium hexametaphosphate (0.5% concentration) was added and the sample sealed and shaken overnight at 170 rpm on a shaker table. Since there was very little organic matter present in the Caoxian loess, H_2O_2 treatment was deemed unnecessary, but as a precaution, a 710 μm sieve was placed over the fluid module to prevent the addition of any roots etc. Immediately prior to analysis the sample was ultrasonically dispersed for 3 minutes. In order to achieve the addition of a representative sample to the fluid

module of the Coulter, the sample was rinsed into a baffle cup, again using 0.5% sodium hexametaphosphate solution and agitated vigorously. A 4ml sample was removed from mid depth and mid radius of the cup by pipette and added to the fluid module through a 710 μm sieve placed over the fluid module opening. The Coulter determines the concentration of particles added to the module by recording the reduction in light passing through the sample. This is displayed as the obscuration value. A range of 8 – 12% obscuration was required for accurate analysis. The addition of 4ml of loess prepared in the method described generally gave obscuration values of between 9 and 11%. The sample was suspended in filtered water in the fluid module and pumped around the lens for 63 seconds. The pump speed was set at 100% and the particle size distribution of the sample was determined using the Fraunhofer optical model (see Chapter4)

Each sample was analysed once. A control sample of Caoxian Malan loess prepared with each batch was analysed in order to monitor any changes in the Coulter operation or sample preparation.

The software produces a file for each sample containing the volume percentage of particles in each particle size 'bin'. The data were combined into particle size windows <4, 4-16, 16-32, 32-63, 63-90, 90-125, 125-250, >250μm, and phi interval windows (0 - 13φ). Metric statistical parameters of each distribution, mean (μm), median (μm), standard deviation, skewness, and kurtosis were also calculated automatically.

3.4.4. Statistical analysis

Frequency distribution plots of the whole section showed that results were not normally distributed. Subdivision of the section into 5 discrete units, based on field descriptions and repeat frequency distribution analysis showed that this approach allowed horizons to tend towards a normal distribution. The normality of the distribution variables was assessed individually for the depth units 6-16 m (split into 6-3 m and 13-16 m) 16-26 and 35-43.5 m. The variability of parameters was described by parametric statistical tests. Initial statistical analysis was carried out in order to determine the significance of the differences between the three main stratigraphical horizons, Units 2, 3, and 5.

One way ANOVA tests were used to evaluate the variability within and between data. The F factor in a single factor ANOVA analysis was used as the measure of the significance of the differences among the means of the classes under investigation. If F is large enough the differences among the means are too great to be explained by sample error.

3.5. Particle Size Distribution Curve Fitting

3.5.1. Introduction

The difficulties of relating the particle size distribution to a particular sedimentary environment have been widely discussed in the literature. The use of a large number of summary statistics may not help in an interpretation. Consequently, particle size distribution analysis appears to have become considered as inadequate for this purpose. The majority of papers regarding loess concentrate on the mass or volume percentages of a particular particle size window or ratios of fractions that are assumed detrital or pedogenic in nature. Very little attention has been paid to the shape of the particle size distributions, and how those characteristics may reflect the erosional, depositional or pedogenic environment. It is generally assumed that aeolian particle size distributions can best be described by a normal or log normal (LN) distribution, most likely with a positive skew. Researchers (Mclaren and Bowles, 1985) have noted progressive changes in textural parameters along an aeolian transport path. It has been suggested that parameters such as mean, sorting and skewness follow trends that identify the direction of transport, the sedimentary process of winnowing, selective and total deposition. Mclaren's (1981) model suggested that transported sediment must be finer and better sorted and more negatively skewed than its source sediment. The lag sediment must become coarser better sorted and more positively skewed. Successive deposits may be finer or coarser but must be better sorted and more positively skewed. They found that sequential deposits may become either coarser, better sorted and positively skewed (high energy) or finer, better sorted and more negatively skewed (low energy) with a decreasing energy regime. Sequential coarse sediments can not become continuously coarse due to the waning energy of the transport mechanism, so eventually the characteristics will be those of a low energy environment. The results of particle size analysis

of unweathered material should be reflected in relative changes of distribution found in interrelated sedimentary deposits.

Having established statistically that loess and palaeosol differed significantly from each other, it was considered reasonable to attempt an assessment of particle size distribution shape. The orthodox method is the method of moments to define skewness and kurtosis; both of these are heavily dependent on the coarse and fine tails of the distribution.

One school of thought states that the tails are the most sensitive indicators of a sediment's depositional environment (Barth, 1984). Another school suggests the tails are unreliable because they reflect different depositional mechanisms (Folk and Ward, 1957; Inman, 1960). The method of moments should only be used when the whole distribution has been determined and it is not suitable for an open ended distribution (Barndorff-Nielsen, 1982). The use of the method of moments on an open distribution will artificially close it and introduce errors. It is generally accepted that the tails of a distribution have a disproportionate effect upon the statistical measures derived. Geometric or arithmetic statistical methods use the central percentiles and not the whole distribution to derive descriptive parameters. Metric parameters only describe the distribution between the third and first quartiles, thus reducing the influence of the tails. A drawback is that parameters calculated from metric quartiles are particle size dependent (expressed in mm). Geometric analyses are size independent. Parameters can cover either 68% (Inman, 1960) or 90% (Folk and ward, 1957) of the distribution and parameters such as the mean are independent of sorting.

For open-ended distributions or those where the origin of variations in the tails of the distribution can not be adequately accounted for, Inman's 68% coverage may be preferable. However, some workers suggest that processes which dictate distribution skewness are partly dependent on particle size, increasingly negative skewness being associated with progressively finer particle sizes (Pye, 1982), the reason for this relationship is not clear, but clearly has implications for the use of skewness however it is calculated.

Combined archaeological and statistical studies of sedimentary proxies of climate change in cave dwellings of mid to late Devensian age showed that the methods outlined above were unable to discriminate satisfactorily between

closely related sedimentary environments (Fieller et al, 1988). It has been suggested that PSD may be better described by a log hyperbolic (LH) curve. This approach is widely used in coastal geomorphology for the distinction of beach and aeolian dune environments. In order to use this approach a suitable model distribution must be ascribed to the 'real' particle size distribution. Bagnold and Barndorff-Nielsen (1980), Barndorff-Nielsen et al, (1982; 1983), state that a LH distribution is the best description of the particle size distribution and provides better summary statistics than a normal distribution. An important reason according to Barndorff-Nielsen (1982) was the poor agreement that the extremes of the distribution show with the LN model. Recent papers (Hartmann and Christiansen, 1992) have also shown that aeolian particle size distributions can be better described by LH than LN models. A useful element of LH models is that sedimentary erosion or deposition leaves a textural fingerprint expressed over a continuum of skewness and peakedness (similar to kurtosis).

An investigation of the benefits of LH over LN with respect to desert dunes in Australia was carried out by Wyrwoll and Smyth (1985). The analysis was applied to data retrieved by sieve analysis. It was noted that sieve analysis is dependent on particle shape (as is laser diffraction analysis). This may contribute to tails i.e. tails may be just as much an artefact of the measuring technique as of the aeolian sorting mechanism. Wyrwoll and Smyth (1985) found that for the time and effort expended in applying a LH, the differences and precision (errors) were only apparent at the tails of the distributions. In summary, they found that in the case of pure aeolian sands there was no advantage of LH over LN models. The aeolian sands analysed were well sorted and uniform in contrast. Loess however, has a much wider, less well sorted distribution. In such a case, the discrepancies between the model LH and LN curves are expected to be more significant.

LH modelling has had inherent problems due to programming instability. Computer programs (e.g SAHARA program by Hartman, 1980; Shefsize 1, Fieller, 1984) may be applicable only to the sediment for which they were designed and are not easily adapted for others sediments. Shefsize version 1a (Robson Sheffield University) has been revised to limit the possibility of different PCs giving different results for the same data set. Although not perfect

Shefsize 1a appears to be an improvement on Shefsize 1 and SAHARA programs, i.e. greater stability with very few samples failing to be modelled.

Fitting LH curves is a lengthy process even with a P.C. In the original Shefsize program, a potentially infinite number of iterations existed to define the δ_{LH} parameter (distribution curvature), which causes instability of the program. This frequently resulted in a LH curve not being fitted at all, with a 35 % failure rate (Fieller, 1988). The new Shefsize 1a program has a limited number of iterations for defining the position of δ_{LH} parameter. If δ_{LH} approaches zero i.e. limited curvature, a Log Skew Laplace (LSL) curve is fitted instead of a LH, a limiting case of LH distributions. LSL distributions are described by 3 parameters (α_{LSL}, β_{LSL}, μ_{LSL}) as opposed to 4 for LH (ϕ_{LH}, γ_{LH}, μ_{LH}, δ_{LH}). Manipulation of LH and LSL parameters allows for an assessment of skewness and degree of sorting.
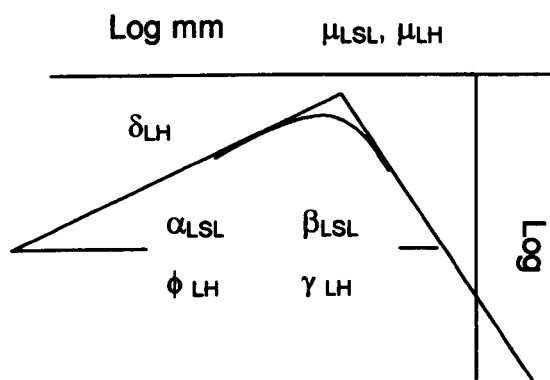
Figure 3.3 schematic representation of LH and LSL parameters

Log Skew Laplace

α_{LSL} – reciprocal of the tangents of the acute angle of the fine fraction (relative abundance of fine fraction)

β_{LSL} - reciprocal of the tangents of the acute angle of the coarse fraction

μ_{LSL} - the point of intersection of the two lines on the abscissa related to modal value. α/β = skewness, $\alpha^2 + \beta^2$ = sorting

Log Hyperbolic

ϕ_{LH} - relative abundance of fine fraction

γ_{LH} - relative abundance of coarse fraction

μ_{LH} - the point of intersection of the two lines on the abscissa related to modal value

δ_{LH} - statistical representation of the degree of peak curvature.

101

Measures of how much a LH fits better than a LSL are $Ncrit_{LH}$-$Ncrit_{LSL}$, also δ; if $\delta = 0$ then the LH reduces to a LSL. In such a case, one would expect that $Ncrit_{LH}$ - $Ncrit_{LSL}$ would also be large. μ_{LSL} is a good summary descriptor of the sample (if the LSL is actually a good model), and values should correspond closely to the modal size class. However, this isn't necessarily true of μ_{LH} (even if LH is a better model than the LSL for the distribution). As the point of intersection of the coarse and fine asymptotes, it can fall outside the size range of the whole sample. This will happen in particular if one arm is very shallow and the other one is quite steep. It can be a useful descriptor i.e. scatter plots using it will show some environmental coherency, but only if the two arms of the distribution are comparable slopes.

Statistical tests of goodness of fit of the model curve rely on knowledge of the population size i.e. number of particles involved. Coulter data is presented as volume percentages not frequency so this could not be carried out. However, within the Shefsize 1a program a parameter called Ncrit can be derived, based on the number of iterations required to define the LH or LSL model i.e. time and standard deviation of factors and number of parameters defined (3 or 4). This allows an estimate of whether it is worthwhile fitting the LH for the extra information gained and the potential inherent errors involved in LH modelling. A lower value of Ncrit indicates a poorer fit. However since Ncrit is related to minimum χ^2 criteria it is possible that maximum likelihood estimates and minimum chi squared estimates may be different. The Ncrit parameter was derived for use on distributions with a known number of particles. If Ncrit values exceeded the number of particles, Fieller et al concluded that neither model was a poor fit. Ncrit has been shown to be so sensitive that distinctions can be made between individual peoples laboratory techniques.

The usefulness of the model curve parameters depends on the purpose for which they are to be used. Studies comparing LN and LH have stated preferences for one or other when applied to various environments. Since LSL curves are a relatively recent development no precedent has been set for this method. To the author's knowledge particle size distribution modelling has not been applied to loess deposits from NW China. Difficulties of interpretation will

arise due to incomplete understanding of the transport mechanisms and the effects of sediment availability and supply at the margins of the loess plateau. Nevertheless, it appears that this approach has the potential to give an additional insight into changes in the depositional history of the loess plateau.

3.5.2. Curve fitting method

The particle size distribution for each sample analysed by laser diffraction was described by 13 particle size windows, phi intervals 1-14 expressed in mm. LN, LSL, and LH curves were fitted using the predefined equations of the Shefsize 1a program. Descriptive statistics were generated in terms of μ_{LN}, σ_{LN}, α_{LSL}, β_{LSL}, μ_{LSL}, ϕ_{LH}, γ_{LH}, δ_{LH} and μ_{LH}.

3.6. Energy Dispersive X-ray Fluorescence Spectrometry

3.6.1. Introduction

XRF analysis was carried out on a group of samples from the zone of transition from Unit 3 to 2, in order to qualify the elemental variability. Energy dispersive XRF (EDXRF) is simple, rapid and non-destructive. The method can be used to give results more quickly than alternative x-ray emission techniques such as wavelength dispersive XRF. However, EDXRF is relatively less sensitive and prone to some instability if operating conditions are variable. EDXRF can establish the presence of elements qualitatively and to an extent quantitatively.

Primary x-rays from a radioactive x-ray source cause a sample to emit x-rays characteristic of the elements present. The fluorescence is produced when an inner shell electron is knocked out of a molecule by the primary x-ray and an electron from another shell falls into the shell. X-rays produced from specific elements are well defined. The detector converts the energies of the x-ray into electrical pulses. The source can only excite characteristic x-rays if its energy is greater than the absorption energy of the particular element. It is the choice of source limits the elements that can be defined.

The Metorex SSPS 2467 was used for analysis of Caoxian loess samples. This is a solid state probe set that uses a silicon lithium (Si (Li)) drifted detector (as opposed to a gas filled detector). The probe is connected to an X-met electronic analyser and controlled by MS-DOS software. In order to

operate the detector it must be cooled with liquid nitrogen. The excitation sources used were Cd – 109 and Am – 241. The SSPS probe has a better energy resolution than a gas filled detector, and therefore it can resolve x-ray peaks from neighbouring elements in a spectrum such as Mn, Fe, Co, etc. Also the spectra produced are characterised by narrow peaks with limited overlap, hence limiting the errors of measurement and improving detection limits.

3.6.2. Sample preparation

Clean sample cups consisting of a ring to hold the plastic film base in place and a snap on plastic collar to secure the plastic film to the cup, were filled to a depth of 4 – 5 mm. This depth is dictated by the thickness required to attenuate the X-ray intensity to 99%, also known as infinite thickness. The infinite thickness depends on the source and the chemical nature of the sample i.e. a Cd – 109 source and a predominantly quartz material has an infinite thickness of 4.8 mm. In the case of loess, the sample is naturally fine grained and homogeneous so grinding was unnecessary. Every effort was made to keep the measuring side of the cup clean. The resulting spectra must be corrected for the influence of organic material. LOI results showed that the organic content of Unit 2 was less than 0.2% and hence defined as negligible.

3.6.3. EDXRF measurements

Liquid nitrogen was added to the probe and left to cool for 30 minutes. Then the machine was calibrated. The X-met compares the signal strength of an unknown sample (loess in this case) with those obtained from known standards. The calibration sample must be representative of the unknown sample to be analysed. After calibration the known samples are used to monitor the operating conditions of the analyser. Two known standard samples were used when running the loess samples and each was re-measured after each batch of 10 loess samples. After analysis the spectra generated was viewed, so spurious results from samples could be removed and re-measured. Relative values for each element were defined from the spectra.

4. Investigation and Refinement of Existing Preparation Methods for the Analysis of Loess Particle Size

4.1. Introduction

Parameters derived from particle size distributions of loess have become widely used as proxies for the strength of the winter monsoon. This chapter is concerned with the implications of preparation of samples prior to PSD analysis for the reliability of particle size as a winter monsoon proxy. As mentioned in Chapter 2 many environmental factors influence the size and distribution of the loess in China and the influences of the majority have not been quantified. However, one may assume a degree of continuity or gradation of environmental influences within and between sites. Therefore, it is reasonable to estimate their effect quantitatively with respect to the climate gradient, so long as laboratory preparation of the samples is consistent.

The analysis of the PSD of loess has been carried out using a variety of techniques, and studies of the comparability of results has been published by Beuselinck et al 1998; Buurman et al 1997; Chappell 1998; Styvitski 1991; Konert and Vandenberghe 1997; McCave et al 1986; Singer et al 1988; and Stein 1985, amongst others. In contrast to magnetic susceptibility analysis, particle size analysis does not follow an established method. A fundamental problem is that several analytical techniques are in use e.g., those based on X-ray attenuation Sedigraph, electroresistance - Coulter counter, laser diffraction etc. These techniques have several advantages over sieve and pipette analysis. They cover a wide range of particle sizes, require small samples and have a relatively short analysis time. This coupled with a variety of preparation methods makes comparisons of high-resolution records difficult.

4.1.1. Instruments used for the analysis of Particle Size.

Devices used for particle size analysis include sieve and pipette, particle counter, Sedigraph, and laser diffraction analyser amongst others. Particle size analysis using sieving and pipette analysis is time consuming and not suitable for the analysis of numerous down core samples (Allen, 1981; Konert and Vandenberghe, 1997). Automated analysis is much more suitable for determining the PSD of a large number of samples. Particle counters measure

the number and volume of particles in an electrolyte. The resulting resistance patterns are related to the resistance values of known volume spherical particles (Stein, 1985). This method of mechanised analysis has been largely superseded by Sedigraph and Laser Diffraction analysis (Buurman et al, 1997). The Sedigraph determines the size distribution of particles using Stokes' Law, (McCave et al, 1986). It measures the attenuation of an X-ray beam as a function of time and height in the settling suspension. Absolute size data in the sub-micron range from the Sedigraph is dubious and it is suggested that the lower limit for gravitational settling methods is set at 1μm (Singer et al, 1988). The laser diffraction analyser uses the angular distribution of forward-scattered light to infer the size distribution of particles suspended in fluid. The majority of published particle size analysis of loess has been carried out on one or other of these machines. The following section discusses the laser diffraction analyser and the operating method used in this research.

4.1.2. Laser diffraction analysis, Coulter LS130

Several manufactures produce laser diffraction analysers, Malvern U.K, Fritsch Germany, and Coulter Inc. USA. Analysis of the Caoxian loess was carried out using a Coulter LS130. Fig 4.1 illustrates the machine's optical configuration. The process involves a laser being deflected by a spherical particle of a particular diameter, and that particle produces a characteristic diffraction pattern on the detectors (figure 4.2). The detectors are arranged in such a way that a small particle is registered at high angle detectors and a large particle at low angle detectors. When a 'real' sample is analysed the light distribution pattern or flux is the sum of the diffraction patterns for the whole particle population. The LS130 has 126 detectors i.e. it can pick out a relatively highly resolved pattern. In contrast, the Malvern laser analyser only has 56 detectors, and the resulting distribution pattern is less well resolved. A laser diffraction analyser with limited detectors is unlikely to interpret bimodal or narrow distributions successfully due to the low detector interval smoothing effect.
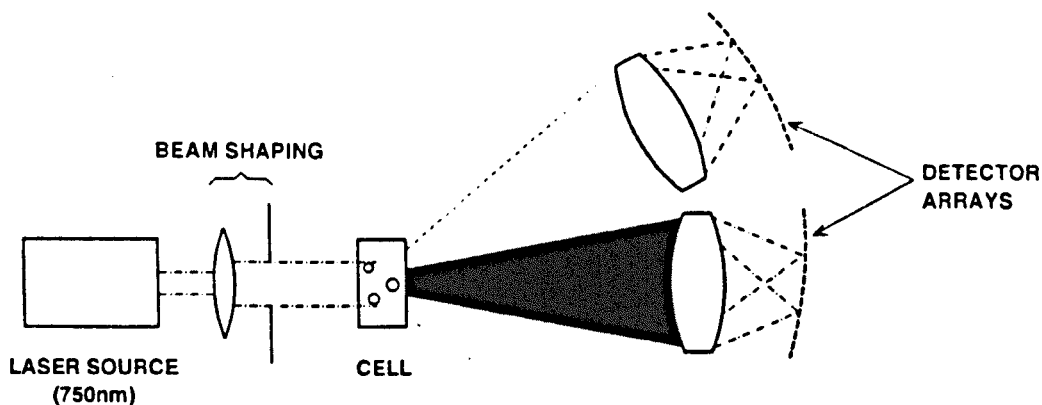
Figure 4.1 The optical configuration of the Coulter LS130

The Coulter laser diffractometer is also an improvement over the Malvern series since it uses a single lens to determine the whole particle size distribution. The Malvern has a series of three lenses with various focal lengths for particular particle sizes; the result from the three lenses can not always be successfully combined (Clifton, 1998).

The Coulter Laser diffraction analyser is set up with a 'beam dump' at the centre of the detectors. The beam dump is directly in line with the laser, and this is where all unaffected light falls. The LS130 uses a laser source of 750 nm wavelength light to recognise particles between 0.4 - 900µm and a white light source for fine particles of 0.1 - 0.4µm (PIDS system). The diffraction pattern is displayed on screen during analysis as a graph of ray intensity at each detector (fig 4.2). Subsequently, the LS130 uses an optical model to match the diffraction pattern to those formed by known particle sizes using an algorithm, and displays the results as a graph of volume % against particle size. The Coulter defines 72 particle 'bins' between 0.4 - 900µm, corresponding to an interval of 0.155ϕ ($\phi = -\log_2 D$, where D is the diameter in mm). When Fraunhofer and PIDS are used together the number of bins increases to 100 covering the whole potential range of 0.1 - 900µm.

The standard optical model used by the LS130 is Fraunhofer theory. The calculations only use the distribution of diffracted, forward travelling light although some will be refracted and reflected. The program also assumes that the diameter of the particles is larger than the wavelength of the light source

107

(750 nm), and is therefore suitable only for particles whose diameter is larger than this. Fraunhofer theory assumes that all light is forward travelling, but this is problematical since refracted light falling on a high angle detector is interpreted as diffracted light from fine particles (Coulter LS130 Operator Manual). This results in an overestimation of the quantity of fine particles sometimes up to 20%. In the distribution pattern this refracted light may be represented as bump in the distribution at ~ 0.75 - 1μm size. In samples where this is apparent, the distribution may be improved by recalculating using a more specific optical model (i.e. altering the Fraunhofer model by using a specific density more relevant to the material being analysed.

Mie theory, modified by Wiscombe (1980) is generally thought most applicable to particles less than 15 μm. However, comparisons of fine material analysed by laser diffraction and interpreted by both Fraunhofer and Mie theory, found Mie theory relatively suppressed the fine tail volume %, when compared to pipette results (Konert and Vandenberghe, 1997). Loizeau et al, (1994) concluded that Fraunhofer theory detects a significantly higher proportion of the clay than Mie theory (applied when using the PIDS system). It was also shown that Fraunhofer rather than Mie theory was better suited to non-spherical fine particles, when compared to orthodox pipette results. Jonasz (1991) showed that the projected area of a non-spherical particle, averaged by orientation, is larger than that of a true sphere. Consequently, coarser results are expected from laser diffraction analysis using Fraunhofer, than from sieve analysis (Styvitski et al, 1991). Konert and Vandenberghe (1997) concluded that the 8 μm of the laser is a good average corresponding with the 2 μm of the classical pipette analysis (on a Fritsch A22 laser diffraction analyser, using Fraunhofer theory), a conclusion based on extensive analysis of Dutch Quaternary aeolian and fluvial material.

4.1.3. The Bench Set-up

The LS130 at Liverpool University uses a fluid module. The water that feeds the fluid module comes from a storage tank and passes through two filters. The filters provide clean water as the suspension fluid in the module. The volume of the fluid module is 1.7l. Two pipes connect the optical and fluid
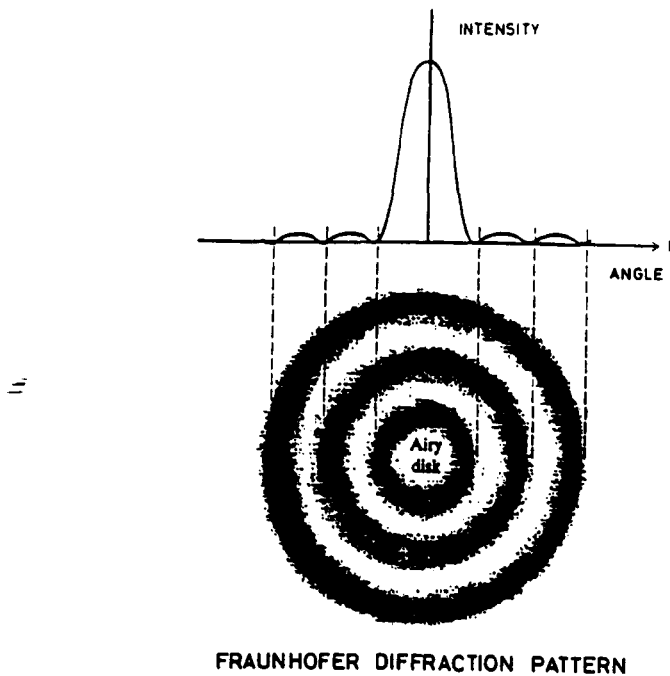
Figure 4.2 The concentric ring pattern of forward scattered light known as the Fraunhofer pattern. Angle and intensity is highly resolved due to the 126 detectors.

modules, allowing the suspension fluid to flow between the fluid module and sample cell in front of the laser in the optical module. The sample is added manually to the fluid module and the pump induces turbulent flow in the suspended sample. The speed of the pump is variable. There is also an option to sonicate the sample whilst it is in the fluid module. The optical module containing the laser is P.C. driven by a windows program, LS Coulter.

4.1.4. Previous published preparation techniques

Assessment of the most suitable fluid for suspension and most effective method of dispersion are a critical part of this preparation review. One of the largest sources of variability is the presence of aggregates. Particle size distributions may differ significantly with and without dispersion (Allen, 1981). Full dispersion is important with respect to certain physical and chemical soil properties (Medvadev, 1996). Other processes, such as wind transport may be

much more dependent on the size distribution of aggregates (Beuselinck et al, 1998). Dispersion prior to analysis is necessary to prevent dispersion to a variable extent during analysis. Due to the large variation in soil type there is no standard method of dispersal. Dispersion was assessed using the measure of obscuration in the laser cell.

Preparation techniques may be divided broadly into two categories. Those which leave, or intend to leave, the material essentially unchanged from the in situ state and those which attempt to return altered material to its 'primary' state, e.g. by chemical treatment to remove secondary carbonate and organic material.

The simplest preparation method is to add water to a quantity of sample. The use of dispersant and agitation is likely to improve dispersion (Chappell, 1998). The next progression is to subject the sample to ultrasonic dispersal, prior to analysis. Thereafter comes chemical treatment, usually the use of hydrochloric or acetic acid of various concentrations, to remove carbonate and hydrogen peroxide to remove organics. Lanzhou, Xian and Beijing laboratories use a preparation method combining all these techniques.

In recent publications particle size used as a winter monsoon proxy, has been recorded in terms of

1. Quartz fraction only (Xiao et al, 1995; Porter and An, 1995). It is accepted that the primary loess dust is dominated by resistant quartz. Pedogenic material, organics, clays and carbonates were removed by chemical treatment. The maximum and median quartz particle sizes were used as proxies of wind strength. Removal of the fine clay mineral particles and carbonates formed during pedogenesis means that parametric curve fitting cannot be done, since the full distribution is not considered.

2. Alternatively the samples may be treated with hydrogen peroxide and hydrochloric acid to remove only the 'organic and inorganic polluting materials like humus and carbonate' (An Z pers comm). Such treatment will remove primary carbonate material. It has been shown that primary carbonate is concentrated in the fine fraction. This procedure is likely to alter specific particle size fractions but be reflected in the mean or median of the PSD as a whole.

3. Samples may be dried, disaggregated, and dispersed in a wetting agent in their 'natural' state. Kemp (pers comm) uses a similar approach, but with removal of organic material using hydrogen peroxide. PSD retrieved using this preparation method are heavily influenced by any pedogenic signal.

Numerous representations of the results have been used in studies of particle size in Chinese loess. Simple graphs of mean, mode, or median particle size against depth are probably the most common. The arithmetic mean is unreliable because it is affected by the distribution. The geometric mean is less affected by extremes of population. The mode or maximum point on the distribution curve is frequently used. The most popular is the median or fiftieth percentile that is less affected by the distribution. More elaborate methods of displaying the results have been used. Ding et al (1995) used the ratio of the two most variable fractions of the Baoji loess i.e. $< 2\ \mu m\ /\ > 10\ \mu m$ sizes applicable to fine loess regions in the south of the plateau. The fraction between $2 \mu m$ and $10 \mu m$ was assumed to be that formed during pedogenesis. Another simple representation was 'the percentage greater than ...' varying with depth. In Luochuan $\% > 20\ \mu m$ was used, in Lanzhou the $\% > 40 \mu m$ was used. The choice of descriptive parameters appears somewhat arbitrary. It is also noted that mechanised methods of particle size analysis produce results in the form of percentages not numbers of particles. Consequently, an apparent increase in one particle size fraction will result in the relative decrease in another. Ratios of such interrelated fractions are not used in this study. However, $> 40\ \mu m$ % is used for comparison between sites

4.2. Method

4.2.1. Introduction

The following results and discussion cover how the best and most efficient run set-up was established and if and how the changes caused by each step in the preparation programme affected the distribution.

A series of experiments was designed to assess the impact of various stages in particle size preparation. Unless otherwise stated experiments were carried out using the control sample, which was subsequently used as a standard during the down core high-resolution analysis of the Caoxian section.

A large amount of sample, approximately 2 kg from an intact block (14m depth Malan loess, L_1L_1) was broken up by hand and homogenised by stirring and separated and re-combined using a riffle box to make the control batches. The method for each experimental set is described below.

4.2.2. Dispersant Concentration: initial study

Initial tests were carried out some time before the rest of the experimental tests and comprised twelve 2g sub-samples from a depth of 5.5 m. Loess powder was placed in 50 ml plastic screw top jars with sodium hexametaphosphate. Concentrations of, 0.5, 1, 5, 10% were used with three repeats of each concentration being prepared. The samples were left overnight on a shaker table. Samples were analysed using the LS 130 by the Fraunhofer model only.

4.2.3. Preparation set 1: Dispersant

Set 1a: six sub-samples of the loess control sample, weighing approximately 2g, were placed in 50ml plastic screw top jars. 25ml of double distilled water was added to wet the samples. The jars were shaken by hand for a minute and then rinsed into a baffle cup. 4 ml was removed from the baffle using a pipette and added to the fluid module giving an obscuration of approximately 9%. Each sample was run through the instrument once.

Set 1b: as in 1a above except the samples were shaken on a shaker table overnight.

Set 1c: as in 1a except samples were subjected to ultrasonic dispersion for 3 minutes immediately prior to measuring.

4.2.4. Preparation set 2: Mechanical agitation

Set 2a: as in 1a above except the samples were wetted using 0.5% Calgon instead of double distilled water.

Set 2b: as in 2a but samples in a 5% Calgon solution were shaken overnight before analysis.

4.2.5. Preparation set 3: Ultrasonic dispersal

Set 3a: as in 2b except after overnight agitation and before measuring the samples were subjected to 3 minutes of ultrasonic dispersion.

Set 3b: as in 3a except the period of sonic treatment was extended to 15 minutes and to 30 minutes for two extra samples.

4.2.6. Preparation set 4: Aliquots

Set 4: Samples of 0.25, 0.35, 0.5, 0.6, 0.75 and 1g where taken and placed in screw top jars and 25ml of 0.5 % sodium hexametaphosphate added. Samples were placed on a shaker table overnight. Prior to analysis, the samples were placed in the sonic bath for 3 minutes. Each sample was added to the fluid module in turn and the obscuration reading noted. The module was rinsed between each reading. From this, it was determined that an aliquot of 0.45 g gave the required obscuration of 9%. This procedure was carried out in order to assess the effect of sub-sampling using a pipette. Six aliquots of 0.45 g were weighed into 50 ml plastic jars and 25ml of 0.5% Calgon added. The samples were shaken overnight and subjected to 3 minutes of ultrasonic treatment immediately prior to the entire contents of the jar being added to the fluid module and analysed.

4.2.7. Preparation set 5: HCl

Set 5a: approximately 2g of loess control sample were added to each of six 100 ml glass beakers. 25ml of 0.5% HCl was added and the samples were heated to 70°C for 30 minutes. Then approximately 25ml of double distilled water was used to rinse the samples into 100ml centrifuge tubes. The samples were centrifuged for 15 minutes, rinsed and pH checked. The rinsing procedure was repeated 3 times. 25ml of Calgon was added to the loess pellet and the solution was shaken overnight. Prior to analysis each sample was rinsed into a baffle cup. 4 ml was removed from the baffle cup using a pipette and added to the fluid module. Each sample was analysed once.

Set 5b: as in 5a but the samples were treated with 10% HCl.

Set 5c: as in 5a except consecutive samples (at 2 cm intervals) between the depth of 5 – 6 m in the section were treated and measured. These were

compared to the same set of consecutive samples treated using the method described in 3a.

4.2.8. Preparation Set 6: Particle Shape

Set 6a: A bulk sample was wetted using double distilled water and simply sieved once through a 90 μm sieve. This initial attempt to prepare the coarse fraction for analysis was unsuccessful. The data show that this method gave variable results so the method given in 6b was used. The method was also modified to use a 63 μm sieve in order to generate a larger amount of material.

Set 6b. Approximately 150g of the control sample was wetted using double distilled water and wet sieved at 63μm. The fraction greater than 63μm was dispersed in Calgon then sieved a second time. After ultrasonic dispersal for 3 minutes, the samples were wet sieved at 63 μm for a second time. After a period of settling the majority of the water was poured of and discarded. Due to the extreme dilution during wet sieving the > 63 μm fraction was dispersed in 0.5% Calgon for a second time and placed on a shaker table overnight and sieved again. After the final wet sieving operation the material was oven dried at 40°C. The mass of loess material > 63μm retrieved from the initial mass of 150g was approximately 27g. Aliquots of 3.3 g where necessary to give an obscuration of 9%. Six sub-samples of the coarse fraction were placed in 50 ml screw top jars with 25ml of 0.5% Calgon. The samples were shaken overnight. The entire aliquot was added directly to the fluid module for analysis.

4.3. Results

4.3.1. Introduction

Each distribution was described in terms of mean, median, skewness and kurtosis (using the method of moments) and the results shown in figure 4.3. Variations in volume LT 4, 4-16, 16-32, 32-63, 63-90, 90-125, 125-250μm, > 250μm for each experimental set are depicted graphically in figure 4.4. The volume percentages in each of the particle size windows, less than 4μm, 4-16, 16-32, 32-63, 63-90, 90-125, 125-250, and greater than 250μm were used to monitor which fractions were most affected by each preparation method.

114

Several statistical tests were considered to help define a 'good' preparation method, but it was decided that simple graphical representation was clearest. Although the total population was usually 6 samples and hence too small for a realistic statistical assessment of variability, depiction of results in the form of box charts including depiction of percentiles was chosen. It was decided that these representations showing the PSD of each preparation technique and the range of results of the sub-samples within, was the most conducive to visual analysis. Each particle size is represented as a box in the following charts. The horizontal lines in the box denote the 25th, 50th, and 75th percentile values. The error bars denote the 5th and 95th percentile values. The two symbols below the 5th percentile error bar denote the 0th and 1st percentile values. The two symbols above the 95th percentile error bar denote the 99th and 100th percentiles. The square symbol in the box denotes the mean of the column of data.

4.3.2. Variations in Mean, Median, Skewness and Kurtosis

All distributions have a modal value of 42.6 μm. All distributions show a mid-point (median) bin size of either 32.4 or 29.6 μm. This illustrates that the logarithmic distribution of the size bin results in an insensitive measure of median particle size values, probably due to the logarithmic distribution of bins in the LS Coulter program. The shape or skewness of the particle size distribution affects the mean particle size value (see chapter 2). All distributions are positively skewed. This adversely affects the usefulness of the standard deviation value for each sample since even distribution about the mean of a skewed distribution is assumed. All distributions had a value of kurtosis greater than or approximately equal to 3 (only 3 distributions had a kurtosis value less than 3, lowest value 2.7). Therefore, parametric curve fitting parameters are used as an alternative to skewness and kurtosis, to compare the most likely preparation techniques (fig 4.8).
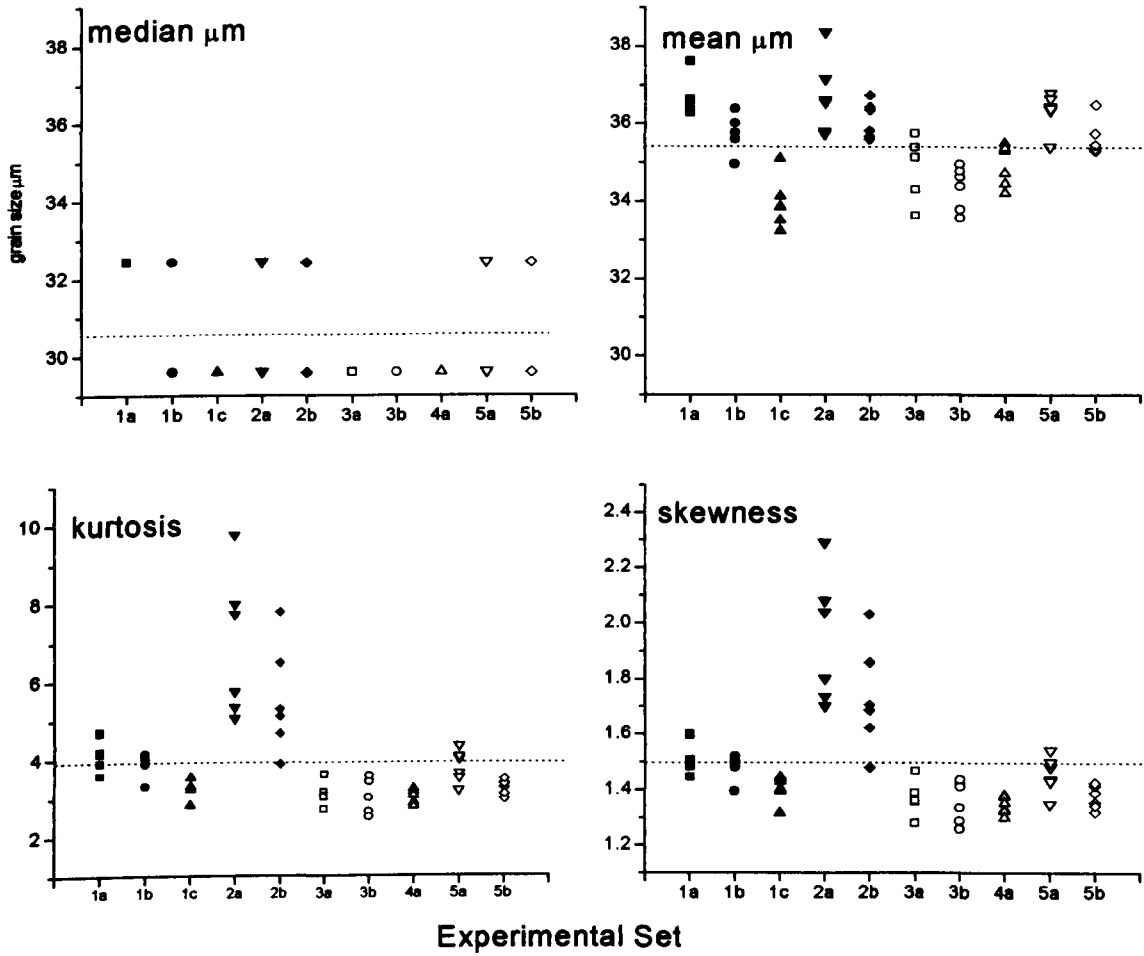
Figure 4.3 The effects of preparation technique on mean, median, skewness and kurtosis (method of moments)

	H_2O	0.5% Calgon	Shaker table	Ultrasonic 3 mins	Other
Set 1a	X				
Set 1b		X			
Set 1c	X		X		
Set 2a		X			green
Set 2b		X	X		yellow
Set 3a		X	X	X	Cyan
Set 3b		X	X	15	magenta
Set 4		X	X	X	Blue ALIQUOT
Set 5a		X	X	X	Red 5 % HCl
Set 5b		X	X	X	black 10 % HCl
Set 5c		X	X	X	5 % HCl 5-6 m
Set 6		X	X	X	> 63 µm

Table 4.1 Summary of experimental preparation techniques
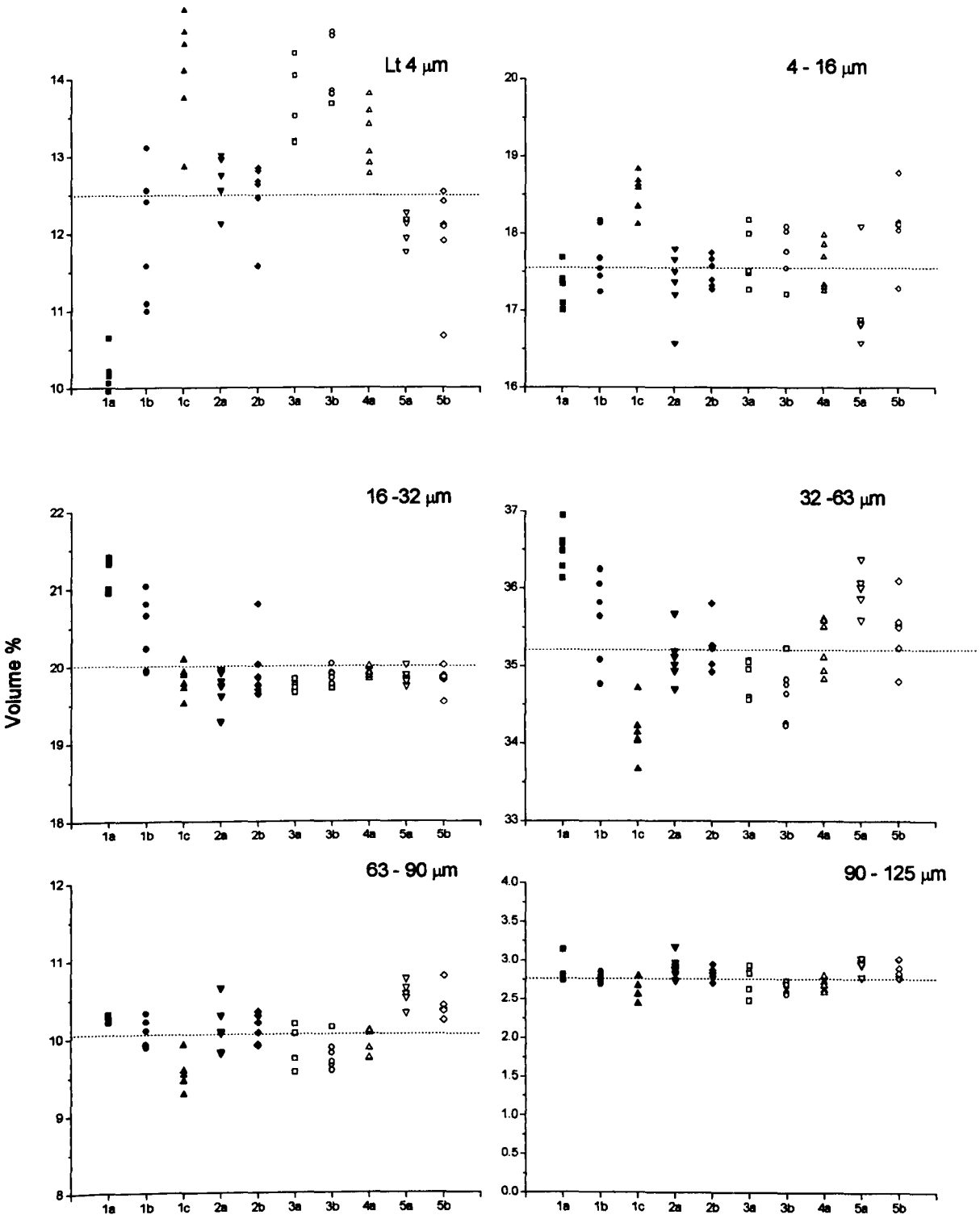
Figure 4.3 The effects of preparation techniques on particle size windows

4.3.3. Results from Set 1: Dispersant

Initial tests were carried out using a sample from 11 m depth not the standard control sample. As a result the actual values are not comparable to those carried out using the control sample. The results are shown in fig 4.4. The range of the values for all the parameters in the initial experiment is much smaller than the range of the results for the 6 experimental sets. This shows that other steps in the preparation method have a greater effect on the distribution than the concentration of the wetting agent. Results for concentrations of 0.5, 1, 5 and 10% are all very similar and there is no obvious trend with increasing concentration. 0.5, 1 and 5% are well grouped; only the results of samples in 10% concentration are significantly more scattered.
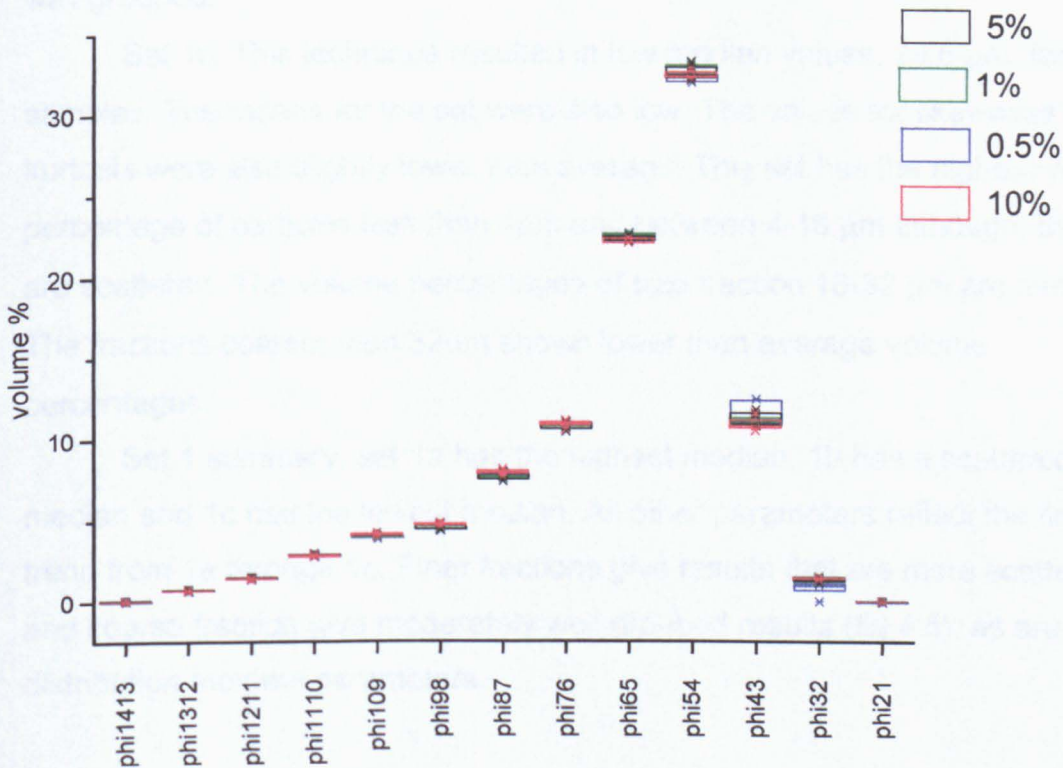
Figure 4.4 The effects of dispersant concentration on the PSD of loess.

Set 1a. This procedure resulted in high median values of 32.4 for all six samples. The means were the second highest of all the experimental sets. The values of skewness and kurtosis were average. The results show the lowest volume percentage of particles less than 4μm and between 4-6 μm but the highest volume percentage 16-32 μm of all sets. The fractions coarser than 32 μm show average volume percentages. Five of the samples were well grouped with one sample outlier.

Set 1b. This technique resulted in variable values of the median for the six samples. The means, skewness and kurtoses were average. The results for particle size fractions less than 4μm are lower than average and the 4-16 μm fractions are average. The 16-32 μm and 32-63 μm fractions are slightly higher than average. The results for the fine fractions are very scattered, making comparison difficult. Fractions coarser than 63 μm are average and moderately well grouped.

Set 1c. This technique resulted in low median values, 29.6 μm, for all six samples. The means for the set were also low. The values for skewness and kurtosis were also slightly lower than average. This set has the highest volume percentage of particles less than 4μm and between 4-16 μm although, the data are scattered. The volume percentages of size fraction 16-32 μm are average. The fractions coarser than 32μm shows lower than average volume percentages.

Set 1 summary: set 1a has the highest median, 1b has a scattered median and 1c has the lowest median. All other parameters reflect the fining trend from 1a through 1c. Finer fractions give results that are more scattered and coarse fraction give moderately well grouped results (fig 4.5), as are the distribution moment parameters.
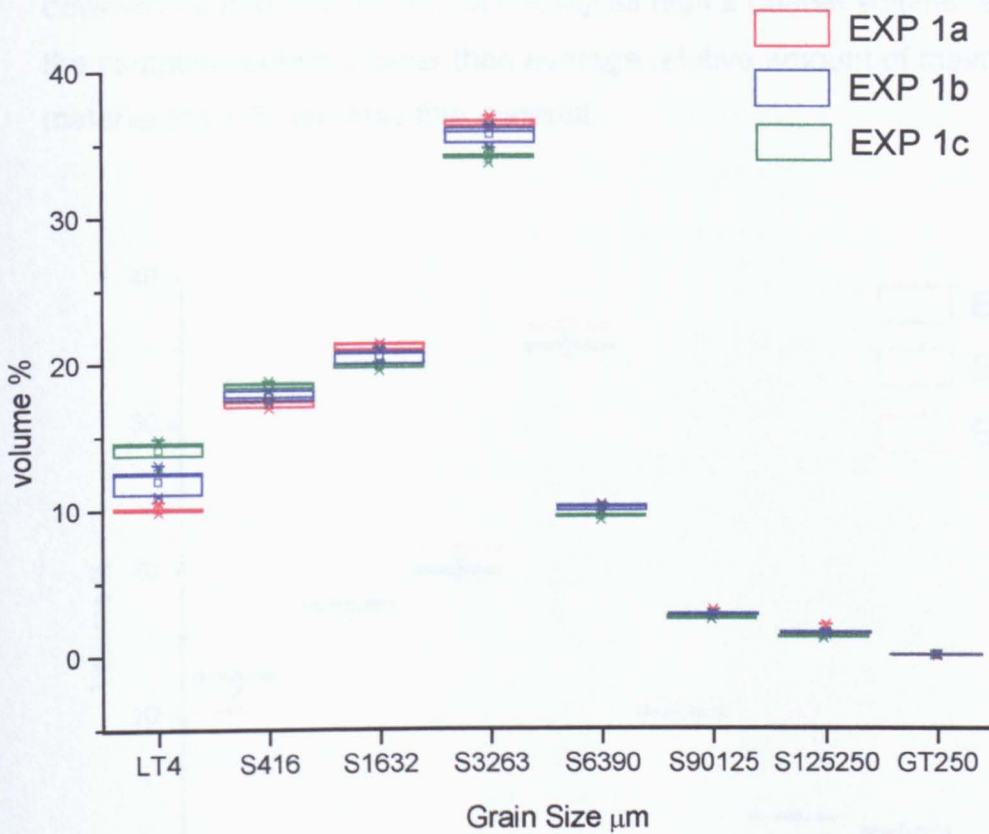
Figure 4.5 The effects of particle dispersal using double distilled water (1A), 0.5% calgon (1B) and 0.5% calgon and ultrasonic treatment (1C)

4.3.4. Results from Set 2: Mechanical agitation

Set 2a. This technique resulted in variable values of the median for the six samples and the highest and most scattered mean, skewness and kurtosis data. The volume percentages of particles less than 4 μm are average but again scattered. Fractions between 4 and 63 μm are slightly below average. The volume percentages of particles in the 63 – 90 μm fraction are average. Coarse fractions between 90 and 250 μm are significantly above average but these results were moderately well grouped. The volume percentages greater than 250μm were higher for this set than others, reaching a small but significant 0.23%.

Set 2b. This technique resulted in variable values of the median for the six samples and above average mean, skewness and kurtosis values that were also scattered, as in 2b. The volume percentages of particles less than 4 μm are average but scattered. Fractions 4-16 and 16-32 μm are average. Fractions

between 32 and 250 μm do not display as high a coarse volume % 2a. Overall the samples contain a lower than average relative amount of mean sized material (fig 4.6) and less fine material.
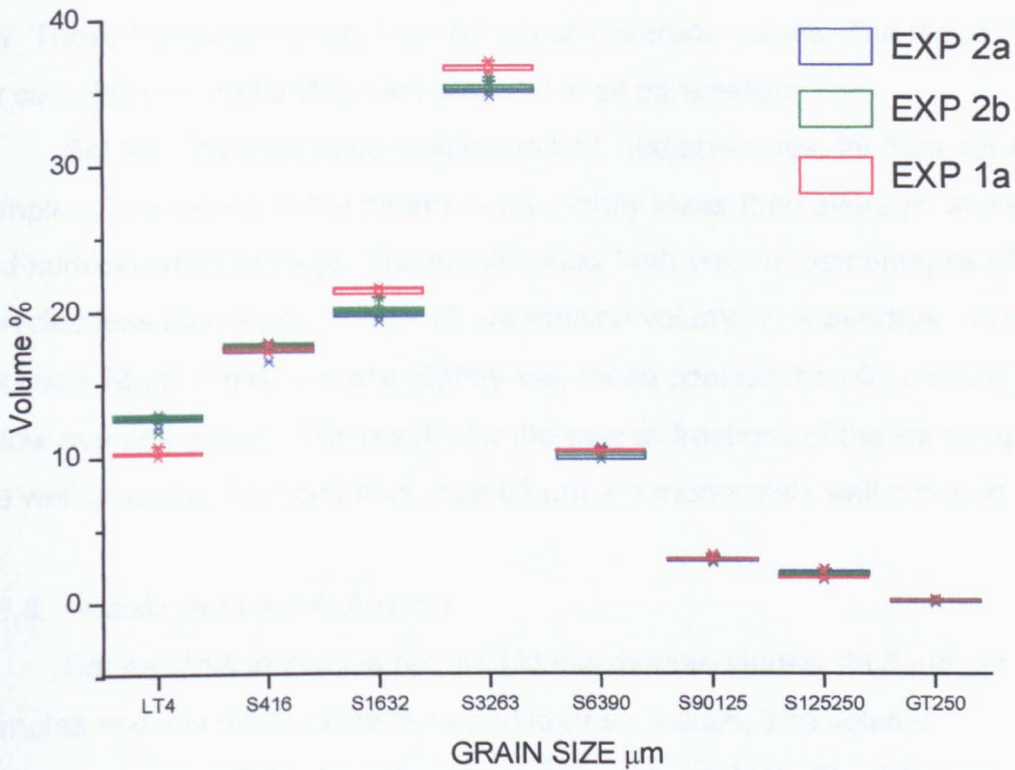
Figure 4.6 The effect of overnight mechanical agitation of loess in 0.5% calgon (2A) compared to samples prepared in 0.5% calgon (2B) and double distilled water without mechanical mixing (1A).

Set 2 summary: both sets gave variable median values and extremely scattered data for all parameters except the fractions coarser than 90μm. In general the values for all parameters for 2a and 2b are similar, 2a showing a slightly coarser distribution than 2b. The volume percentages less than 4 μm and coarser than 90μm are higher for set 2 than 1b, but the volume percentage of the fractions at the centre of the distribution 16 to 63 μm are lower for set 2 than 1b. Most significant is the difference in shape of set 2 data from all the others, more positively skewed.

4.3.5. Results from set 3: ultrasonic treatment

Set 3a. This technique resulted in low median values, 29.6 μm, for all six samples. The mean, skewness and kurtosis values were less than other sets. The results show high volume percentages of particles less than 4 μm. The 4-16 μm fractions is representative, fractions between 16 and 63 μm are slightly low. Those fractions coarser than 63 μm are average values. The results for the six samples are moderately well grouped in all parameters.

Set 3b. This technique resulted in low median values, 29.6μm, for all six samples. The values of the means were slightly lower than average, skewness and kurtosis were average. The results show high volume percentages of particles less than 4 μm. The 4- 16 μm fraction volume % is average. Fractions between 16μm and 63 μm are slightly low, those coarser than 63 μm are just below average values. The results for the coarse fractions of the six samples are well grouped, fractions finer than 63 μm are moderately well grouped

4.3.6. Results from set 4: Aliquots

Set 4a. This technique resulted in low median values, 29.6 μm, for all six samples and low mean, skewness and kurtosis values. The volume percentages of particles less than 4 μm are relatively high. The fractions between 4μm and 90 μm are average, those coarser than 90 μm are just below average values. When compared to 3a and 3b, the drop in the volume percentages of particles less than 4 μm appears to be matched by slightly increased volume percentages of the fraction 32-63 μm (fig 4.7). The results for the six samples are well grouped for all parameters except the finest fractions < 4μm and 4-16μm.
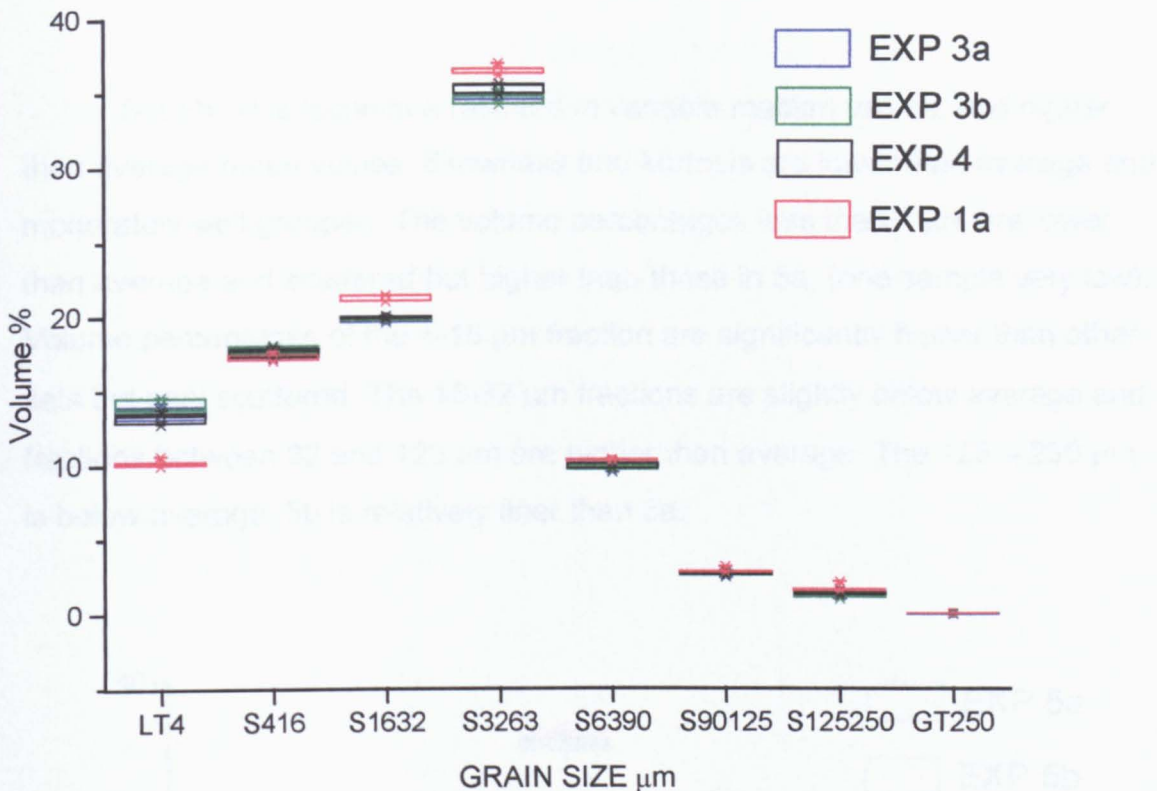
Figure 4.7 The effects of the period of ultrasonic treatment, 3 and 15 mins, 3A and 3B respectively. Preparation of an aliquot of sub-sample in 0.5% calgon with 3 mins ultrasonic treatment. All compared to minimal dispersion in double distilled water (1A).

Summary of sets 3 and 4: all three sets gave a low median value and similar mean values. However, the treatment resulted in a small but significant increase in the fine fractions over samples dispersed in double distilled water. The extended period of ultrasonic treatment of method 3b resulted in the finer distributions. Method 4 showed more clustered results for the coarse fraction but the repeatability of the fine fraction was not significantly improved.

4.3.7. Results from set 5: HCl

Set 5a. This technique resulted in generally high median values of 32.4 (1 low value, 29.6). The values for the means are higher than average, skewness and kurtosis were average and moderately well grouped. The volume % for fractions < 4 μm are much lower than average. The 4-16 μm fractions are also lower than average and scattered. Fractions 16-32μm are average, and fractions coarser than 32 μm are higher than average. These coarser fractions are moderately well grouped.

Set 5b. This technique resulted in variable median values, and higher than average mean values. Skewness and kurtosis are lower than average and moderately well grouped. The volume percentages less than 4 μm are lower than average and scattered but higher than those in 5a, (one sample very low). Volume percentages of the 4-16 μm fraction are significantly higher than other sets but very scattered. The 16-32 μm fractions are slightly below average and fractions between 32 and 125 μm are higher than average. The 125 – 250 μm is below average. 5b is relatively finer than 5a.
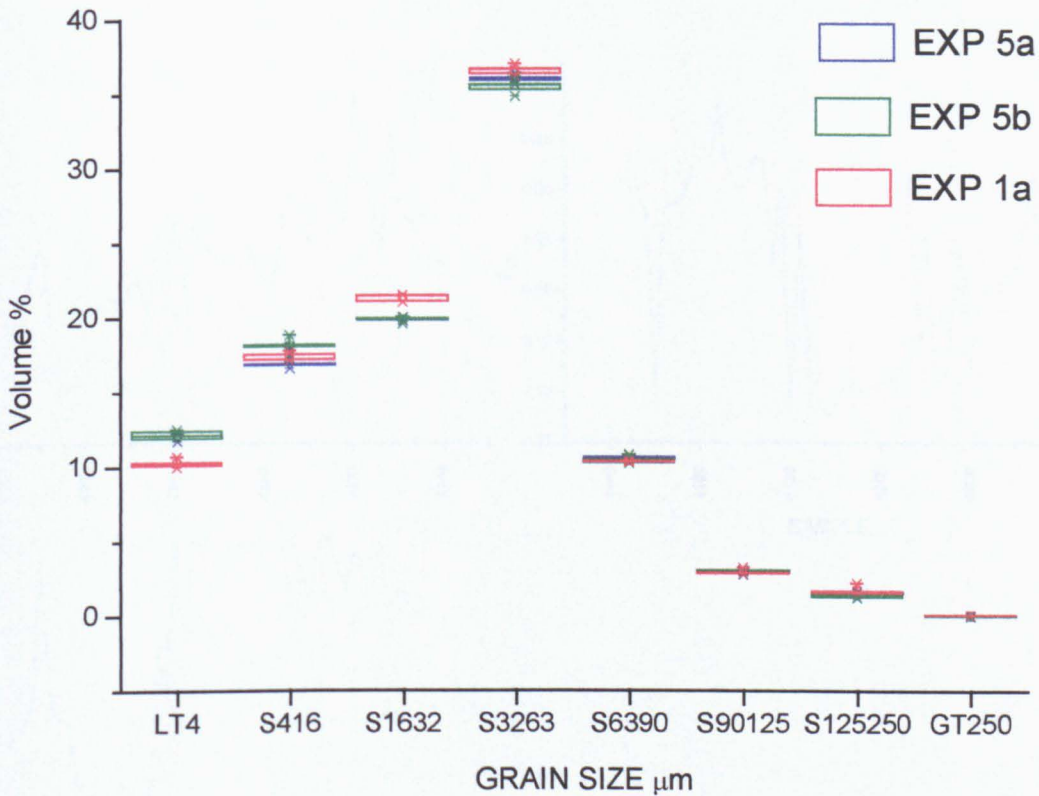
Figure 4.8 The effects of carbonate remove using 5% and 10% HCl, 5A and 5 B respectively

Set 5c. The results of this down section investigation are illustrated in fig 4.9 to allow comparison of samples prepared with and without 5% HCl. Covariance of each of the particle size windows occurs in the down core samples as in the control samples 5a. Acid treated samples have approximately 0.5-1% lower volume % < 4μm fraction. The volume percentages in the 4-16 μm fraction are very similar in both the acid treated and untreated samples. In fractions coarser than 16 μm the volume percentage in each fraction in acid treated samples is greater than those left untreated. The sensitivity of skewness and kurtosis to variability at the tails of the distribution results in a poorer correlation.
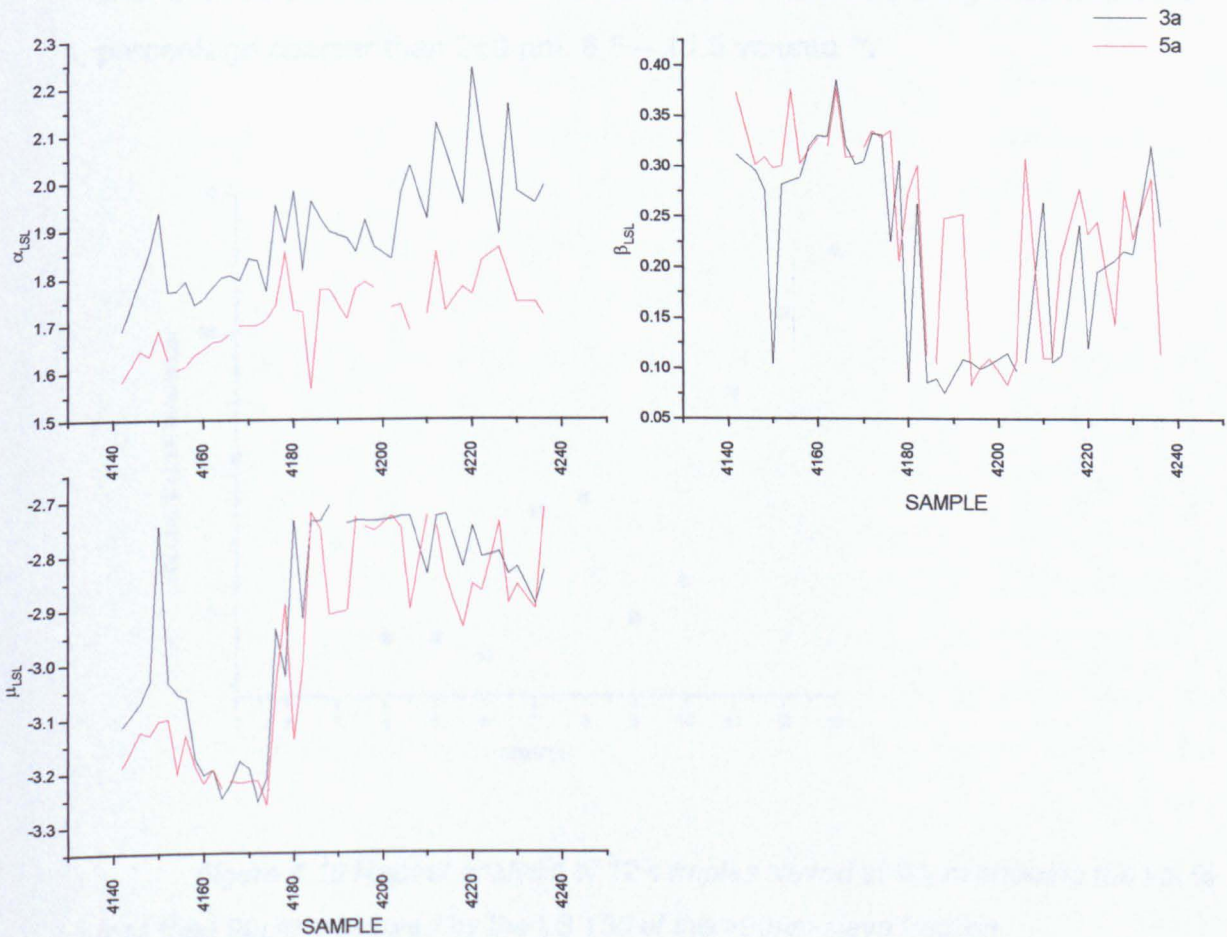
Figure 4.9 Preparation using method 3A (0.5 % calgon and overnight mixing) and 5A (5% HCl treatment and dispersal in 0.5% calgon with overnight mixing). Comparison using LSL parametric curve parameters.

Summary of set 5: Acid treatment and rinsing using the centrifuge coarsens the distribution significantly. Loss of fine material results in a steepening of the coarse gradient. Acid treatment alters the parametric parameters to a greater extent than is indicated by the bulk particle size (see appendix 4)

4.3.8. Results from set 6: Particle Shape

Set 6a. The results from this preparation method gave variable values for the mode (116 or 167μm) and median values of 106 or 116μm. The mean values ranged from 139 - 153μm for the six samples taken from the same bulk coarse fraction. Most significantly, the Coulter measured between 25 and 38 volume % finer than 90 μm i.e. the size sieve size used. There was a significant volume percentage coarser than 250 μm, 8.5 – 11.5 volume %.
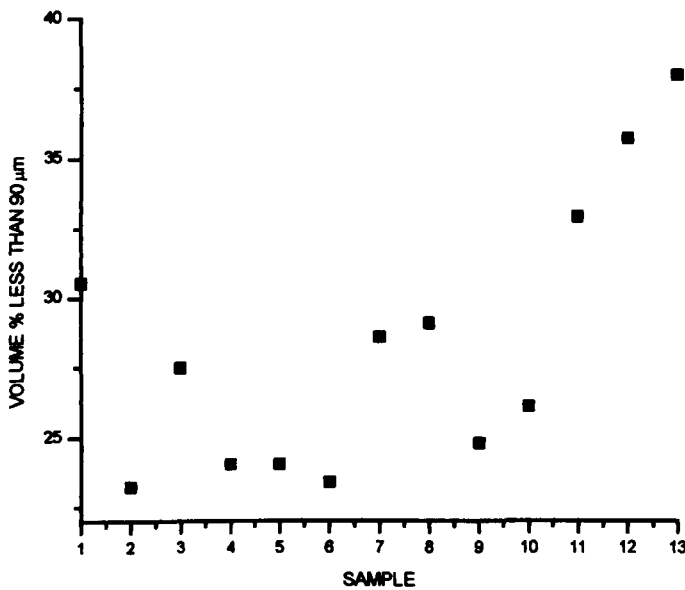
Figure 4.10 Repeat analysis of 12 samples sieved at 90μm showing the vol % less than 90μm measured by the LS 130 of the >90μm sieve fraction.

Set 6b. The results from this method gave much more consistent results than 6a, values of 88 μm for both the median and the mode, the mean ranged from 95.1 to 96.5 μm. The volume percentage less than 63μm, the sieve size

used, was between 16.2 and 16.5%. Although the results from this preparation method show a significant fraction finer than 90 μm was present. It is can be difficult to ensure that the shortest axis of a flat particle is orientated in such a way that it can pass through the sieve prior to diffraction analysis; it was unlikely that over 25% had failed to do so. It seems more likely that the coarse fraction was not 'clean' and the fine particles shown in the distribution where separated from the coarse fraction after sieving by the sodium hexametaphosphate and sonication.

4.4. Discussion

4.4.1. Suspension fluid and dispersion method

It is important to incorporate the dry loess powder into a liquid in such a way that particles are dispersed evenly before the sample is added to the fluid module to ensure air bubbles and particle clusters do not affect the results. Two methods of dispersing materials are considered: chemical dispersal using sodium hexametaphosphate as a wetting agent and physical dispersal by mechanical shaking and ultrasonication. These methods are compared to samples mixed only in double distilled water.

It is necessary to draw the distinction between different types of particle groupings in loess soils. The first group consists of loosely held clusters of clay and silt particles formed during pedogenesis, while the second consists of particles of various sizes that are held more strongly by cement of re-precipitated material. Both occur naturally in the sediment pile. These must be evenly and consistently dispersed during preparation. The formation of floccules caused by the attraction of fine particles during immersion of the loess in a liquid (either water or wetting agent, see following discussion) needs to be prevented.

There are differences between the concentration of dispersant, sodium hexametaphosphate, used in laboratories for the preparation of loess samples for particle size analysis. The standard concentration used at Liverpool is 4%, whereas the concentration used at Royal Holloway (RHUL) is 0.5%. It is stated that the most effective concentration of sodium hexametaphosphate is below the micelle limit, 0.8% (Meng X. M pers comm). Above this concentration, flocculation is increasingly likely. The random motion of particles in the liquid

will bring them into close contact, and whether they flocculate depends on the relative strengths of the attractive and repulsive forces. These forces define how stable the dispersal of the powder will be in the liquid. To be affective the wetting agent should have a greater affinity for the surface of the particles than water alone. Once on the surface it should reduce the attractive forces between particles and prevent particles flocculating. In order to ascertain whether flocculation was evident at concentrations higher than 0.8%, the initial investigation was carried out.

4.4.2. Dispersant concentration

The criticality of concentration of wetting agent was investigated by preparing 24 sub-samples, six of each concentration 0.5, 1, 5, 10% as described in the initial test method. The variability of the tails of the distribution was of most importance. It was expected that there would be the highest volume percentage of fines in samples dispersed in the 0.5% concentration, and a decrease in the volume percentage of fines in samples dispersed in concentrations above and below the micelle limit due to flocculation and incomplete wetting respectively. The adverse effects of wetting agent concentrations above the micelle limit (>0.8 %) were not apparent (figure 4.4).

Samples added to the fluid module of the Coulter are diluted in 1.7 litres of water. Flocculation of the clay fraction once in the fluid module may occur, due to the dilution of the wetting agent below its effective concentration. The concentration of the dispersant is not as critical as at first thought, since small changes could only be seen when high concentrations (10%) were used. It is likely that once dispersed, the pump in the fluid module and the size of the laser aperture destroys any flocs that form because of the water in the fluid module. Since little variation with concentration occurred it was decided to use a concentration of 0.5%, i.e. below the micelle limit for the experimental sets (fig 4.4).

4.4.3. Assessment of dispersion

An assessment of the effectiveness of the sodium hexametaphosphate to wet the surfaces of the particles can be done by comparison of the results from experimental sets 1a and 2a. Simply adding a wetting agent does

increase the volume particles finer than 16 µm. The data show that when a wetting agent is added and not agitated samples are affected to a variable degree, leading to a the scatter in the results. Data from sets 1b and 2b show whether dispersal by a wetting agent can be improved when combined with overnight mechanical shaking. Comparing sets 1a and 1b, mechanical shaking overnight increases the volume of fines when the loess is only mixed with water, although the value is still below average. As may be expected, comparison of 2a and 2b demonstrates that overnight shaking decreases the scatter of the data, and the effect of adding a wetting agent is improved by overnight mechanical shaking.

These results can be compared to those of sets 3a and 3b to assess the effect of physical dispersal by sonication. Three minutes of sonic treatment increases the volume percentage of material less than 4µm significantly and slightly increases the volume percentage between 4 – 16 µm. There is a decrease in all fractions coarser than 32 µm, cf. sets 2a and b with 3a and b (figure 4.7). An increased period of sonication, 15 minutes, does not appear to have a further significant effect on the distribution other than to slightly reduce scatter in fractions coarser than 90 µm. Although the increase in temperature was significant; this can cause the Calgon to thicken. Evidence for the destruction of coarse particles due the action of sonic waves is not apparent (lower percentage of coarse material and higher percentage of fine material in 3b than 3a). Extending the period of sonication to 30 minutes did significantly affect the distribution, reducing the median from 29.6 – 32.4 to 27.0 µm, increasing the amount of material in the less than 4 µm fraction to 15 vol % and reducing all fractions coarser than 32 µm. This is taken as evidence of the destruction of intact particles. Both Mcave (1986) and Chappell (1998) noted that after initial dispersion, an extensive period of ultrasonic treatment (>10 mins) caused reduced dispersion of samples suspended in Calgon, probably due to flocculation. In McCave's experiment (1984), samples subjected to ultrasonic treatment when suspended in DD water dispersed continually with time, as shown by increasing obscuration, indicating the break up of individual particles.

4.4.4. Sample size and method of introduction to the fluid module

The standard method of sample addition to the fluid module used at Liverpool is sub-sampling from a baffle cup using a pipette. This method was compared with the alternative method of the addition of an aliquot of sample. Method 4a was compared to 3a to monitor the repeatability of pipette addition since this was a preferable method on the basis of time.

The most significant difference between sets 3a and 4a is the slightly lower percentage of fines (approximately 0.5% less) in 4a and slightly higher percentage of the 32-63 μm fraction also by about 0.5%. The statistical parameters are slightly less scattered when using aliquot addition rather than pipette addition. It is unlikely that a short period in the baffle cup could make the 32 – 63μm fraction finer by its action after overnight shaking and 3 minutes sonication. Since all other aspects of preparation are identical these results suggest that use of the pipette removes approximately 0.5 vol % of fines at the cost of sizes close to the modal size.

4.4.5. Chemical treatment

An extension of the previous discussion about dispersal of particle clusters is the use of hydrochloric acid to dissolve the carbonate that cements the particles together to form secondary aggregates. In loess from more southerly sites where carbonate enhanced horizons are significant and nodules are prevalent, removal of secondary carbonate is probably necessary. As mentioned previously the lower precipitation levels in the north of the plateau results in less primary carbonate material being dissolved and re-precipitated. Up to 12% of the total loess may be primary carbonate and treatment using hydrochloric acid will affect both primary and secondary material. HCl may also cause clay particles to flocculate. It was hoped that acid treatment would disaggregate coarse secondary aggregates (>100μm), present as small but significant 'aggregate humps' (3-5 volume %) at the coarse end of the distribution in and below soil horizons (see chapter 5). This experiment was carried out to see if treatment with HCl would break up the small volume percentage of coarse aggregates sufficiently to drop them into the main distribution, thus reducing their effect on the distribution tails.

Experimental set 3a is compared to sets 5a and 5b. After treating sets 5a and 5b with 5 and 10% HCl respectively, rinsed and centrifuged the 3 sets were identically treated. Results of acid treated samples were more scattered than 3a showing that it is difficult to ensure that acid treatment and centrifuging affect the samples evenly. The data do not show that the action of the HCl decreases the volume percentage of coarse material i.e. disaggregation. In fact the opposite is evident: results show a relatively higher percentage of coarse material in acid treated samples. The data show that acid treatment causes a decrease in the fine fraction. Samples treated with 5% concentration show a lower percentage of fines than those treated with the higher concentration do. It seems incongruous that a higher concentration of acid would not result in increased flocculation. It is more likely that the decrease in fines and the relative increases in the coarse fractions are the result of the loss of a variable amount of fine particles during rinsing to remove the acid after centrifuging.

Samples between 5 and 6m prepared with and without acid treatment are compared in fig 4.9. Again, it can be seen that acid treatment causes apparent coarsening of the distribution. The mean particle size of acid treated samples is 1to 2 µm coarser than those prepared using method 3a. It is also worth noting that the even after acid treatment the profiles for the two preparation methods are well correlated for the mean and for all particle size fractions, there merely being a shift in the size or percentage.

4.4.6. The effect of non-spherical particles on the distribution

This experiment was carried out in order to assess whether the flat / platy particles in the coarse fraction were consistently measured by the LS130. SEM photos of loess samples shows that quartz particles are sub-angular to sub-rounded, not spherical. There is a significant percentage of mica particles, which are platy.

Since non-spherical particles are evident in the samples it was important to see whether matching the diffraction patterns of these natural samples to those formed by known artificial particle sizes using an algorithm can be done repeatedly on the same sample and the same results be achieved. It was

expected that the results would be highly variable since flat platy particles would pass through the beam in a random orientation.

The results from the first preparation method, (6a) appeared to show that the non-sphericity of the coarse fraction was a significant factor in the variability of results of a repeatedly measured sample. By using method 6b, repeatedly sieving the coarse fraction and addition of the samples to the fluid module in aliquots, the results were much more consistent. Under these preparation conditions it may more reasonable to conclude that non-spherical particles do affect the repeatability of the sample even if the sample is well dispersed. Although the results are repeatable the presence of 16 vol % finer than the sieve size used may indicate that the 'coarse' fraction is underestimated due to the random orientation of non-spherical or platy particles as they pass the laser. It is possible that there is also a contribution from fines that could not be removed even by the more rigorous method of 6b.

4.5. Selection of preparation method and summary

The Coulter is known to underestimate the size of fine particles but to over estimate the total volume percentage of fines present (due to refracted high angle light). It is assumed that these effects are constant for all samples Loess distributions analysed in the Coulter LS 130 are not sensitive to the concentration of wetting agent used so long as it is less than 5%. Mechanical agitation is vital to ensure even dispersal. Ultrasonic treatment and the addition of 0.5% Calgon improves clustering of data i.e. repeatability. Ultrasonic treatment in excess of 15 minutes may destroy intact particles. Coarsening in the distribution caused by HCl treatment and subsequent removal of the acid by centrifuging were not quantifiable. Water and ultrasonic treatment was surprisingly effective at dispersing the fine fraction of the loess with no flocculation evident. The results were slightly more scattered than those combining shaking and ultrasonic treatment with 0.5% Calgon. The technique used for the preparation of samples down section was method 3a. The raw Coulter particle size 'bin' data was processed using Gsize, Wind, and Phi programs suitable for the Unix system.

5. Experimental Results from Caoxian

5.1. Introduction

This chapter will describe the results of analysis of magnetic properties, particle size distribution, and some elemental analysis of loess and palaeosols. These results will be used in the subsequent discussions on the potential of the Caoxian site for high resolution magnetic and particle size studies and the usefulness of these profiles as proxies for variability in the intensity of the Asian summer and winter monsoon.

5.2. Field Section

The stratigraphy noted in the field is presented first. The topsoil is dark brown and the surface is vegetated with grass and trees. Below this is an extensive thickness of light beige - yellow loess, which is homogeneous and friable. At depth, the deposit was more consolidated, redder in colour and contained large (up to 4cm) elliptical nodules. The section contains natural joints, possibly caused by cyclic wetting and drying, creep induced tension, or earthquake shock, (Derbyshire et al, 1999). Fractures were closely spaced (15 - 20cm) running diagonally across all columns marked out for sampling blocks dipping at ~ 45°SW.

It is possible that there was also a relict circular slip surface in the sample area. Several parallel fractures were evident along the brow of the hill. A fracture dipping west, in the same direction as the slope but at an angle of 30° exited the hillside at twelve metres depth. A second dipped gently into the hillside below the bottom of the trench. However, no evidence of movement along the fractures was found. These large fractures were not apparent until sampling was well under way and several more fractures opened on the surface, both parallel and perpendicular to the trench. These cracks eventually resulted in the collapse of the sides of the section with the loss of six metres of block samples (between 12 - 17 m). These may have been relict fracture surfaces that became more visible due to disturbance during and after trench excavation. Alternatively, the fractures may be newly formed due to the disturbance and pressure release caused by the excavations.

CX	Depth (m)	
		Unit 1 dark brown, heavily vegetated surface, mod clay content,
	0.00	
		Unit 2 light yellow, beige. Coarse grained homogeneous texture. Fractures.
	16.66	
		Unit 3 darker coloured sub horizons. Slightly finer texture. Bio reworking? Occasional nodules (small gritty)
	26.00	
		Unit 4 yellow –beige colour homogeneous coarse texture. Some large nodules (> 1cm = Gypsum?). More consolidated than unit 2, less friable.
	35.32	
		Unit 5. Mid-dark red-beige. Clayey mass with gritty nodules. Variable texture down unit. Bio reworking. Root channels.
	42.50	

Figure 5.1 Stratigraphic field section at Caoxian

Five stratigraphic horizons or units were defined in the field (fig 5.1). Unit 1, the upper most part of the section, was 80cm thick including the vegetated surface layer. Unit 2 is pale buff yellow and uniformly coarse silt in texture. There is little evidence of contemporaneous organic material. Unit 3 is a little darker in colour when dry. It is also finer in texture. There are a few coarse inclusions 0.5 - 2 mm in the lower part of the unit, which appear to be composed of gypsum. Unit 4 is very similar in colour in a dry state to Unit 2 and appears homogeneous in texture. The boundary between Unit 4 and Unit 5 is indicated by a dramatic darkening and fining in texture. Unit 5 is much redder than the previous units. The clay content also appears to be considerably higher. The upper part of Unit 5 contains some relatively large loess dolls, 5-15 mm. A lightening in colour and a coarsening in particle size mark the base of Unit 5.

Table 5.1 Depth of units resolved from χ_{LF} data.

Unit	Height at the top of each Unit
1	00
2	-2.24
Transition	13.42
3	16.66
4	25.94
5	35.36

5.3. PSD analysis by parametric curve fitting

5.3.1. Introduction

The hypothesis is that changes on the land surface, dominance of deposition or erosion, transport by low level suspension/ saltation or high level suspension would leave different textural characteristics that could be described by parameters derived from model curves, (see chapter 6). This may allow a down section profile of variation that can be linked to shifting environmental boundaries during interglacials and glacials. Curve fitting analysis using LSL and LH models was carried out on all particle size

distributions. Results of the descriptive parameters are summarised and presented as scatter and down core plots.

5.3.2. PSD classification

Since the range of values for all parameters for the various units was small, it was found that clarity could be achieved by colour coding PSDs types. Initial colour coding was based simply on the stratigraphic horizons defined in the stratigraphic section. However, this failed to subdivide incipient soils from interbedded loess layers within a unit, especially Units 3 and 5. In an effort to group like with like, it was found that division of sub-horizons could be made using curve fitting parameters. For example, it appears that low level pedogenic sub-horizons in Unit 3 have distinct PSDs from late glacial Unit 2 loess. It is important to note that subdivision and colour coding is based on PSD parameters. This has implications for interpretation of magnetic parameters when based on PSD groupings.

5.3.3. Characteristic PSD of loess and palaeosols.

Coarse PSD have very little curvature around the modal value. Consequently no δ_{LH} value (peak curvature) can be defined, so these PSD are only described by the 3 parameter LSL model, μ_{LSL} - equivalent mode, α_{LSL} – relative abundance of fine material and β_{LSL} - relative abundance of coarse material. μ_{LSL} is approximately equivalent to the mode used in orthodox particle size analysis. Samples that are finer than those described by LSL alone, have a considerable range of PSD shape, i.e. increase in peakedness and increasing variability in δ_{LH} with fining. The finer PSD are best characterised by the 4 parameter LH distribution, μ_{LH} asymptote intersection, ϕ_{LH} - fine fraction, γ_{LH} - coarse fraction and δ_{LH} -measure of PSD peak curvature. Figure 5.2 shows a scatter Plot of μ_{LSL} versus μ_{LH}. Not only does this show that μ_{LSL} - modal equivalent and μ_{LH} - asymptote intersection, are not identical; it illustrates the potential to subdivide types of PSDs. The 4 groups of PSD defined by this analysis were coloured red, green, light blue and dark blue. In the subsequent text, μ_{LSL} is referred to as the LSL modal equivalent

and, because of the non-modal equivalent nature of μ_{LH}, μ_{LH} is referred to as the LH asymptote intersection (see following section).

5.3.4. Parametric curves and PSD peakedness

The most dramatic difference between the plots of LSL and LH curve models other than a defined δ value, is the shift in the position of μ values for some PSD. In PSD with a significant curvature about the mode, the LH model has a greater potential to fit the gradient of the fine loess fraction than a LSL model. However, this means that the intersection of the coarse and fine asymptotes in LH models may result in an apparently coarser 'modal' parameter μ, than those described by a LSL model (fig 5.2). In this respect, LSL parameters are more comparable to actual particle size variations (fig 5.3). Nevertheless, LH curves make a value contribution in allowing subdivision of PSD types, as shown in the following sections. The characteristic properties of these PSD types are discussed below. Fig 5.4 shows α_{LSL}, β_{LSL} and μ_{LSL} plotted as scatter graphs. Figure 5.5 shows the corresponding LH distribution parameters ϕ_{LH}, γ_{LH}, μ_{LH}, for comparison with LSL model parameters
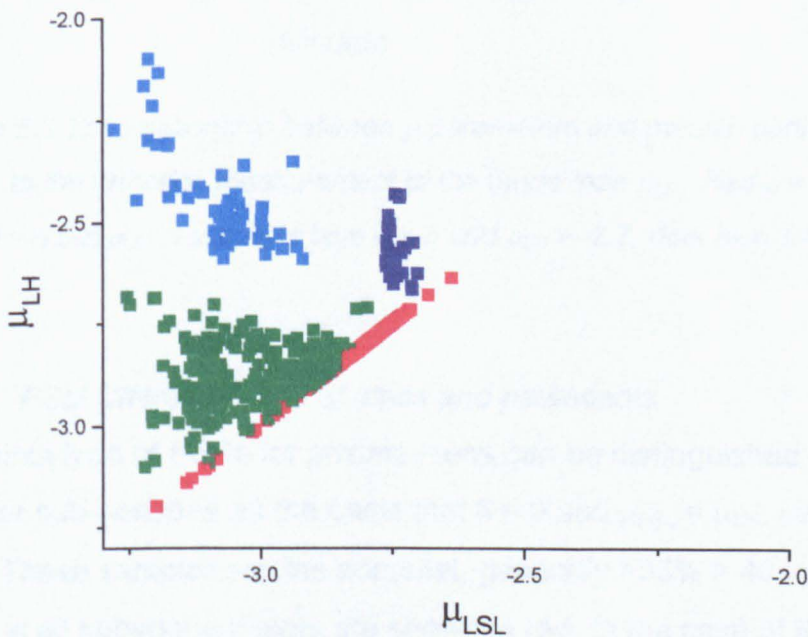
5.2 Examples of how pristine loess PSDs and pedogenically altered loess may be distinguished by differences in μ_{LSL} and μ_{LH}. When $\delta = 0$ then $\mu_{LH} = \mu_{LSL}$. μ_{LH} and μ_{LSL} are not equivalent.

138
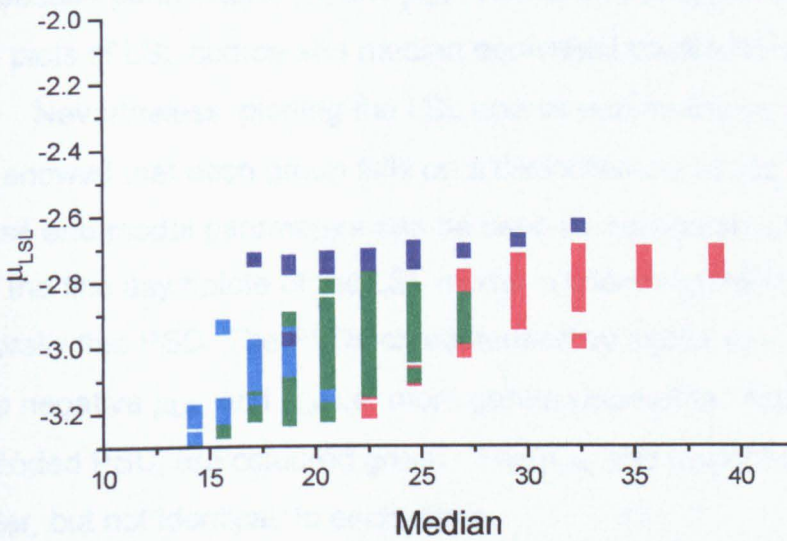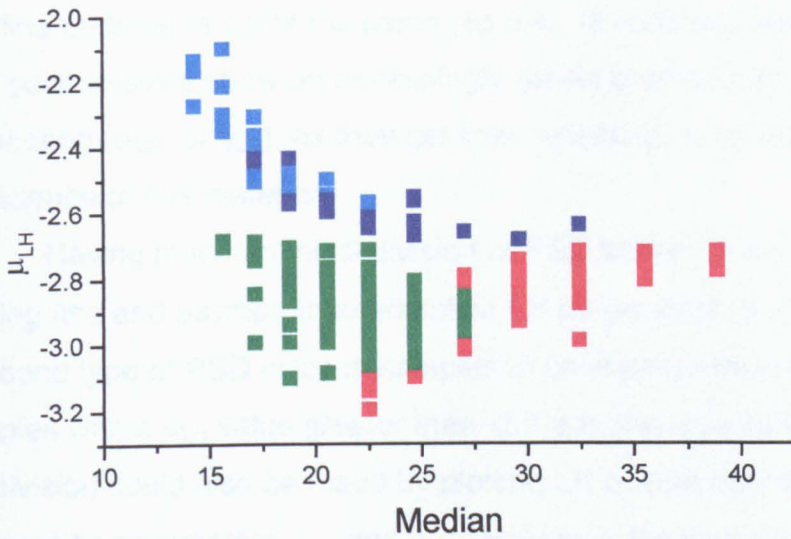
Figure 5.3 The relationship between μ parameters and median particle size. ,μ_{LSL} is closer to the orthodox measurement of the mode than μ_{LH}. Red $\delta = 0$ and μ_{LSL} =μ_{LH}, green $\delta = n$ but $\mu_{LSL} \approx \mu_{LH}$, light blue $\delta = n$ and $\mu_{LH} > -2.7$, dark blue $\delta = n$ and β_{LSL} < 0. 15.

5.3.5. PSD Characteristics of loess and palaeosols

A distinct type of PSDs for pristine loess can be distinguished from the PSDs of other sub-horizons on the basis that $\delta = 0$ and $\mu_{LSL} = \mu_{LH}$, i.e. LSL distribution. These samples are the coarsest, generally >35% > 40μm, very peaked and in all subsequent plots are shown in red. In the case of these coarse samples, if μ_{LSL} shifts towards more negative values i.e. finer PSD, the shape of the distribution remains more or less the same and the values of α_{LSL} and β_{LSL} remains relatively unchanged i.e. the relative abundance of coarse

and fine material remains the same (fig 5.4). In contrast, those samples with finer particle sizes show an increasingly gentle gradient of the fine half of the distribution (α_{LSL} or ϕ_{LH}), as they get finer reflecting an increase in the relative abundance of fine material.

Having made an initial division of PSD based on μ_{LH} and μ_{LSL} values, plotting fine and asymptote intersection LH parameters, ϕ_{LH} against μ_{LH} allowed a second type of PSD in loess samples to be distinguished (fig 5.5). Those samples with a μ_{LH} value greater than -2.7 are coloured light blue. This subdivision could also be made by plotting LH coarse against the asymptote intersection parameters, γ_{LH} and μ_{LH}. However, the division was not apparent from plots of LSL coarse and median equivalent parameters (α_{LSL} and μ_{LSL}).

Nevertheless, plotting the LSL coarse and modal parameters β_{LSL} and μ_{LSL} showed that each group falls on a distinctive curve (fig 5.4). Although LSL coarse and modal parameters can be used to distinguish variations in PSD, the fit of the fine asymptote of the LSL model is inferior to the LH model for generally fine PSD. The PSDs characterised by higher α_{LSL} and ϕ_{LH} values and more negative μ_{LSL} and μ_{LH} i.e. more gentle slope of the fine gradient than the red coded PSD, are coloured green. The μ_{LSL} and μ_{LH} of these samples are similar, but not identical, to each other.

The final group is made up of PSDs that have particularly low values of β_{LSL} - coarse fraction abundance; when fitted by a LH model curve the equivalent γ_{LH} values fall within the range of the previously described light blue coded PSDs. The shape of the PSD of blue and green coded PSDs is similar. However, they have high μ_{LSL} values indicating a high modal value, this is due to a coarse tail which the LSL model incorporates into the coarse fraction gradient value but the LH model does not, giving a more appropriate model for these generally fine grained PSDs.

5.3.6. Ncrit: use in PSD classification

As described in Chapter 3, the parameter Ncrit can be used to show a non statistical analysis of goodness of fit for PSD fitted with LSL and LH. Fieller et al (1992) concluded that so long as the values of Ncrit are greater than the number of particles either model could be deemed a good model.

Ncrit values for loess and palaeosol horizons are in the range of 1500 - 2000. Whether this is greater than the number of particles in the loess distributions is unclear since results were generated as volume % not number of particles. It is unlikely due to the relatively high clay size particle content of some samples,
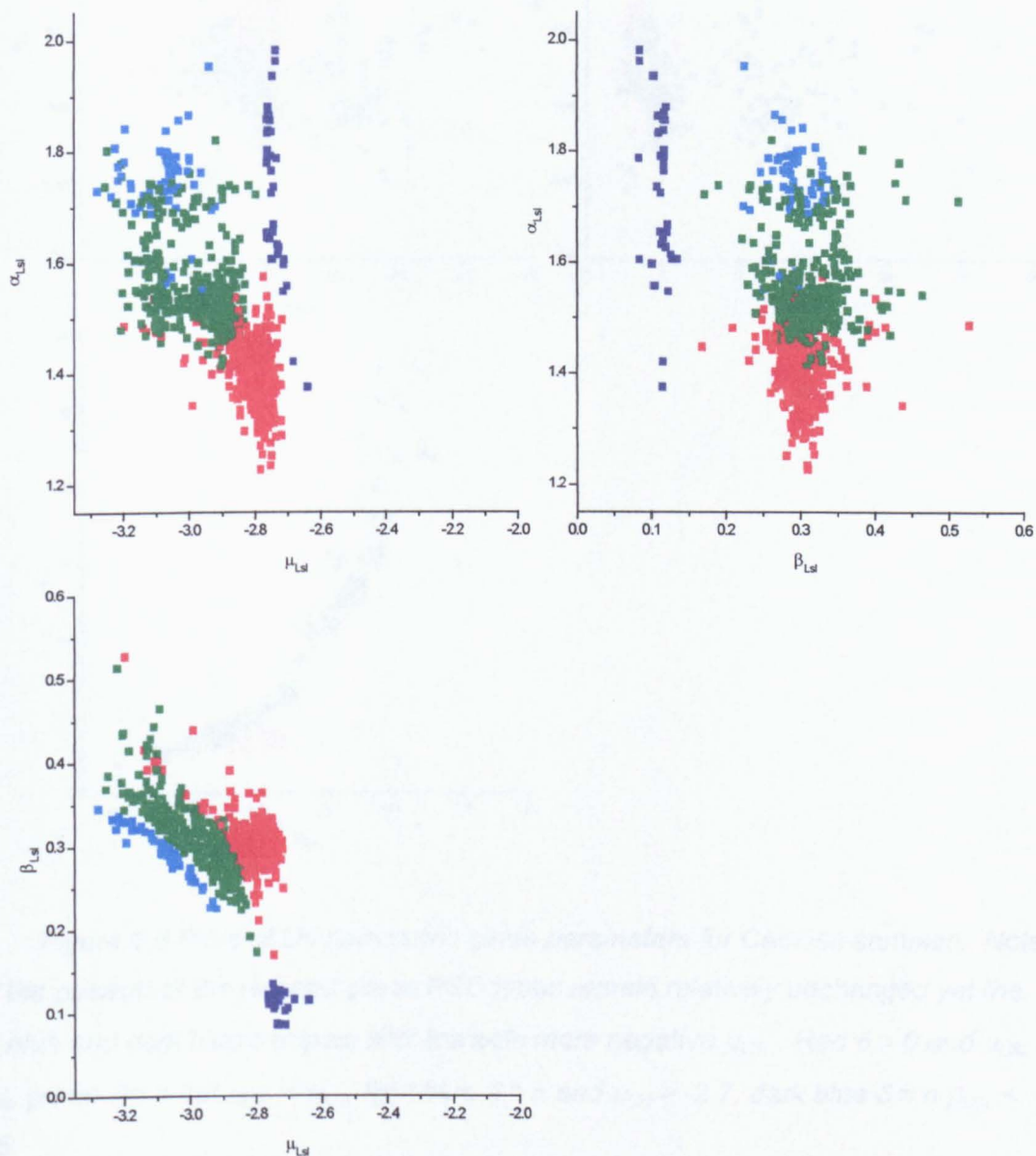
Figure 5.4 Plots of $_{LSL}$ parametric curve parameters for Caoxian samples. There is a high potential for classification of distinct types of PSDs. Red $\delta = 0$ and $\mu_{LSL} = \mu_{LH}$, green $\delta = n$ but $\mu_{LSL} \approx \mu_{LH}$, light blue $\delta = n$ and $\mu_{LH} > -2.7$, dark blue $\delta = n$ $\beta_{LSL} < 0.15$.
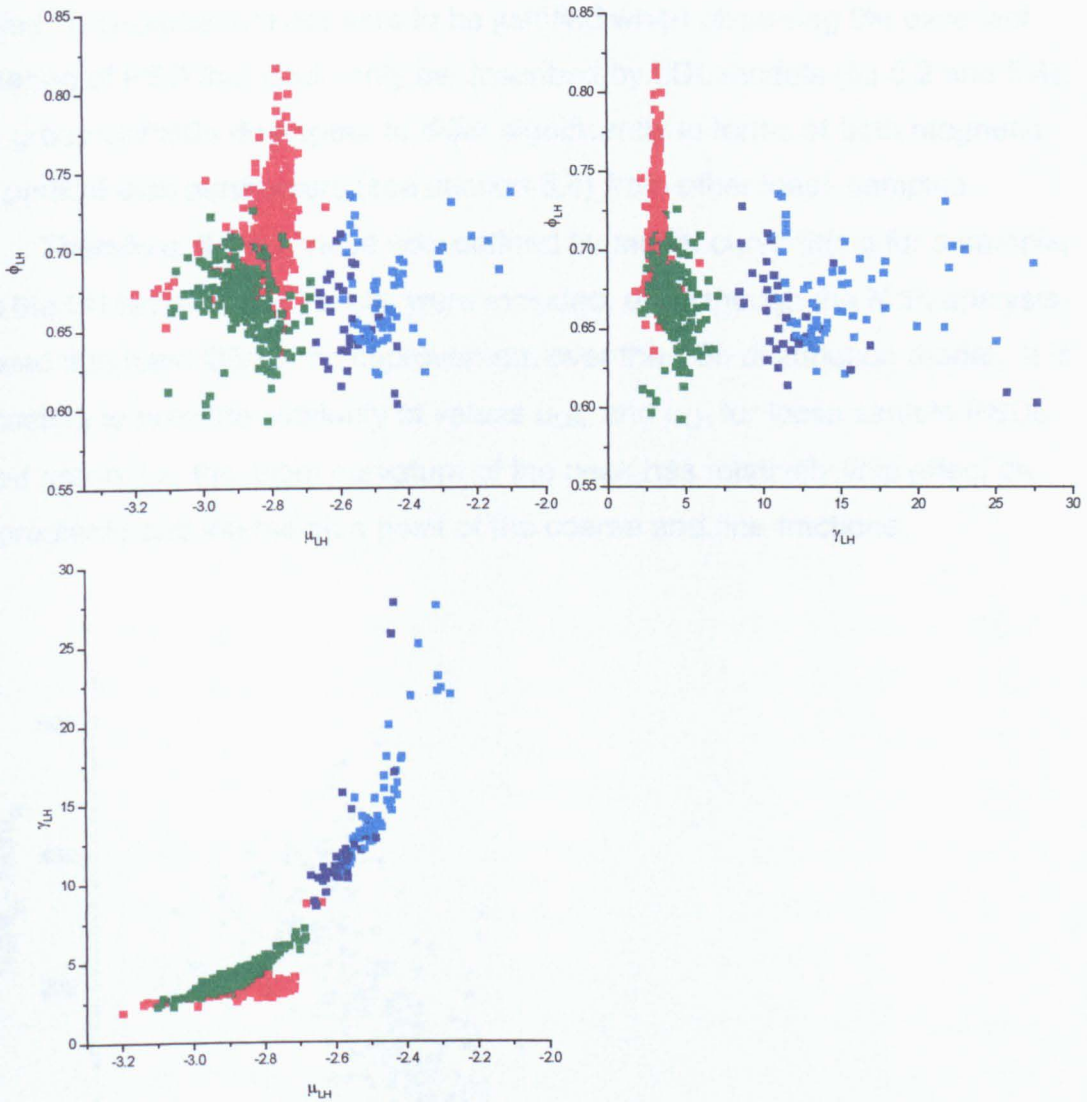
Figure 5.5 Plots of LH parametric curve parameters for Caoxian samples. Note how the position of the red and green PSD types remain relatively unchanged yet the light blue and dark blue samples shift towards more negative μ_{LH}. . Red $\delta = 0$ and μ_{LSL} = μ_{LH}, green $\delta = n$ but $\mu_{LSL} \approx \mu_{LH}$, light blue $\delta = n$ and $\mu_{LH} > -2.7$, dark blue $\delta = n$ $\beta_{LSL} <$ 0. 15.

the implications of which are unquantified. The LSL Ncrit values were subtracted from the LH Ncrit values. Those PSD with a value of Ncrit greater than 0 are, according to Fieller et al (1982), best fitted by a LH model (fig 5.6).

A significant number of loess samples (in green) have Ncrit values below zero, i.e. according to defining thresholds of Ncrit, a 4 parameter LH curve has no advantage over a 3 parameter LSL even though, a δ_{LH} value for peak

curvature was defined. However, in the following the Ncrit rule is not stringently applied. This procedure appears to be justified when observing the excellent clustering of PSD that could only be described by LSL models (fig 5.2 and 5.4). This group of PSDs do appear to differ significantly in terms of both magnetic and particle size parameters (see section 5.4) from other loess samples.

Therefore, if a δ_{LH} value was defined by model curve fitting for a sample, then the LH curve model results were included, even though the Ncrit analysis showed it to have little or no improvement over the LSL distribution model. It is interesting to note the similarity of values μ_{LSL} and μ_{LH} for loess sample PSDs coded green, i.e. the slight curvature of the peak has relatively little effect on the gradients and intersection point of the coarse and fine fractions.
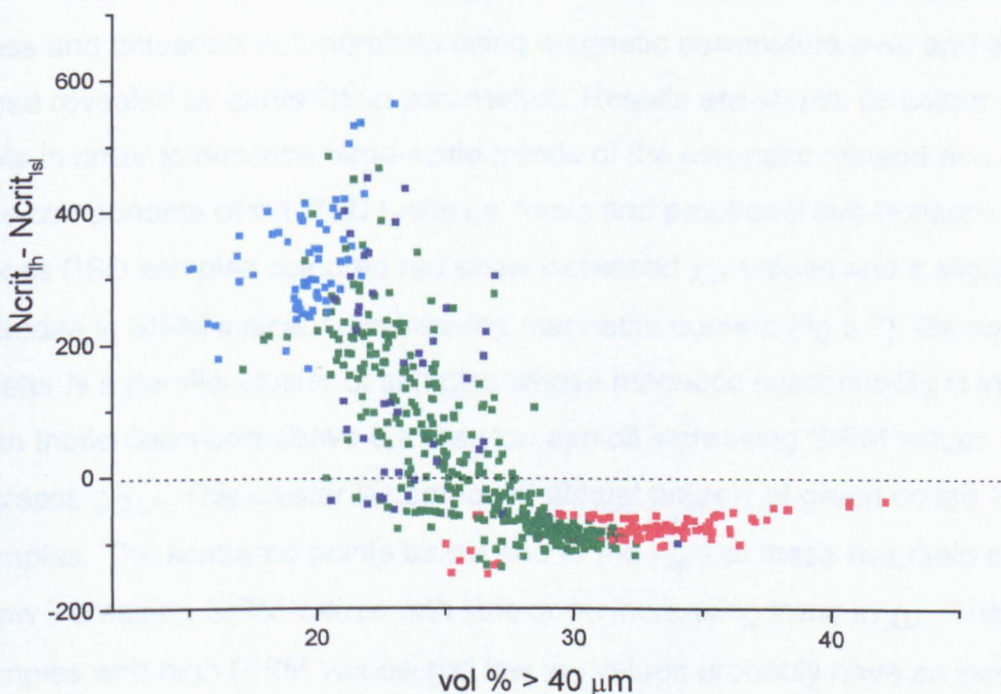
Fig 5.6 Defining factors imply that samples with Ncrit values below 0 show no improvement by fitting a LH curve. However, the distinction between PSD type is aided by the use of LH parametric models for all PSDs that can accommodate a LH curve. Colours as before.

Consequently, the LSL and LH models are nearly the same for green coded PSD. In summary, when red PSDs are modelled by a LH model, the plot is identical to its LSL plot (fig 5.4 and 5.5). Since LSL is a limiting case of

the LH model where $\delta = 0$. Green PSDs, where a δ_{LH} parameter can be defined but is generally low, show there are only slight changes between LSL and LH models due to the subtle increase in peak curvature. As δ values increase in green, blue and light blue coded PSD, their positions in the LH plots are increasingly different from LSL plots and this is reflected in the increasing Ncrit$_{LSL}$-Ncrit$_{LH}$ (fig 5.6) δ_{LH} and μ_{LH} values. Since there appears to be no precursor to this research using aeolian silt, comparisons are made of both LSL and LH parameters for those horizons where both models could be fitted (N Fieller, pers com).

5.4. Magnetic properties of PSD classes

5.4.1. Introduction

The following results concentrate on the potential for further distinction of loess and palaeosol sub-horizons using magnetic parameters over and above those revealed by curve fitting parameters. Results are shown as colour scatter plots in order to describe large-scale trends of the magnetic mineral and grain size components of the PSD types i.e. loess and palaeosol sub-horizons. Those PSD samples coloured red show increased χ_{LF} values and a slight increase in SIRM indicating increasing magnetite content (fig 5.7). Below this cluster is a parallel cluster of samples whose magnetic susceptibility is lower than those described above but they too exhibit increasing SIRM values with increasing χ_{LF}. This cluster is composed almost entirely of green coded PSD samples. The scattered points below and to the right of these two main clusters show increasing SIRM values with little or no increasing trend in χ_{LF}. These samples with high SIRM values and low χ_{LF} values probably have an increased imperfect canted antiferromagnetic content, possibly hematite and are dominated by green and light blue coded PSD samples. Those samples plotting above the main groups showing high χ_{LF} values and low SIRM,

144
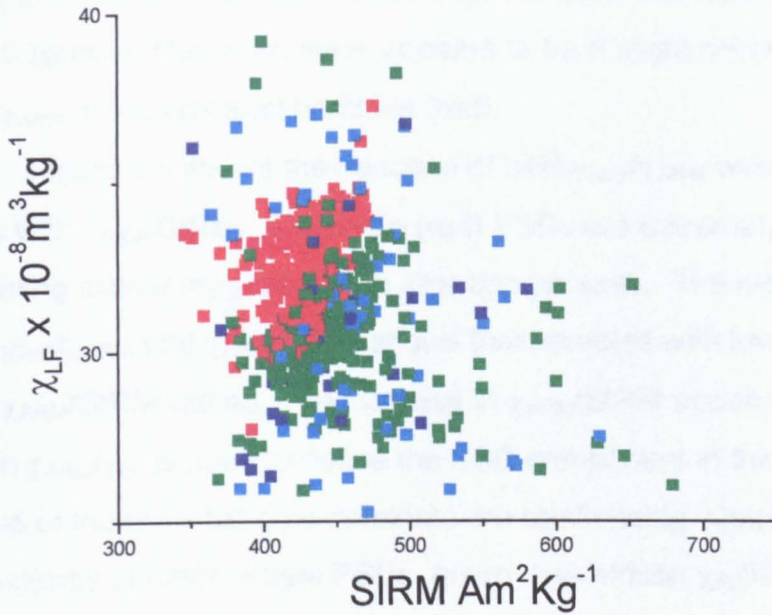
Figure 5.7 The relationship between χ_{LF} and SIRM. χ_{LF} is commonly used as a proxy for precipitation on the Chinese loess plateau. However, the relationship is scattered and complex in sections close to the plateau margin. . Red $\delta = 0$ and $\mu_{LSL} = \mu_{LH}$, green $\delta = n$ but $\mu_{LSL} \approx \mu_{LH}$, light blue $\delta = n$ and $\mu_{LH} > -2.7$, dark blue $\delta = n$ $\beta_{LSL} < 0$. 15.

probably on account of their superparamagnetic or multidomainal domain size and again includes blue and green samples. The general scatter in this plot may be indicative of the variable effects of paramagnetic material at these relatively low magnetite concentrations.

5.4.2. Relationships between magnetic and bulk particle size parameters

Figure 5.8 shows that PSDs coded light blue and dark blue with the lowest coarse bulk particle size component and the highest χ_{LF} show rapidly decreasing values of $\chi_{FD}\%$ and χ_{ARM}/χ_{LF} as the coarse component increases from 15 -25 % > 40 µm. PSDs in green show a gradual decrease in χ_{ARM}/χ_{LF} values and $\chi_{FD}\%$ is low but scattered. Thereafter, red PSDs that are relatively coarse have consistently low $\chi_{FD}\%$, χ_{ARM}/χ_{LF} and $\chi_{ARM}/SIRM$ values. The variation of IRM_{-20mT}/χ_{ARM} with bulk particle size is the approximate inverse of the χ_{ARM}/χ_{LF} relationship. Fine PSDs (blue) show rapidly increasing values of

IRM_{-20mT}/χ_{ARM} as the coarse component increases from 15 -25 % > 40 μm. IRM_{-20mT}/χ_{ARM} is relatively invariable for samples with between 25 and 35% > 40 μm (green). However, there appears to be a slight decrease in IRM_{-20mT}/χ_{ARM} in the coarsest horizons (red).

Figure 5.9 shows the variation of IRM_{-20mT}/χ_{ARM} with $\chi_{ARM}/SIRM$ and χ_{FD}% with $\chi_{ARM}/SIRM$. All coarse (red) PSDs are extremely closely clustered indicating similar magnetic grain size components. The relationship between IRM_{-20mT}/χ_{ARM} and $\chi_{ARM}/SIRM$ shows that samples with low IRM_{-20mT}/χ_{ARM} have high $\chi_{ARM}/SIRM$ values. The increase in $\chi_{ARM}/SIRM$ appears to be exponential. When χ_{ARM}/χ_{LF} is used to define the SSD component in this way, the high χ_{LF} values of the red PSD type dominate the relationship. Coarse PSDs, red, and the majority of intermediate PSDs, green, has similar χ_{FD}% values, as shown in fig 5.9 and are distinguished on the basis of the greater influence of χ_{LF} in the χ_{ARM}/χ_{LF} ratio. The coarse horizons shown in red in scatter plots show an unexpectedly high total magnetic mineral concentration with high χ_{LF} but χ_{FD} % values remain very low (fig 5.8). Their χ_{LF} and SIRM values (fig 5.7) indicate that in general, these samples have a higher magnetite content than the majority of other layers analysed.

Figure 5.8 shows that the magnetic characteristics of green and light and dark blue PSD types fall on a continuum of increasing SP/SSD content. The magnetic composition and grain size characteristics of red PSDs do not fall on a continuum of magnetic composition with the other PSD types. This may reflect the unquantified paramagnetic component of the red PSD samples.

Assuming χ_{FD}%, χ_{ARM}/χ_{LF} and $\chi_{ARM}/SIRM$ and IRM_{-20mT}/χ_{ARM} are indicators of SSD/SP, SD and MD magnetic grain sizes respectively; the following relationships between bulk grain size and magnetic grain size can be defined. Fine bulk particle size fractions with increasing coarse component from 15 - 25 % > 40μm have a corresponding increase in MD magnetic grain size proportion and decreasing SP/SSD and SSD magnetic grain size proportion and correspond generally to light blue and dark blue PSDs. Bulk particle size fractions with between 25 - 35 % >40μm have a low but variable SP proportion, a gradually decreasing SSD proportion and an invariable MD

proportion and correspond to green PSDs. The coarsest bulk particle size samples have low but variable SP/SSD proportion, low invariable SSD proportion and a slight decrease in the MD proportion and correspond to red PSDs.

Plots of LSL and LH μ parameters against IRM$_{-20mT}$/χ_{ARM}, χ_{ARM}/χ_{LF} and χ_{FD}% are shown in the appendix. The magnetic parameters reflect PSD classes well but no further subdivision could be made on the basis of magnetic grain size. Plots of α_{LSL} and γ_{LH}, and β_{LSL} and ϕ_{LH} versus IRM$_{-20mT}$/χ_{ARM}, χ_{ARM}/χ_{LF} and χ_{FD}% did not allow further subdivision of PSD types. However, they summarise well the generally higher proportion of MD grains in coarse material and the higher proportion of SSD and SP/SSD grains in fine material.

Figure 5.10 shows down core plots of magnetic parameters IRM$_{-20mT}$/χ_{ARM} (MD) compared to volume % > 40μm and γ_{LH} (coarse), μ_{LH} compared to χ_{LF}, χ_{ARM}/χ_{LF} (SSD) and α_{LSL} (fine). As expected there is a close correlation between values for the coarse asymptote and volume % >40 μm since they are derived from the same data. Comparison with IRM$_{-20mT}$/χ_{ARM} shows covariance with coarse horizons especially Unit 2, having a larger MD component than the intervening incipient soils. Down section plots of μ_{LH} and bulk susceptibility shows that horizons of enhanced χ_{LF} correspond to μ_{LH} values larger than -2.7, and this is particularly clear in unit 5. χ_{ARM}/χ_{LF} shows a similar pattern with maxima corresponding to larger μ_{LH} values and lower α_{LSL}.

5.5.   High resolution variation in magnetic composition and bulk particle size

5.5.1. Introduction

Consecutive down core data are illustrated graphically in fig 5.11 in SI units. Subsequent figures for each stratigraphic horizon are expanded for ease of correlation. Magnetic and particle size data for each unit (5-1), delimited in the field, are plotted with depth and described in turn. The magnetic and particle size results are discussed in order of stratigraphic units, starting with Unit 5 the oldest.
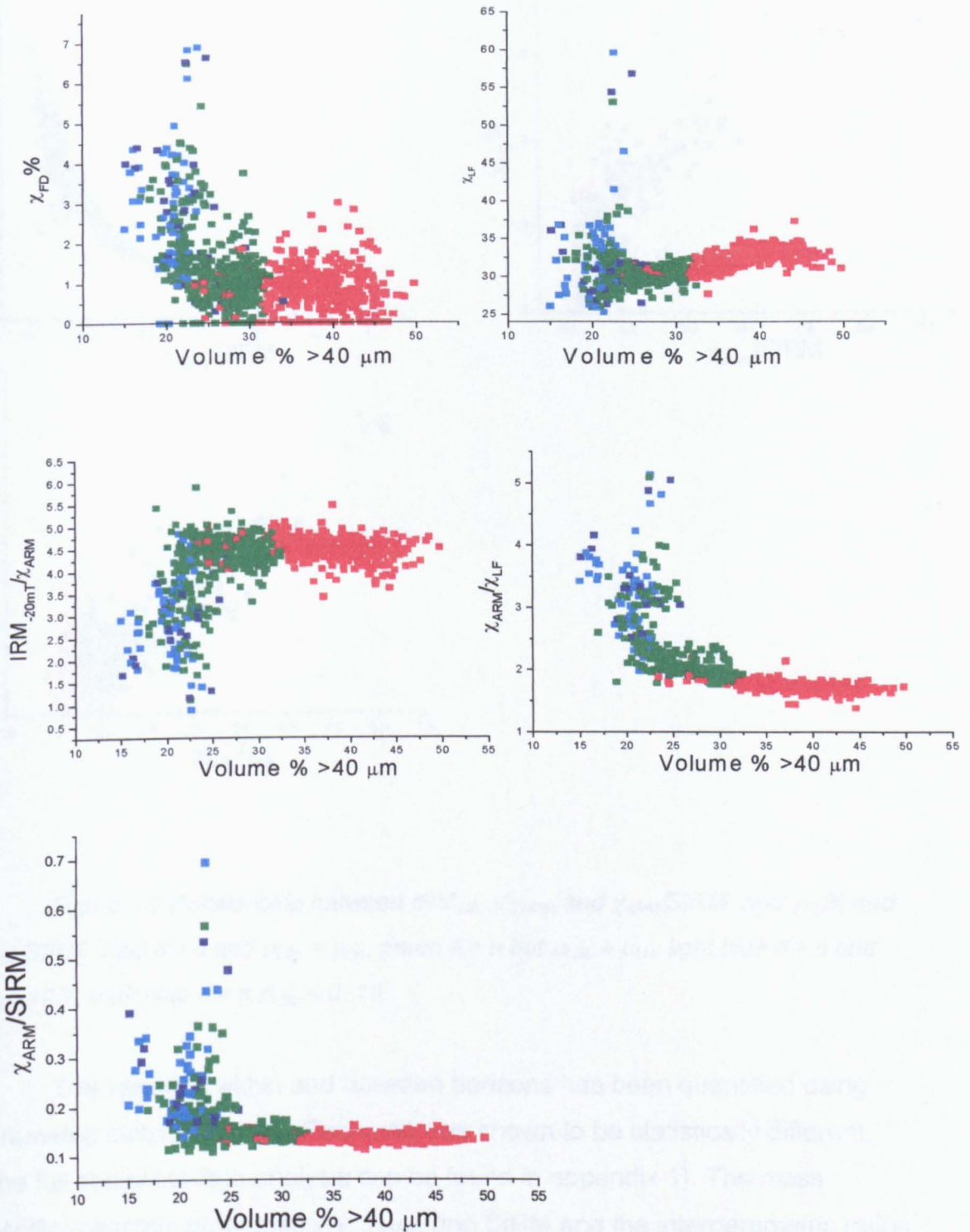
Figure 5.8 Relationship between bulk particle size (> 40,um) and χ_{FD} %, χ_{LF}, χ_{ARM}/χ_{LF}, $\chi_{ARM}/SIRM$ and IRM_{-20mT}/χ_{ARM}. It is clear that χ_{FD}% and χ_{ARM}/χ_{LF} and $\chi_{ARM}/SIRM$ decrease in value as the coarse fraction increases. IRM_{-20mT}/χ_{ARM} behaves in the opposite way. However, χ_{LF} shows a small but significant increase for the coarsest fraction. Colours as before.
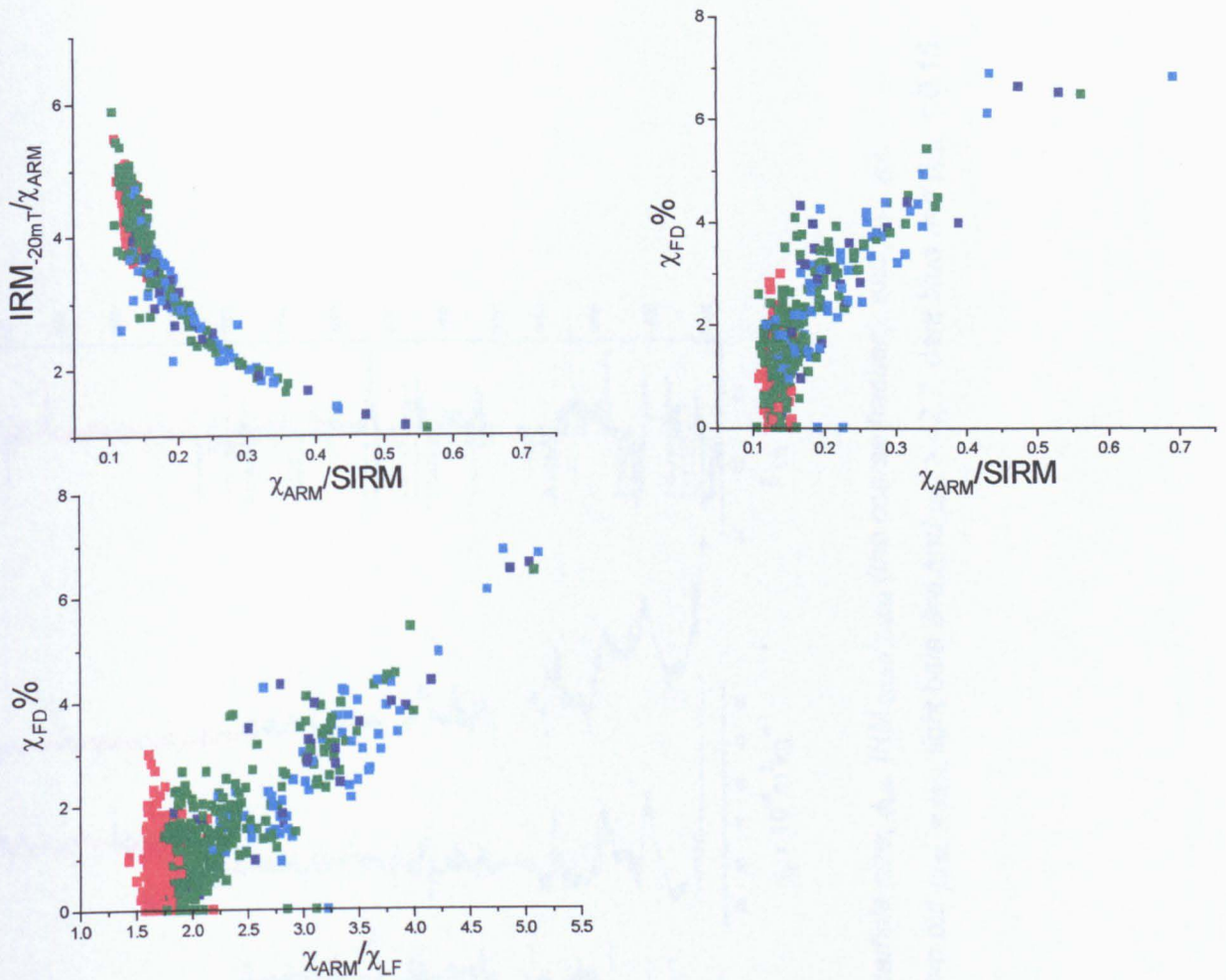
Figure 5.9 Relationship between IRM$_{-20mT}$/χ_{ARM} and χ_{ARM}/SIRM, and χ_{FD}% and χ_{ARM}/SIRM. Red $\delta = 0$ and $\mu_{LSL} = \mu_{LH}$, green $\delta = n$ but $\mu_{LSL} \approx \mu_{LH}$, light blue $\delta = n$ and $\mu_{LH} > -2.7$, dark blue $\delta = n$ $\beta_{LSL} < 0.15$.

The variance within and between horizons has been quantified using parametric statistical tests. Each unit was shown to be statistically different. (The full statistical data analysis can be found in appendix 1). The mass specific magnetic properties χ_{LF}, χ_{ARM}, and SIRM and the interparametric ratios χ_{FD} %, χ_{ARM}/χ_{LF}, IRM$_{-20mT}$/χ_{ARM}, SIRM/χ_{LF}, HIRM, S-ratio and coarse bulk particle size, (volume % > 40µm) are shown for the entire section.
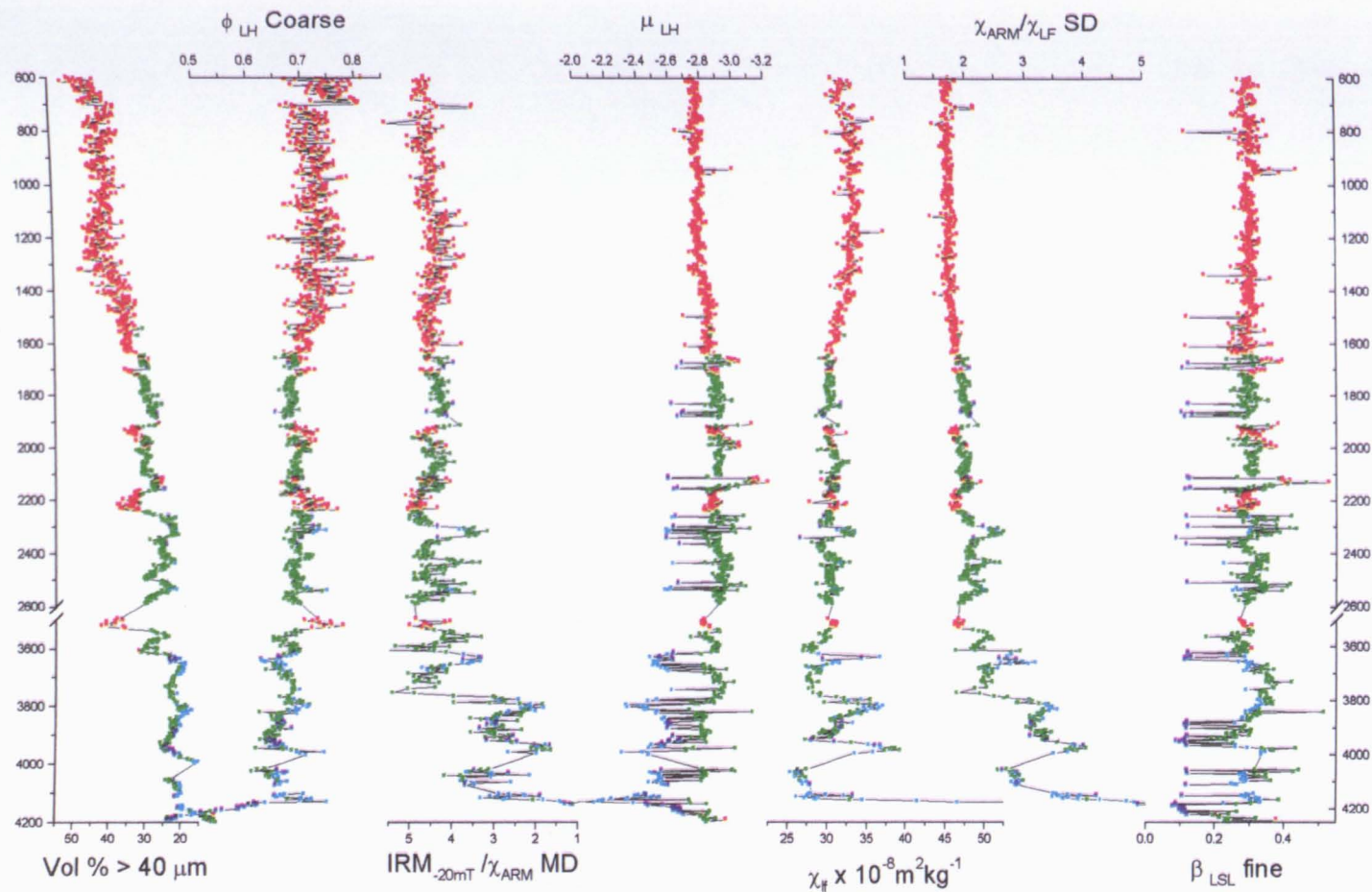
Figure 5.11 Down section plot showing the relationship between bulk particle size, ϕ_{LH}, IRM_{-20mT}/χ_{ARM} (the coarse fraction), and μ_{LH}, χ_{LF}, χ_{ARM}/χ_{LF}, and β_{LSL} (the fine fraction). Red $\delta = 0$ and $\mu_{LSL} = \mu_{LH}$, green $\delta = n$ but $\mu_{LSL} \approx \mu_{LH}$, light blue $\delta = n$ and $\mu_{LH} > -2.7$, dark blue $\delta = n$ $\beta_{LSL} < 0.15$.
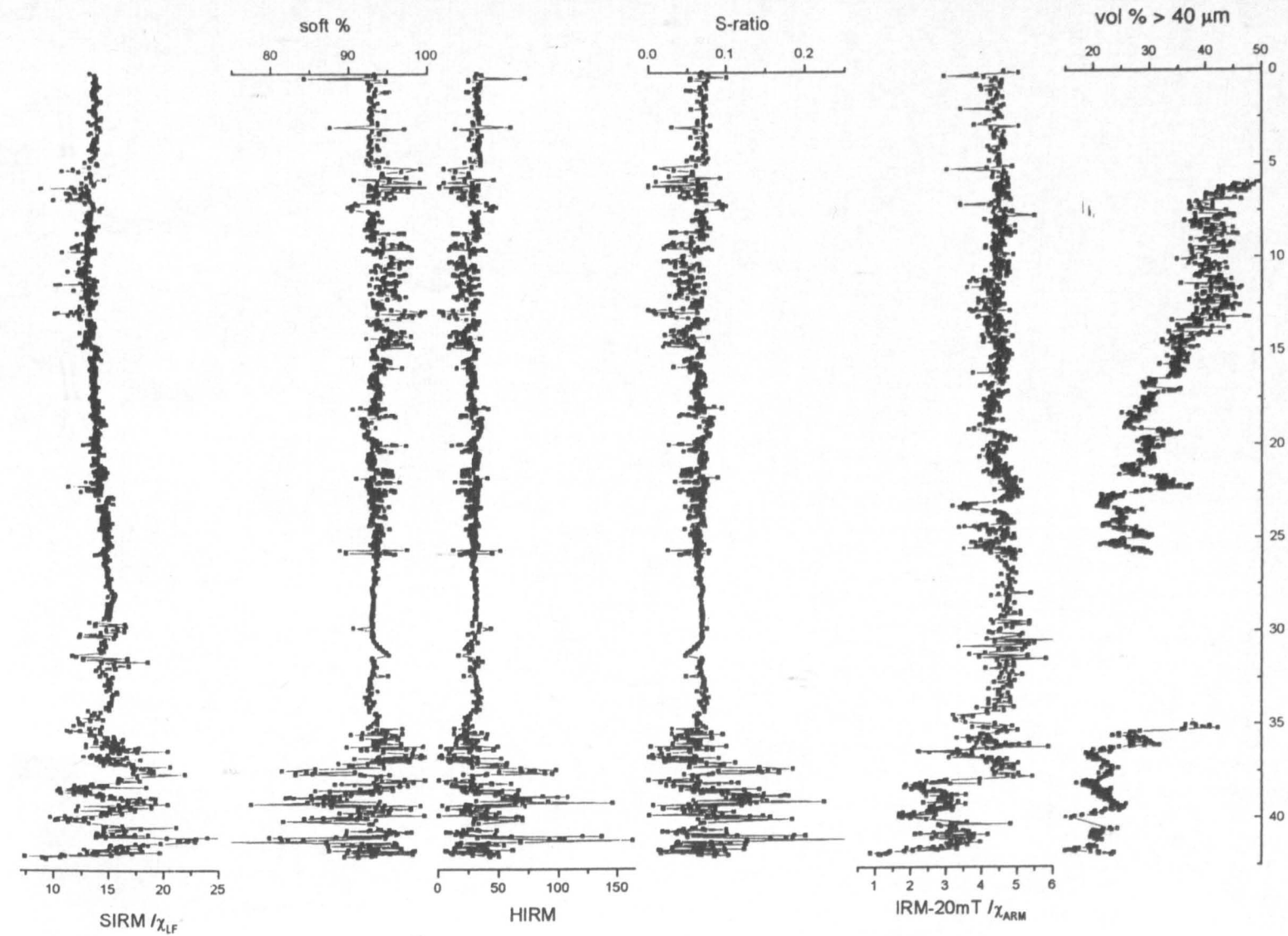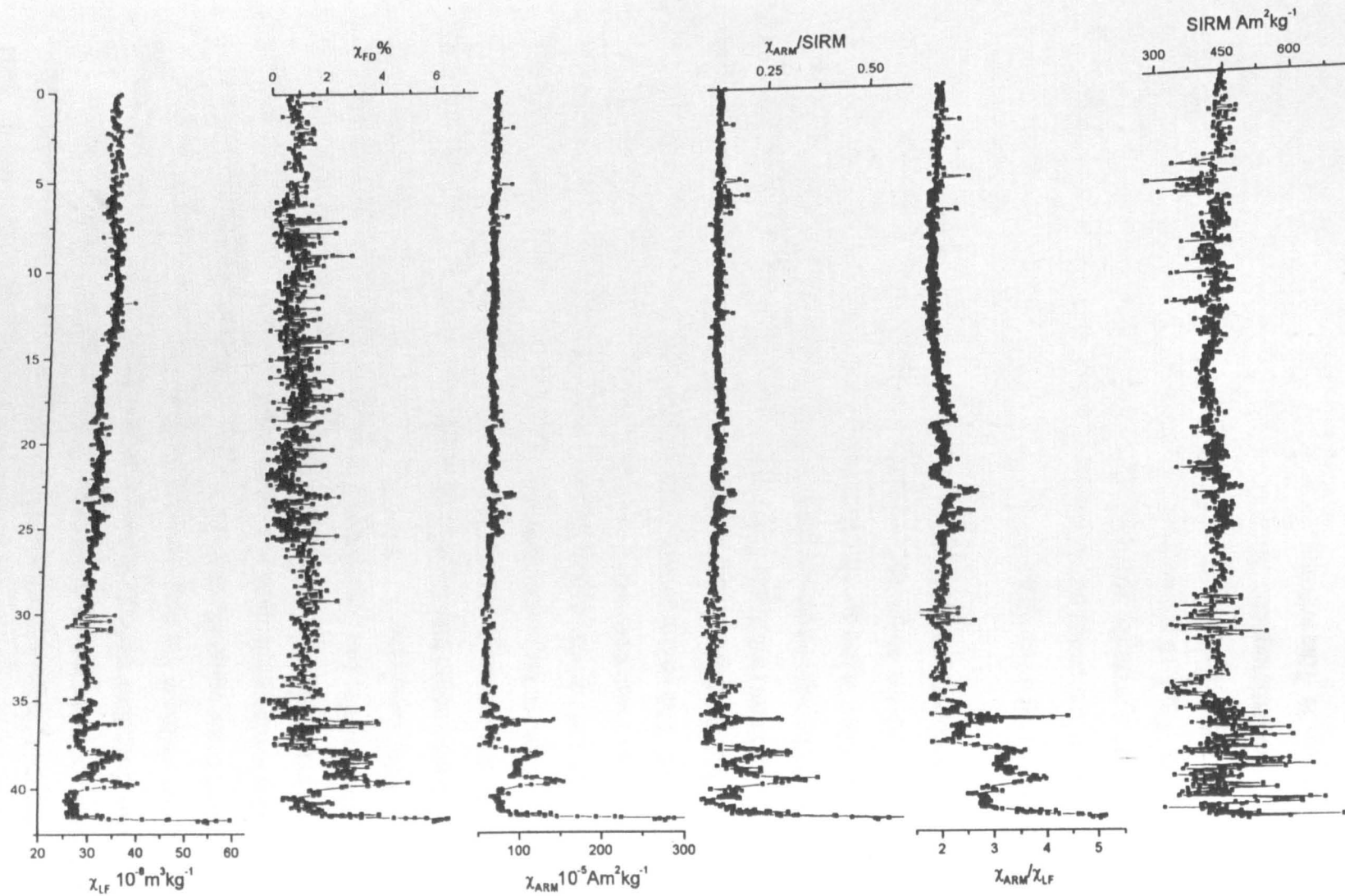
Figure 5.12 Magnetic and grain size data for the whole Caoxian section

5.5.2. Amplitude and frequency of variations

Three classes of variability are applied to the section as a whole. First order variability is generally linked to field horizons (Units 5 -1) i.e. generally pedogenic or loessial on a depth scale of 10s of metres. Second order variability describes pedogenic development within those horizons that may have been visible in the field but not accurately defined, at a depth scale of 12m. Third order variability was not evident in the field but was distinct and repeatable in laboratory tests at a scale of less than 0.4 m thickness. It was expected that increasing pedogenesis and an associated decrease in sedimentation rate; and consolidation at depth would reduce the resolution of the third order variability.

It is also noted that a combination of these factors and compaction of the lower horizons means the scales of variability in each horizon can not be directly equated to temporal variations. Based on field observations, Unit 5 at Caoxian has the highest degree of pedogenic development in the section. Three scales of variability can be observed. Unit 3 shows less pedogenic development. The variation in the magnetic mineral assemblage is of lower amplitude but discrete i.e. single steep well defined peaks. In horizons of great thickness, such as Unit 2, any first order variation is not evident and the horizon is dominated by high frequency third order variations. It will become increasingly clear in the subsequent discussion in chapter 6 that horizons such as these can not be interpreted in exactly the same way as those with significant pedogenic characteristics such as Unit 5.

5.5.3. Unit 5 (43 -35m)

Unit 5 is the oldest part of the section analysed. As illustrated in the field log description it is clayey and reddened. It shows a considerable degree of pedogenesis. Fig 5.13 shows the particle size and magnetic profile of Unit 5 in detail. This unit is characterised by the highest values for parameters indicative of fine grained ferrimagnetic minerals; χ_{LF}, χ_{ARM}, χ_{ARM}/SIRM, and χ_{ARM}/χ_{LF} covary with χ_{FD} %. This soil unit exhibits large amplitude, first order variability. Although there is a high degree of pedogenesis visible in the field, significant second order variability is evident within the soil and intervening loess layers,
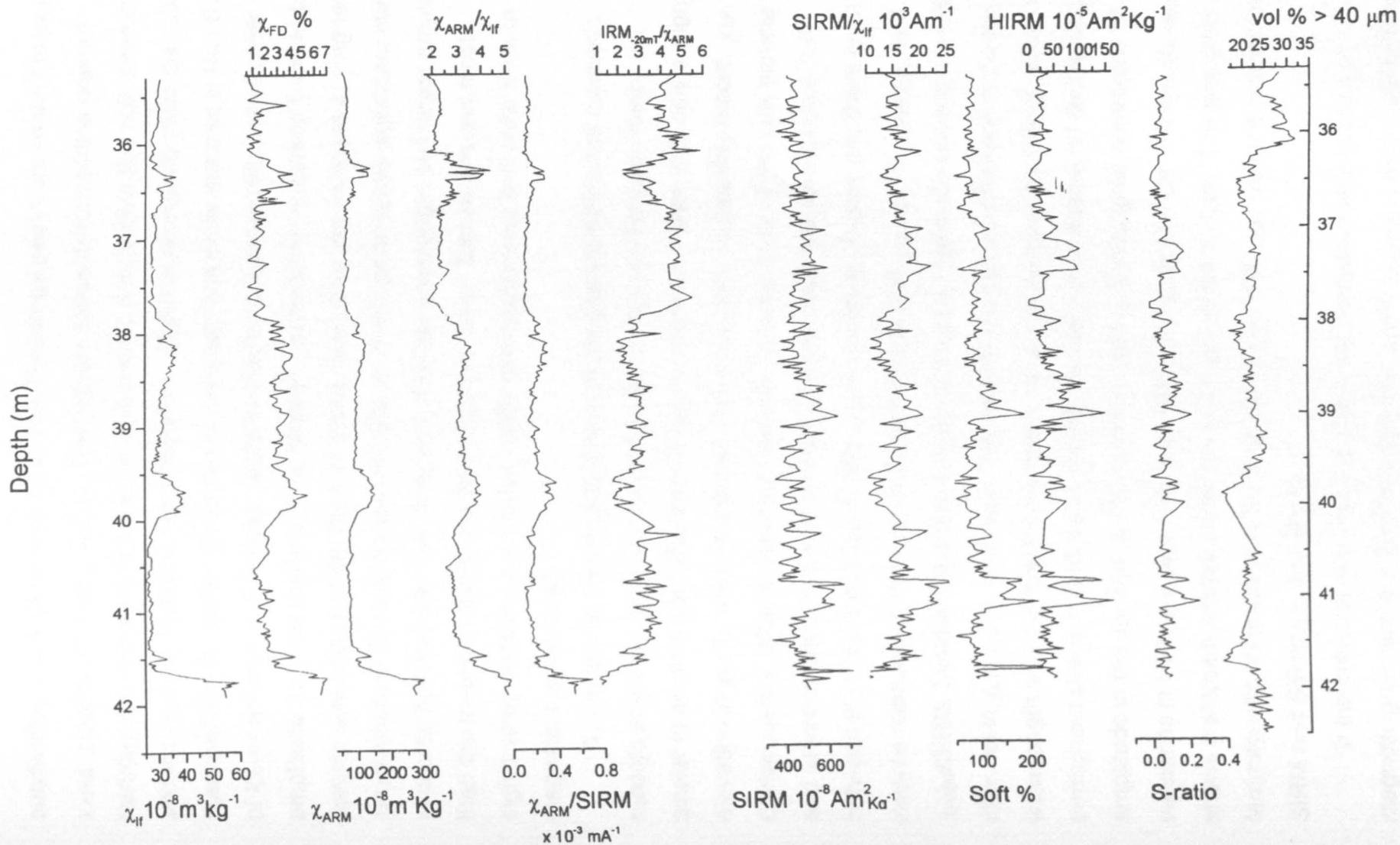
Figure 5.13 Magnetic and bulk grain size parameters of unit 5

subdividing major minima and maxima. Four large peaks are evident in χ_{FD} χ_{ARM}, χ_{ARM}/SIRM, and χ_{ARM}/χ_{LF}. The highest concentration of fine grained ferrimagnetic minerals is between 42.5 and 41.5 m. Within this soil, three short second order fluctuations are discernible. There is an equally rapid decrease in susceptibility thereafter. The three subsequent first order maxima in Unit 5 are of lower amplitude. The latter peaks in magnetic susceptibility are of wider amplitude than the first and more skewed (up section). A marked fining in bulk particle size occurs at the base of Unit 5, preceding any increase in magnetic concentration. The soil horizon (42.5 to 41.5 m) contains two significant minima in coarse bulk particle size. They are of longer wavelength and larger amplitude than the magnetic signal; incorporating third order fluctuations and most significantly correlate to a second order and subsequent first order peak in magnetic concentration.

There is also dissimilarity between the granulometric and magnetic records at the top of Unit 5. A coarse fraction bulk particle size minimum, similar in amplitude to others in the section here correlates with only a slight elevation in χ_{FD}%, which is masked in the magnetic susceptibly record, χ_{LF}. Consequently, differences in wavelength and amplitude of the bulk particle size and environmental magnetic records give low statistical correlation (- 0.48 between 90-125μm and χ_{FD} % and χ_{ARM}). However, in generally there is an inverse relationship between bulk particle size and χ_{LF}, χ_{FD}% χ_{ARM}/χ_{LF}, and χ_{ARM}/SIRM. Minima in the bulk particle size record generally correspond with maxima in χ_{LF}, χ_{FD}%, and χ_{ARM}. The most conspicuous difference is the longer wavelength and the similarity in amplitude of consecutive particle size minima throughout Unit 5 in contrast to shorter wavelength variations of decreasing amplitude in the χ_{LF} and χ_{FD} % records. There is a very good correlation of variations in IRM$_{-20mT}$/χ_{ARM} with grain size volume % >40 μm. IRM$_{-20mT}$/χ_{ARM} shows a stepped increase between each palaeosol horizon. The proportion of ferrimagnetic minerals (soft %) does not covary with χ_{LF}; rather it covaries with SIRM and SIRM/χ_{LF}, and HIRM.

If the previous assumptions regarding interparametric ratios and magnetic grain size are applied again then χ_{FD}% χ_{ARM}/χ_{LF}, and χ_{ARM}/SIRM may be taken as indicators of SP/SSD and SD content and therefore, indicators of in

situ pedogenic alteration. Fine grained viscous superparamagnetic grains (SP) and stable single domain grains (SSD) ferrimagnetic minerals dominate the χ_{LF} record. χ_{ARM}/SIRM indicates that SSD grains are concentrated within horizons also enhanced by SP and SD grains. Intercalated loess horizons are characterised by distinct peaks in HIRM and S-ratio parameters indicating a higher concentration of imperfect antiferromagnetic minerals coinciding with minima in parameters indicative of SP/SSD and SD. The peaks in SIRM, SIRM/χ_{LF}, in intercalated loess horizons also suggests a relatively increased proportion of coarse MD ferrimagnets. The good correlation of variations in IRM$_{-20mT}$/χ_{ARM} with grain size volume % >40 μm suggests that bulk particle size and MD content are closely linked.

5.5.4. Unit 4 (35 to 26 m)

In the field, this horizon is characterised by low pedogenic development. At the boundary between Unit 4 and Unit 5 the records show a change in character to large and distinct lower frequency, high amplitude second order fluctuations. Third order fluctuations are somewhat obscured by the increased sampling interval (8 cm) of this unit. No particle size data has been collected for this unit, it is assumed to be similar in PSD character to Unit 2. The magnetic parameters show a similar pattern of variability to Unit 2. The results of magnetic measurements show a horizon of increased χ_{LF} and χ_{ARM} values between 30 and 32m (fig 5.14) suggesting ferrimagnetic enhancement. These second order fluctuations are very clear with rapid changes occurring over 0.04m. This portion is also significant in that the amplitude of the χ_{LF} variation is large and the frequency of variation is high; and yet this is not reflected in the χ_{FD} % record. Remanence parameters increase immediately above and below the enhanced layer. This indicates increases in ferrimagnetic particle size and increased imperfect antiferromagnetic content immediately either side of the SD enhanced horizon.

Those parameters showing a positive correlation with χ_{LF} (where no enhancement is evident) are remanence parameters SIRM, SIRM/χ_{LF}, HIRM, and soft %. Evidence from the field and magnetic analysis suggest that, the low levels of pedogenic alteration means coarse ferrimagnetic and imperfect

155
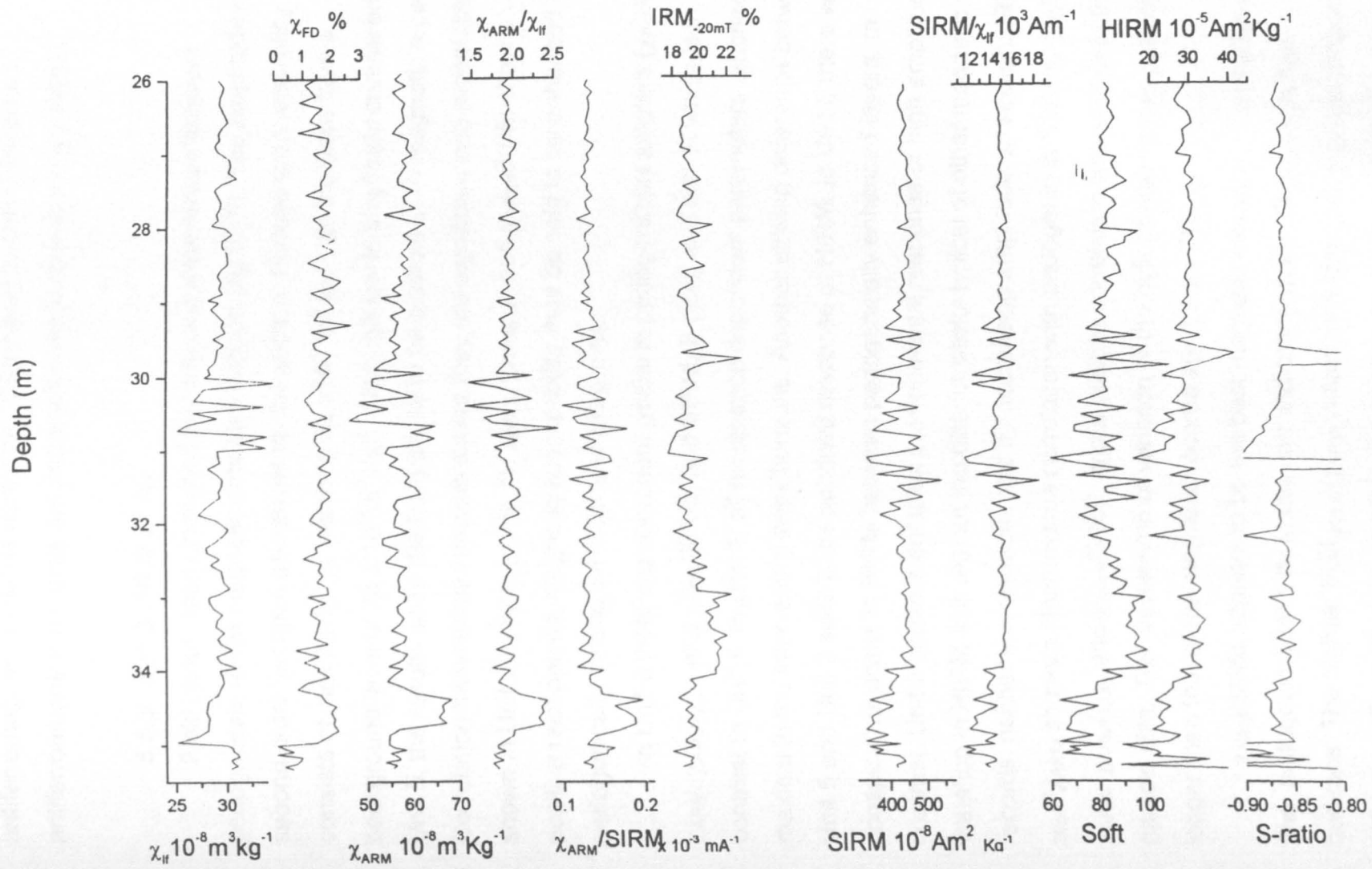
Figure 5.14 Magnetic parameters of unit 4

antiferromagnetic minerals dominate. Compared to Unit 5 imperfect antiferromagnetic minerals are important contributors to the χ_{LF} signal.

5.5.5. Unit 3 (16 to 26 m)

Field observations indicated that this unit experienced incipient pedogenesis which magnetic data also support (fig 5.15). The amplitude of second order variation decreases up the section. Second order variability consists of maxima in χ_{LF} reaching 32×10^{-8} m^3 kg^{-1}, an increase from a background level of $30 \times 10^{-8} m^3$ kg^{-1}. Although low in amplitude compared to Unit 5, the results show the fluctuations to be discrete in all magnetic records. Correlation between parameters shows they are significant and repeatable. As shown in Unit 5, where χ_{LF}, $\chi_{FD}\%$, χ_{ARM}, χ_{ARM}/χ_{LF}, and $\chi_{ARM}/SIRM$ show a visual positive relationship, magnetic susceptibility may be said to be enhanced by pedogenically formed SP/SSD and SD grains.

In Unit 3 there are coincident peaks in pedogenic parameters ($\chi_{FD}\%$, χ_{ARM}, χ_{ARM}/χ_{LF}, and $\chi_{ARM}/SIRM$) and SIRM, S-ratio, and soft % which is in contrast to Unit 5. In Unit 5, all remanence dependent parameters reached maxima in the intervening loess horizons. Another striking difference between Unit 5 and Unit 3 soils is the subdued response of HIRM. In Unit 5 there were conspicuous peaks in HIRM between pedogenically enhanced layers. In contrast, Unit 3 shows a complex environmental response of high amplitude variation in HIRM, but without the distinct peaks typical of other magnetic records: neither is it characterised by decreasing amplitude up section. IRM_${20mT}/\chi_{ARM}$ shows a clear inverse correlation with pedogenic indicators, $\chi_{FD}\%$, χ_{ARM}, χ_{ARM}/χ_{LF}, and $\chi_{ARM}/SIRM$, and a positive correlation with coarse bulk particle size. The wavelength of variation of the bulk granulometric records is longer than that of the magnetic records apart from IRM_${20mT}/\chi_{ARM}$.

$\chi_{ARM}/SIRM$ appears to be the best magnetic indicator of variations in fine, pedogenic grain size in this unit, indicating more SD grains in fine horizons. The highest IRM_${20mT}/\chi_{ARM}$ values indicating the greatest proportion of MD magnetic grain sizes occur in the coarser loess horizons. IRM_${20mT}/\chi_{ARM}$ appears to reflect the coarse, possibly detrital component, and certainly the coarse MD magnetic grain sizes. Profiles indicating hard or imperfect
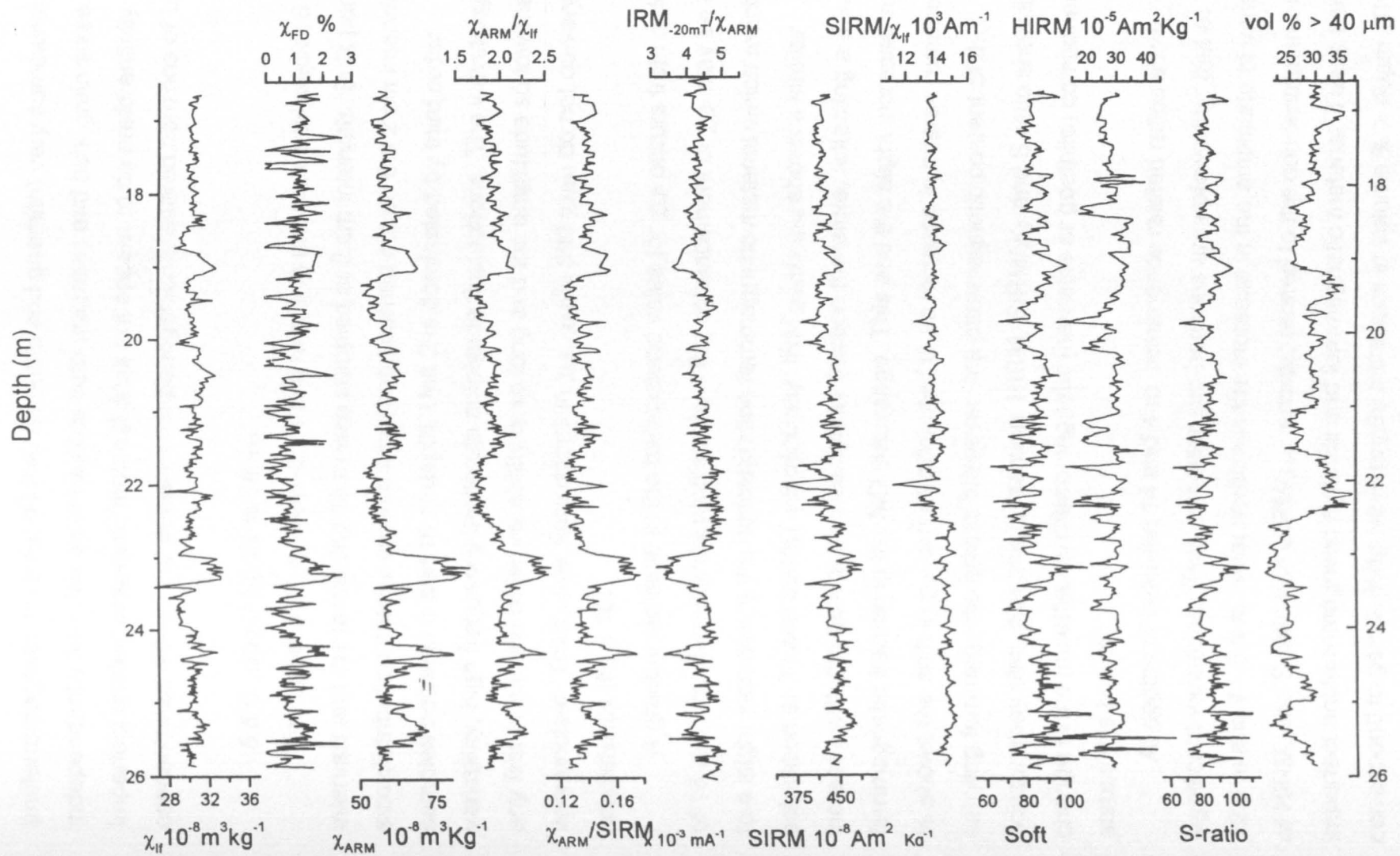
Figure 5.15 Magnetic and bulk grain size parameters of unit 3

antiferromagnetic material (HIRM, hematite and goethite) vary somewhat independently from the other records both magnetic and bulk grain sizes. Imperfect antiferromagnetic material does not appear to be preferentially concentrated either in or between the pedogenically altered horizons of Unit 3.

5.5.6. Unit 2 (-2.24 to 16 m)

The upper 8.24 m, from -2.24 to 6 m of this unit was analysed at 8 cm intervals and the remaining 10 m was sampled at 2 cm intervals. Bulk particle size distribution measurements have been carried out on the 2 cm interval samples between 6 and 16 m depth. Unit 2 is dominated by third order variability, high frequency moderate amplitude fluctuations. The wavelength of any first or second order variability is so long and the amplitude so low that it is very unclear. Third order fluctuations in χ_{LF}, $\chi_{FD}\%$ and χ_{ARM} do not co-vary consistently (fig 5.16).

A gradual increase in the background value for χ_{LF} occurs from a depth of 16 to 13 m. Remanence profiles show the enhancement of χ_{LF} may be due to a slight increase in the concentration ferrimagnetic material which reaches saturation at 20 and 300mT respectively. IRM$_{-20mT}$/χ_{ARM} shows a similar increase with the bulk grain size coarse fraction therefore, reflecting a dominant ferrimagnetic fraction in the MD size range. This and the slight increase in soft % shows the shift in χ_{LF} can be attributed to an increase in coarse remanence carrying ferrimagnetic grains. However, the paramagnetic content of this horizon may also increase up section. HIRM, SIRM/χ_{LF} and S ratio show little change in the imperfect antiferromagnetic (hematite or goethite) component across this horizon.

At depths of between 14 and 4 m, remanence related ratios show significant variations. Two particular sub-horizons are noteworthy: that at 13.5 12.5 m and 7 - 5.5 m. Most notable is the increase in the amplitude of variability of HIRM, and S-ratio and SIRM/χ_{LF} records; related to the concentration of imperfect antiferromagnetic material and ferrimagnetic material. These horizons correspond to gentle (long wavelength) increases in volume % > 40μm. This characteristic is not reflected to any significant fluctuations in the χ_{LF}, χ_{ARM}, or $\chi_{FD}\%$ 'pedogenic' parameters (see chapter 6).
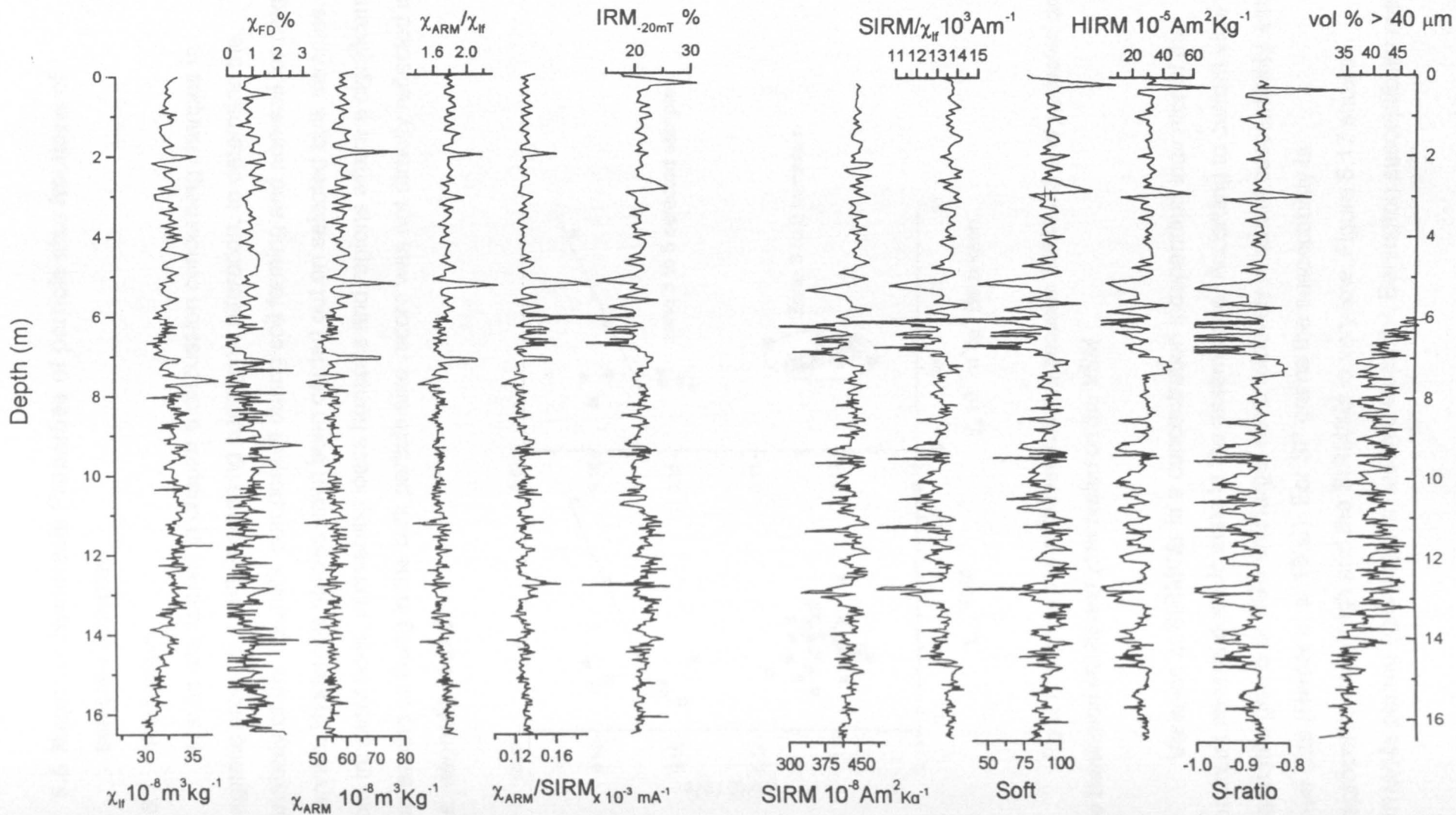
Figure 5.16 Magnetic and bulk grain size parameters of unit 2

5.6. Magnetic Hysteresis Properties of particle size fractions of selected samples

5.6.1. Introduction

Results are applied in chapter 6 discussion concerning changes in magnetic properties with increasing pedogenic alteration, to determine the variability of the magnetic component during soil forming and non-soil forming intervals. Hysteresis studies have been carried out on selected bulk samples, from incipient soils, intervening loess horizons and regions where a significant coarsening or fining in the bulk particle size record was not directly reflected in the magnetic record.
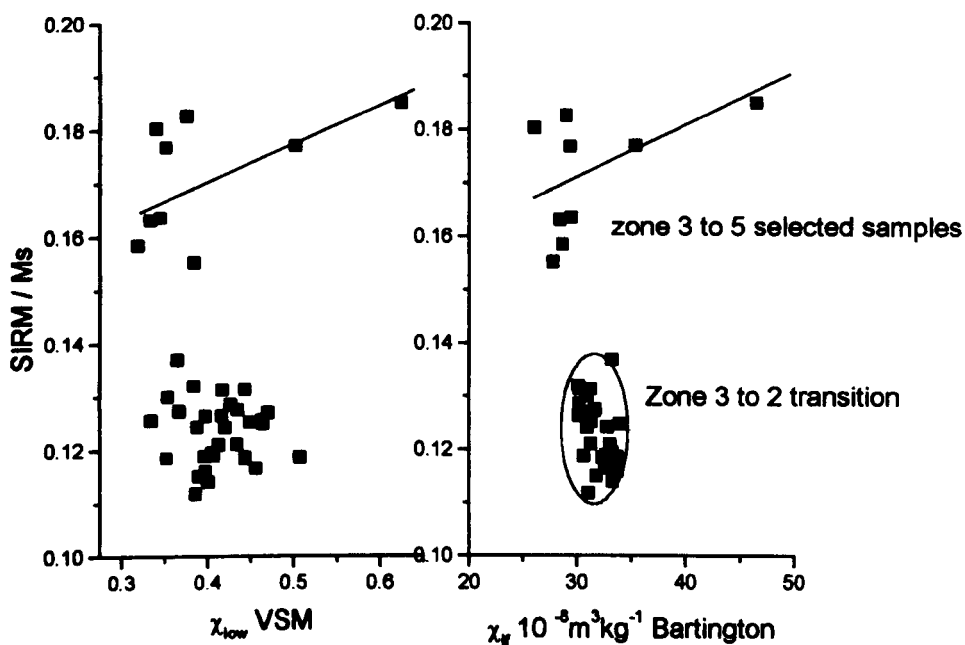
Fig 5.17 comparison of the relationship between SIRMI MS and χ_{LF} tested on the Bartington MS2B and χlow tested on the VSM

Variation in SIRM/Ms is a concentration independent indicator of the dominant mineral domain state in the assemblage. According to current view magnetite grains of SSD and larger have relatively invariant susceptibility with grain size (Heider et al 1996). For SP grains the susceptibility is disproportionately high and the SIRM/Ms is very low. Figure 5.17 shows SIRM/Ms plotted against χ_{LF} measured using the Bartington susceptibility meter

and χlow measured on the VSM. The patterns are similar. The Unit 3 to 2 transition shows no obvious increase in SIRM/Ms and χ_{LF} therefore little or no change in domain size is inferred. Samples from Units 3 to 5 show the expected trend indicating a dominance of small domain sizes in Unit 5 soils with high χ_{LF} values.

5.6.2. Results of VSM analysis of particle size fractions

VSM analysis was carried out on three particle size fractions; > 63μm 63-40 μm and <40 μm. As expected the < 40 μm has the highest bulk susceptibility and ferrimagnetic content. Results for HIRM shows that the <40 μm fraction has the highest imperfect antiferromagnetic content. The < 40 μm fraction contained the highest paramagnetic content. One noteworthy pattern may be the convergence of the fractions with depth; i.e. increased pedogenesis means the differences between these fractions become less distinct. This is probably an effect of the generally fining trend with depth of the bulk grain size. This convergence is obvious in χ_{ferri}% and χ_{high}% and may have implications for the future analysis of first order detrital material (chapter 6). Some results are shown in fig 5.18. The plot shows the χ_{LF} variation measured on the Bartington meter for comparison. It also shows that the > 63 μm fractions have the lowest total ferrimagnetic content of the 3 fractions analysed. The remaining two fractions 40-63 μm and <40 μm have a ferrimagnetic content relatively similar to the bulk sample. χ_{low} results indicate the potential magnetism of the 63μm fraction is lowest but increases with depth as the degree of pedogenesis increases with depth and the loess becomes generally finer. The 40-63 μm fraction and the < 40 μm fraction contain the majority of the magnetically susceptible material and there is an apparent decrease in values with depth, with the exception of the 2 samples from the well developed palaeosol horizons in unit 5. VSM analysis of imperfect antiferromagnetic content (HIRM) shows an increase in proportion with depth in bulk samples. The imperfect antiferromagnetic content of the >63 μm fraction also increases with depth. The remaining 2 fractions show the proportion of imperfect
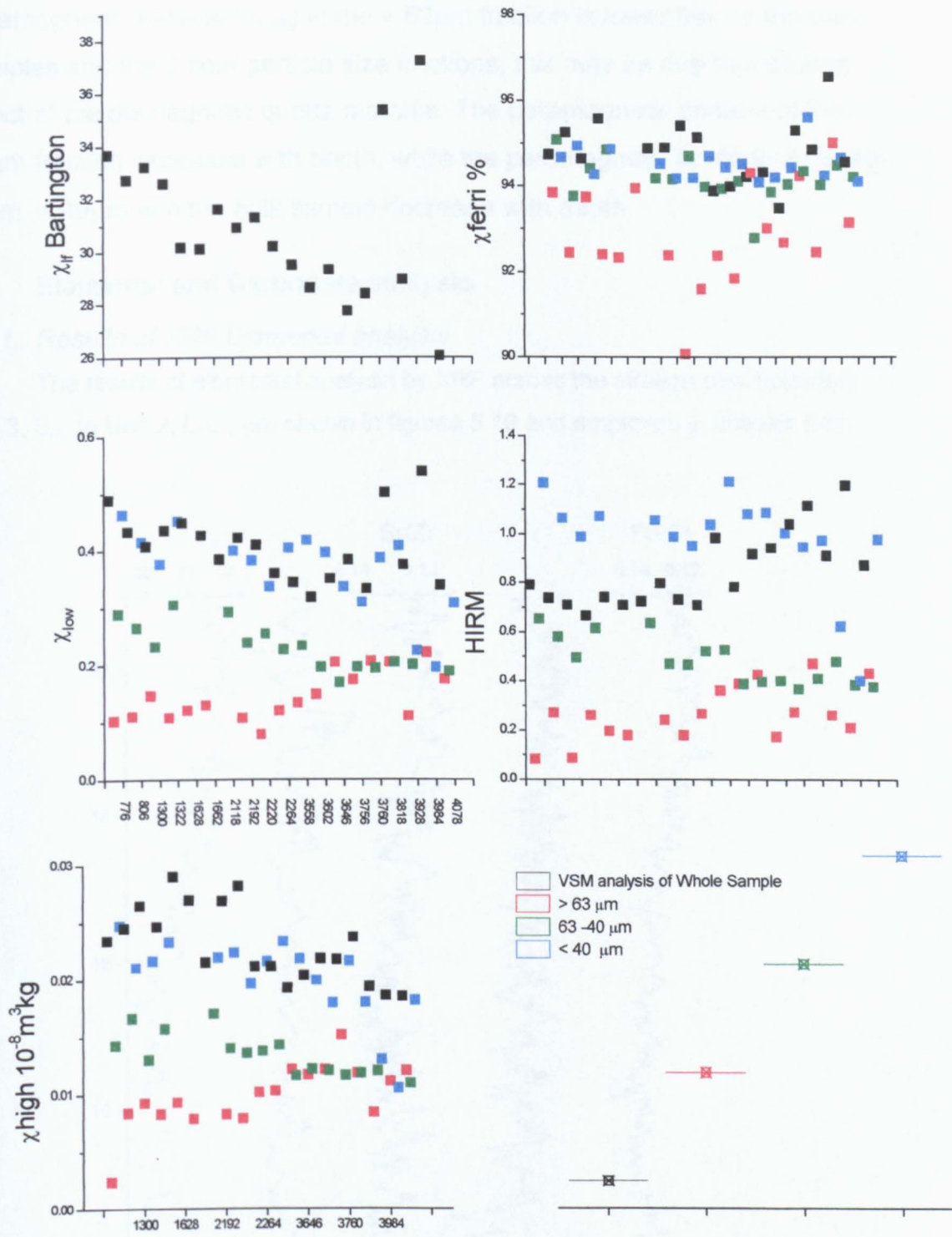
Figure 5.18 Hysteresis properties of particle size fractions. χ_{LF} Bartington eater results are shown for comparison. % ferri (ferrimagnetic material), χlow (~ equivalent to χ_{LF}), HIRM (imperfect antiferromagnetic material), χhigh (paramagnetic mineral content)

antiferromagnetic material decreases with depth. The proportion of paramagnetic material (χ_{high}) in the > 63μm fraction is lower than in the bulk samples and the 2 finer particle size fractions, this may be due to a diluting effect of the diamagnetic quartz material. The paramagnetic content of the > 63μm fraction increases with depth, while the paramagnetic content of the 40-63μm, < 40μm and the bulk sample decrease with depth.

5.7. Elemental and Carbonate analysis

5.7.1. Results of XRF Elemental analysis

The results of elemental analysis by XRF across the stratigraphic boundary Unit 3, S_m. to Unit 2, L_1L_1, are shown in figures 5.19 and employed in chapter 6 to
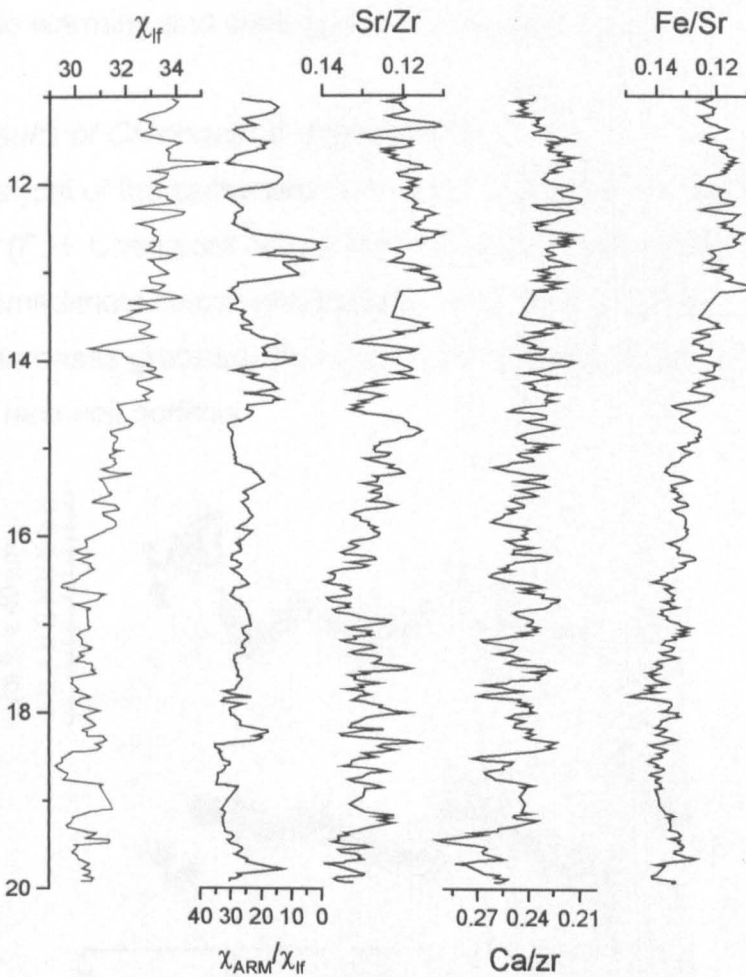
Fig 5.19 Trends in Sr, Ca, and Fe across the horizon of increasing coarse grained ferrimagnets. All elements are normalised.

further elucidate temporal changes in source and transport of dust on to the plateau. Three elements show a broad relationship to environmental and bulk particle size parameters: iron, calcium and strontium. As susceptibility and bulk particle size increases with increasing dominance of coarse ferrimagnets, the relative proportion of Fe, Ca, Sr show small but significant decreases. The method used was not precise enough to pick out anything more than general trends. The variation of Sr/Zr is very similar to that of χ_{LF}. This may indicate that it responds to the same environmental factors as χ_{LF}. However, Zr as a primary heavy mineral may be influenced by wind intensity such that it increases in relative proportion as bulk grain size increases. It should be noted that this inverse relationship is most obvious in sub- horizons with some pedogenic magnetic characteristics. Any apparent cyclicity could not be verified, and may be linked to warming and cooling due to the liquid nitrogen.

5.7.2. Results of Carbonate analysis of unit 5

Analysis of the carbonate content of Unit 5 was carried out at Lanzhou University (F.H. Chen pers.com.). Results show horizons of high carbonate content immediately below magnetically enhanced horizons. The carbonate content decreases gradually through the coarser horizons, peaking abruptly below the next soil horizon.
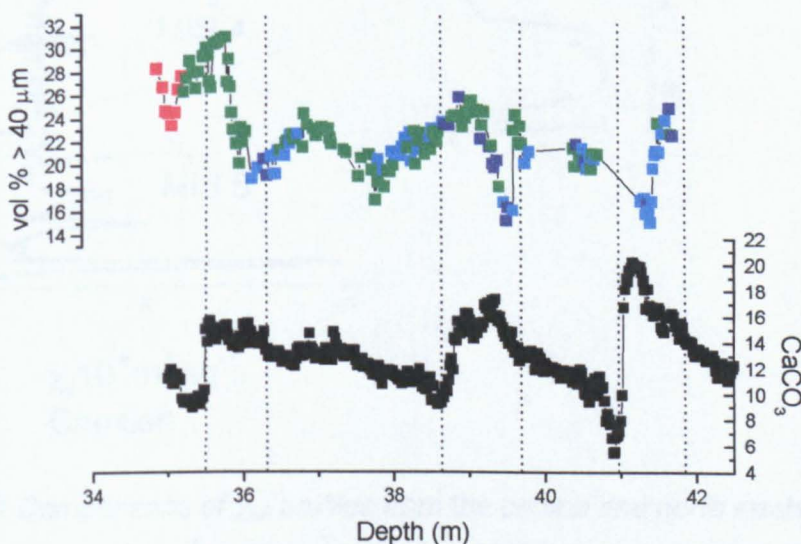
Figure 5.20 variations in carbonate content of Unit 5 compared to bulk grain size volume % >40um

6. Chronology and Environmental interpretation of PSD variations

Type Sites for the loess plateau are located in the central loess plateau where extensive deposits have been dated to an age of 2.4 my. Sites at Baoji and Luochuan have successfully shown that the terrestrial environment of central China responds to large scale glacial interglacial fluctuations (Ding et al. 1995). However such sites are unsuitable for analyses of rapid climate variability. Because of the low sedimentation rate and pedogenic overprinting.
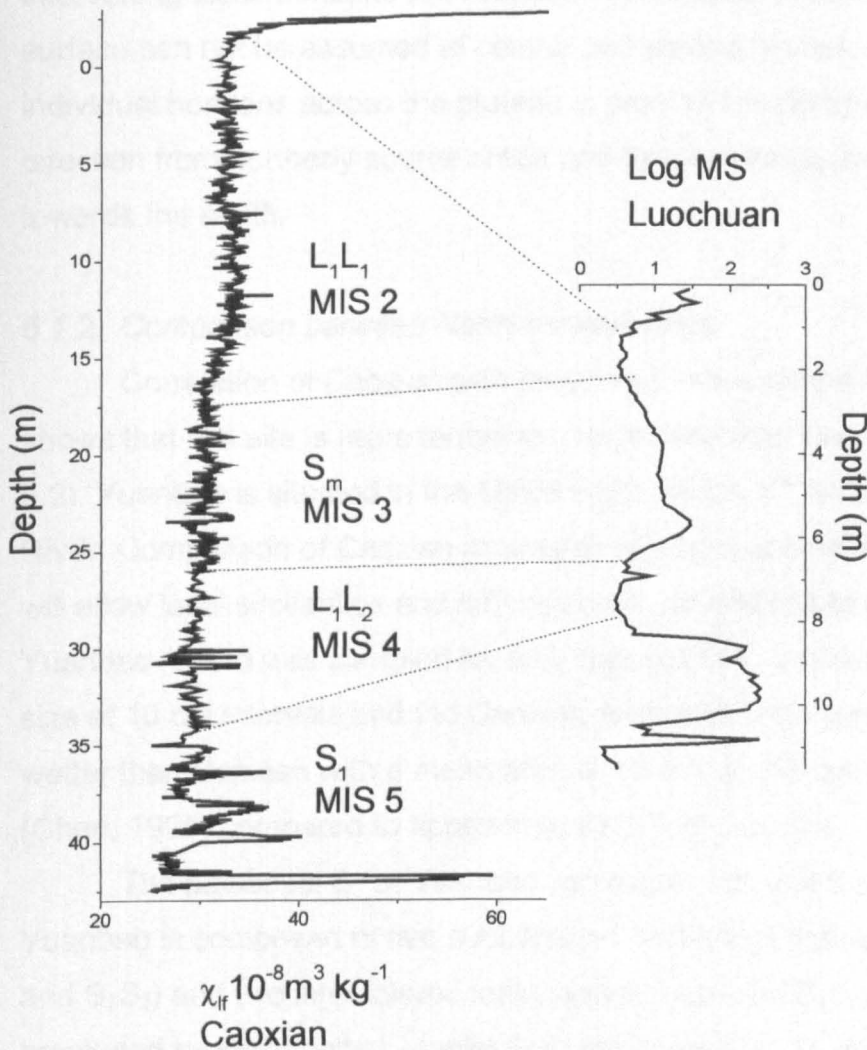
6.1 Comparisons of χ_{LF} profiles from the central and north western loess Plateau, Luochuan and Caoxian respectively. MIS 2, 3, 4, and 5 = marine oxygen isotope stages corresponding to the loess stratigraphy classification.

6.1. Chronology

6.1.1. Comparison of Central and North-western sites

A correlation of Caoxian and Luochuan section from the central loess plateau shows the striking difference in thickness of the sedimentary pile across the loess plateau during the last glacial interglacial cycle. Luochuan shows enhanced bulk susceptibility between 12 – 8 m and 6.5 - 2 m. These horizons have been well dated and correlate with marine oxygen isotope stage (MIS) 5 and MIS 3 of the ice and deep sea marine record. Due to the reduced sedimentation rate there is considerable overprinting of the susceptibility signal, intervening loess horizons are reduced in thickness. A constantly aggrading surface can not be assumed at central and southerly sites. The wedge shape of individual horizons across the plateau is proof of the dominant aeolian transport direction from northerly source areas and the increasing precipitation gradient towards the south.

6.1.2. Comparison between North-western sites

Correlation of Caoxian with other sites in the northwest of the plateau shows that this site is representative of high resolution loess records (see fig 6.2). Yuanbao is situated in the Linxia basin on the 4th terrace of the Daxia River. Comparison of Caoxian to another site across a relatively short distance will allow local similarities and differences in parameters to be assessed. The Yuanbao record was sampled for bulk susceptibility at 5 cm intervals, particle size at 10 cm intervals and the Caoxian section at 2 cm intervals. Yuanbao is wetter than Caoxian with a mean annual rainfall of approximately 500mm (Chen, 1999) compared to approximately 300 at Caoxian.

The palaeosol S_1 at Yuanbao correlates with unit 5 at Caoxian. S_1 at Yuanbao is composed of five subhorizons; three well defined soils (S_1S_1, S_1S_2 and S_1S_3) and two intercalated loess layers (S_1L_1 and S_1L_2). Palaeosol S_1 is bracketed by loess units L_1 (units 4, 3, and 2) and L_2. TL dates for a weathered loess layer in the Yuanbao section, close to the L_1 S_1 boundary is given as 65 ± 5 ka (Chen et al, 1999). The base of S_1S_1 is 90 ± 10 ka, and the lower part of S_1S_3 has been dated as 125 ± 10 ka indicating that this soil was formed during the Eemian interglacial. Comparison of the Caoxian and Yuanbao sections

shows that MIS 5, 4, 3, and 2 correspond to units 5, 4, 3, and 2, S_1, L_1L_2, L_1S_1 (S_m), L_1L_1 using Chinese loess nomenclature.
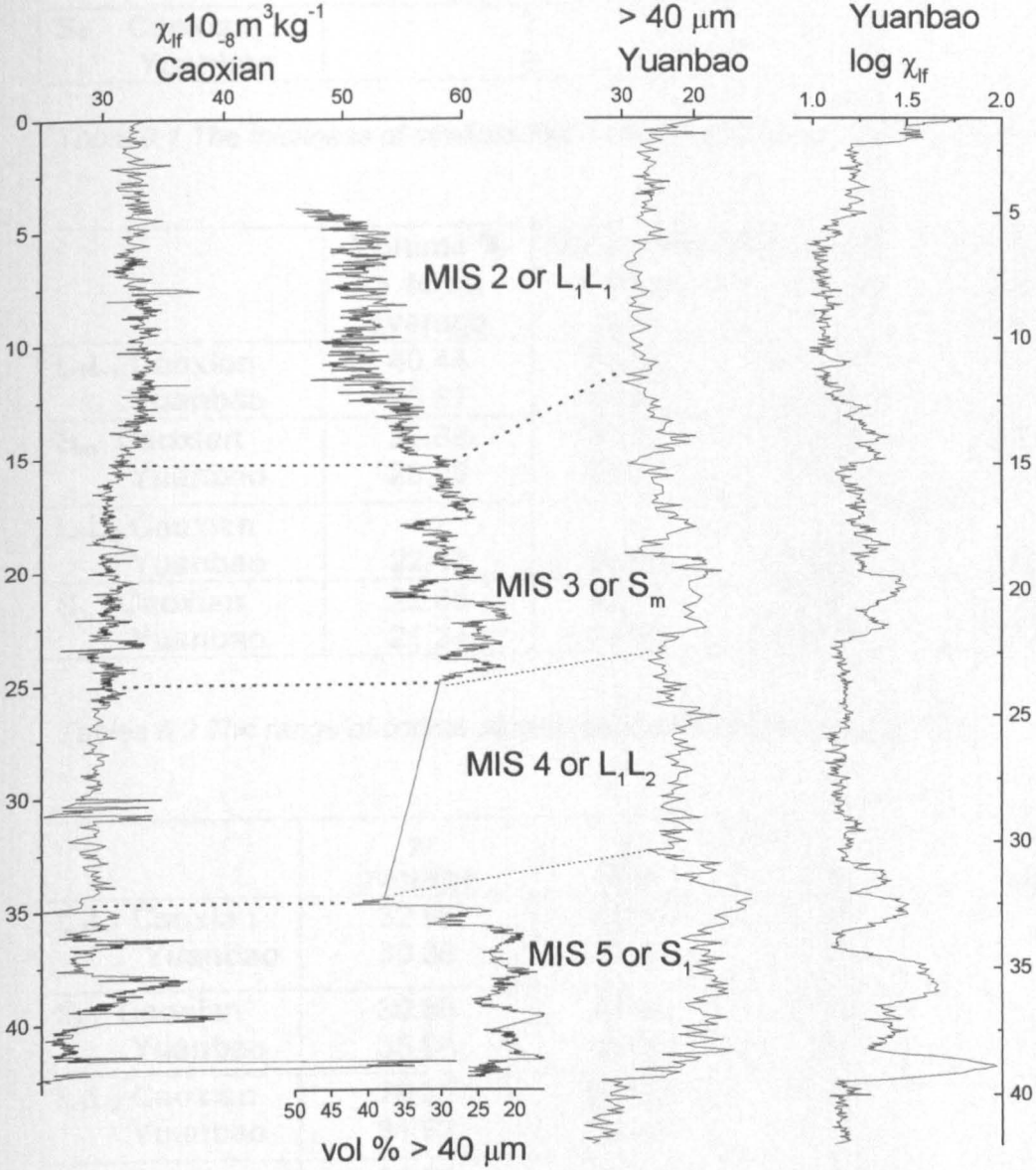
Figure 6.2 Comparison of the χ_{LF} and coarse particle size fraction of 2 northwestern sites, Caoxian and Yuanbao (Chen et al, 1997)

	Thickness in M (approx.)
L_1L_1 Caoxian	16
Yuanbao	9
S_m Caoxian	9
Yuanbao	11
L_1L_2 Caoxian	10
Yuanbao	8.5
S_1 Caoxian	7
Yuanbao	9

Table 6.1 The thickness of stratigraphic horizons at Caoxian and Yuanbao

	Volume % > 40µm average	Volume % > 40µm max	Volume % > 40µm min	Volume % > 40µm range
L_1L_1 Caoxian	40.44	51.52	30.30	21.22
Yuanbao	26.87	29.67	23.23	6.44
S_m Caoxian	28.88	37.52	20.60	16.92
Yuanbao	23.25	29.42	16.10	13.32
L_1L_2 Caoxian				
Yuanbao	22.62	26.43	16.52	9.90
S_1 Caoxian	22.85	42.14	15.05	27.09
Yuanbao	21.34	34.98	11.33	23.65

Tables 6.2 The range of coarse particle sizes at Caoxian and Yuanbao

	χ average	χ max	χ min	χ range
L_1L_1 Caoxian	32.90	38.01	30.41	7.61
Yuanbao	30.38	36.73	26.83	9.91
S_m Caoxian	30.56	33.45	26.54	6.91
Yuanbao	35.94	44.43	29.42	15.01
L_1L_2 Caoxian	29.26	34.82	25.15	9.67
Yuanbao	31.92	36.49	29.10	7.39
S_1 Caoxian	31.02	59.62	25.06	34.56
Yuanbao	39.64	71.60	29.74	41.86

Tables 6.3 The range of χ_{LF} values at Caoxian and Yuanbao

6.1.3. Characteristics of S_1 at Caoxian and Yuanbao

The χ_{LF} profiles show that the concentration of magnetic material is lower at Caoxian with a smaller range of values and the amplitude and wavelength of variability is smaller i.e. less variation than at Yuanbao and lower χ_{LF} values. The susceptibility record of Yuanbao is smoother than at Caoxian. This may be due to the closer sampling interval, or alternatively a greater influence of precipitation and soil moisture allowing a higher level pedogenesis leading to a degree of overprinting.
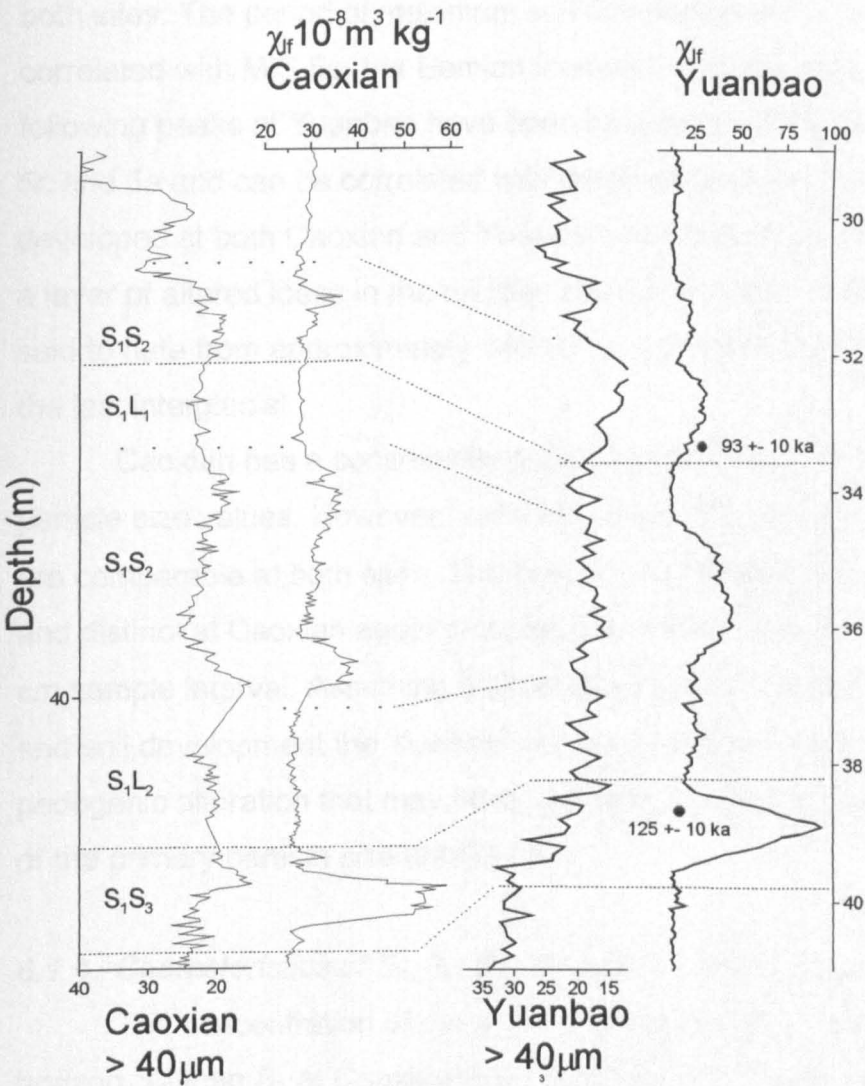
Figure 6.3 Characteristics of the magnetic susceptibility and bulk particle size records for S_1 (Unit 5) at Caoxian and Yuanbao (Yuanbao data from Chen et al, 1997)

Soil horizons at Caoxian are consistently thinner than at Yuanbao. However, the pattern of variability is similar. The χ_{LF} profile at Caoxian shows abrupt shifts to magnetically enhanced layers even though the total thickness of the MIS 5 horizon is approximately 2 m less than at Yuanbao. The apparent rapidity of change may also be a feature at Yuanbao but a similar sampling interval would be required to demonstrate this. Caoxian shows some of the best evidence for the rapidity of response of MIS 5 soils to changing environmental factors.

The greatest degree of magnetic enhancement occurs in the lower most soil horizon S_1S_3, with consecutive soils becoming gradually less enhanced at both sites. The period of maximum soil development is dated at Yuanbao and correlated with MIS 5e, the Eemian interglacial (Chen et al, 1997). The following peaks at Yuanbao have been labelled as the subsequent interstadials 5c and 5a and can be correlated with those at Caoxian. S_1S_3 is the best developed at both Caoxian and Yuanbao. At Caoxian palaeosol S_1S_2 contains a layer of altered loess in the middle. The base of the Caoxian section can be said to date from approximately 140 ka i.e. the beginning of amelioration into the last interglacial.

Caoxian has a consistently coarser particle size, and a greater range of particle size values. However, variations in coarse particle size (vol % > 40μm) are comparable at both sites. The five minima in particle size are more abrupt and distinct at Caoxian again probably the result of a 2cm as opposed to a 10 cm sample interval. Assuming a direct relationship between χ_{LF} enhancement and soil development the Yuanbao profile indicates a higher degree of pedogenic alteration that may have resulted in a greater degree of weathering of the primary particle size distribution.

6.1.4. Characteristics of S_m (L_1 S_1) at Caoxian and Yuanbao

The concentration of magnetic material is much lower during soil forming horizon S_m than S_1 at Caoxian than Yuanbao, with a smaller range of values. The amplitude and wavelength of variability is smaller than the equivalent S_m horizon at Yuanbao. The abrupt shifts are again more apparent at Caoxian
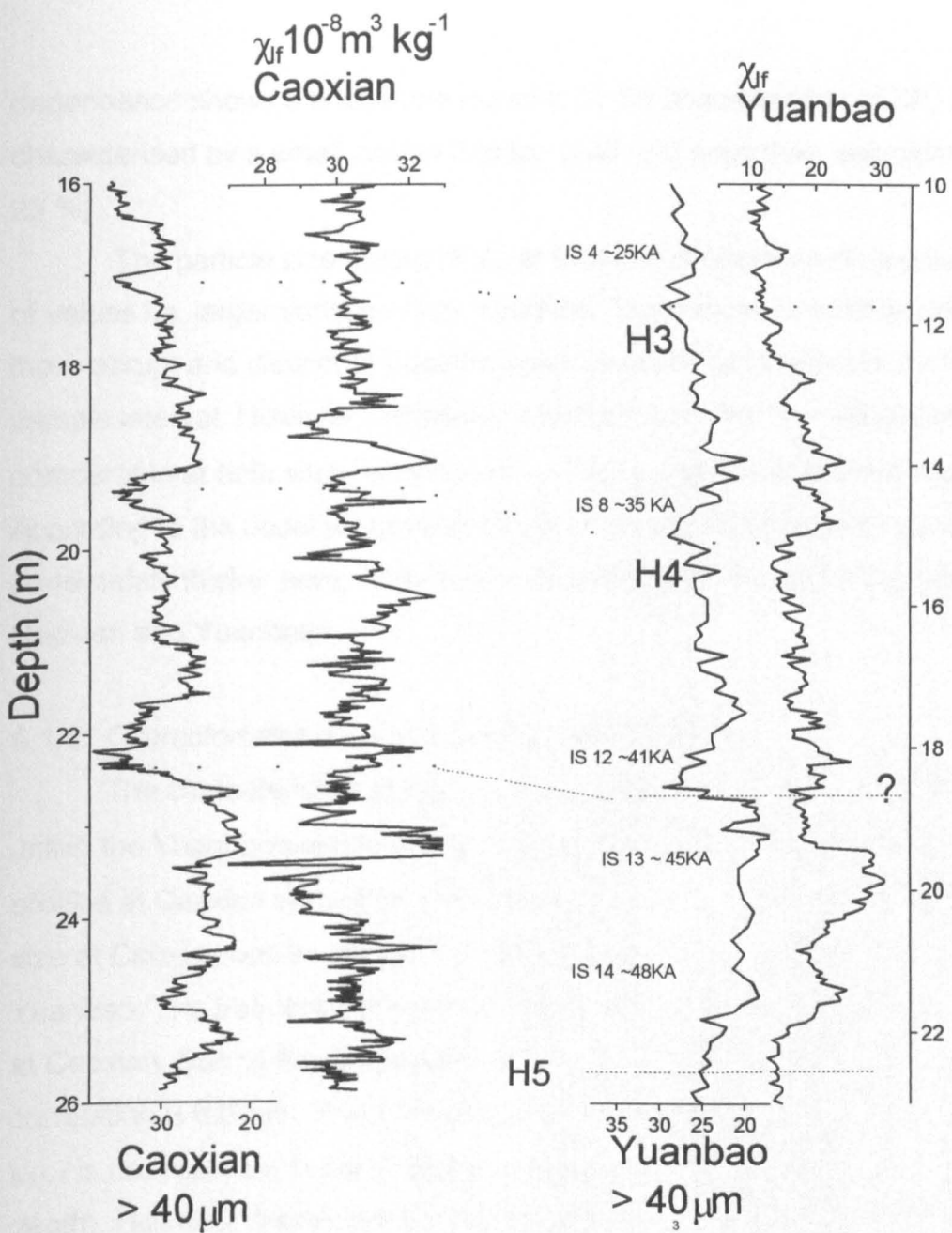
Figure 6.4 Characteristics of S_m (L_1 S_1) at Caoxian and Yuanbao

than at Yuanbao, most likely due to the closer sample interval and perhaps lower levels of pedogenic alteration. The χ_{LF} profile at Caoxian shows abrupt shifts to magnetically enhanced layers even though the total thickness of the S_m horizon is approximately 2 m less than at Yuanbao, similar to S_1. Since this soil horizon is again thinner at Caoxian than Yuanbao, this abruptness can not be a response to sedimentation rate. As the degree of magnetic enhancement decreases up profile at Caoxian, the differences between it and its particle size counterpart and Yuanbao records increases. Soils at Caoxian, where frequency

dependence shows a noticeable increase in the concentration of SP, are also characterised by a small coarse fraction (>40 μm) (less than approximately 23-25 %).

The particle size record of S_m at Caoxian is coarser with a greater range of values i.e. larger variation than Yuanbao. The minima in particle size are more abrupt and distinct at Caoxian again probably as a result of the finer sample interval. However, variations in particle size (vol % > 40μm) are comparable at both sites, much more so than χ_{LF} profile at the two sites. According to the usual assumptions one would expect the coarser site to have consistently thicker beds, both loess and palaeosols this is not the case at Caoxian and Yuanbao.

6.1.5. Characteristics of L_1L_1 at Caoxian and Yuanbao

The characteristics of the χ_{LF} and particle size records at Caoxian are unlike the Yuanbao particle size and χ_{LF} profile. The particle size and χ_{LF} profiles at Caoxian show little similarity to each other, unlike Yuanbao. Particle size at Caoxian has a volume % > 40μm generally 10 –15% higher than Yuanbao. The frequency of variation of the particle size profile is much higher at Caoxian. Due to the dissimilarity of the sections of this unit detailed correlation is difficult. The pronounced shift in background χ_{LF} at the base of L_1L_1 is not apparent in the Yuanbao section (see fig 6.2 between 17 and 13m depth). However, there appears to be a stepped increase at Yuanbao between depths of 6 and 5 m but the relationship of these shifts between the two sites is unclear.
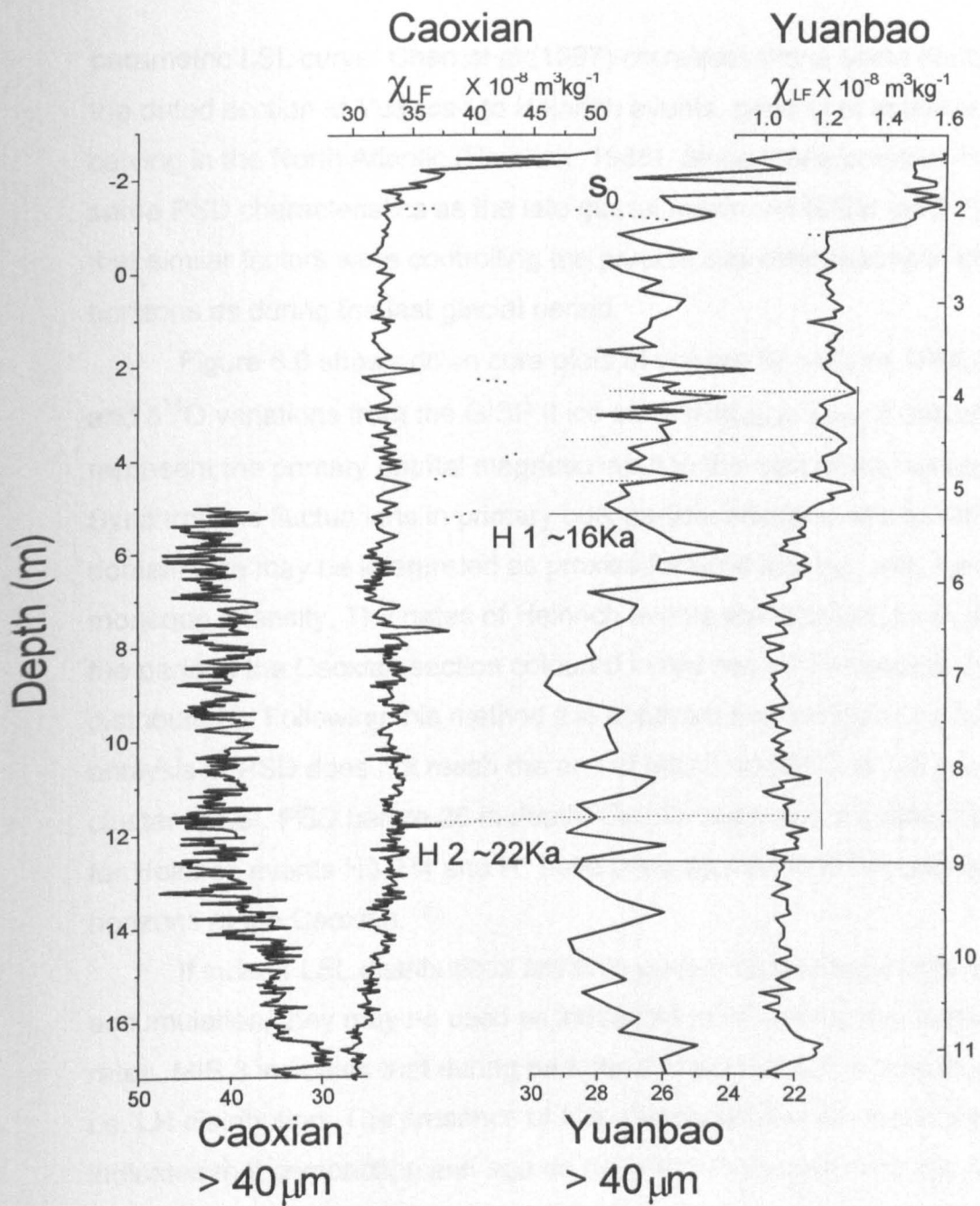
Figure 6.5 Comparison of L_1L_1 at Caoxian and Yuanbao. Magnetic susceptibility and coarse fraction grain size fraction. H – Heinrich Events.

6.2. Heinrich Event signatures in the PSD of NW Chinese Loess

The similarity of particle size curves from Caoxian and Yuanbao allows tentative dates to be applied to the Caoxian profile (fig 6.4). As shown in Chapter 5 it is possible to describe loess and altered loess - palaeosol by fitting LSL and LH distributions respectively. Figures 5.12 and 5.13 showed that sub-horizons of coarse material within MIS 3 were generally modelled well by a

parametric LSL curve. Chen et al (1997) correlates these same horizons from the dated section at Yuanbao to Heinrich events, periods of massive iceberg calving in the North Atlantic (Heinrich, 1988). Since these horizons have the same PSD characteristics as the late glacial maximum (LGM -MIS 2) it appears that similar factors were controlling the particle size distributions in these horizons as during the last glacial period.

Figure 6.6 shows down core plots of volume % >40 μm, IRM$_{-20mT}$/χ_{ARM}, and δ^{18}O variations from the GISP II ice core. IRM$_{-20mT}$/χ_{ARM} is assumed to represent the primary detrital magnetic input to this part of the section. Synchronous fluctuations in primary bulk particle size and coarse MD magnetic domain size may be interpreted as proxies for wind strength and, hence winter monsoon intensity. The dates of Heinrich events are labelled. As in chapter 5, the parts of the Caoxian section coloured in red mark PSD modelled by LSL distributions. Following this method it is apparent that the high resolution analysis of PSD does not reach the end of MIS 3 since H5 is not evident as a cluster of LSL PSD before 26 m depth. On the basis of this correlation, dates for Heinrich events H3, H4 and H* have been applied to these coarse LSL sub-horizons at the Caoxian.

If indeed LSL distributions are only preserved during periods of rapid accumulation, they may be used as indicators of extremely high sedimentation rates. MIS 3 indicates that during periods of lower flux some alteration occurs, i.e. LH distribution. The presence of LSL distributions at the base of MIS 5 (L2) indicates that compaction and age do not affect the potential to fit a parametric LSL PSD. If it is assumed that LSL PSD indicated environments of rapid dust deposition then the sedimentation between H events can not be linear. When calculating the sedimentation rate based on this hypothesis on the mean accumulation rate can be estimated.
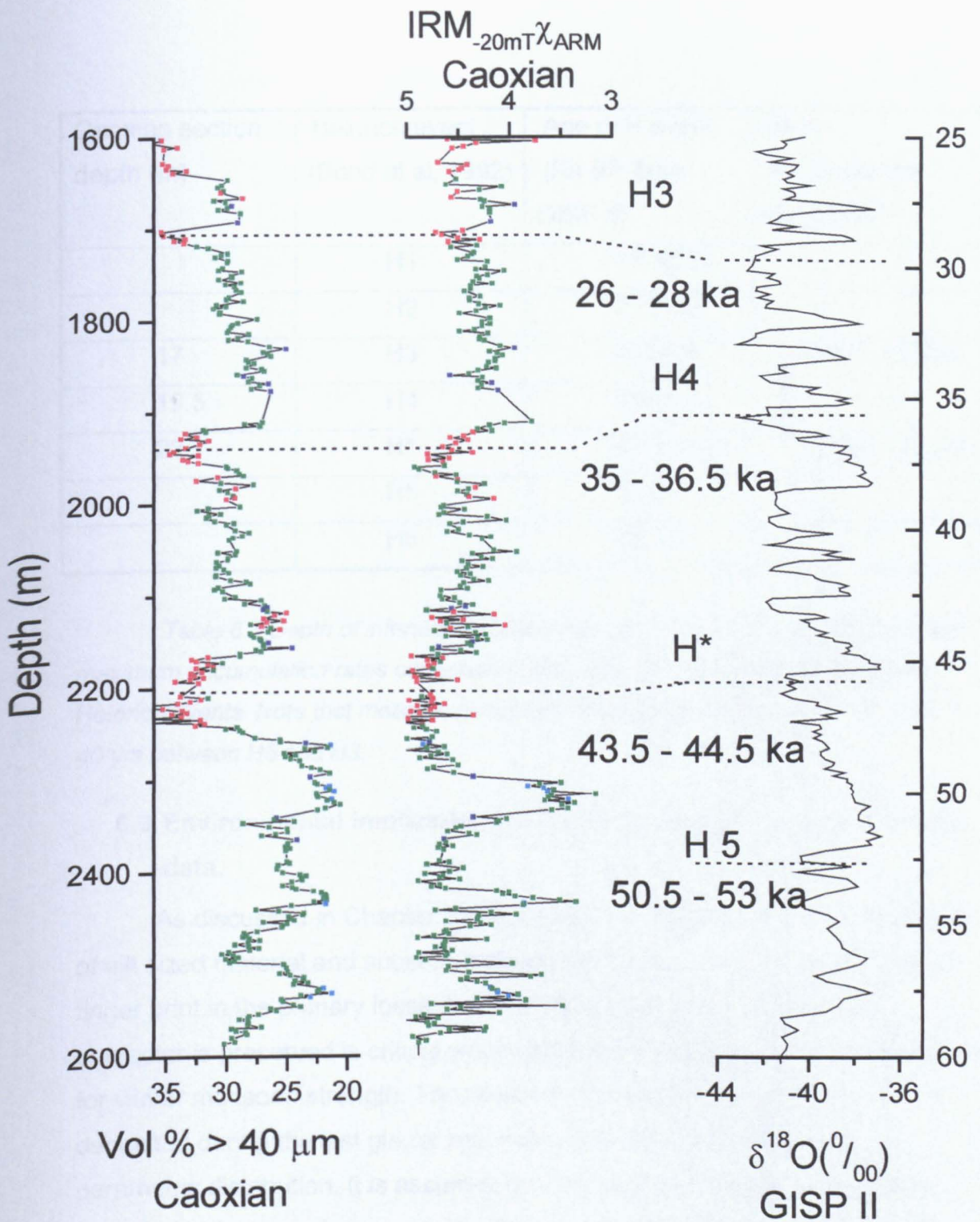
Figure 6.6 Down Section plot of volume % > 40 μm, IRM$_{-20mT}$/χ$_{ARM}$, and δ^{18}O
variations from the GISP II ice core. All ages are in yr BP (AD 1950 = 0 yr BP) GISP
data after Sowers et al (1993). H – Heinrich events.

Caoxian section depth (m)	Heinrich event (Bond et al, 1992)	Age of H event (Ka BP from GISP II)	Mean Accumulation Rate (m/y)
	H1	15-16.5	
	H2	21.5-22	
17	H3	26.5-28	0.025 – 0.036
19.5	H4	35-36.5	
22	H*	43.5-44.5	0.026 – 0.036
	H5	51-53	
	H6	68.5-70	

Table 6.3 Depth of inferred Heinrich event position at Caoxian. Minimum and maximum accumulation rates calculated from oldest and youngest possible dates of Heinrich events. Note that mean accumulation rate shows a thickness of 1 m in 30 – 40 yrs between H5 and H3.

6.3. Environmental implications of the bulk particle size and magnetic data.

As discussed in Chapter 2 and chapter 3 initial stages in the production of silt sized material and subsequent transport processes will leave a textural finger print in the primary loess deposit. The extent to which this primary character is preserved is critical when using particle size parameters as a proxy for winter monsoon strength. The results in Chapter 5 showed that dust deposited during the last glacial maximum is best modelled by a LSL parametric distribution. It is assumed that this is characteristic of cold loess. The magnetic mineralogy suggests that L_1L_1 loess has undergone very little pedogenic alteration. However, the magnetic susceptibility shows that L_1L_1 loess has a slightly different composition from sub-horizons within S_m. Several causes are suggested. LSL horizons in S_m may have undergone some alteration changing the magnetic particle size and mineralogy form one originally similar to that of L_1L_1. Alternatively the primary magnetic composition of LSL horizons in S_m may have been different to that of L_1L_1 and this has been preserved. The latter scenario is preferred, on the basis that LSL horizons in

L_1L_1 occur during the glacial maximum and S_m LSL horizons correlate with H events in the north Atlantic.

It was shown in chapter 5 that although the distribution of those samples best described by an LSL model may shift finer, the shape of the distribution remains the same and that this may be indicative of a consistent transport mechanism. It is generally accepted that the collapse of thick ice sheets during temperature minima resulted in the iceberg calving events and allowed major atmospheric circulation reorganisations, thus influencing dust transport (Dansgaard et al, 1993; Taylor et al, 1993a; Ding et al, 1995). The differing magnetic compositions may reflect the longevity of the 'dusty' period. Rapid warming follows Heinrich events, as illustrated in the GISP II ice core (Bond et al, 1992; Taylor et al, 1993a). During these periods of rapid warming, one may assume a rapid decrease in dust flux and a possible coincident change in dominant transport mechanism. The magnetic properties of the loess at the beginning of L_1L_1 are similar to those of the S_m sub-horizons. As the L_1L_1 period continued, the magnetic phase changed in both composition and domain size. This may reflect a shift in the dominant wind direction i.e. change in source area or extensive deflation of the source area exposing material of a different composition. It may be expected that some weathering will occur in the source area during warm intervals. Indeed Lehmkuhl (1998a) found evidence of subtropical soil development and planation surfaces on the Tibetan Plateau margin and alluvial fans. It is logical to assume that some of this pedogenically altered material will be eroded and transported to the loess plateau at the initiation of dusty periods. During extended dusty periods, subsoil may be exposed i.e. different magnetic mineralogy. Alternatively, increased weathering intensity during cold periods will eventually provide a supply of freshly weathered bedrock material.

If a constant transport mechanism can be assumed for these LSL distributions, it is likely to be a combination of low level suspension perhaps with a saltation component ascertained by the large particle size. Such a statement may imply that LH distributions are characteristic of a greater degree of suspended or finer material. This is misleading since environmental magnetic evidence suggests a significant degree of pedogenic alteration. In line with the results of this study, the author does not assume that the primary PSD

178

representative of warm dust deposition events differs significantly in PSD shape i.e. better modelled by a LH curve.

Zhang et al (1999) noted that the present day PSD is similar to the PSD of S_1 at Luochuan. S_1 at Luochuan shows high pedogenic alteration as indicated by χ_{FD} %. If warm loess deposition is indeed characterised by a LH distribution then the change may reflect a change in the dominant aeolian transport mechanism. Differences in the magnetic character may reflect alteration along the transport pathway as well as in situ post depositional changes. It is possible that characteristic PSD differs between cold and warm loess depositional periods (Zhang's (1996) dust storm and non dust storm periods). Chapter 2 discussed previously published evidence for different PSD and possibly different compositions of present day dust-storm and non dust-storm dust. On a longer time scale this scenario would appear appropriate since the wind regime is unlikely to have been the same during stadials and interstadials, due to the shifting position of the Siberian – Mongolian high and Aleutian low pressure systems as the polar vortex waxed and waned.

Evidence against this hypothesis is that PSD parametric models show PSD are altered on a continuum from loess layers in S_m to the most well developed soils in S_1 (see fig 5.9 and 5.10). Therefore, the author believes that the majority of LH particle size distributions reflect the degree of in situ alteration. The PSD of the oldest part of the Caoxian section (top of S_2) changes from a LSL distribution to a LH. PSD within S_1 or MIS 5 are shown to be best represented by a LH parametric curve represented by the most extreme LH PSD in the entire section. Combining parametric curve fitting results and high levels of magnetic enhancement, it may be postulated that the higher degree of weathering in MIS 5 has significantly altered the PSD. Although the relationship between PSD, coarse particle size % and in situ ferrimagnetic enhancement shown in chapter 5 is complex it may be said that the coarse fraction at Caoxian in MIS 5 no longer reflects the primary PSD. Since the degree of ferrimagnetic enhancement is greater, the amount of weathering of particles may be even higher at Yuanbao

This means that past publications using particle size windows as proxies of the winter monsoon are somewhat flawed. The author believes that those

samples that generally fall as a cluster of outliners coloured dark blue are unrepresentative of the section as a whole. They are described by LH parametric curves with a μ_{LH} and μ_{LSL} of -2.7. The similarity of μ values of LSL and LH implies that they should be best described by a LSL (where $\delta = 0$, μ_{LH} $=\mu_{LSL}$). They have scattered Ncrit LH $-$Ncrit LSL values and therefore may be best fitted by a LH or LSL distribution. Figure 5.20 showing CaCO3 measured by calcimetery indicates that the majority of these samples fall in horizons of re-precipitated CaCO3, and therefore may represent PSD containing carbonate aggregates that have not been removed by the minimal preparation technique. It should be noted that bulk particle size does not show any significant degree of coarsening compared to other fine horizons. Although this conclusion would indicate pedogenic alteration of the PSD it substantiates the potential of parametric models to distinguish between pristine and pedogenically altered loess.

It is the light blue samples that show the greatest shift in μ value between LSL and LH parametric parameters i.e. appear coarser in LH models. They also have the highest Ncrit values i.e. definitely should be LH PSD. Since they do not coincide with CaCO3 enhancement, the apparent coarsening is not due to carbonate nodule. It may reflect the dissolution of fine grained primary carbonate thus causing a relative coarsening of the distribution. It should be noted that examination of individual phi particle size windows of these distributions failed to identify any relatively depleted or enhanced fractions.

Soils at Caoxian are consistently thinner than at Yuanbao. That this is a symptom of overprinting into previously deposited loess at Yuanbao can not be discounted i.e. increasing the apparent thickness of the soil at the expense of the underlying loess layer. Alternatively thinner soil horizons at Caoxian may imply that a smaller gross flux was deposited at the site during interglacials / stadials. The implications of this are that Caoxian was in a depositional shadow, the majority of material may have been carried further east to Yuanbao. Increased vegetation during interglacials and interstadials may be expected to limit saltation and low level suspension processes. If indeed Caoxian received a significant saltation and low level suspended sediment input during stadials and glacials, this would be rapidly curtailed by an increase

in surface roughness i.e. vegetation. Assuming a transport mechanism dominated by suspension, this may be a logical conclusion. If, during interglacials and interstadials the area surrounding Caoxian had a low trapping potential of higher level suspended dust (vegetation etc.) and did not reduce the upward wind velocity the material may have remained in suspension for a longer distance, thus a relatively higher flux reaching Yuanbao's position. Conversely initial fluxes reaching Caoxian may have been similar or higher than at Yuanbao, but significant redistribution occurred i.e. winnowing of the surface by (modified) saltation and suspension due to a lower degree of surface protection, indicating the vegetation factor again. Increased magnetic enhancement may indicate greater organic material, hence denser vegetation cover at Yuanbao, assuming a higher precipitation level than Caoxian in the past. This would have acted not only to cause deposition but also to prevent significant resuspension at Yuanbao. This may account for differences in the PSD of dust deposited during an intense soil forming interval and that deposited during an intense glacial period. The fact that soil horizons are thinner yet coarser at Caoxian reveals a non linear relationship across the north western part of the loess plateau between sedimentation rate and particle size. According to the usual assumptions on would expect the coarser site to have consistently thicker beds this is not the case of Caoxian and Yuanbao.

6.4. The possible significance of changes in the magnetic mineralogical assemblage

In horizons of significant magnetic enhancement by fine grained SP and SD ferrimagnetic material one may expect the SIRM S-ratio and SIRM/χ_{LF} profile also to reflect this enhancement. This is not the case in MIS 5 at Caoxian. The large peaks in these profiles occur in the horizon between those that are pedogenically enhanced. Since these horizons of relatively increased coarse magnetic material correspond to coarser particle size a number of potential formation mechanism may be put forward. 1) It is simply a reflection of the primary magnetic component deposited in the detrital component during stadial periods. 2) Antiferromagnetic material and coarse ferrimagnetic material is relatively concentrated in the intercalated coarser horizons. This may be directly related to primary dust composition or to a lesser/different type of

pedogenesis in cooler environment. The stadial horizons of Unit 5 are as coarse as Unit 3 or MIS 3. This section shows a small but significant degree of magnetic enhancement indicating significant soil moisture content. It may be assumed that MIS 5 stadial loess is not unaffected by pedogenesis. MIS 5 shows soil development in line with assumptions usually made about pedogenesis on the loess plateau i.e. that $\chi_{FD}\%$ is a good indicator of the degree of pedogenic development and may be proportional to degree of soil moisture and oxidative and reducing conditions within the soil.

Comparison of north western and central loess plateau sites presumes that there is a significant difference in sedimentation rate, higher in the north than in the centre. This does not appear to be the case at a smaller scale and may be due to local topography acting as shelters, funnels etc. The S_m soil horizon is again thinner at Caoxian than Yuanbao. The apparently more abrupt changes in the magnetic mineralogy and domain size in the can not be said to be solely a caused by rapid sedimentation rate, whereby the material is more rapidly covered and protected from weathering than at Yuanbao. Within the north western area the difference in soil moisture and organic content between sites, known to be prerequisites for situ ferrimagnetic production, appear to be the dominant variables rather than flux in interglacials and interstadials. Given the low levels of in situ ferrimagnetic enhancement in S_m at Caoxian, this increases the evidence for the rapid response time of the deposits in the north western loess plateau to react to changing environmental factors. However, there appears to be a critical level of soil moisture, organic activity or some other factor that generates a measurable concentration of SP ferrimagnetic material. This may indicate that initial enhancement occurs at a particle size outside the range picked up by frequency dependent measurement. Since χ_{ARM} and χ_{ARM}/χ_{LF} appear to be good pedogenic proxies one may assume that initial enhancement begins with the formation of grains at the coarse SP or SD range. A possible mechanism may be simple weathering of coarse MD primary ferrimagnetic grains broken up into SD grains. More intense weathering allows the freeing of iron oxides and particular wetting and drying (oxidising and reducing) conditions allows inorganic precipitation of SP ferrimagnetic material.

As the degree of magnetic enhancement (χ_{FD} %) decreases up profile at Caoxian, the differences between it and its particle size counterpart and Yuanbao magnetic and bulk particle size records increase. Variations in particle size (vol % > 40μm) are comparable for S_m at both sites, and much more so than χ_{LF} profiles at the two sites. Until the end of S_m the same particle size forcing mechanism is mirrored at both sites but the χ_{LF} forcing mechanism differs between sites. The profiles for Caoxian and Yuanbao provide some insight into a possible critical requirement for the formation of detectable frequency dependent SP grains. Coarser grains are deposited at Caoxian, the S_m deposit is thinner and the degree of enhancement is low. The similarity in the two coarse particle size profiles must imply that, although χ_{LF} is higher, little alteration of the primary particle size distribution has occurred at Yuanbao i.e. the finer deposit at Yuanbao is due predominantly to increased distance from source area compared to Caoxian and not a result of weathering. During periods where the A horizons is subjected to pedogenesis for a relatively long time, the particle size profile may come to vary more in the manner of pedogenic indicators such as χ_{FD}%. However, if one assumes a primary magnetic composition similar to pristine loess horizons at Caoxian on initial deposition, Yuanbao shows that variations in χ_{LF} become more like those in the particle size profile not vice versa, under a wetter regime.

Consequently, a causal link is proposed between particle size and initiation of enhancement. Higher values of α_{LSL} and lower values of μ_{LSL} indicate not only a finer shift but also a subtle change in PSD of the fine fraction in those samples with measurable χ_{FD}%. It was noted in chapter 5 that horizons with measurable χ_{FD}% occurred in horizons ~< 25% volume % > 40μm. Two possible mechanisms are proposed. First, the intensity of the winds must drop below a critical strength i.e. that which can support no more than 23-25 % > 40μm particles (as far as Caoxian is concerned). A critical reduction in a major driving force of the wind regime, either a northward shift of pressure or a decrease of the Siberian-Mongolian high must occur before significant penetration of the moisture carrying winds from the south.

Reduced evaporation and/or increased precipitation and elevated soil moisture may then result in the production of frequency dependent SP grains.

Second, an internal mechanism may be responsible where by a suitable environment for SP production is dictated by a critical PSD and therefore packing structure, pore size and 'micro niche' environment in combination with soil moisture retention and organic acid concentration.

An increase in coarse ferrimagnetic material has been shown responsible for the increase in background χ_{LF} in Unit 2 (Chapter 5). During the upward coarsening horizon in L_1L_1 the PSD μ_{LSL} becomes more positive reflecting the coarsening, and the fine asymptote αLSL becomes steeper. The greatest variability is in the PSD fine parameter α_{LSL} rather than the coarse parameter β_{LSL} that remains relatively constant. If one assumes no pedogenic alteration, a procedure similar to that used to analyse beach sand may be used. α_{LSL} represents variation in the transport mechanism of the fine fraction mid – low suspension and β_{LSL} represents variation in the saltation and creep component. This procedure could only be applied realistically to the least weathered material.

6.5. Global implications

The amount of primary sediment supplied, weathering mechanism, amount of silt sized particles deflated, the method of transportation and deposition are closely linked to long and short term variations in the East Asian Monsoon regime. What part an increasing number and intensity of dust storms played in the production of the perennial winter monsoon is unclear. A positive feedback cooling cycle would depend on how long-lived individual storms were and combined regional effect. There is also ambiguity regarding the effect of increased dust loading and any change in vegetation. Decreased 'light' may cause a decrease in vegetation allowing more dust to be deflated. There are two questions that appear to have been given little attention so far in published literature. Could the Chinese climate vary in the short term due to dust loading and feedback effects, or do the high latitude variations dominate? In addition, can a period of intense dust transport be independent of high latitude variations? Feedback in the 'climate change - silt production - wind transport' cycle is complex. Originally, it was assumed that mineral aerosol dust in the

Figure 6.7 changes in the degree of skewness (ϕ/γ) in coarse and fine horizons

atmosphere resulted in a reduction in the net energy reaching the surface and so caused cooling (Carlson and Benjamin, 1980). It has since become clear that increased dust in the atmosphere can affect the climate by shutting out solar radiation and by holding in terrestrial radiation. The dominance of solar or thermal radiation flips depends on the concentration, composition, size, and shape of particles in the atmosphere and external factors such as albedo (Tegen and Lacis 1996, Tegen et al, 1996). Until recently, it was believed that the energy output from the sun was relatively stable. Since 1978, high precision monitoring of the solar radiance has been possible and it is evident that the solar constant changes in phase with the solar activity by 1-1.5%. It has also been proposed that several processes within the atmosphere directly or indirectly amplify any solar radiation effect. All these interactions are complex and no one process can be considered in isolation.

It is accepted that mineral aerosols act as micro-nutrients for terrestrial and especially marine systems (Martin et al, 1994). Martin hypothesised that iron added to the ocean would act as a fertiliser, augment photosynthesis, remove CO_2 and encourage cooling. Dust may also be associated with the export of carbon to the deep oceans and thus regulate CO_2 and the adsorption

of SO_2 reducing the radiative cooling effect of sulphate aerosols. Surface reactions on the mineral particles may reduce ozone concentrations. Moreover, mineral dust has been shown to act as a cloud concentration nucleus.

Overpeck et al (1996) conducted global climate model simulations to examine the potential role of tropospheric dust in glacial climates, comparing "modern dust" with "glacial dust" conditions. He found patterns of regional warming increased at progressively higher latitudes. The warming was greatest (up to 4.4 degrees Celsius) in regions with dust over snow and ice covered areas. The team conducted another set of simulations using interactive sea surface temperatures. The mid-to high-latitude warming was reduced from 4.4 degrees C to 2.4° C, but the main regions of significant warming remained concentrated in areas where the dust loading coincided with snow or ice covered land areas. The authors point out that their results are conservative, the regional warming may have been significantly greater than 2.4 degrees during some extreme dust events. Episodic dust loading may have provided the warming needed to trigger the ice, ocean and atmospheric changes associated with abrupt climatic events during the past 100,000 years (Overpeck et al, 1996).

Water vapour is a very effective greenhouse gas the lower the concentration of vapour the less heat is trapped. A decrease in water vapour would cool the tropics by several degrees (Broecker et al, 1996). Shifts in water vapour content could easily produce decadal shifts. Although further exploration into the link between the ocean circulation and convective activity in the tropical atmosphere is required, such changes may have significantly impacted on the Asian Monsoonal system and may go some way to accounting for the limited extent of glaciation and the weak pedogenesis in MIS 3 observed on the plateau. However, U/Th ages indicated transitions from high to low lake levels at 302 +/- 56 ka, at 138 +/-6 ka, and at 16.3 +/- 2.2 ka in the Qaidam Basin. These ages indicate that high lake stands were terminated at the end of continental glacial maxima. This result is unexpected because previously the large aeolian dust fluxes out of Central Asia during glacial maxima have been considered to be associated with increased aridity in the region, not increased humidity.

7. Conclusions and Future Work

7.1. Conclusions

This research shows that rapid and abrupt changes occurred in the area influenced by the Asian monsoon throughout the last 130 ka. The area influenced by the monsoonal regime includes China, India, Pakistan, and Thailand, which constitutes over 60% of the world's population. A greater understanding of earth-ocean-atmosphere interactions is essential to help formulate global climate prediction models.

This study has shown that high resolution climate proxies from north western China can rival those from the area in and around the North Atlantic. Ding (1 994) speculated that during glacial periods the enlarged ice sheets of the Northern hemisphere intensified the Mongolian-Siberian high and/or displaced it southwards, so linking high and low latitudes. Inferred increases in aridity of the source areas of the loess dust and extension of deserts combined with strengthened cold, dry winds caused an increase in dust flux and particle size that could potentially be transported on to the plateau. Once deposited the loess material was subjected to a range of environmental conditions. Subsequent soil forming processes were dictated by temperature, precipitation and sedimentation rate i.e. the intensity of the East Asian summer and the winter monsoon. The usual assumption is that susceptibility increases as the degree of pedogenesis increases due to enhancement by SSD/SP grains reflected in the frequency dependent susceptibility magnetic parameter χ_{FD}%.

Previous analyses of loess-palaeosol sections have concentrated on magnetic susceptibility and bulk particle size as indicators of the East Asian summer and winter monsoons respectively. This author believes that for north western China, where the sedimentation rate is high and the degree of pedogenesis low, the simple assumptions made regarding climate proxy use of magnetic susceptibility, and bulk grain size are oversimplified. The relevance of climate induced changes to environmental processes in the source area and along the transport route become more critical when analysing thick depositional profiles at small sample intervals.

In Chapter 2 the standard assumptions regularly made in published literature regarding silt production, provenance and deposition in China were

discussed. From an extensive literature review, several conclusions can be drawn. The majority of silt particles are probably formed by high altitude weathering processes, not only by glacial grinding but also frost shattering and fluvial erosion in flashy ephemeral rivers. Large quantities of poorly sorted material is subsequently deposited at the foot of mountain ranges and sorted by fluvial and aeolian processes. Further weathering and erosion of this sediment in desert dune and playa environments may generate a small but significant quantity of silt. Evidence suggests that during periods of increased aridity, coarse fanglomerates were deposited by ephemeral streams and active-layer structures were produced by permafrost within the alluvial fan sediments. The Mu Us desert bounds the loess plateau directly and it has been proposed that the desert has expanded into the loess region during arid periods in the past (Ding et al, 1999). This would appear to be a major contributory factor in the extensive thickness deposited at the loess plateau margin during the last glacial cycle, as compared to other loess deposits.

Most alluvial fans in north western China are aggrading at present, characterised by sheet flooding and lateral channel migration. Since new material is regularly supplied, boulder cover does not form and the silt can be readily deflated (Derbyshire et al, 1998). It appears that the source material is regularly replenished although the character of the alluvial material may vary between cold and warm periods.

In general, the source regions for proto loess are likely to have remained the same. However, over the short term dust is not derived from a spatially and temporally constant source area. Distinctions can be made between the characteristics of dust from different source areas at present. Distinctions can also be made between the granulometric and elemental character of floating dust and dust storm proto loess. Mass spectrometry results of elemental concentrations (Al, Fe, Mg, Sc) in modern dust, collected during storm and "non-storm" events, showed significant differences between storm and non-storm aerosols. In addition, the signature of a particular source was traceable between source area and site over 400 km apart (Zhang et al, 1996). Non dust storm dust travels under quite different conditions from dust storm dust and therefore a distinct particle size distribution may be expected (see Chapter 6).

It may be expected that during a sustained period of erosion the source will become better sorted until a point where grains susceptible to deflation have been removed. The author envisages that this period will be seasonal unless a reduction in seasonality occurs where either silt production or transportation is limited. Then replenishment or a change in the environment (drying, reduction in vegetation etc.) will be required before significant deflation can resume. The simple assumption that particle size is directly proportional to wind speed and therefore a useful proxy for winter monsoon intensity is subject to question since it takes no account of changes in aeolian transport mechanisms and sediment availability.

Mineral aerosol monitoring from the Taklimakan desert has shown that coarse silt and sand particles can be transported significant distances by storm winds (Chen, 1995). Deposition of dust storm dust is often associated with precipitation. Present dust flux maxima occur in March - July, with corresponding storm minima during November. Silt particles and aggregates may by subjected to a significant degree of pedogenic alteration along the transport pathway. Hence, it cannot be said that incipient soil development in the north western loess plateau reflects in situ alteration or that soil formation occurs on a previously deposited loess base during periods of high dust flux.

The processes that form the loess pile are summarised, in the context of north western loess as follows; 1) formation of silt sized particles; 2) transport and sorting of the material into a deflation-prone sediment, 3) wind velocity reduction and dust trapping elements, i.e. deposition > erosion; 4) post depositional modification.

Moisture is an important factor in sediment availability i.e. precipitation in the source area, weathering and erosion etc. Perhaps the most critical factor in the development of a loess profile is soil moisture at the source and depositional sites. An increase in the moisture content of the soil at source can double or treble the drag velocity required to entrain the material compared to that for dry sand (Mckenna-Neuman and Maljaars, 1998). The degree of vegetation cover is also dictated by soil moisture. The deflation potential in the source area is dominated by vegetation related roughness elements which, can respond quickly to changes in the climate. Changes in roughness boundary positions and heights will also influence deposition.

Soil moisture and organic acids appear to be critical in the production of in situ superparamagnetic and stable single domain ferrimagnetic material. Within she mountainous north eastern Tibetan Plateau soil development in basins is evident in loess-like deposits (Lehmkuhl, 1998b) indicating that periodic increases in soil moisture in the past were significant even beyond the plateau margins. Large pores, formed by roots and plant capillaries and intergranular or inter-aggregate pores formed by bioturbation, may be critical for the in situ formation of SP/SSD grains. Field experiments showed that higher infiltration rates were associated with a greater degree of vegetation cover (Derbyshire et al 1999). It is feasible that some root penetration provides sufficient water and increased porosity allowing SP/SSD oxidation and reduction processes to occur in an increasingly massive and spongy soil. Crusts formed in arid environments are strong enough to significantly reduce soil erodibility, deflation potential and water infiltration. They may also significantly limit SP/SSD production. Only very limited infiltration can explain the presence of highly soluble salts within recent loess layers. In order for a soil layer to become 'enhanced' magnetically some paramagnetic or antiferromagnetic iron oxides, silicates or oxyhydroxides must convert to ferrimagnetic material. Migration of organic rich water helps to keep any dissolved iron in suspension. A suitable environment for the production of secondary magnetic minerals may form even earlier due to the adhesion of water, charged micelle films and water held by capillary action. Sections from the western loess plateau at Beiyuan and Yuanbao contain incipient soil development within S_m characterised by organic enrichment of the A horizon and lacking a B horizon (Chen, 1997). The profile at Caoxian also shows similar characteristics. This indicates that the accumulation rate was rapid (Feng et al, 1998) and the depth of influence of weathering was low.

Although Caoxian lacks an independent chronology, the similarities of the section to the proximal Yuanbao section allowed tentative dates to be applied. The stratigraphic units 5, 4, 3, and 2, defined in the field were found to correspond to MIS 5, 4, 3, and 2: S_m L_1L_2, L_1S_1 (S_m), and L_1L_1 using Chinese loess nomenclature. By fitting parametric curves to the PSDs of samples, 4 types of characteristic curves were defined. The author believes that the most important finding of this research is that glacial and stadial loess has a

characteristic PSD. The mean value may increase or decrease but the shape remains constant. It is likely that this reflects the transport mechanism and it is proposed that the coarse fraction is dominated by saltation and low level suspension, and the fine fraction is dominated by low to mid level suspension (< 1 km height). All these PSD have very similar magnetic grain size and mineralogy and reflect the primary loess magnetic composition.

The remaining three PSD types defined fall on a continuum. They may reflect a different transport mechanism but this can not be proved since the magnetic mineralogy suggests increasing pedogenesis along the continuum. High resolution analysis of remanence parameters has shown that in incipient soils, in situ ferrimagnetic profiles vary independently from imperfect antiferromagnetic parameters. As the degree of pedogenesis increases, the in situ ferrimagnetic and imperfect antiferromagnetic parameters come to vary simultaneously. This indicates that there is a primary imperfect antiferromagnetic signal recognisable in pristine loess such as L_1L_1, but, under intense weathering conditions in situ production of imperfect antiferromagnetic material occurs, reflecting the same environmental forces as in situ ferrimagnetic material. The results also indicate the speed of response of SP/SSD formation to soil moisture production must occur rapidly in the upper most 0.5 m of the constantly aggrading loess pile.

In summary, PSD curves can be used to discriminate between weathered and non-weathered loess, as well as being indicative of the degree of pedogenesis or energy of the transporting medium. χ_{LF} is not a reliable indicator of East Asian summer monsoon intensity, since changes in environment factors other than increased precipitation can cause an increase in the value. In the case of Caoxian, the author believes that the increase in χ_{LF} in L_1L_1 is due to the encroaching desert margin bringing large quantities of well sorted, saltated and low level suspended material to the site, the material being dominated by paramagnetic mineral. IRM_{-20mT}/χ_{ARM} appears to be an effective proxy for the primary detrital magnetic profile for all but the Eemian loess.

Fluctuations in ice conductivity on scales of <5-20 yrs reflect rapid oscillations of the dust content of the atmosphere (Reader et al, 1999), suggesting extremely rapid reorganisations of atmospheric circulation as well

as ocean circulation (Taylor et al, 1993). The Late glacial stage record of the Guliya ice core from the Tibetan Plateau contains 200 year oscillations in $\delta^{18}O$ values and in dust content. Shifts in the Aleutian low in the 1970's and early 1990's resulted in rapid and abrupt warming of ~5°C over Alaska (NOAA, Arctic Research Initiative). All of these proxies are linked to variations in the intensity of the Asian monsoon system. The results of this study also indicate that the north western loess plateau responded abruptly to climate variations during the last 130 ka.

7.2. Further work

It is imperative that an equally highly resolvable dating technique can be defined for high resolution records such as Caoxian. Without one, the rapidity of change can only be estimated. Chapter 4 discussed the importance of the preparation technique in the interpretation of PSD results. A logical progression from this study would be to investigate the comparability of PSD prepared in different ways to Caoxian loess PSDs. This will prove to be a useful technique only if it is widely applicable.

References

Adkins, J. F., Boyle, E. A., Keigwin, L., Cortijo, E., 1997. Variability of the North Atlantic thermohaline circulation during the last interglacial. *Nature*, 390: 154-156.

Alley, R. B., Meese, D. A., Shuman, C. A., Gow, A. J., Taylor, K. C., Grootes, P. M., White, J. W. C., Ram, M., Waddington, E. D., Mayewski, P. A., Zielinski, G. A., 1993. Abrupt Increase in Greenland Snow Accumulation at the End of the Younger Dryas Event. *Nature* 362: 527-529

An, Z. S., Kukla, G., Porter, S. C., Xiao, J. L., 1991. Late Quaternary dust flow on the Chinese Loess Plateau. *Catena*, 18:125-132.

An, Z. S., Porter, S. C., Zhou, W. J., Lu, Y. C., Donahue, D J., Head, M. J., Wu, X. H., Ren, J. Z., Zheng, H. B., 1993. Episode of Strengthened Summer Monsoon Climate of Younger Dryas Age on the Loess Plateau of Central China. *Quaternary Research*, 39: 45-54

An, Z., Kukla, G. J., Porter, S. C., Xiao, J., 1994. Magnetic susceptibility evidence of monsoon variation on the loess plateau of central China during the last 130,00years. *Quaternary Research*, 36: 29-36.

Andersen, K. K., Armengaud, A., Genthon, C., 1998. Atmospheric dust under glacial and interglacial conditions. *Geophysical Research Letters*, 25: 2281-2284

Andrews. J., T., 1998. Abrupt changes (Heinrich events) in Late Quaternary North Atlantic marine sediments: a history and review of data and concepts. *Journal of Quaternary Science* 13: 3-16.

Asahara, Y., Tanaka, T., Kamioka, H., Nishimura, A., Yamazaki, T., 1999. Provenance of the north Pacific sediments and process of source material transport as derived from Rb-Sr isotopic systematics. *Chemical Geology*, 158: 271-291

Assallay, A. M., 1998, Structure and Hydrocollapse Behaviour of Loess. PhD thesis, Loughborough University

Bagnold R. A., 1941. The physics of wind blown Sands and dune sands. Methuen & Co. Ltd. London. Pp265

Bagnold, R. A., 1983. The Nature and Correlation of Random Distributions. Proceedings of the Royal Society Of London Series A-Mathematical Physical And Engineering Sciences, 388: 273-291

Banerjee, S. K., Hunt, C. P., Liu, X., 1993. Separation of local signals from the regional paleomonsoon record of the Chinese loess plateau: a rock magnetic approach. *Geophysical Research letters* 20: 843-846.

Barndorff-Nielsen, O., Dalsgaard, K., Halgreen, C., Kuhlman, H., Moller, J. T., Schou, G., 1982. Variation in Particle-Size Distribution over a Small Dune. Sedimentology, 29: 53-65

Barndorff-Nielsen, O., 1982. The Hyperbolic Distribution in Statistical Physics. Scandinavian Journal of Statistics 9: 43-46

Barnola, J. M., Raynaud, D., Korotkevich, Y. S., Loorius, C., 1987. Vostok ice core provides 160,000 year record of atmospheric CO2. *Nature*, 329: 408-414

Barth, H. G., 1984. Modern Methods of particle size analysis.

de Beaulieu, J. L., Reille, M., 1992. The last climatic cycle at La Grande Pile (Vosges, France) and new pollen profile. *Quaternary Science Reviews*, 11: 431-438.

Beer, J., Shen, C., Heller, F., Liu, T. S., Bonani, G., Dittrich, B., Suter, M., Kubik, P. W., 1993. ^{10}Be and magnetic susceptibility in Chinese loess. *Geophysical Research Letters*, 20: 57-60.

Behl, R. J., Kennett, J. P., 1996. Brief interstadial events in the Santa Barbara basin, NE Pacific, during the past 60 kyr. *Nature*, 379: 243-246.

Belnap, J., and Gillette, D. A., 1998. Vulnerability of desert biological crusts to wind erosion: the influences of crust development, soil texture, and disturbance. Journal of Arid Environments. 39:139-142.

Best, J., 1992. On the entrainment of sediment and initiation of bed defects: insights from recent developments within turbulent boundary layer research. *Sedimentology*, 39: 797-811.

Beuselinck, L., Govers, G., Poesen, J., Degraer, G., Froyen, L., 1998. Grain size analysis by laser diffractometry: comparison with the sieve pipette method. *Catena*, 32: 193-208.

Biscaye, P. E., and Grousset, F. E. 1998. The Chinese Loess Plateau Far and Wide. *PAGES Conference Proceedings* 6: 8.

Bloemendal. J., King, J. W., Hall, F. R., Doh, S. J., 1992. Rock magnetism of late Neogene and Pleistocene deep sea sediments: Relationship to sediment source, diagenic processes, and sediment lithology. *Journal of Geophysical Research*, 97: 4361-4375.

Bloemendal, J., Liu, X., Rolph, T. C., 1995. Correlation of the magnetic susceptibility stratigraphy of Chinese loess and the marine oxygen isotope record: chronological and palaeoclimatic implication. *Earth and Planetary Science Letters*, 131: 371-380.

Bond, G., Heinrich, H., Broecker, W. S., Labeyrie, L., McManus, J., Andrews, J., Huon, S., Jantschik, R., Clasen, S., Simet, C., Tedesco, K., Klas, M., Bonani, G., Ivy, S., 1992. Evidence for massive discharges of icebergs into the north Atlantic ocean during the last glacial period. *Nature*, 360: 245-249.

Bond, G., Broecker, W. S., Johnsen, S., McManus, J., Labeyrie, L., Jouzel, J., Bonani, G., 1993. Correlations between climate records from North Atlantic sediments and Greenland ice. *Nature*, 365: 143-147.

Bond, G. C, Lotti, R. 1995 Iceberg Discharges into the North-Atlantic on Millennial Time Scales during the Last Glaciation. *Science*, 267: 1005-1010

Braaten, D. A., 1994. Wind tunnel experiments of large particle re-entrainment-deposition and development of large particle scaling parameters. *Aerosol Science and Technology*, 21: 157-169.

Brady, N. C., and Weil, R. R., 1999. The Nature and Properties of soils. Prentice Hall

Brookfield, M. E., and Ahlbrandt, T. S.1983. Eolian sediments and Processes. *Elsvier*

Broecker, W. S., Peteet, D. M., Rind, D., 1985. Does the ocean-atmosphere system have more than on e stable mode of operation? *Nature*, 315: 21-25.

Broecker, W. S., Denton, G. H., 1989. The role of ocean-atmosphere reorganisations in glacial cycles. *Geochimica et Cosmochimica Acta*, 53: 2465-2501.

Bronger, A., Heinkele, T. 1989: Micromorphology And Genesis Of Palaeosols In The Luochuan Loess Section, China - Pedostratigraphic And Environmental Implications *Geoderma*, 45: 123-143

Bronger, A., Winter, R., Derevjanko, O., Aldag, S., 1993. Loess-paleosol-sequences in Tajikistan as a palaeoclimatic record of the quaternary in central Asia. *Quaternary Proceedings*, 5: 69-81.

Buurman, P., Pape, Th., Muggler, C. C., 1997. Laser grain-size determination in soil genetic studies 1. *Practical problems. Soil Science*, 162: 211-228.

Butler, H. J., Hogarth, W. L., McTainsh, G. H., 1996. A source-based model for describing dust concentrations during wind erosion events: an initial study. *Environmental Software*, 11: 45-52.

Catt, J. A., 1995. Soils in Aeolian sequences as evidence of quaternary climatic change: problems and possible solutions. *Quaternary proceedings*, 4: 59-68.

Chappell, D., 1998. Dispersing sandy soil for the measurement of Particle size distributions using optical laser diffraction. *Catena*, 31: 271-281.

Chen, F.H., Qie, X. S., Zhang, Y. T., Cao, J. X. 1993. Climatic Record of Lanzhou Loess and Climatic Cycles on the Scale of 10000 Years. *Chinese Science Bulletin* 38: 1181-1185

Chen, F. H., Bloemendal, J., Wang, J. M., Li, J. J., Oldfield, F 1997. High-resolution multi-proxy climate records from Chinese loess, evidence for rapid climatic changes over the last 75 kyr. Palaeogeography Palaeoclimatology Palaeoecology, 130: 323-335

Chen, F. H., Bloemendal, J., Feng, Z. D., Wang, J. M., Parker, E., Guo, Z. T., 1999a. East Asian monsoon variations during Oxygen Isotope Stage 5: evidence from the northwestern margin of the Chinese loess plateau *Quaternary Science Reviews* 18: 1127-1135

Chen, F. H., Bloemendal. J., Zhang, P. Z., Liu, G. X., 1999b. An 800 ky proxy record of climate from lake sediments of the Zoige Basin, eastern Tibetan Plateau. *Palaeogeography Palaeoclimatology Palaeoecology*, 151: 307-320

Chen, J., Qiu, G., Lu, H. Y., Ji, J. F., 1997. Variation of Summer Monsoon Intensity on the Loess Plateau of Central China during the last 130000 A - Evidence From Rb And Sr Distribution. *Chinese Science Bulletin*, 42: 473-476

Chen, W., Fryrear, D. W., 1996. Grain-size distributions of wind-eroded material above a flat bare soil. *Physical Geography*, 17: 554-584.

Chen, W., Yang, Z., Dong, Z., 1995. Vertical distribution of grain-size parameters of drifting particles during sand storms in the Taklimakan desert. *Physical Geography*, 16: 503-523.

Cilek. V., 1999. The loess deposits of the Bohemian Massif: Silt Provenance Paleometeorology and the loessification process. *Loessfest '99 Conference Proceedings*, extended abstracts edited by E. Derbyshire.

Clarke, M. L., 1995a. A comparison of magnetic fabrics from loessic silts across the Tibetan front, Western China. *Quaternary proceedings*, 4: 19-26.

Clarke, M. L., 1995b. Sedimentalogical Characteristics and rare Earth Element fingerprinting of Tibetan silts and their relationship with the sediments of the Western Chinese loess Plateau. *Quaternary Proceedings*, 4: 41-51.

Clemens, S. C., Prell, W. L., 1990. Late Pleistocene variability of Arabian Sea summer monsoon winds and continental aridity: Eolian records from the lithologic component of deep sea sediments. *Paleoceanography*, 5: 109-145.

Clemens, S. C., Prell, W. L., Murray, D., Shimmield, G., Weedon, G., 1991. Forcing mechanisms of the Indian Ocean Monsoon. *Nature*, 353: 720-725.

Clemens, S. C., Prell, W. L., 1992. Comments on "palaeoclimatic significance of the mineral magnetic record of the Chinese loess and palaeosols". *Quaternary Research* 38: 265-267.

Clifton J 1998, Relationships between radionuclide activity and sediment composition in Eastern Irish sea intertidal environments. Liverpool University : Thesis Ph.D., 1998

Colonna, M., Casanova, J., Dullo, W. C., Camoin, G., 1996. Sea-level changes and $\delta^{18}O$ record for the past 34,000 yr from Mayotte reef, Indian Ocean 46:335-339.

Dansgaard, W., Johnsen, S. J., Clausen, H.B., Dahl-Jensen, D., Gundestrup, N. S., Hammer, C. U., Hvidberg, C. S., Steffensen, J. P., Sveinbjonsdottir, A. E., Jouzel, J., Bond, G., 1993. Evidence for general instability of past climate from a 250 kyr ice core record. *Nature*, 364: 218-220.

Dearing, J., 1994. Environmental magnetic susceptibility: using the Bartington MS2 system. Unpublished guidebook for using the Bartington magnetic susceptibility meters.

Dearing, J. A., Dann, R. J. L., Hay, K., Lees, J. A., Loveland, P. J., Maher, B. A., O'Grady, K., 1996a. Frequency-dependent susceptibility measurements of environmental materials. *Geophysical Journal International*, 124: 228-240.

Dearing, J., Livingstone, I., Zhou, L. P., 1996b. A late Quaternary magnetic record of Tunisian loess and its climatic significance. *Geophysical Research Letters*, 23: 189-192.

Dearing, J. A., Hay, K., Baban, S. M. J., Huddleston, A. S., Wellington, E. M. H. Loveland, P. J., 1996c. Magnetic susceptibility of soil: an evaluation of conflicting theories using a national data set. *Geophysical Journal International*, 127: 728-734.

Dearing, J. A., Bird, P. M., Dann, R. J. L., Benjamin, S. F., 1997. Secondary ferrimagnetic minerals in Welsh soils: a comparison of mineral magnetic detection methods and implications for mineral formation. *Geophysical Journal International*, 130: 727-736.

Dearing, J., 1999. Magnetic Susceptibility. In Walden, J., Oldfield, F., Smith, J., 1999. *Environmental magnetism A practical Guide. Technical Guide No.6. Quaternary research Association*, London

DeMenocal, P. B., and Rind, D., 1993. Sensitivity of Asian and African Climate to variations in seasonal insolation, glacial ice cover, sea-surface temperature, and Asian orography. Journal of Geophysical Research – Atmospheres, 98: 7265-7287.

Derbyshire, E., Shi, Y. F., Li, J.J., Zheng, B. X., Li, S. J., Wang, J. T., 1991. Quaternary Glaciation Of Tibet - The Geological Evidence. *Quaternary Science Reviews* 10: 485-510

Derbyshire, E., 1991. Quaternary Environments in China *Quaternary Science Reviews* 10: R5

Derbyshire, E., Dijkstra, T. A., Billard, A., Muxart, T., Smalley, I. J., Li, Y. J., 1993. Thresholds in a sensitive landscape: The loess region of central China. From *'Landscape Sensitivity'* eds., Thomas D. S. G., Allison, R. J.

Derbyshire, E., Kemp, R., Meng, X., 1995a. Variations in loess and paleosol properties as indicators of palaeoclimate gradients across the loess plateau of North China. *Quaternary Science Reviews*, 14: 681-697

Derbyshire, E., Keen, D. H., Kemp, R. A., Rolph, T. A., Shaw, J., Meng, X., 1995b. Loess-Paleosol sequences as recorders of palaeoclimatic variations during the last glacial-interglacial cycle: some problems of correlation in North central China. *Quaternary Proceedings*, 4: 7-18.

Derbyshire, E., 1995c. Quaternary glacial sediments, glaciation style, climate and uplift in the Karakoram and north west Himalayas: review and speculations. *Palaeogeography, Palaeoclimatology, Palaeoecology*, 120: 147-157.

Derbyshire, E., 1995d. Aeolian sediments in the Quaternary record: an introduction. *Quaternary Science Reviews*, 14: 641-643.

Derbyshire, E., Kemp, R. A., Meng, X. M., 1997. Climate change, loess and palaeosols: Proxy measures and resolution in North China. *Journal of the Geological Society*, 154: 793-805

Derbyshire, E., Meng, X. M., Kemp, R. A., 1998. Provenance, transport and characteristics of modern aeolian dust in western Gansu Province, China, and interpretation of the Quaternary loess. *Journal of Arid Environments*, 39: 497-516

Derbyshire, E., Meng, X., Dijkstra, T. A., in press 1999 *Landslides in the Thick Loess Terrain of North West China*. Wiley and Sons Ltd.

Ding, Z., Rutter, N., Han, J., Liu, T. S., 1992. A coupled environmental system formed at about 2.5Ma in East Asia. *Palaeogeography, Palaeoclimatology, Palaeoecology*, 94: 223-242.

Ding, Z., Yu, Z., Rutter, N., Liu, T. S., 1994. Towards an orbital time scale for Chinese loess deposits. *Quatemary Science Reviews*, 13: 21-30

Ding, Z., Liu, T. S., Rutter, N., Yu, Z., Guo, Z., Zhu, R., 1995. Ice-volume forcing of East Asian winter monsoon variation in the past 800,00 years. *Quatemary Research*, 44: 149-159.

Ding, Z. L., Rutter, N. W., Liu, T. S., 1997. The onset of extensive loess deposition around the G/M boundary in China and its palaeoclimatic implications. *Quatemary International*, 40: 53-60

Ding, Z. L., Sun, J. M., Liu, T. S., Zhu, R. X., Yang, S. L., Guo, B., 1998. Wind-blown origin of the Pliocene red clay formation in the central Loess Plateau, China. *Earth And Planetary Science Letters* 161: 135-143

Ding, Z. L., Sun, J. M., Rutter, N. W., Rokosh, D., Liu, T. S., 1999a. Changes in sand content of loess deposits along a north-south transect of the Chinese Loess Plateau and the implications for desert variations *Quatemary Research*, 52: 56-62

Ding, Z. L., Xiong, S. F., Sun, J. M., Yang, S. L., Gu, Z. Y., Liu, T. S., 1999b. Pedostratigraphy and paleomagnetism of a similar to 7.0 Ma eolian loess-red clay sequence at Lingtai, Loess Plateau, north- central China and the implications for paleomonsoon evolution. *Palaeogeography Palaeoclimatology Palaeoecology* 152: 49-66

Dodonov, A. E., Baiguzina, L. L., 1995. Loess stratigraphy of central Asia: palaeoclimatic and palaeoenvironmental aspects. *Quatemary Science Reviews* 14: 707-720.

Dunlop, D., 1981. The rock magnetism of fine particles. *Physics of Earth and Planetary Interiors*, 26: 1 –26.

Dunlop, D., 1995. Magnetism in rocks. *Journal of Geophysical Research*, 100: 2161-2174.

Duplessy, J. C., Labeyrie, L., Arnold, M., Paterne, M., Duprat, J., van Weering, T. C. E., 1992. Changes in surface salinity of the North Atlantic ocean during the last deglaciation. *Nature*, 358: 485-487.

Eleftheriaddis, K., Colbeck, I., Harrison, R. M., 1991. Size distributions of atmospheric coarse aerosol species by a tunnel sampler employing single stage impactors. *Journal of aerosol Science*, 22: S321-S324.

Emeis, K., Anderson, D. M., Doose, H., Kroon, D., Schulz-Bull, D., 1995. Sea-surface temperature and the history of monsoon upwelling in the north west Arabian Sea during the last 500,000 years. *Quatemary Research*, 43: 355-361.

Evans, M. E., Heller, F., 1994. Magnetic enhancement and palaeoclimate: study of a loess / paleosol couplet across the Loess Plateau. *Geophysical Journal International* 117: 257-264.

Eyre, J. K., Shaw, J., 1994. Magnetic enhancement of Chinese loess – the role of γFe_2O_3? *Geophysical Journal International*, 117: 265-271.

Eyre, J. K., 1996. The application of the high resolution IRM acquisition to the discrimination of the remanence carriers in Chinese loess. *Studia Geographica et Geodica*, 40: 234-242.

Eyre, J. K., 1997. Frequency dependence of magnetic susceptibility for populations of single domain grains. *Geophysical Journal International*, 129: 209-211.

Fang, J., 1993a. Lake evolution during the last 3000 years in China and its implications for environmental change. *Quaternary Research*, 39: 175-185.

Fang, J., 1993b Lake evolution during the past 30,000 years in China, and its implications for environmental change. *Quaternary Research*, 36: 37-60.

Fang, X. M., Li, J. J., Derbyshire, E., Fitzpatrick, E. A., Kemp, R. A., 1994. Micromorphology of the Beiyuan Loess Paleosol Sequence in Gansu Province, China - Geomorphological and Paleoenvironmental Significance. *Palaeogeography Palaeoclimatology Palaeoecology*, 111:289-303

Fang, X. M., Li, J. J., Banerjee, S. K., Jackson, M., Oches, E. A., VanderVoo, R., 1999a. Millennial-scale climatic change during the last interglacial period: Superparamagnetic sediment proxy from paleosol S1, western Chinese Loess Plateau. *Geophysical Research Letters* 26: 2485-2488

Fang, X. M., Li, J. J., VanderVoo, R., 1999b. Rock magnetic and grain size evidence for intensified Asian atmospheric circulation since 800,000 years BP Related to Tibetan uplift. *Earth and Planetary Science Letters*, 165: 129-144

Fanning, A. F. and Weaver, A. J., 1997. Temporal-geographical melt water influences on the North Atlantic Conveyor: Implications for the Younger Dryas *Paleoceanography*, 12: 307-320

Feng, Z., 1996. Climatic Implications of Magnetic Susceptibility and 10Be Flux in Chinese Loess. *Catena*, 27: 143-147.

Feng, Z. D., Chen, F. H., Tang, L. Y., Kang, J. C., 1998. East Asian monsoon climates and Gobi dynamics in marine isotope stages 4 and 3. *Catena* 33: 29-46

Field, M. H., Huntley, B., Muller, H., 1994. Eemian Climate Fluctuations Observed In A European Pollen Record. *Nature*, 371: 779-783

Fieller, N. R. J., Gilbertson, D. D., Olbricht, W., 1984. A New Method For Environmental-Analysis Of Particle-Size Distribution Data From Shoreline Sediments. Nature, 311: 648-651

Fieller, N. R. J., Flenley, E. C., Gilbertson, D. D., Thomas, D. S. G., 1990. Dumb-Bells - A Plotting Convention for Mixed Grain-Size Populations. *Sedimentary Geology*, 69: 7-12

Fieller, N. R. J., Flenley, E. C., Olbricht, W., 1992. Statistics Of Particle-Size Data. *Applied Statistics-Journal Of The Royal Statistical Society Series C* 41: 127-146

Folk, R. L., and Ward, W. C., 1957. Brazos river bar: a study in the significance of grain size parameters. Journal of sedimentary Petrology, 27: 3-27.

Forman, S., 1991. Late Pleistocene Chronology of the loess Deposition near Luochuan, China. *Quatemary Research*, 36: 19-28.

Forster, Th., Evans, M. E., Heller, F., 1994. The frequency dependence of low field susceptibility in loess sediments. *Geophysical Journal International*, 118: 636-642.

Forster, Th., Heller, F., Evans, M. E., Havlicek, P., 1996. Loess in the Czech republic: Magnetic properties and palaeoclimate. *Studia Geographica et Geodica*, 40: 243-261.

Frakes, L. A., Sun, J., 1994. A carbon isotope record of the upper Chinese loess sequence: Estimates of plant types during stadials and interstadials. *Palaeogeography, Palaeoclimatology, Palaeoecology*, 108: 183-189.

Fronval, T., Jansen, E., Bloemendal, J., Johnsen, S., 1995. Oceanic evidence for coherent fluctuations in the Fennoscandian and Laurentide ice sheets on millennial time scales. *Nature*, 374: 443-446.

Gallet, S., Jahn, B., Torii, M., 1996. Geochemical characterisation of the Luochuan loess-paleosol sequence, China, and palaeoclimatic implications. *Chemical Geology*, 133: 67-88.

Gao, G. R., 1988. Formation and Development of the Structure of Collapsing Loess in China. *Engineering Geology* 25:235-245

Gasse, F., Derbyshire, E., 1996. Environmental changes in the Tibetan Plateau and surrounding areas - Preface. *Palaeogeography, Palaeoclimatology, Palaeoecology*, 120: 1-3.

Genthon, C., 1992. Simulations of Desert Dust and Sea-Salt Aerosols in Antarctica with A General-Circulation Model of the Atmosphere. *Tellus Series B-Chemical and Physical Meteorology* 44: 371-389

Goslar, T., Kuc, T., Ralska-Jasiewiczowa, M., Rozanski, K., Arnold, M., Bard, E., van Geel., B., Pazdur, M. F., Szeroczynska, K., Wicik, B., Wieckowski, K., Walanus, A., 1993. High-resolution lacustrine record of the late glacial/ Holocene transition in central Europe. *Quatemary Science Reviews*, 12: 287-294.

Goudie, A. S., Cooke, R. U., Doornkamp, J. C., 1979. The formation of silt from quartz dune sand by salt weathering processes in deserts. *Journal of Arid Environments* 2: 105-112.

Greenley, R., Iversen, J. D., 1985. Wind as geological process on Earth, Mars, Venus and Titan. Cambridge University Press, Cambridge.

Greenley, R., Blumberg, D. G., Williams, S. H., 1996. Field measurements of the flux and speed of wind blown sand. *Sedimentology*, 43: 41-52.

GRIP members, 1993. Climate instability during the last interglacial period recorded in the GRIP ice core. *Nature*, 364: 203-207.

Grootes, P. M., Stuiver, M., White, J. W. C., Johnsen, S., Jouzel, S., 1993. Comparison of oxygen isotope records from the Greenland ice cores. *Nature*, 366: 552-554.

Guo, Z., Fedoroff, N., An, Z. S., Liu, T. S., 1992. Interglacial dust fall and the origin of iron oxides-hydroxides in the paleosols of the Xifeng loess section, China. *Scientica Geolgica Sinica*, 2: 91-100.

Guo, Z., Fedoroff, N., Liu, T. S., 1996. Micromorphology of the loess-paleosol sequence of the last 130 ka in China and palaeoclimatic events. *Science in China Series D*. 39: 468-477.

Guo, Z. T., Liu, T. S., Fedoroff, N., Wei, L. Y., Ding, Z..L., Wu, N. Q,. Lu, H. Y., Jiang, W. Y., An, Z. S., 1998. Climate extremes in Loess of China coupled with the strength of deep-water formation in the North Atlantic Global and Planetary Change 18: 113-128

Han, J., Lu, H., Wu, N., Guo, Z., 1996. The magnetic susceptibility of modem soils in China and its use for palaeoclimate reconstruction. *Studia geophysica. Geodica.* 40: 262-275.

Harrison, S. P., Kutzbach, J. E., Prentice, I. C., Beheling, P. J., Sykes, M. T., 1995. The response of Northern Hemisphere extra-tropical climate and vegetation to orbitally induced changes in insolation during the last interglacial. *Quatemary Research*, 43: 174-184.

Harrison, S. P., Yu, G., Tarasov, P. E., 1996. Late Quaternary lake-level record from northern Eurasia. *Quaternary Research*, 45: 138-159.

Hartman, D., Christiansen, C., 1992. The hyperbolic shape triangle as a tool for discriminating populations of sediment samples of closely connected origin. *Sedimentology*, 39: 697-708.

He, X., Tang, K., Lei, X., 1997. Heavy mineral record of the Holocene environment on the loess plateau in China and its pedogenic significance. *Catena*, 29: 323-332.

Head, M. J., Zhou, W. J., Zhou, M.F., 1989. Evaluation of C-14 Ages of Organic Fractions of Paleosols from Loess-Paleosol Sequences near Xian, China. *Radiocarbon*, 31: 680-696

Heintzenburg, J., Strom, J., Ogren, J. A., 1991. Vertical profiles of Aerosol properties in the summer troposphere of central Europe, Scandinavia and the Svalbard region. *Atmospheric environment*, 25A: 621-627.

Heinrich, H., 1988. Origin and Consequences of Cyclic Ice Rafting in the Northeast Atlantic-Ocean during the past 130,000 Years. *Quatemary Research*, 29: 142-152

Heller, F., Liu, T. S., 1982. Magnetostratigraphical Dating of Loess Deposits in China. *Nature*, 300: 431-433.

Heller, F., Liu, T. S., 1984. Magnetism of Chinese Loess Deposits. *Geophysical Journal of the Royal Astronomical Society*, 77: 125 et seq.

Heller, F., Liu T. S., 1986. Paleoclimatic and Sedimentary History from Magnetic-Susceptibility of Loess in China. *Geophysical Research Letters* 13: 1169-1172

Heller, F., Liu, X., Liu, T. S., Xu, T., 1991. Magnetic susceptibility of loess in China. *Earth and planetary Science Letters* 103: 301-310.

Heller, F., Shen, C. D., Beer, J., Liu, X. M., Liu, T. S., Bronger, A., Suter, M., Bonani, G., 1993. Quantitative Estimates of Pedogenic Ferromagnetic Mineral Formation in Chinese Loess and Paleoclimatic Implications. *Earth and Planetary Science Letters* 114: 385-390

Heller, F., 1995. Loess magnetism. Review of geophysics, 33: 211-240.

Heslop, D. C. 1998 Sub-Millennial scale in East Asian monsoon systems recorded by dust deposits from the north-western Chinese plateau. Liverpool University: Thesis Ph.D.

Heusser, L. and Morley, J., 1997. Monsoon Fluctuations over The Past 350kyr: High Resolution Evidence From Northeast Asia / Northwest Pacific Climate Proxies (Marine Pollen and Radiolarians). *Quaternary Science Reviews*, 16: 565-581.

Heider, F., Zitzelsberger, A. and Fabian, K. 1996. Magnetic Susceptibility and Remanent Coercive Force in Grown Magnetite Crystals from 0.1 Mu M to 6 Mm. *Physics of the Earth and Planetary Interiors*. 93: (3-4): 239-256

Hovan, S. A., Rea, D. K., Pisias, N. G Shackleton, N. J., 1989. A direct link between the China loess and marine $\delta^{18}O$ records: aeolian flux to the North Pacific. *Nature*, 340: 296-298.

Hovan, S. A., Rea, D. K., 1991. Late Pleistocene continental climate and oceanic variability recorded in north west pacific sediments. *Paleoceanography*, 6: 349-370.

Huang, Q., Phillips, F. M., 1990. Preliminary-Study on Chlorine-36 Dating Of Halite In Salt Lakes From Qaidam Basin. *Chinese Science Bulletin* .35: 32-36

Hughen, K. A., Overpeck, J. T., Peterson, L. C., Trumbore, S., 1996. Rapid climate changes in the tropical Atlantic region during the last deglaciation.
Nature, 380: 51-54

Hus, J. J., Han, J., 1992. The Contribution of Loess Magnetism in China to the Retrieval of Past Global Changes - Some Problems. *Physics Of the Earth and Planetary Interiors*, 70: 154-168

Imbrie et al 1984 *In* A. Berger, J. Imbrie., J. D. Hays. G. Kukla., and B. Saltzman (Eds.) *Milankovitch and Climate Part 1* (pp 671-686 Dordrecht, Netherlands: Reidel.

Imbrie, J., Berger, A., Boyle, E. A., Clemens, S. C., Duffy, A, Howard, W. R., Kukla, G., Kutzbach, J., Martinson, D. G., McIntyre, A., Mix, A. C., Molfino, B., Morley, J. j., Peterson, L.C., Pisias, N.G., Prell, W. I., Raymo, M. E., Shackleton, N. J., Toggweiler, J. R., 1993. On The Structure and Origin of Major Glaciation Cycles .2. The 100,000-Year Cycle. *Paleoceanography*, 8: 699-735

IPCC Summary for Policymakers: The Science of Climate Change 1995. Http://www

Janecek, T. R, Rea, D. K., 1985. Quaternary Fluctuations In The Northern Hemisphere Trade Winds And Westerlies *Quaternary Research* 24: 150-163

Johnsen, S. J., Claussen, H. B., Dansgaard, W., Furher, K., Gundestrup, N., Hammer, C. U., Iversen, P., Jouzel, J., Stauffer, B., Steffensen, J. P., 1992. Irregular interstadials recorded in a new Greenland ice core. *Nature*, 359: 311-313.

Johnsen, S. J., Clausen, H. B., Dansgaard, W., Gundestrup, N. S., Hammer, C. U., Tauber, H., 1995. The Eem stable Isotope record along the GRIP ice core and its interpretation. *Quatemary Research*, 43: 117-124.

Jonasz, M., 1991. Size, Shape, composition and structure of microparticles from light scattering. In: *Principles, methods and applications of particle size analysis.* Ed. By J. P. M. Styvitski, pp 143-162. Cambridge University Press. New York.

Jouzel, J., Petit, J, R., Raynaud, D., 1990. Palaeoclimatic information from ice cores: the Vostok records. *Transactions of the royal society of Edinburgh: Earth Sciences*, 81: 349-355.

Joussaume, S., 1990. 3-Dimensional Simulations of the Atmospheric Cycle of Desert Dust Particles using a General-Circulation Model. *Journal Of Geophysical Research-Atmospheres* 95: 1909-1941

Joussaume, S., Jouzel, J., 1993. Paleoclimatic Tracers - An Investigation Using An Atmospheric General-Circulation Model Under Ice-Age Conditions. *Journal Of Geophysical Research-Atmospheres* 98: 2807-2830

Kalm, V.E., Rutter, N. W., Rokosh, C. D., 1996. Clay minerals and their paleoenvironmnetal interpretation in the Baoji loess section, Southern Loess Plateau, China. *Catena*, 27: 49-61

Kapsner, W. R., Alley, R.B., Shuman, C.A., Anandakrishnan, S., Grootes, P.M., 1995. Dominant Influence Of Atmospheric Circulation On Snow Accumulation In Greenland Over The Past 18,000 Years. *Nature*, 373: 52-54

Keen, D., 1995. Molluscan assemblages from the loess of north central China. *Quatemary Science Reviews*, 14: 699-706.

Keigwin, L. D., Curry, W. B., Lehman, S. J., Johnsen, S., 1994. The role of the deep ocean in North Atlantic climate change between 70 and 130 kyr ago. *Nature*, 371: 323-325.

Kemp, R. A., Derbyshire, E., Meng, X., Chen, F., Baotian, P., 1995. Pedosedimentary reconstruction of a thick loess-paleosol sequence near Lanzhou in north-central China. *Quatemary Research*, 43: 30-45

Kemp, R. A., 1999. Micromorphology of loess-paleosol sequences: a record of paleoenvironmental change *Catena*, 35: 179 -196

Kemp, R. A, Derbyshire, E., Meng, X. M., 1999. Comparison of proxy records of Late Pleistocene Climate Change from a sequence in North Central China. *Journal of Quatemary Science* 14: 91-96.

Kennett, J. P., Ingram, B. L., 1995. A 20,000-year record of ocean circulation and climate change from the Santa Barbara basin. *Nature*, 377: 510-513.

Kezao, C., Bowler, J. M., 1986. Late Pleistocene Evolution Of Salt Lakes In The Qaidam Basin, Qinghai Province, China. *Palaeogeography Palaeoclimatology Palaeoecology* 54, 87-104

Kiladis, G. N., Meehl, G. A., Weickmann, K. M., 1994. Large-Scale Circulation Associated with Westerly Wind Bursts and Deep Convection over the Western Equatorial Pacific. *Journal of Geophysical Research-Atmospheres*, 99: 18527-18544

Kind, R. J., One-dimensional aeolian suspension above beds of loose particles – A new concentration-profile equation. *Atmospheric Environment*, 26A: 927-931.

Konert, M., Vandenberghe, J., 1997. Comparison of laser grain size analysis with pipette and sieve analysis: a solution for the underestimation of the clay fraction. *Sedimentology*, 44: 523-535.

Kotilainen, A. T., Shackleton, N. J., 1995. Rapid Climate Variability in the North Pacific-Ocean during the Past 95,000 Years. *Nature*, 377: 323-326

Kukla, G., Heller, F., Ming, L. X., Chun, X. T., Sheng, L. T., Sheng, A. Z., 1988. Pleistocene Climates in China Dated By Magnetic-Susceptibility Geology, 16: 811-814

Kukla, G., An, Z., 1989. Loess stratigraphy in central China. . *Palaeogeography, Palaeoclimatology, Palaeoecology*, 72: 203-225.

Kukla, G., An, Z. S., Melice, J. L., Gavin, J., Xiao, J. L., 1990. Magnetic susceptibility record of Chinese loess. *Transaction of the royal society of Edinburgh: Earth Sciences*, 81: 263-288.

Kukla, G., Cilek, V., 1996. Plio-Pleistocene megacycles: record of climate and tectonics. *Palaeogeography, Palaeoclimatology, Palaeoecology*, 120: 171-194.

Kukla, G., McManus, J.F., Rousseau, D., Chuine, I., 1997. How Long And How Stable Was the Last Interglacial. *Quaternary Science Reviews*, 16: 605-612.

Kutzbach, J. E, Prell, W. I, Ruddimann, W. F., 1993. Sensitivity of Eurasian Climate to Surface Uplift of the Tibetan Plateau. *Journal of Geology*, 101: 177-190

Larsen, E., Sejrup, H. P., Johnsen, S. J., Knudsen, K. L., 1995. Do Greenland ice cores reflect NW European interglacial climate variations. *Quaternary Research*, 43: 125-132.

Lauritzen, S., 1995. High-resolution Paleotemperature proxy record for the last interglacial based on Norwegian speleothems. *Quaternary Research*, 43: 133-146.

Lehman, S. J., Keigwin, L. D., 1992. Sudden changes in North Atlantic circulation during the last deglaciation. *Nature*, 356: 757-762.

Lehman, S., 1997. Sudden end of an interglacial. *Nature*, 390: 117-119.

Lehmkuhl, F., 1998a. Quaternary glaciations in central and western Mongolia. *Journal of Quaternary Science*, 13: 153-167

Lehmkuhl, F., 1998b. Extent and spatial distribution of Pleistocene glaciations in eastern Tibet. *Quaternary International*, 45-6: 123-134

Leroux, M., 1993. The mobile polar high: a new concept explaining present mechanisms of meridional air-mass and energy exchanges and global propagation of palaeoclimatic changes. *Global and Planetary Change*, 7: 69-93.

Levesque, A. J., Mayle, F. E., Walker, I. R., Cwynal, L. C., 1993. The Amphi-atlantic oscillation: A proposed late glacial climatic event. *Quaternary Science Reviews*, 12: 629-643.

Li, J., Feng, Z., 1988. Late quaternary monsoon patterns on the loess plateau of China. *Earth surface processes and land forms*, 13: 125-135.

Li, J. J, Zhu, J. J, Kang, J. C, Chen, F. H, Fang, X. M., Mu, D. F., Cao, J. X., Tang, L. Y., Zhang, Y. T., Pan, B. T., 1992. The Comparison of Lanzhou Loess Profile with Vostok Ice Core in Antarctica over the Last Glaciation Cycle. *Science in China Series B-Chemistry*, 35: 476-488

Li, J., Fang, X., Ma, H., Zhu, J., Pan, B., Chen, H., 1996. Geomorphological and environmental evolution in the upper reaches of the Yellow River during the late Cenozoic. *Science in China Series D*, 39: 380-390.

Li, J. J., Fang, X. M., van der Voo, R., Zhu, J. J., Niocaill, C. M., Ono, Y., Pan, B. T., Zhong, W., Sasaki, T., Zhang, Y. T., Cao, J. X., Kang, S. C, Wang, J. M., 1997. Magnetostratigraphic dating of river terraces: Rapid and intermittent incision by the Yellow River of the north eastern margin of the Tibetan Plateau during the Quaternary. *Journal of Geophysical Research* 102: 10121-10132.

Lindstrom, D. R., MacAyeal, D. R., 1986. Palaeoclimatic constraints on the maintenance of possible ice shelf cover in the Norwegian and Greenland seas. *Paleoceanography*, 1: 313-337.

Lister, G. S., Kelts, K., Zao, C. K., Yu, J. Q., Niessen, F., 1991. Lake Qinghai, China - Closed-Basin Lake Levels and The Oxygen Isotope Record for Ostracoda since the Latest Pleistocene. *Palaeogeography, Palaeoclimatology, Palaeoecology*, 84: 141-162

Liu, D. S., An, Z. S., 1984. A Preliminary Magnetostratigraphic Study of the Beihanzhai Loess Section. Geochimica 2:134-137

Liu, J., Wu, X., Li, S., Zhang, M., 1997. The Last Glacial Stratigraphic Sequence, Depositional Environment and Climate Fluctuations from the Aeolian Sand Dune in Hongguang, Pengze, Jiangxi (China). *Quaternary Science Reviews*, 16: 535-546.

Liu, K. B., 1988. Quaternary history of the temperate forests of China. *Quaternary Science Reviews*, 7: 1-20.

Liu, K. B., Yao, Z. J, Thompson, L. G., 1998. A pollen record of Holocene climatic changes from the Dunde ice cap, Qinghai-Tibetan Plateau. *Geology, 26: 135-138*

Liu, T. S., An, Z. S., Yuan, B. Y., Han, J. M 1985. The Loess-Paleosol Sequence In China and Climatic History. *Episodes*, 8: 21-28

Liu, T. S., Ding, Z., 1993. Stepwise coupling of monsoon circulations to global ice volume variations during the late Cenozoic. *Global and Planetary Change*, 7: 119-130.

Liu, T. S., Ding, M., Derbyshire, E., 1996. Gravel deposits on the margins of the Qinghai-Xizang Plateau, and their environmental significance. *Palaeogeography, Palaeoclimatology, Palaeoecology*, 120: 159-170.

Liu, X. M., Shaw, J, Liu, T. S., Heller, F, Yuan, B . Y., 1992. Magnetic Mineralogy of Chinese Loess And Its Significance. *Geophysical Journal International*, 108: 301-308

Liu, X., Shaw, J., Liu, T. S., Heller, F., Cheng, M., 1993. Rock magnetic properties and palaeoclimate of Chinese loess. *Journal of Geomagnetism and Geoelectricity*, 45: 117-124.

Liu, X., Shaw, J., Liu, T. S., Heller, F., 1993. Magnetic susceptibility of the Chinese loess-paleosol sequence: environmental change and pedogenesis. *Journal of the Geological Society, London*, 150: 583-588.

Liu, X., Rolph, T., Bloemendal, J., Shaw, J., Liu, T. S., 1994a. Remanence Characteristics of Different magnetic grain size categories at Xifeng, Central Chinese Loess Plateau. *Quaternary Research*, 42: 162-165.

Liu, X. M., Bloemendal, J., Rolph, T., 1994b. Pedogenesis And Paleoclimate - Interpretation Of The Magnetic- Susceptibility Record Of Chinese Loess-Paleosol Sequences – Comments. *Geology* 22: 858-859

Liu, X., Rolph, T., Bloemendal, J., 1995. The Citrate-Bicarbonate-Dithionate (CBD) Removable Magnetic Component of Chinese Loess. *Quaternary Proceedings*, 4: 53-58.

Lorius, C., Jouzel, J., Raynaund, D., 1993. Glacials – interglacials in Vostok: climate and greenhouse gases. *Global and Planetary Change*, 7: 131-143.

Lovley, D. R., Stolz, J. F., Nord, G. L., Phillips, E. J. P., 1987. Anaerobic production of the magnetite by a dissimilatory iron-reducing micro-organism. *Nature*, 330: 252-254.

Lowell, T., Teller, J. T., 1994. Radiocarbon Vs calendar ages of major late glacial hydrological events in North America. *Quaternary Science Reviews*, 13: 801-803.

Lozhkin, A. V., Anderson, P. M., 1995. The last interglaciation in North east Siberia. *Quaternary Research*, 43: 147-158.

Lund, D. C., Mix, A. C., 1998. Millennial-scale deep water oscillations: Reflections of the North Atlantic in the deep Pacific from 10 to 60 ka. *Paleoceanography*, 13: 10-19

Lu, H. Y., Van Huissteden, K. O., An, Z. S., Nugteren, G., Vandenberghe, J., 1999. East Asia winter monsoon variations on a millennial time-scale before the last glacial-interglacial cycle. *Journal Of Quaternary Science* 14: 101-110

Ma, Y. Z., Zhang, H. C., Li, J. J., 1998. On the evolution of the palynoflora and climatic environment during late Pleistocene in Tengger Desert, China *Acta Botanica Sinica* 40: 871-879

MacAyeal, D. R., 1993. Binge/purge oscillations of the Laurentide ice sheet as a cause of the North Atlantic's Heinrich events. *Paleoceanography*, 8: 775-784.

Maher, B. A., 1988. Magnetic-Properties Of Some Synthetic Sub-Micron Magnetites *Geophysical Journal-Oxford* 94: 83-96

Maher, B. A., Taylor, R. M., 1988. Formation of ultrafine-grained magnetite in soils. *Nature*, 336: 368-370.

Maher, B. A., Thompson, R., 1992. Palaeoclimatic significance of the mineral magnetic record of the Chinese Loess and Paleosols. *Quaternary Research*, 37: 155-170.

Maher, B. A., Thompson, R., 1995. Paleorainfall reconstructions from pedogenic magnetic susceptibility variations in the Chinese loess and paleosols. *Quaternary Research*, 44: 383-391

Maher, B. A., 1998. Magnetic properties of modern soils and Quaternary loessic paleosols: paleoclimatic implications. *Palaeogeography Palaeoclimatology Palaeoecology*, 137: 25-54

Mahowald, N., Kohfeld, K., Hansson, M., Balkanski, Y., Harrison, S P., Prentice, I. C., Schulz, M., Rodhe, H., 1999. Dust sources and deposition during the last glacial maximum and current climate: A comparison of model results with paleodata from ice cores and marine sediments. *Journal of Geophysical Research-Atmospheres*, 104: 15895-15916

Marchitto, TM, Curry, WB, Oppo, DW 1998 Millennial-scale changes in North Atlantic circulation since the last glaciation. *Nature*, 393: 557-561

Marticorena, B., Bergametti, G., Gillette, D., Belnap, J., 1997. Factors controlling threshold friction velocity in semiarid and arid areas of the United States. *Journal of Geophysical Research*, 102: 23277-23287.

Martin, J. H., Coale, K. H., Johnson, K. S., Fitzwater, S. E., Gordon, R. M., Tanner, S. J., Hunter, C. N., Elrod, V. A., Nowicki, J. L., Coley, T. L., Barber, R. T., Lindley, S., Watson, A. J., Vanscoy, K., Law, C. S., Liddicoat, M. I., Ling, R., Stanton, T., Stockel, J., Collins, C., Anderson, A., Bidigare, R., Ondrusek, M., Latasa, M., Millero, F. J., Lee, K., Yao, W., Zhang, J. Z., Friederich, G., Sakamoto, C., Chavez, F., Buck, K., Kolber, Z., Greene, R., Falkowski, P., Chisholm, S. W., Hoge, F., Swift, R., Yungel, J., Turner, S., Nightingale, P., Hatton, A., Liss, P., Tindale, N. W., 1994. Testing the Iron Hypothesis In Ecosystems of the Equatorial Pacific-Ocean. *Nature*, 371: 123-129

Mayewski, P. A, Meeker, L. D, Whitlow, S., Twickler, M. S, Morrison, M. C., Bloomfield, P., Bond, G. C., Alley, R. B., Gow, A. J., Grootes, P. M., Meese, D. A., Ram, M., Taylor, K. C., Wumkes, W., 1994. Changes in Atmospheric Circulation and Ocean Ice Cover over the North-Atlantic during the Last 41,000 Years. *Science*, 263: 1747-1751

McCave, I. N., Bryant, R. J., Cook, H. F., Coughanowr, C. A., 1986. Evaluation of a laser-diffraction-size analyser for use with natural sediments. (Research Methods Papers) *Journal of Sedimentary petrology* Vol.56, No.4, pp.561-564

McLaren, P., 1981. An Interpretation of Trends in Grain-Size Measures. *Journal Of Sedimentary Petrology*, 51: 611-624

McLaren, P. and Bowles, D., 1985. The effect of sediment transport on grain size distributions. *Journal of Sedimentary Petrology*, 55: 457-470.

McManus, J. F., Bond, G. C., Broecker, W. S., Johnsen, S., Labeyrie, L., Higgins, S., 1994. High-resolution climate records from the North Atlantic during the last interglacial. *Nature*, 371: 326-329.

McManus, J.F., Oppo, D.W., Cullen, J.L., 1999. A 0.5-million-year record of millennial-scale climate variability in the North Atlantic. *Science*, 283: 971-975

McTainsh, G. H., Nickling, W.G., Lynch, A. W., 1997. Dust deposition and particle size in Mali, West Africa. *Catena*, 29: 307-322.

Medvadev, V. V., 1996. Mechanisms of microaggregate formation in chernozems. *Eurasian Soil Science*, 28: 13-23.

Meng, X. M., Derbyshire, E., Kemp, R. A., 1997. Origin of the magnetic susceptibility signal in Chinese loess. *Quaternary Science Reviews*, 16: 833-839

McElhinny, M. W, McFadden, M. W. Merril, R. T., 1996. The time averaged palaeomagnetic field 0 – 5Ma. *Journal of Geophysical Research – Solid Earth* 101:25007 – 25027.

McKenna-Neuman, C., and Maljaars, S. M., 1998. A wind tunnel study of the influence of pore water on aeolian sediment transport. *Journal of Arid Environments*, 39: 403-419.

McLaren, P., 1981. An Interpretation of trends in grain size measures. *Journal of Sedimentary Petrology*. 51:611 – 624

McLaren, P., and Bowles, D., 1985. The effect of sediment transport on grain size distributions. *Journal of Sedimentary Petrology*. 55:457 – 470

McTainsh, G. H., Nickling, W.G., Lynch, A.W., 1997. Dust deposition and particle size in Mali, West Africa. *Catena*, 29:307-322

Merrill, J., Arnold, E., Leinen, M., Weaver, C., 1994. Mineralogy of Aeolian Dust Reaching the North Pacific-Ocean .2. Relationship of Mineral Assemblages to Atmospheric Transport. *Journal of Geophysical Research-Atmospheres*, 99: 21025-21032

Medvedev, V. V., 1996. Mechanisms of microaggregate formation in chernozems. *Eurasian Soil Science*, 28:13-28.

Middleton, N.J., 1991. Dust storms in the Mongolian Peoples Republic. *Journal of Arid Evironments*, 20: 287-297.

Miehe, G., 1996. On the connection of vegetation dynamics with climatic changes in High Asia. *Palaeogeography, Palaeoclimatology, Palaeoecology*, 120: 5-24

Morner, N., 1993a. Global change: the last millennia. *Global and Planetary change*, 7: 211-217.

Morner, N., 1993b. Global Change: the high-amplitude changes 13-10 ka ago – novel aspects. *Global and Planetary Change*, 7: 243-250.

Nesje, A., Johannessen, T., 1992. What were the primary forcing mechanisms of high-frequency Holocene climate and glacier variations? *The Holocene*, 2: 79-84.

Obruchev, V.A., 1911. The question of the origin of loess – in defense of the aeolian hypothesis. Izvestiya Tomskogo Tekhnologicheskogo Instituta 23 (in Russian) – section translated by I. J Smalley.

Oches, E. A., McCoy, W. D., 1995. Amino acid geochronology applied to the correlation and dating of central European loess deposits. *Quaternary Science Reviews*, 14: 767-782.

Oches, E. A., Banerjee, S, K., 1996. Rock-magnetic proxies of climate change from loess-paleosol sediments of the Czech republic. *Studia Geographica et Geodica*, 40: 287-300.

Oke, T., R. 1987. Boundary Layer Climates, second edition. Routlege, pp 435.

Oldfield, F., 1991. Environmental magnetism – A personal perspective. *Quaternary Science Reviews*, 10: 73-85.

Oldfield, F., 1992. The source of fine grained magnetite in sediments. *The Holocene*, 2: 180-182.

Oldfield, F., 1994. Towards the discrimination of fine grain ferrimagnets by magnetic measurements in lake and near shore marine sediments. *Journal of Geophysical Research*, 99: 9045-9050.

Oppo, D 1997. Palaeoclimatology - Millennial climate oscillations. *Science*, 278: 1244-1246

Owen, L. A., Bailey, R. M., Rhodes, E. J., Mitchell, W. A., Coxon, P., 1997. Style and timing of glaciation in the Lahul Himalaya, northern India: A framework for reconstructing late Quaternary palaeoclimatic change in the western Himalayas. *Journal of Quaternary Science*, 12: 83-109

Pachur, H., Wunnemann, B., Zhang, H., 1995. Lake evolution in the Tengger Desert North western China, during the last 40,000 years. *Quaternary Research*, 44:171-180.

Paillard, D., 1998. The timing of Pleistocene glaciations from a simple multiple-state climate model. *Nature*, 391: 378-381.

Parkin, D. W., 1973. Trade wind and temperature correlations down a deep sea core off the Saharan coast. *Nature*, 245: 455-456.

Petit, J. R., Mounier, L., Jouzel, J., Korotkevich, Y. S., Kotlyakov, V. I., Lorius, C., 1990. Palaeoclimatological and chronological implications of the Vostok core dust record. *Nature*, 343: 56-58.

Phillips, F. M., Zreda, M.G., Ku, T.L., Luo, S., Huang, Q., Elmore, D., Kubik, P.W., Sharma, P. 199*. 230Th/234U and 36Cl dating of evaporite deposits from the western Qaidam Basin, China: Implications for glacial-period dust export from Central Asia. htttp://amos.physics.purdue.edu/web/primelab/papers/PH93a.html

Pleim, J. E., Chang, J. S., 1992. A non-local closure model for vertical mixing in the convective boundary layer. *Atmospheric environment*, 26A: 965-981.

Polubesova, T. A., Shishova, L. T., Lefevre, M., Romanenkov, V. A., 1996. Effect of freezing and thawing on the surface chemical properties of soils. *Eurasian soil Science*, 28: 104-114.

Pons, A., Guiot., de Beaulieu, J. L., Reille, M., 1992. Recent contributions to the climatology of the last glacial-interglacial cycle based on French pollen sequences. *Quaternary Science Reviews*, 11: 439-448.

Porter, S. C., An, Z., Zheng, H., 1992. Cyclic Quaternary Alluviation and terracing in a non glaciated drainage basin on the north flank of the Qinling Shan, Central China. *Quaternary Research*, 38: 157-169.

Porter, S. C., An, Z., 1995. Correlation between climate events in the North Atlantic and China during the last glaciation. *Nature*, 375: 305-308.

Prell, W. L., Kutzbach, J. E., 1992. Sensitivity of the Indian Monsoon to Forcing Parameters and Implications for its Evolution. *Nature*, 360: 647-652

Prieto, A. R., 1996. Late Quaternary vegetational and climatic changes in the Pampa Grassland of Argentina. *Quaternary Research*, 45: 73-88.

Pye, K., 1982. Negatively skewed aeolian sands from a humid tropical coastal dune field, Northern Australia. *Sedimentary Geology*, 31: 249-266.

Pye, K., 1983. Formation of quartz silt during humid tropical weathering of dune sands. *Sedimentary Geology*, 34:267-282.

Pye, K., 1987. Aeolian dust and dust deposits. London: Academic Press, pp334

Pye, K., Zhou, L. P., 1989. Late Pleistocene and Holocene aeolian dust deposition in north China and the north west pacific ocean. *Palaeogeography, Palaeoclimatology, Palaeoecology*, 73: 11-23.

Pye, K., Mazzullo, J., 1994. Effects of tropical weathering on quartz grain shape: an example from north eastern Australia. *Journal of sedimentary Research*, A64: 500-507.

Pye, K., Winspear, N. R., Zhou, L. P., 1995. Thermoluminescence Ages of Loess and Associated Sediments In Central Nebraska, Usa. *Palaeogeography Palaeoclimatology Palaeoecology* 118: 73-87

Rahmstorf, S., 1994. Rapid climate transitions in a coupled ocean-atmosphere model. *Nature*, 372: 82-85.

Rahmstorf, S 1996. On the freshwater forcing and transport of the Atlantic thermohaline circulation. *Climate Dynamics*, 12: 799-811

Raymo, M. E., Ruddimann, W. F., 1992 Tectonic Forcing of Late Cenozoic Climate. *Nature*, 359: 117-122

Raymo, Me, Ruddimann, W Cooling In The Late Cenozoic - Reply *Nature*, 1993, 361: 124

Raymo, M. E., 1997 The timing of major climate terminations. *Paleoceanography*, 12: 577-585

Raymo, ME, Ganley, K, Carter, S, Oppo, DW, McManus, J 1998, Millennial-scale climate instability during the early Pleistocene epoch. *Nature*, 394: 809

Rea, D. K., 1994. Palaeoclimatic record provided by eolian deposition in the deep sea: the geologic history of wind. *Review of Geophysics*, 32: 159-195.

Reader, M.C., Fung, I., McFarlane, N., 1999. The mineral dust aerosol cycle during the Last Glacial Maximum *Journal Of Geophysical Research-Atmospheres*, 104: 9381-9398

Rhodes, T. E., Gasse, F., Ruifen, L., Fontes, J., Wei, K., Bertrand, P., Gigert, E., Melieres, F., Tucholka, P., Wang, Z., Cheng, Z., 1996. A late Pleistocene – Holocene lacustrine record from lake Manas, Zunggar (northern XinJiang, western China). *Palaeogeography, Palaeoclimatology, Palaeoecology*, 120: 105-121.

Ridgwell, A. J., Watson, AJ, Raymo, M. E., 1999. Is the spectral signature of the 100 kyr glacial cycle consistent with a Milankovitch origin? *Paleoceanography*, 14: 437-440

Rind, D., Overpeck, J., 1993. Hypothesised causes of decade to century scale climate variability: climate model results. *Quaternary Science Reviews*, 12: 357-374.

Robert, A., Roy, A. G., de Serres, B., 1992. Changes in velocity profiles at roughness transitions in coarse grained channels. *Sedimentology*, 39: 725-735.

Robinson, S. G., 1997. Environmental Magnetism and Environmental Change", University of Liverpool. PhD thesis

Rogers, C. D. F., Smalley, I. J., 1993. The Shape of Loess Particles. *Naturwissenschaften* .80: 461-462

Rogers, C. D. F., Dijkstra, T. A., Smalley, I. J., 1994. Particle Packing from an Earth-Science Viewpoint. *Earth-Science Reviews*, 36:59-82

Rowell, D, L., 1996. Soil science: Methods and Applications. Longman Ltd.

Ruddimann, W., F., and McIntyre, A., 1984. An evaluation of ocean-climate theories on the north Atlantic. *In* A. Berger, J. Imbrie., J. D. Hays. G. Kukla., and B. Saltzman (Eds.) *Milankovitch and Climate Part 1* (pp 671-686 Dordrecht, Netherlands: Reidel.

Ruddimann, W. F., Kutzbach, J. E., 1990. Late Cenozoic plateau uplift and climate change. *Transaction of the royal society of Edinburgh: Earth Sciences*, 81:301-314.

Ruddimann, W. F., 1997. *Tectonic Uplift and Climate Change*. Kliver Academic Press *

Rutter, N., Ding, Z., Evans, M. E., Liu, T. S., 1991. Baoji-Type pedostratigraphic section, loess plateau, north-central China. *Quaternary Science Reviews*, 10: 1-22.

Rutter, N., 1992. Presidential Address, XIII INQUA congress 1991: Chinese loess and global change. *Quaternary Science Reviews*, 11: 275-281.

Sabin, A. L., Pisias, N. G., 1996. Sea surface temperature changes in the North eastern Pacific Ocean during the Past 20,000 years and their relationship to climate change in north western North America. *Quaternary Research*, 46: 48-61.

Sayago, J. M., 1995. The Argentine Neotropical loess: an overview. *Quaternary Science Reviews*, 14: 755-766.

Schubel, K. A., Lowenstein, T. K., 1997. Criteria for the recognition of shallow-perennial-saline-lake halites based on recent sediments from the Qaidam Basin, western China *Journal Of Sedimentary Research* 67: 74- 87

Seppala, M., 1995. Deflation and redeposition of sand dunes in Finnish Lapland. *Quaternary Science Reviews*, 14: 799-809.

Sequeira, R., 1993. On the large-scale impact of arid dust on precipitation chemistry of the continental northern hemisphere. *Atmospheric Environment*, 27A: 1553-1565.

Shackleton, N. I., Imbrie, J., Hall, M. A., 1983. Oxygen And Carbon Isotope Record Of East Pacific Core V19-30 - Implications For The Formation Of Deep-Water In The Late Pleistocene North-Atlantic *Earth And Planetary Science Letters,* Vol.65, No.2, Pp.233- 244

Shackleton, N. J., An, Z., Dodonov, A. E., Gavin, J., Kukla, G. J., Ranov, V. A., Zhou, L. P., 1995. Accumulation rate of loess in Tajikistan and China: relationship with global ice volume cycles. *Quaternary Proceedings*, 4: 1-6.

Shen, C. D., Beer, J., Liu, T. S., Oeschger, H., Bonani, G., Suter, M., Wolfli, W., 1992. Be-10 in Chinese Loess. *Earth and Planetary Science Letters*, 109: 169-177

Shen, C. D., Yi, W. X, Zhou, Z., Liu, D.S., Beer, J., Oeschger, H., Bonani, G., Suter, M., Wolfli, W., 199*. A Study on [10]Be in Quartz from Loess of China .1. In situ Cosmogenic [10]Be and Erosion Rates of Source Regions of Loess. *Science in China Series B-Chemistry*, 35: 329-339

Shi, Y., Kong, Z., Wang, S., Tang, L., Wang, F., Yao, T., Zhao, X., Zhang, P., Shi, S., 1993. Mid-Holocene Climates and Environments in China. *Global and Planetary Change*, 7: 219-233.

Singer, J. K., Anderson, J. B., Ledbetter, M. T., McCave, I. N., Jones, K. P. N., Wright, R., 1988. An assessment of the analytical techniques for the size analysis of fine-grained sediments. *Journal of sedimentary Petrology*, 58: 534-543.

Soldatova, Y. F., Ivanov, A. V., Romanyuk, A. V., Solov'ev, A. A., 1993. Forms of iron compounds in dry steppe soils on ancient weathering crusts. *Eurasian soil Science*, 25: 54-67.

Smalley, I., 1995. Making the material: The formation of silt sized primary mineral particles for loess deposits. *Quaternary Science Reviews*, 14: 645-651.

Smalley, I.J and Smalley, V., 1983. Loess material and Loess deposits: formation distribution and consequences. (in *Eolian Sediments and Processes Eds. M.E. Brookfield and T.S. Ahlbrandt. Elsvier*)

Smith, B. J., Whalley, W. B., 1982. Observations On The Composition And Mineralogy Of An Algerian Duricrust Complex. *Geoderma* 28: 285-311

Smith, J., 1999. An introduction to the magnetic properties of natural materials. In Walden, J., Oldfield, F., Smith, J., 1999. *Environmental magnetism A practical Guide*. Technical Guide No.6. *Quaternary research Association, London*.

Starkel, L., 1993. Late Quaternary continental paleohydrology as related to future environmental change. *Global and Planetary Change*, 7: 95-108.

Stein, R., 1985. Rapid Grain-size analyses of clay and silt fraction by Sedigraph 5000D: comparison with Coulter Counter and Atterburg methods. *Journal of Sedimentary Petrology*, 55: 590-593.

Stocker, T. F., 1998. A glimpse of the Glacial. Nature, 391: 338-339.

Stuiver. M., Braziunas, T. F., Grootes, P. M., Zielinski, G. A., 1997. Is there Evidence for solar forcing of climate in the GISP2 oxygen isotope record? *Quatenary Reserarch*, 48: 259-266.

Styvitski J. P. M., 1991. Principles, methods and applications of particle size analysis. Cambridge University Press. New York.

Sun, X., Chen, Y., 1991. Palynological records of the last 11,000 years in China. *Quaternary Science Reviews*, 10: 537-544.

Sun, D. H., Shaw, J., An, Z. S., Rolph, T., 1993. Matuyama/Brunhes (M/B) Transition Recorded In Chinese loess. *Journal of Geomagnetism and Geoelectricity* 45: 319-330

Sun, D. H., Shaw, J., An, Z. S., Cheng, M. Y., Yue, L. P., 1998. Magnetostratigraphy and paleoclimatic interpretation of a continuous 7.2Ma Late Cenozoic eolian sediments from the Chinese Loess Plateau. *Geophysical Research Letters* 25: 85-88

Sun, J. M., and Ding, Z. L., 1998. Deposits and soils of the past 130,000 years at the desert-loess transition in northern China. *Quaternary Research, 50*: 148-156

Sviridenkov, M. A., Gillette, D., Isakov, A. A., Sokolik, I. N., Sminov, V. V., Belan, B. D., Pachenko, M. V., Andronova, A. V., Kolomiets, S. M., Zhukov, V. M., Zhukovsky, D. A., 1993. Size distributions of dust aerosol measured during the Soviet-American experiment in Tajikistan, 1989. *Atmospheric Environment*, 27A: 2481-2486.

Taylor, K. C., Lamorey, G. W., Doyle, G. A., Alley, R. B., Grootes, P. M., Mayewski, P. A., White, J. W. C., Barlow, L. K., 1993a. The flickering switch of late Pleistocene climate change. *Nature*, 361: 432-435.

Taylor, K. C., Hammer, C. U., Alley, R. B., Clausen, H. B., Dahl-Jensen, D., Gow, A. J., Gundestrup, N. S., Kipfstuhl, J., Moore, J.C., Waddington, E.D., 1993b. Electrical Conductivity Measurements from the GISP2 and GRIP Greenland Ice Cores. *Nature*, 366: 549-552.

Taylor, K. C., Alley, R. B., Lamorey, G. W., Mayewski, P., 1997. Electrical measurements on the Greenland Ice Sheet Project 2 core. *Journal of Geophysical Research-Oceans*, 102: 26511-26517

Taylor, R. M., Maher, B. A., Self, P. G., 1987. Magnetite in Soils 1. The Synthesis of Single-Domain and superparamagnetic Magnetite Clay Minerals 22: 411-422

Teller, J. T., Kehew, A. E., 1994. Introduction to the late glacial history of large proglacial lakes and melt water runoff along the Laurentide ice Sheet. *Quaternary Science Reviews*, 13: 795-799.

Thompson, L. G., Mosley-Thompson, E., Dansgaard, W., Grootes, P. M., 1986. The Little Ice-Age As Recorded In The Stratigraphy Of The Tropical Quelccaya Ice Cap. *Science*, 234: 361-364

Thompson, L. G., Mosley-Thompson, E., Davis, M., Lin, P.N., Yao, T., Dyurgerov, M., Dai, J., 1993. Recent Warming - Ice Core Evidence from Tropical Ice Cores with Emphasis on Central-Asia. *Global and Planetary Change*, 7:145-156.

Thompson, L. G, Mosley-Thompson, E., Davis, M. E., Lin, P. N., Henderson, K. A., Coledai, J., Bolzan, J. F., Liu, K. B., 1995. Late-Glacial Stage and Holocene Tropical Ice Core Records from Huascaran, Peru. *Science* 269: 46-50

Thompson, L. G., Yao, T., Davis, M. E., Henderson, K. A., Mosley-Thompson, E., Lin, P. N., Beer, J., Synal, H. A., ColeDai, J., Bolzan, J. F., 1997. Tropical climate instability: The last glacial cycle from a Qinghai-Tibetan ice core. *Science*, 276: 1821-1825

Thompson, R., Maher, B. A., 1995. Age models, sediment fluxes and palaeoclimate reconstructions for the Chinese loess and paleosol sequences. Geophysical *Journal International*, 123: 611-622.

Thorp, J., 1936. Geography of Chinese soils. Nanking.

Thunell, R. C., Mortyn, P. G., 1995. Glacial Climate Instability in the Northeast Pacific-Ocean. *Nature*, 376: 504-506

Tite, M. S., Linington, R. E., 1975. Effect of climate instability on the magnetic susceptibility of soils. *Nature*, 256: 565-566.

van Campo, E., Gasse, F., 1993. Pollen and diatom inferred climatic and hydrological changes in Sumxi Co Basin (western Tibet) since 13,000 yr BP. *Quaternary Research*, 39: 300-313.

van Campo, E., Cour, P., Hang, S., 1996. Holocene environmental changes in Bangong Co basin (western Tibet). Part 2: the pollen record. *Palaeogeography, Palaeoclimatology, Palaeoecology*, 120: 49-63.

Vandenberghe, J., An, Z. S., Nugteren, G., Lu, H. Y., VanHuissteden, K., 1997. New absolute time scale for the Quaternary climate in the Chinese loess region by grain-size analysis. *Geology* 25: 35-38

Van Huisstenden, J., Nugteren, G., Vandenberghe, J., An, Z., 1997. Spectral analysis of a grain size record of the loess deposit in central China. *Proc. 30th International Geological Congress 2&3*: 313-325

van Tatenhove, F. G. M., van der Meer, J. J. M., Koster, E. A., 1996. Implications for Deglaciation chronology from New AMS age determinations in Central West Greenland. *Quaternary Research*, 45: 245-253.

Verosub, K. L., Fine, P., Singer, M. J., TenPas, J., 1993. Pedogenesis and palaeoclimate: Interpretation of the magnetic susceptibility record of Chinese loess-paleosol sequences. *Geology*, 21: 1011-1014.

Verosub, K. L., Roberts, A. P., 1995. Environmental magnetism: Past, present, and future. *Journal of Geophysical Research*, 100: 2175-2192.

Walker, M. J. C., Bjorck, S., Lowe, J. J., Cwynar, L. C., Johnsen, S., Knudsen, K. L., Wohlfarth, B., 1999. Isotopic 'events' in the GRIP ice core: a stratotype for the Late Pleistocene. *Quaternary Science Reviews*, 18: 1143-1150

Wang, H., van Strydonck, M., 1997. Chronology of Holocene Cheniers and Oyster reefs on the coast of Bohai Bay, China. *Quaternary Research*, 47: 192-205.

Wang, W. C., Li K. R., 1990. Precipitation Fluctuation over Semiarid Region in Northern China and The Relationship with El-Nino Southern Oscillation. *Journal of Climate*, 3: 769-783

Webster, P. J., and Yang, S., 1992. Monsoon and ENSO – selectively interactive systems. Quarterly Journal of the Royal Meteorological Society. 118:877-926.

Whalley, W. B., Marshall, J. R., Smith, B. J., 1982. Origin Of Desert Loess From Some Experimental-Observations. *Nature*, 300; 433-435.

Williams, T., Thouveny, N., Creer, K. M., 1996. Palaeoclimatic significance of the 300 ka mineral magnetic record from the sediments of Lac du Bouchet, France. *Quaternary Science Reviews*, 15: 223-235.

Winograd, I. J., and Ludwig, K. R., 1996. High Resolution palaeotemperature proxy record for the last interglacial based on Norwegian speleothems – comment. Quaternary Research. 45: 102.

Wright, J. S., 1995. Glacial comminution of quartz and sand grains and the production of loessic silt: a simulation study. *Quaternary Science Reviews*, 14: 669-680.

Wu, J. L., Wang, S. M., 1997. Climatic variation during the Last Interglacial Period recorded in the lake carbonate deposit, eastern Qinghai-Xizang Plateau. *Chinese Science Bulletin*, 42: 1017-1020

Wu, N. Q., Rousseau, D. D, Liu, D. S., 1996. Land Mollusk Records from the Luochuan Loess Sequence and their Paleoenvironmental Significance. *Science in China Series D-Earth Sciences*, 39: 494-502

Wu, X., Zhan, X., 1991. Tree-ring width and Climate change in China. *Quaternary Science Reviews*, 10: 545-549.

Wyrwoll, K. H., Smyth, G. K., 1985. On Using the Log-Hyperbolic Distribution To Describe the Textural Characteristics Of Eolian Sediments. *Journal of Sedimentary Petrology*, 55; 471-478

Xiao, J., Porter, S. C. An, Z., Kumai, H., Yoshikawa, S., 1995. Grain size of quartz as an indicator of winter monsoon strength on the loess plateau of central China during the last 130,000yr. *Quaternary Research*, 43: 22-29.

Xiao, J., Inouchi, Y., Kumai, H., Shasaku, Y., Kondo, Y., Liu, T. S., An, Z., 1996. Biogenic Silica Record In Lake Biwa of Central Japan over the Past 145, 000 Years. *Quaternary Research*, 47: 277-283.

Xiao, J., Inouchi, Y., Kumai, H., Yoshikawa, S., Kondo, Y., Liu, T. S., An, Z., 1997. Biogenic silica record in Lake Biwa of Central Japan over the Past 145,000 years. *Quaternary Research*, 47: 277-283.

Xiao, J. L., An, Z. S., Liu, T. S., Inouchi, Y., Kumai, H., Yoshikawa, S., Kondo, Y., 1999. East Asian monsoon variation during the last 130,000 Years: evidence from the Loess Plateau of central China and Lake Biwa of Japan. *Quaternary Science Reviews* 18: 147-157.

Xu, T. C., Liu, T. S., 1993. Implication of the magnetic susceptibility curve from the Chinese loess profile at Xifeng. *Quaternary Science Reviews* 12: 249-254.

Yakimenko, E. Y., 1995. Pleistocene paleosols in the loess and loess-like sediments of the central part of the Russian plain. *Quaternary Science Reviews*, 14: 747-753.

Yang, W. B., Spencer, R. J., Krouse, H. R., Lowenstein, T. K., Cases, E., 1995. Stable Isotopes of Lake and Fluid Inclusion Brines, Dabusun Lake, Qaidam Basin, Western China - Hydrology and Palaeoclimatology in Arid Environments. *Palaeogeography Palaeoclimatology Palaeoecology*, 117: 279-290

Yao, T. D., Thompson, L. G., Qin, D. H., Tian, L. D., Jiao, K. Q., Yang, Z. H., Xie, C., 1996. Variations in temperature and precipitation in the past 2000a on the Xizang (Tibet) Plateau - Guliya ice core record. *Science in China Series D-Earth Sciences*.39: 425-433

Yao, T. D., Thompson, L. G., Shi, Y.F., Qin, D. H., Jiao, K.Q., Yang, Z.H., Tian, L. D., Thompson, E.M., 1997. Climate variation since the last interglaciation recorded in the Guliya ice core. Science In *China Series D-Earth Sciences*, 40: 662-668

Yatagai, A., Yasunari, T., 1995. *Journal of the Meteorological Society of Japan*, 73: 909-923.

Yin, A., Nie, S., Craig, P., Harrison, T. M., Ryerson, F. J., Qian, X. L., Yang, G. 1998. Late Cenozoic tectonic evolution of the southern Chinese Tian Shan. *Tectonics* 17: 1-27

Yung, Y. L., Lee T., Wang, C. H., Shieh, Y. T., 1996. Dust: A diagnostic of the hydrologic cycle during the last glacial maximum *SCIENCE,* 271: 962-963

Zhang, J., 1990. Drainage basin weathering and major element transport of two large Chinese rivers (Huanghe and Changjiang). *Journal of Geophysical Research,* 95: 13277-13288.

Zhang, J., Huang, W. W., 1992. Potential Chemical Link Between Continental Wind Deposits, Marine Aerosol and Pelagic Sediments - An Example from Chinese Loess. *Deep-Sea Research, Part A-Oceanographic Research Papers,* 39: 1809-1816

Zhang, J., and Lin, Z., 1992. Climate of China. John Wiley and Sons.

Zhang, X., An, Z., Chen, T., Zhang, G., Arimoto, R., Ray, B. J., 1994. Late quaternary records of the centre of the Chinese loess Plateau. *Quaternary Research,* 41: 35-43.

Zhang, X., Shen, Z., Zhang, G., Chen, T., Liu, H., 1996. Remote mineral aerosols in westerlies and their contributions to the Chinese loess. *Science in China (Series D)* 39: 134-143.

Zhang, X. Y., Arimoto, R., An, Z. S., 1997. Dust emission from Chinese desert sources linked to variations in atmospheric circulation *Journal Of Geophysical Research-Atmospheres,* 102: 28041-28047

Zhang, X. Y, Arimoto, R., Zhu, G.H., Chen, T., Zhang, G.Y., 1998. Concentration, size-distribution and deposition of mineral aerosol over Chinese desert regions. *Tellus Series B-Chemical and Physical Meteorology,* 50: 317-330

Zhang, X. Y., Arimoto, R., An, Z. S., 1999. Glacial and interglacial patterns for Asian dust transport. *Quaternary Science Reviews,* Vol.18, No.6, pp.811-819

Zhang, Z., Zhang, Z., Wang, Y., 1991. Loess deposits in China. *Geological Publishing House, Beijing.* P202

Zhao, S. Q., Xia, X. C., 1984. Evolution of The Lop Desert And The Lop-Nor. *Geographical Journal,* 150: 311-321

Zheng, B. X., Rutter, N., 1998. On the problem of quaternary glaciations, and the extent and patterns of Pleistocene ice cover in the Qinghai-Xizang (Tibet) Plateau. *Quaternary International* 45-6: 109-1

Zheng, H. B., 1989. Controversy regarding the existence of a large ice sheet on the Quinghai-Xizang (Tibetan) Plateau during the Quaternary Period. *Quaternary Research,* 32: 121-123.

Zheng, H. B., Oldfield, F., Yu, L. H., Shaw, J., An, Z. S., 1991. The Magnetic-Properties of Particle-Sized Samples from the Luochuan Loess Section - Evidence for Pedogenesis. *Physics Of the Earth and Planetary Interiors,* 68: 250-258

Zhou, L. P., Oldfield, F., Wintle, A. G., Robinson, S. G., Wang, J. T., 1990. Partly pedogenic origin of magnetic variations in Chinese loess. *Nature,* 346: 737-739.

Zhou, L. P., Dodonov, A. E., Shackleton, N. J., 1995. Thermoluminescence dating of the Orkutsay loess section in Tashkent region, Uzbekistan, Central Asia. *Quatemary Science Reviews* 14: 721-730.

Zhou, W., Donahue, D. J., Porter, S. C., Jull, T. A., Li, X., Stuiver, M., An, .Z., Matsumoto, E., Dong, G., 1996. Variability of monsoon climate in East Asia at the end of the last glaciation. *Quatemary Research*, 46: 219-229.

Zhou, W. J., Donahue, D., Jull, A. J. T., 1997. Radiocarbon AMS Dating of Pollen Concentrated from Eolian Sediments: Implications for Monsoon Climate Change since the Late Quatemary. *Radiocarbon*, 39: 19-26

Zielinski, G. A. and Mershon, G. R., 1997. Paleoenvironmental implications of the insoluble microparticle record in the GISP2 (Greenland) ice core during the rapidly changing climate of the Pleistocene-Holocene transition. *Geological Society Of America Bulletin*, 109: 547-559

APPENDIX 1 STATISTICAL ANALYSES AND CORRELATIONS

Summary of One Way ANOVA results for Mean, Volume % > 40μm and χ_{LF} for Units 2 – 5.

Groups	Count	Sum	Average	Variance
Mean Unit 2	246	9467.738	38.48674	3.410089
Mean Unit3	151	4964.795	32.87944	5.051282
Mean Unit 4	254	7638.633	30.07336	5.804439
Mean Unit 5	267	7029.953	26.32941	11.34348

ANOVA   sumsq   deg free

Source of Variation	SS	df	MS	F	P-value	F crit
Between Groups	19913.98	3	6637.994	998.0382	8.9E-288	2.614641
Within Groups	6079.053	914	6.651042			
Total	25993.04	917				

Groups	Count	Sum	Average	Variance
Gt 40um Unit 2	246	10164.27	41.31816	9.120718
Gt 40um Unit3	151	4870.127	32.2525	10.60852
Gt 40um Unit 4	254	7116.092	28.01611	13.18749
Gt 40um Unit 5	267	6273.364	23.49575	23.39321

ANOVA

Source of Variation	SS	df	MS	F	P-value	F crit
Between Groups	43723.18	3	14574.39	995.2269	2.4E-287	2.614641
Within Groups	13384.88	914	14.64429			
Total	57108.06	917				

Groups	Count	Sum	Average	Variance
xlf Unit 2	246	8147.859	33.12138	0.863464
xlf Unit3	151	4663.941	30.88703	0.809279
xlf Unit 4	254	7764.818	30.57015	0.806171
xlf Unit 5	240	7560.034	31.50014	38.16099

ANOVA

ource of Variatio	SS	df	MS	F	P-value	F crit
Between Groups	917.5273	3	305.8424	28.09067	2.34E-17	2.614939
Within Groups	9657.378	887	10.88769			
Total	10574.9	890				

	xLF	xFD%	xARM	gt40	SIRM	IRM-20	IRM-300	20mT/xA	ARM/SIR	IRM/xAR	SIRM/xLF	xARM/xLF	HIRM	soft%	sirm-300	mt300-20
xLF																
xFD%	0.825184															
xARM	0.952602	0.872429														
gt40		-0.40651														
SIRM																
IRM-20					0.613287											
IRM-300					-0.37887	-0.4033										
IRM20mT/xARM	-0.63767	-0.77765	-0.7857	0.539354												
xARM/SIRM	0.874223	0.844365	0.94253					-0.84051								
SIRM/xARM	-0.68196	-0.79144	-0.78543	0.469503				0.925963	-0.8843							
SIRM/xLF	-0.63917	-0.53501	-0.57391		0.676233			0.614457	-0.75828	0.794017						
xARM/xLF	0.772867	0.862587	0.917578	-0.45527				-0.87773	0.87816	-0.85683	-0.4619					
HIRM					0.662702						0.52792					
soft%					-0.52845		-0.4099				-0.40805		-0.9744			
sirm-300					0.666511						0.541051		1	-0.97475		
mt300-20							-0.74385							0.488093		
S-ratio					0.52641		0.41209				0.406643		0.974009	-1	0.974364	-0.48932
Mean		-0.49264	-0.4152	0.976501				0.596498	-0.45895	0.530345		-0.54472				
Median		-0.49142	-0.42187	0.947654				0.605762	-0.47847	0.536866		-0.54096				
Mode				0.757224												
Stnd. Dev.		-0.42377		0.836214				0.491591		0.445862		-0.4795				
Skewness																
Kurtosis		-0.31997														
LT 20		0.507905	0.427216	-0.96501				-0.62292	0.488053	-0.55445		0.55609				
LT 40		0.40816		-1				-0.53698		-0.46539		0.455862				
LT 63		0.47029		-0.97015				-0.55949	0.428252	-0.49698		0.516726				
LT 90		0.480714	0.429147	-0.79292				-0.5336	0.415384	-0.48278		0.541049				
LT 4		0.527436	0.451139	-0.71893				-0.67813	0.574494	-0.62057		0.556596				
4-16		0.414716		-0.95237				-0.56677	0.416556	-0.49392		0.461255				
16-32		-0.46587	-0.46442					0.532199	-0.63318	0.573428		-0.4611				
32-63				0.966074				0.544013		0.465198		-0.43078				
63-90		-0.41405		0.991117				0.522916		0.457391		-0.44592				
90-125		-0.53737	-0.4791	0.876324				0.599215	-0.48636	0.538379		-0.5975				
125-250				0.623665				0.408322				-0.42461				
GT 250																

Correlation coefficients for MIS 5

	xlf	xfd%	xarm	sirm	back-20	back-300	20mT/xar	xarm/sirm	sirm/arm	Sirm/xlf	xarm/xlf	xarm/xlf-hf	HIRM	hard %	soft%	sirm-300	mt300-20
xlf																	
xfd%																	
xarm																	
sirm	0.451547																
back-20	0.468671			0.930138													
back-300	-0.52669			-0.95872	-0.91164												
irm20mT/x	0.406641		-0.59646	0.770349	0.826675	-0.73824											
xarm/sirm				0.614722	-0.82001	-0.75401	0.767874	-0.93066									
sirm/arm			-0.60864	0.826466	0.762288	-0.7755	0.95045	-0.9814									
Sirm/xlf				0.853709	0.765585	-0.76279	0.617448	-0.69174	0.688553								
xarm/xlf	-0.63337		0.835682			-	-0.69153	0.697964	-0.69342								
xarm/xlf-hf		-0.64958															
HIRM				0.60731	0.471256		0.4343	-0.54608	0.547128	0.629168							
hard %													-0.8569				
soft%				0.880242	0.644496	-0.81684	0.527864			0.727127	0.788277		0.64617				
sirm-300				0.60731	0.471256	-0.41209		-0.54608	0.547128	0.629168			1	-0.8569	0.64617		
mt300-20				0.735011	0.502326	-0.79148		-0.55769	0.560289	0.599459					0.867538		
sratio														-0.9819			0.827391

Correlation coefficients for MIS 4

	xLF	xFD%	xARM	gt40	SIRM	IRM-20	IRM-300	20mT/xA	ARM/SIR	IRM/xAR	SIRM/xLF	xARM/xLF	HIRM	soft%	sirm-300	mt300-20
xLF																
xFD%																
xARM																
gt40	0.608874	0.461123														
SIRM			-0.73154													
IRM-20	0.54249		0.708079	-0.63964												
IRM-300			0.481055	-0.60072	0.729939											
RM20mT/xARM	-0.5656		-0.70526	0.616032	-0.88592	-0.78281	1									
xARM/SIRM	-0.49026	-0.52632	-0.7969	0.439518												
SIRM/xARM	0.473225	0.534084	0.893715	-0.58462				-0.40701	-0.87544							
SIRM/xLF	-0.43748	-0.5301	-0.87384	0.587512					0.876475	-0.99412						
xARM/xLF				-0.65317	0.773721	0.668704	-0.61656									
HIRM		0.410829	0.959051	-0.81586	0.645755	0.479844	-0.63398	-0.76197	0.880426	-0.87192	0.489142					
soft%													1			
sirm-300													-0.96435			
mt300-20														-0.96435		
S-ratio	0.570012		0.51135		0.483596			-0.59951	-0.60253							
Mean													0.936715	-0.97567	0.936715	
Median			-0.71536	0.987714	-0.61761	-0.58074	0.585976	0.431638	-0.57572	0.576613	-0.63063	-0.79793				
Mode			-0.7077	0.960217	-0.61051	-0.57542	0.59684	0.427611	-0.57059	0.572549	-0.62045	-0.7875				
Stnd. Dev.			-0.59311	0.84773	-0.53097	-0.52334	0.509101		-0.4646	0.472534	-0.58298	-0.68135				
Skewness			-0.4906	0.747116	-0.44666	-0.45053					-0.48169	-0.55629				-0.17436
Kurtosis																
LT 20																
LT 40			0.760686	-0.98741	0.631378	0.575356	-0.61401	-0.48628	0.627731	-0.62848	0.607294	0.832349				
LT 63			0.73154	-1	0.639636	0.600716	-0.61603	-0.43952	0.58462	-0.58751	0.653165	0.815859				
LT 90			0.690867	-0.98513	0.618156	0.601289	-0.59015		0.542788	-0.54482	0.650918	0.778872				
LT 4			0.570287	-0.86467	0.495549	0.492982	-0.44338		0.456083	-0.45835	0.558863	0.661881				
4-16			0.74011	-0.9446	0.582823	0.488538	-0.56043	-0.51796	0.628788	-0.62736	0.552832	0.808133				
16-32			0.753268	-0.97734	0.631813	0.593939	-0.62036	-0.46603	0.617609	-0.61922	0.604117	0.822283				
32-63			0.572533	-0.89678	0.598852	0.616343	-0.56048		-0.40699		0.69562	0.673796				
63-90			-0.76881	0.970386	-0.63686	-0.56729	0.621721	0.503143	-0.63589	0.638284	-0.60306	-0.83724				
90-125			-0.69621	0.951923	-0.63209	-0.60783	0.623216	0.392776	-0.54109	0.542746	-0.64136	-0.77238				
125-250			-0.63634	0.917214	-0.55035	-0.54172	0.523364	0.375122	-0.514	0.52198	-0.58645	-0.72366				
GT 250	.		-0.4241	0.689065							-0.45713	-0.5123				

Correlation coefficients for MIS 3

	xLF	xFD%	xARM	gt40	SIRM	IRM-20	IRM-300	20mT/xA	ARM/SIR	IRM/xAR	SIRM/xLF	xARM/xLF	HIRM	soft%	sirm-300	mt300-20
xLF																
xFD%																
xARM	0.608874	0.461123														
gt40			-0.73154													
SIRM	0.54249		0.708079	-0.63964												
IRM-20			0.481055	-0.60072	0.729939											
IRM-300	-0.5656		-0.70526	0.616032	-0.88592	-0.78281	1									
IRM20mT/xARM	-0.49026	-0.52632	-0.7969	0.439518												
xARM/SIRM	0.473225	0.534084	0.893715	-0.58462				-0.40701	-0.87544							
SIRM/xARM	-0.43748	-0.5301	-0.87384	0.587512					0.676475	-0.99412						
SIRM/xLF				-0.65317	0.773721	0.668704		-0.61656								
xARM/xLF		0.410829	0.959051	-0.81586	0.645755	0.479844	-0.63398	-0.76197	0.880426	-0.87192	0.489142					
HIRM													1			
soft%													-0.96435			
sirm-300														-0.96435		
mt300-20	0.570012		0.51135		0.483596			-0.59951	-0.60253							
S-ratio													0.936715	-0.97567	0.936715	
Mean			-0.71536	0.987714	-0.61761	-0.58074	0.585976	0.431638	-0.57572	0.576613	-0.63063	-0.79793				
Median			-0.7077	0.960217	-0.61051	-0.57542	0.59684	0.427611	-0.57059	0.572549	-0.62045	-0.7875				
Mode			-0.59311	0.84773	-0.53097	-0.52334	0.509101		-0.4646	0.472534	-0.58298	-0.68135				
Stnd. Dev.			-0.4906	0.747116	-0.44666	-0.45053					-0.48169	-0.55629				-0.17436
Skewness												.				
Kurtosis												.				
LT 20			0.760686	-0.98741	0.631378	0.575356	-0.61401	-0.48628	0.627731	-0.62848	0.607294	0.832349				
LT 40			0.73154	-1	0.639636	0.600716	-0.61603	-0.43952	0.58462	-0.58751	0.653165	0.815859				
LT 63			0.690867	-0.98513	0.618156	0.601289	-0.59015		0.542788	-0.54482	0.650918	0.778872				
LT 90			0.570287	-0.86467	0.495549	0.492982	-0.44338		0.456083	-0.45835	0.558863	0.661881				
LT 4			0.74011	-0.9446	0.582823	0.488538	-0.56043	-0.51796	0.628788	-0.62736	0.552832	0.808133				
4-16			0.753268	-0.97734	0.631813	0.593939	-0.62036	-0.46603	0.617609	-0.61922	0.604117	0.822283				
16-32			0.572533	-0.89678	0.598852	0.616343	-0.56048		-0.40699		0.69562	0.673796				
32-63			-0.76881	0.970386	-0.63686	-0.56729	0.621721	0.503143	-0.63589	0.638284	-0.60306	-0.83724				
63-90			-0.69621	0.951923	-0.63209	-0.60783	0.623216	0.392776	-0.54109	0.542746	-0.64136	-0.77238				
90-125			-0.63634	0.917214	-0.55035	-0.54172	0.523364	0.375122	-0.514	0.52198	-0.58645	-0.72366				
125-250			-0.4241	0.689065							-0.45713	-0.5123				
GT 250																

Correlation coefficients for MIS 3

|	xLF	xFD%	xARM	gt40	SIRM	IRM-20	IRM-300	20mT/xA	ARM/SIR	IRM/xAR	SIRM/xLF	xARM/xLF	HIRM	soft%	sirm-300	mt300-20
xLF																
xFD%																
xARM																
gt40	0.492816															
SIRM	0.560565															
IRM-20				-0.4733												
IRM-300	-0.78497				-0.70381			1								
IRM20mT/xARM			-0.5067				0.666161									
xARM/SIRM	-0.40082		0.620099	-0.41007	-0.5093				-0.40702							
SIRM/xARM			-0.63258	0.402841	0.493623				0.406437	-0.99694						
SIRM/xLF	-0.42364				0.512461											
xARM/xLF	-0.63387	0.744652	-0.55567						0.75898	-0.762	0.533039					
HIRM							0.443317				0.704342					
soft%	0.437188						-0.56131				-0.66262		-0.99002			
sirm-300							0.443317				0.704342			-0.99002		
mt300-20	0.741566			0.517038	0.469896	-0.47906	-0.7921	-0.57428					-0.46168	0.546524	-0.46168	
S-ratio	-0.43914						0.563769				0.661456			0.989613	-1	-0.54826
Mean	0.436725		0.979668		-0.50904				0.394335			-0.52741				0.502989
Median	0.470356		0.932726		-0.46975							-0.5225				0.498479
Mode			0.728009									-0.45688				
Stnd. Dev.			0.672052		-0.50493											
Skewness																
Kurtosis					-0.30475											
LT 20	-0.50973		-0.97593		0.450794				0.401129		0.559424					-0.5237
LT 40	-0.49282		-1		0.473298				0.410068	-0.40284	0.555667					-0.51704
LT 63	-0.43205		-0.98068		0.492345				0.404554		0.524642					-0.48483
LT 90			-0.82882		0.45641						0.425895					-0.41403
LT 4			-0.85585		0.404564						0.452733					-0.41835
4-16	-0.56202		-0.98074		0.445093				0.416987	-0.411	0.594153					-0.55722
16-32			-0.89093		0.443745						0.462539					-0.43641
32-63	0.539118		0.928626									-0.54611				0.518473
63-90	0.472277		0.963735		-0.45052							-0.5286				0.470334
90-125			0.90857		-0.41751				-0.42185	0.417432		-0.49251				0.4285
125-250			0.630084		-0.41492											
GT 250																

*Correlation coefficients for transition between MIS 3 and MIS 2*

|	xLF	xFD%	xARM	gt40	SIRM	IRM-20	IRM-300	20mT/xA	ARM/SIR	IRM/xAR	SIRM/xLF	xARM/xLF	HIRM	soft%	sirm-300	mt300-20
xLF																
xFD%																
xARM																
gt40																
SIRM	0.404245		0.417527													
IRM-20																
IRM-300	-0.63844		-0.48478		-0.55517	-0.55689										
IRM20mT/xARM			-0.50099			0.632013										
xARM/SIRM					-0.67526											
SIRM/xARM			-0.39093		0.666489				-0.98642							
SIRM/xLF					0.912031				-0.68451	0.675635						
xARM/xLF			0.883074					-0.46427	0.458585	-0.47202						
HIRM					0.707842				-0.47603	0.504143	0.799709					
soft%					-0.63127				0.47511	-0.50214	-0.76075		-0.99366			
sirm-300					0.707842				-0.47603	0.504143	0.799709			-0.99366		
mt300-20	0.472815					-0.44991	-0.49723	-0.56216								
S-ratio					0.656342				-0.50472	0.533847	0.788384		0.96803	-0.97497	0.96803	
Mean				0.91542												
Median				0.842164												
Mode				0.696271												
Stnd. Dev.				0.62856												
Skewness																
Kurtosis																
LT 20				-0.93745	0.394974											
LT 40				-1												
LT 63				-0.97074												
LT 90				-0.88583												
LT 4				-0.77777			-0.39997									
4-16				-0.94709												
16-32				-0.84592												
32-63				0.772817	-0.3989		0.399121									
63-90				0.945746												
90-125				0.918914												
125-250				0.724271												
GT 250																

Correlation coefficients for MIS 2

APPENDIX 2 PARAMETRIC CURVES
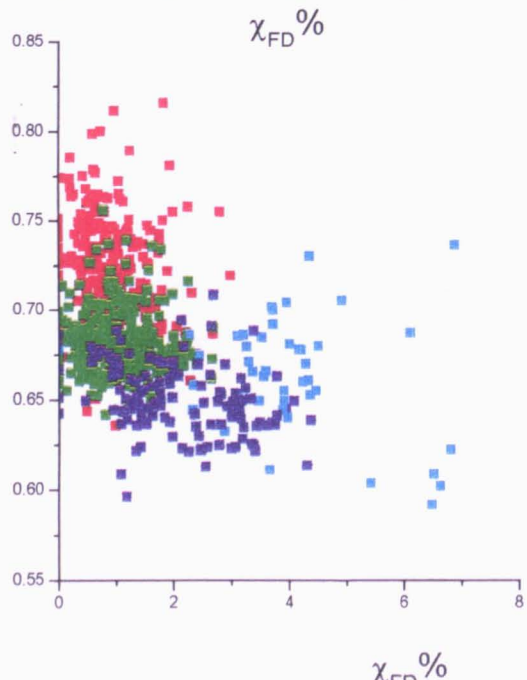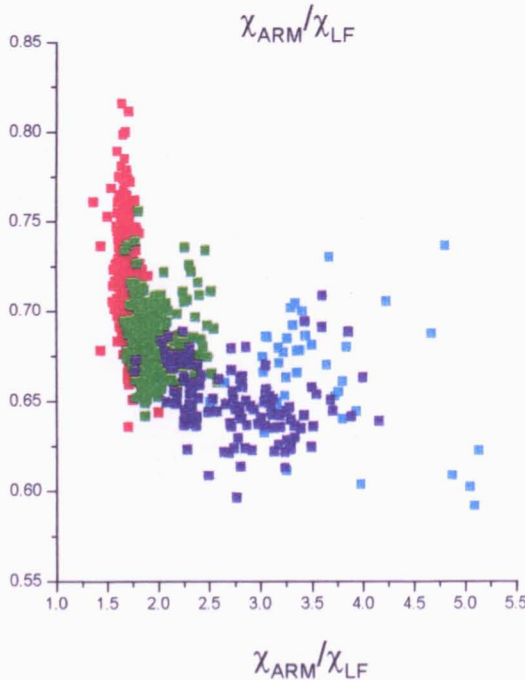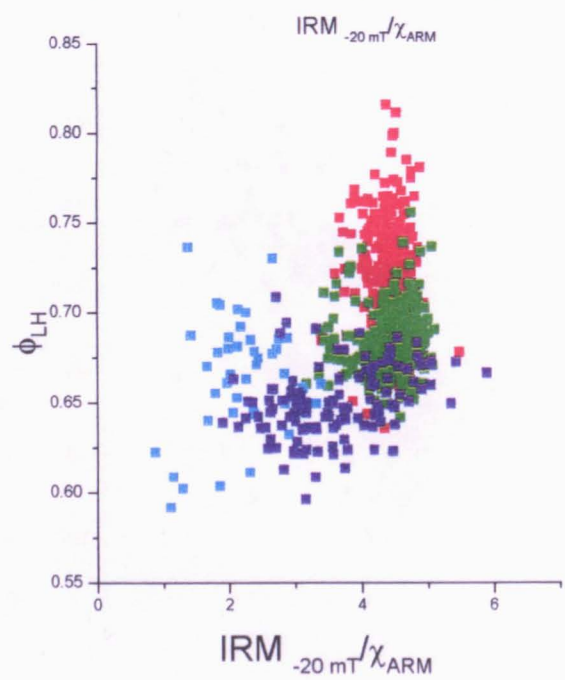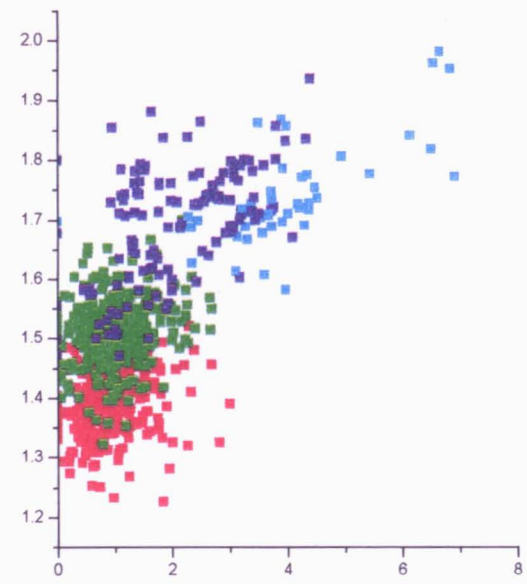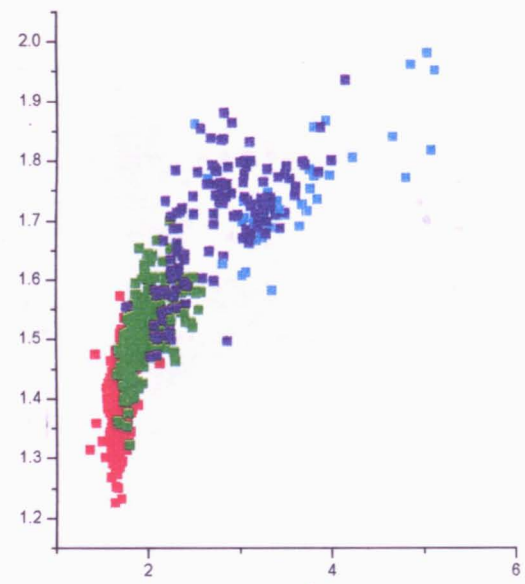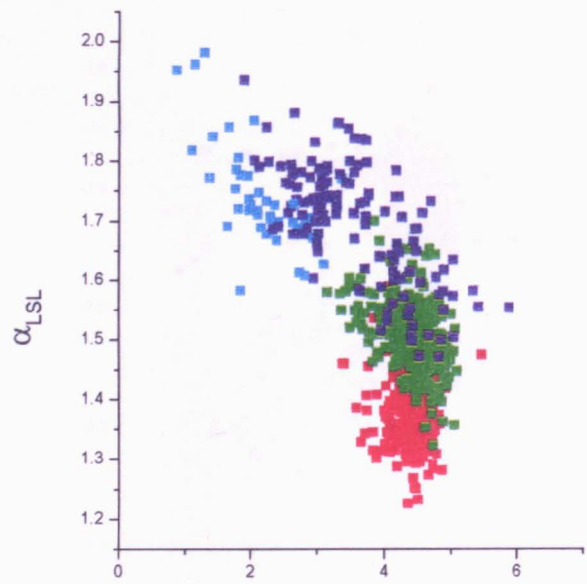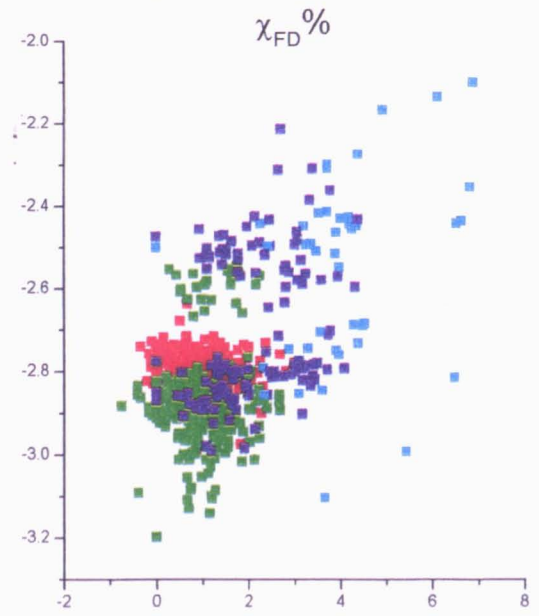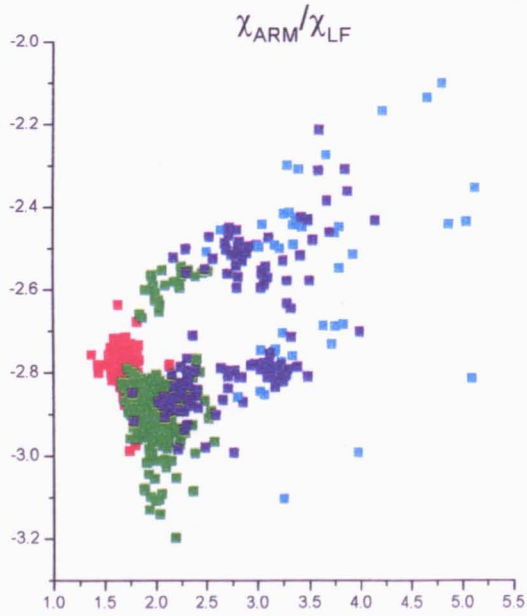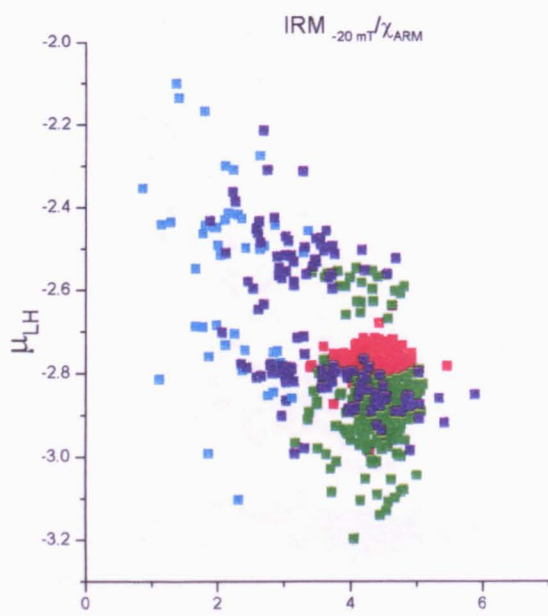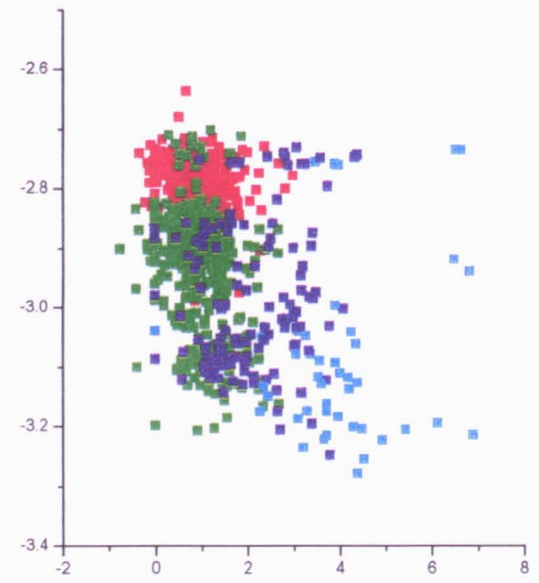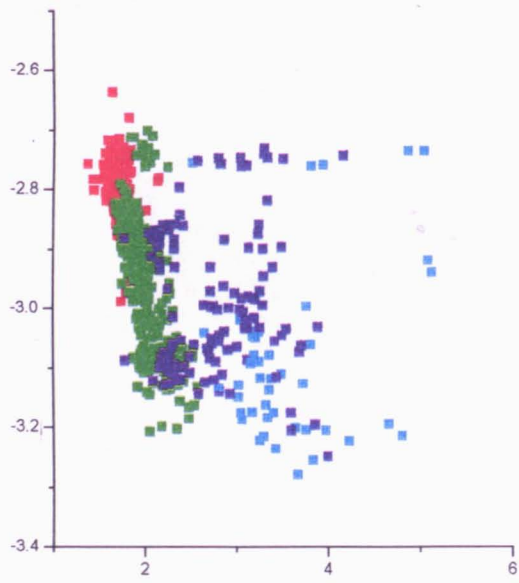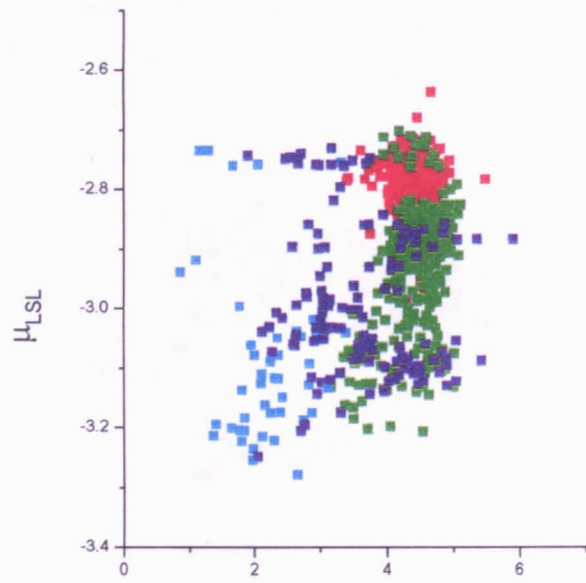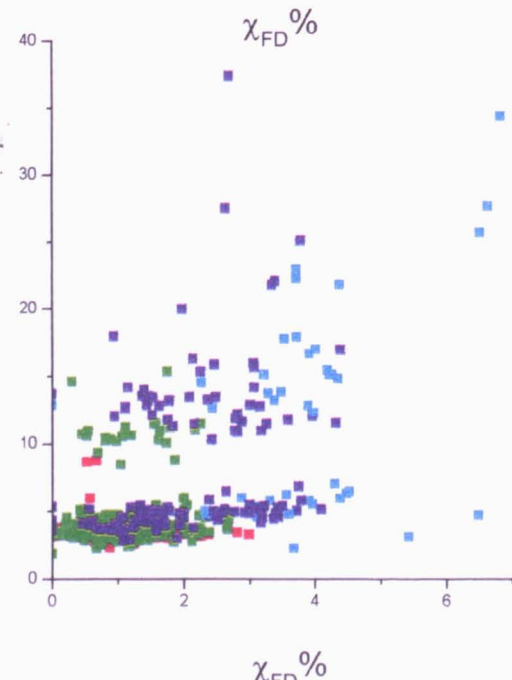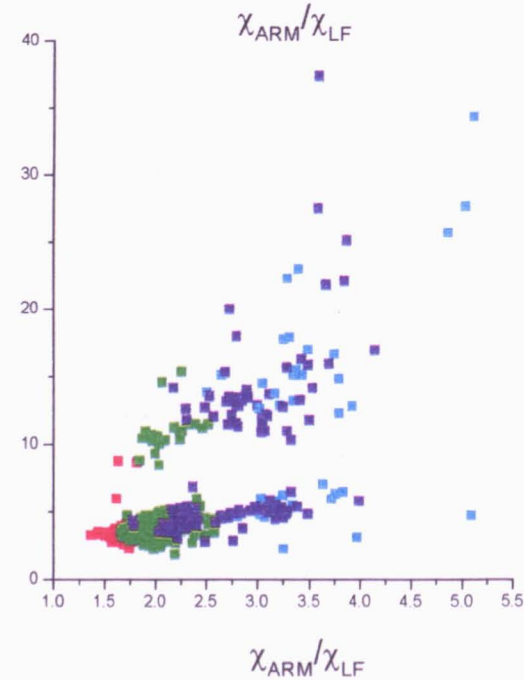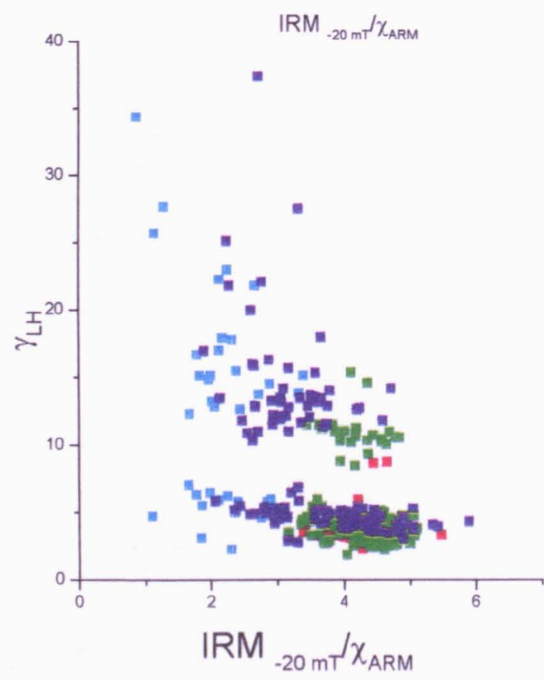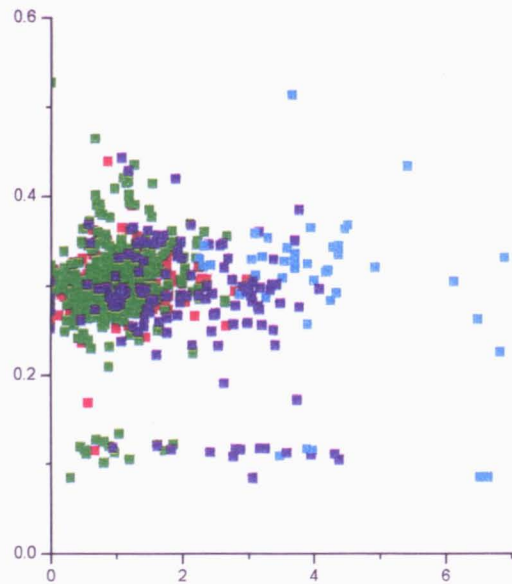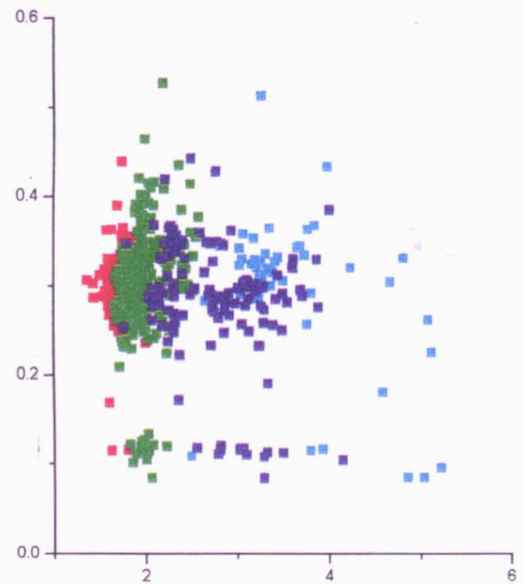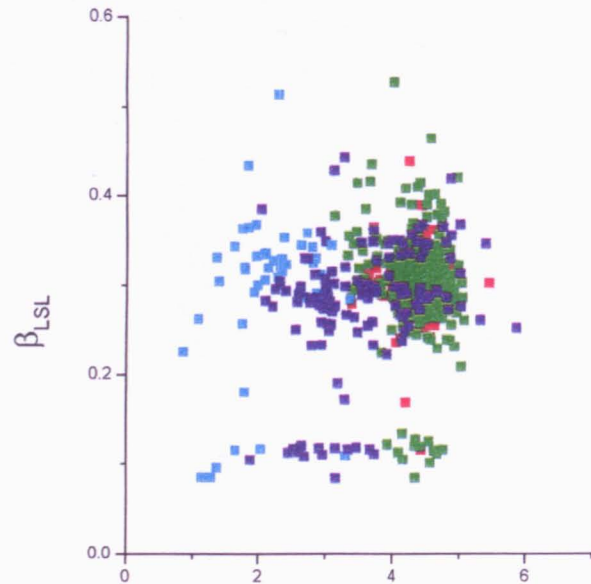
Appendix 3 Down Core Data

(See CD ROM – contact El Parker for password and most recent data and publications on elparker@hotmail.com)
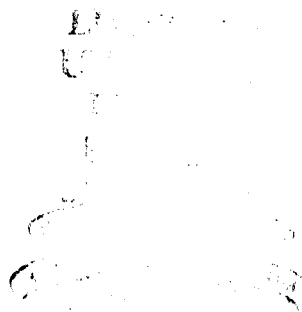
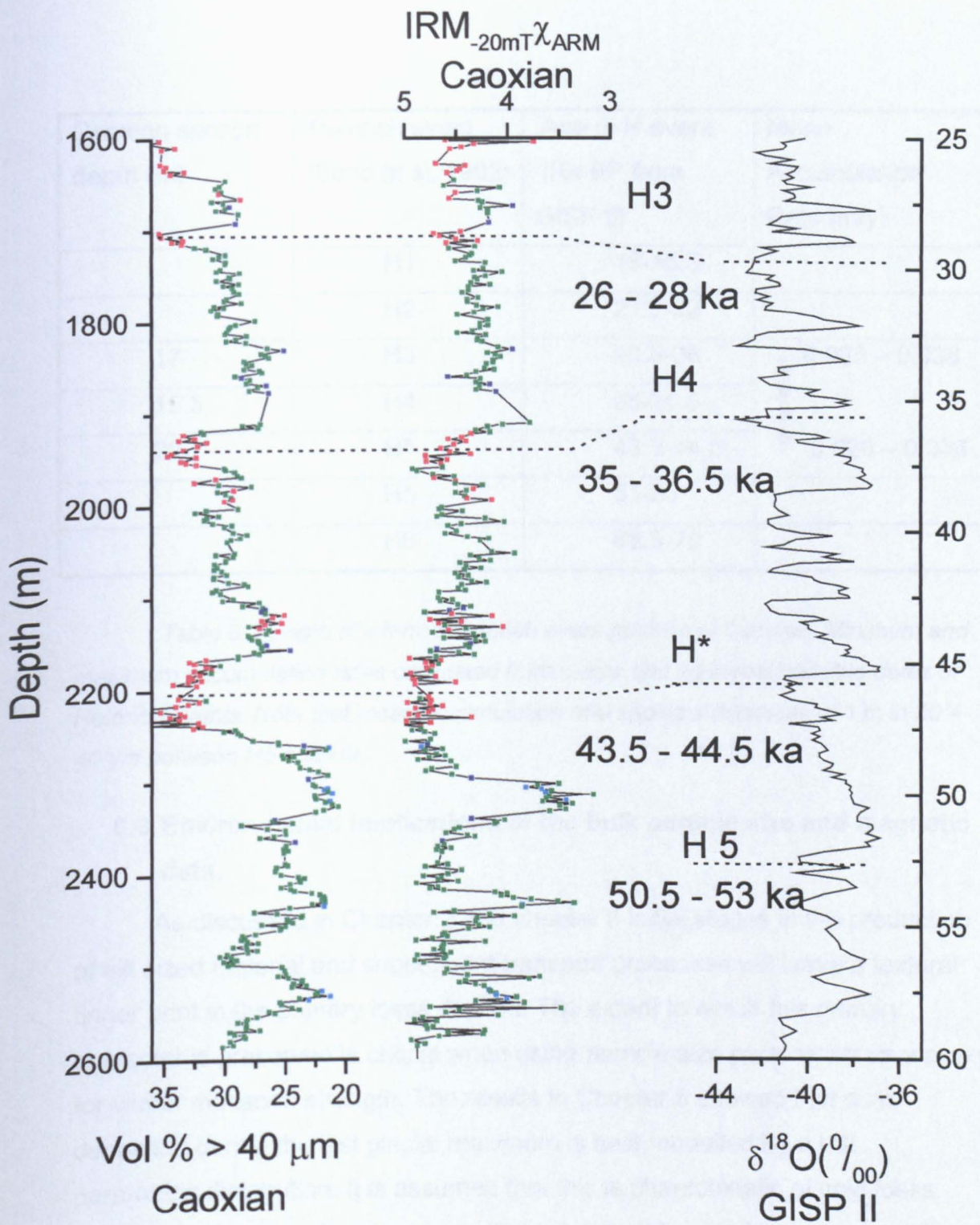Figure 6.6 Down Section plot of volume % > 40 μm, IRM$_{-20mT}$/χ$_{ARM}$, and δ^{18}O variations from the GISP II ice core. All ages are in yr BP (AD 1950 = 0 yr BP) GISP data after Sowers et al (1993). H – Heinrich events.
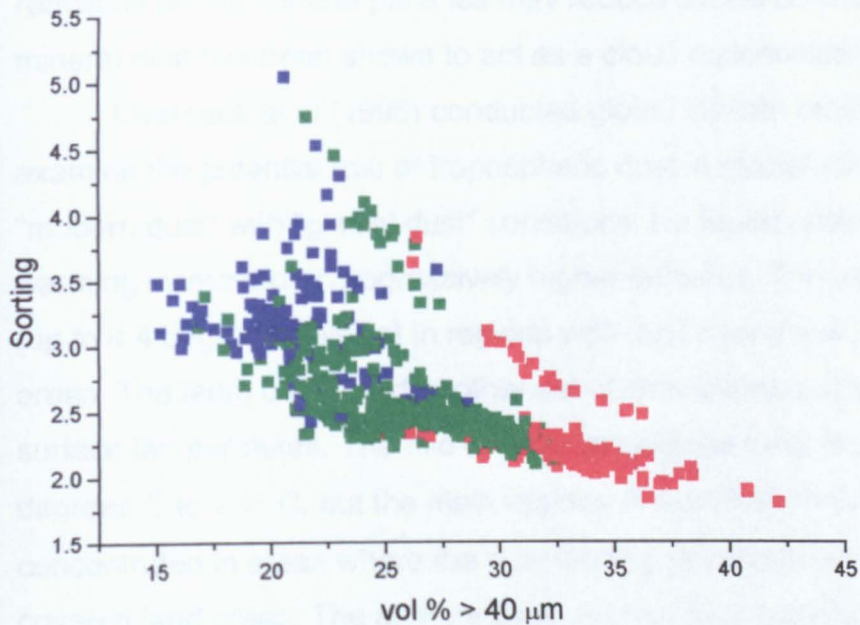
Figure 6.7 changes in the degree of skewness (φ/γ) in coarse and fine horizons

atmosphere resulted in a reduction in the net energy reaching the surface and so caused cooling (Carlson and Benjamin, 1980). It has since become clear that increased dust in the atmosphere can affect the climate by shutting out solar radiation and by holding in terrestrial radiation. The dominance of solar or thermal radiation flips depends on the concentration, composition, size, and shape of particles in the atmosphere and external factors such as albedo (Tegen and Lacis 1996, Tegen et al, 1996). Until recently, it was believed that the energy output from the sun was relatively stable. Since 1978, high precision monitoring of the solar radiance has been possible and it is evident that the solar constant changes in phase with the solar activity by 1-1.5%. It has also been proposed that several processes within the atmosphere directly or indirectly amplify any solar radiation effect. All these interactions are complex and no one process can be considered in isolation.

It is accepted that mineral aerosols act as micro-nutrients for terrestrial and especially marine systems (Martin et al, 1994). Martin hypothesised that iron added to the ocean would act as a fertiliser, augment photosynthesis, remove CO_2 and encourage cooling. Dust may also be associated with the export of carbon to the deep oceans and thus regulate CO_2 and the adsorption